PSL UNIVERSITÉ PARIS

THÈSE DE DOCTORAT
DE L'UNIVERSITÉ PSL

Préparée à MINES ParisTech

# Cellulose based aerogels: properties and shaping as beads

# Aérogels à base de cellulose : propriétés et production sous forme de billes


Soutenue par

**Lucile Druel**

Le 10 mai 2019


École doctorale n°364

**Sciences Fondamentales et Appliquées**

Spécialité

**Mécanique numérique et Matériaux**

Composition du jury :

| | |
|---|---|
| Irina Smirnova<br>Professor, Hamburg University of Technology | *Rapporteur* |
| Herbert Sixta<br>Professor, Aalto University | *Rapporteur* |
| Lennart Salmén<br>Professor, RISE Innventia AB - KTH Royal Institute of Technology | *Président* |
| Yves Grohens<br>Professeur des universités, Université Bretagne Sud | *Examinateur* |
| Tatiana Budtova<br>Directeur de recherche, Cemef - Mines ParisTech | *Directrice de thèse* |

MINES ParisTech | PSL

# Acknowledgements

Tout d'abord, j'aimerai remercier ma directrice de thèse Tatiana Budtova pour m'avoir donné l'opportunité de réaliser cette thèse sous son encadrement.
Merci Tania, pour tout ce que tu m'as apporté, aussi bien au niveau professionnel que personnel ! La découverte du milieu de la recherche et des aérogels bio-sourcés à tes côtés a été un véritable plaisir. Durant ces trois ans tu m'as accompagnée, soutenue et enrichie. Merci pour ta patience, ton adaptabilité, ton sourire et ta gentillesse ainsi que tes encouragements et toutes nos discussions intéressantes.

This work was performed in the frame of the European project "NanoHybrids" and we would like to thank all partners for the fruitful collaboration. A particular thank to :

- RISE-Innventia for providing the pulps and hemicellulose, for helping with elemental analysis and moisture sorption tests and for the very welcoming and productive stay in their institution.
- DLR and Philipp Niemeyer for the opportunity to work in their institution to use the JetCutter and for the very welcoming stay.
- Victor Baudron and Pavel Gurikov for the kind advices and very fruitful discussions on emulsions.
- Irina Smirnova and her staff for the excellent project coordination.

I would also like to thank the members of my evaluation committee for their comments and the very interesting discussions on my work. My thanks to Lennart Salmén, Yves Grohens and especially Herbert Sixta and Irina Smirnova for being my reviewers and for writing very complete reviews of my manuscript.

J'aimerai aussi remercier tout le personnel du Cemef Mines ParisTech pour leur aide tout au long de ma thèse. Un merci tout particulier à Suzanne Jacomet pour sa gentillesse et son aide avec le MEB. Un grand merci à Romain Castellani pour avoir toujours été disponible et pour avoir répondu à mes nombreuses questions lorsque je désespérais en rhéologie et en rhéo-optique. Merci également pour nos discussions aux divers sujets =) Merci à Marie-Françoise Guenegan, Sylvie Massol, Geneviève Anseeuw, Florence Morcamp, Isabelle Iota, Alain Burr, Elisabeth Massoni, Marc Bouyssou, Gabriel Monge, Gilbert Fiorucci et Francis Fournier pour leur aide.

Un grand merci à l'équipe de Persée Mines ParisTech et tout particulièrement à

Pierre Ilbizian pour sa gentillesse, sa disponibilité et son aide avec le séchage supercritique et tous les autres instruments et problèmes rencontrés. Merci Pierre, de nous avoir soutenues et aidées tout au long de notre thèse, tout en nous rappelant qu'il fallait aussi savoir se ménager. Merci à Aravind Parakkulam Ramaswamy et Arnaud Rigacci pour avoir été d'excellents partenaires de projet.

Il me tient aussi à cœur de remercier tous mes collègues du Cemef et de Persée sans qui cette "aventure" n'aurait pas eu le même goût. Merci à Ghislain, Antoine, Patou, Guillaume, Maxime, Kevin, Adrian, Fabien, Lucia, Pedro et Alexis pour avoir accepté "une Cemef" dans votre équipe =) Merci Vincent, Manon, Pierrick, Marc, Suzanne, Antoine, Christophe, Fabien, Emilie et Catheline pour votre présence et nos discussions. Je voudrais remercier tout particulièrement Gerry et Romain pour leur gaieté et pour m'avoir fait découvrir un nouveau monde plein de magie ;) Vous faites partie des inspirateurs de cette nouvelle voie qui s'offre à moi ^^ Merci aussi à Benjamin pour nous avoir rejointes dans notre bureau et pour nous avoir soutenues lors de ces derniers mois de thèse. Thank you Feng for having shared great experiences with us and thank you Oona for being sooooo great ! I am really grade I met you :) I would also like to thank my interns for their nice work and their kindness : Amelie, Omar and Isadora, thank you for your help !

Merci aussi à mes amis, en dehors du travail, Jean, Jeff, Vincent, Emma et Iris, qui m'ont permis de m'évader de ma routine.

Un super méga merci à Julien (Sunaku), Nicolas (oYo) et François (Fifou) pour toutes les découvertes, le soutien et le bon temps que vous m'avez apportés =D Un merci tout particulier à Julien pour m'avoir écoutée et supportée lors de nos longues discussions, parfois bien trop tard dans la nuit. Merci ! Merci ! Merci ! Merci ! Merci ! Merci ! Merci ! Merci ! Merci ! Merci ! Merci !.....

Milles mercis à toute ma famille, en particulier à mes parents, Marie-Laure et Fabrice, mon frère, Godefroy, son fils, Marius et sa femme, Marie. Merci de m'avoir soutenue et accompagnée comme vous l'avez toujours fait. Je vous aime de tout mon cœur ! Merci également à ma tante, Natalie, et mon cousin, Antoine, pour m'avoir soutenue et pour avoir toujours été aussi adorable !

Un grand merci, comme toujours, à Thomas, Tatiana, Guylaine et Hervé qui m'ont offert beaucoup d'instants précieux.

Enfin, j'aimerai remercier du fond du cœur Sophie. Comment t'exprimer toute ma gratitude et mon amour avec de simples mots ? Je pense sincèrement que cette thèse, et ma vie, n'aurait pas été la même sans toi. Tu m'as tellement apporté d'un point de vu professionnel mais surtout personnel et je t'en suis infiniment reconnaissante. Ces trois années ont été heureuses et remplies d'émotions grâce à toi. Encore des milliards de merci et un nombre infini de bisous <3 J'espère ne jamais perdre une amie aussi précieuse que toi ! Love yoooouuuu !

# Table des matières

# Abbreviations and symbols

## Abbreviations and acronyms

| | |
|---|---|
| **aq** | Aqueous |
| **BET** | Brunauer-Emmett-Teller (theory) |
| **BJH** | Barrett–Joyner–Halenda (theory) |
| $\mathbf{C}_a$ | Capillary Number |
| $\mathbf{C}_a^{Crit}$ | Critical Capillary Number |
| **CNC** | Cellulose nanocrystals |
| **Cr.I.** | Crystallinity Index |
| **C*** | Overlap concentration |
| **DP** | Degree of Polymerisation |
| $\boldsymbol{I}_a$ | Integrated area of cellulose amorphous phase |
| $\boldsymbol{I}_c$ | Integrated area of cellulose crystalline phase |
| **IL** | Ionic liquid |
| **ILs** | Ionic liquids |
| **MCC** | Microcrystalline cellulose |
| **MFC** | Microfibrillated cellulose |
| **NFC** | Nanofibrillated cellulose |
| **RTILs** | Room temperature ionic liquids |
| $\mathbf{S}_{\mathbf{BET}}$ | Specific surface area from BET method |
| **Sc** | Supecritical |
| **SEM** | Scanning Electron Microscopy |
| $\mathbf{V}_{ini}$ | Initial volume |
| $\mathbf{V}_{final}$ | Final volume |

# Chemical compounds

| | |
|---|---|
| **AA** | Acetic acid |
| **C** | Carbon |
| **$CS_2$** | Carbon disulphide |
| **CED** | Cupriethylenediamine |
| **$CO_2$** | Carbon dioxide |
| **DBN** | 1,5-diazabicyclo[4.3.0]non-5-ene |
| **[DBNH][Pr]** | 1,5-diazabicyclo[4.3.0]non-5-ene Propionate |
| **DMSO** | Dimethyl sulfoxide |
| **[Emim][OAc]** | 1-ethyl-3-methyl imidazolium acetate |
| **$EtCO_2H$** | Propionic acid |
| **EtOH** | Ethanol |
| **HCl** | Hydrochloric acid |
| **$H_2O$** | Water |
| **$H_2SO_4$** | Sulphuric acid |
| **Na** | Sodium |
| **NaOH** | Sodium Hydroxide |
| **$Na_2S$** | Sodium sulphide |
| **NMMO** | N-methylmorpholine N-oxide |
| **$SO_2$** | Sulphur dioxide |
| **Span 80** | Sorbitane monooleate |
| **Zn** | Zinc |
| **ZnO** | Zinc Oxide |

# Symbols

| | |
|---|---|
| % | Weight percent (all percent are given in weight percent otherwise mentioned) |
| **vol.%** | Volume percent |
| $\boldsymbol{\rho_{bulk}}$ | Bulk density |
| $\boldsymbol{\rho_{sk}}$ | Skeletal density |
| $\boldsymbol{\eta}$ | Viscosity |
| $[\boldsymbol{\eta}]$ | Intrinsic viscosity |
| **m** | Mass |
| $\boldsymbol{\sigma}$ | Interfacial tension |
| **V** | Volume |

# General introduction

Ecology, environmental awareness, sustainable development - these terms are now in everyone's mind. As a matter of fact, the extensive use of fossil resources for the production of energy, textiles and other materials have led to a concerning global warming and multiple environmental issues. Governments are now trying to promote the development of new materials and energies that would be sustainable and environmentally friendly. The scientific community is fully involved in this process and great efforts are done for discovering and improving eco-responsible products.

One class of materials that could contribute in lowering human impact on environment are the aerogels. They were discovered in 1931 by Kistler (Kistler (1931)). He developed a new method to dry wet materials without damaging their structure : the supercritical drying. Aerogels obtained are ultra-lightweight with a fine, highly porous and interconnected 3D network. Their remarkable properties render them versatile materials to be used in multiple industries, from construction to medical. One of the most famous aerogel is made from silica. Silica aerogels have demonstrated outstanding properties in thermal insulation, showing thermal conductivity as low as 0.013 W $m^{-1}$ $K^{-1}$. These aerogels are, however, very fragile and brittle which brought to the development of aerogels based on metal oxides or synthetic polymers. Polyurethane aerogels are now commercialised by BASF, as thermal insulation panels (BASF (2019)-https ://www.basf.com) ; yet, one issue remains, these products still involve the petrochemical industry.

Around 15 years ago, a new class of aerogels was made, the bio-aerogels. Based on polysaccharides, polymers found in nature, these aerogels have properties similar to their synthetic counterparts. However, contrary to synthetic polymer based aerogels, bio-aerogels are sustainable and environmentally friendly, with no toxic chemicals involved in their preparation. As a result, this class of aerogels can be used in new applications which directly involve human health. Nevertheless, several problems are to be tackled :

- The first one is economical ; the production of aerogels is expensive, mostly because of the supercritical drying.
- The second problem is related to their shape ; the production of aerogels shaped as monoliths is now mastered but other shapes, such as microspheres, are required

for use in different fields, for example in pharma, cosmetic and food.

The **goals of the work** presented in this manuscript were as follows :

- Preparation and characterisation cellulose aerogels in the shape of beads of various controlled sizes.
- Using various pulps in order to make raw material cheaper than classically used microcrystalline cellulose.
- Trying to find the ways to avoid drying under supercritical conditions.

This work was performed in the frame of the European project "NanoHybrids" (Nanohybrids (2019)-https ://nanohybrids.eu/). As its title indicates *"NanoHybrids - New generation of nanoporous organic and hybrid aerogels for industrial applications : from laboratory to pilot scale production"*, the main objective of this project is the development of industrialisable methods for the production of aerogels. The focus is especially set on the production of aerogels shaped as beads or particles and on the adaptation of their properties to different applications. NanoHybrids consortium regrouped several academic and industrial partners, all leaders in their field :

- TUHH, the Hamburg University of Technology, coordinated the project.
- DLR, Institute of Materials Research, German aerospace centre.
- KU, Koç University.
- Mines ParisTech (Armines), Center of Material Forming (Cemef) and Centre for Processes, Renewable Energies and Energy Systems (Persée).
- RISE-Innventia AB, Research Institutes of Sweden.
- MUCTR, Mendeleev University of Chemical Technology of Russia.
- The University of Patras.
- The National and Kapodistrian University of Athens.
- BASF, Polyurethanes GMBH.
- Nestlé, Production Technology Centre York.
- Dräger, Safety AG & Co. KGAA
- Arçelik A.Ş.

Academic partners focused on developing techniques to produce tuned aerogel beads from different sources at the industrial scale and each industrial partner was testing the produced aerogels for their applications.

As the most abundant polysaccharide on earth, cellulose is a first choice for the production of bio-aerogels. It was hence logical to choose this polysaccharide for the purpose of producing cellulose aerogel beads. Several steps are to be followed for their production. Figure 1 below shows the pathway used to produce cellulose aerogels in the frame of our work. It also includes the methods used to shape them as beads.

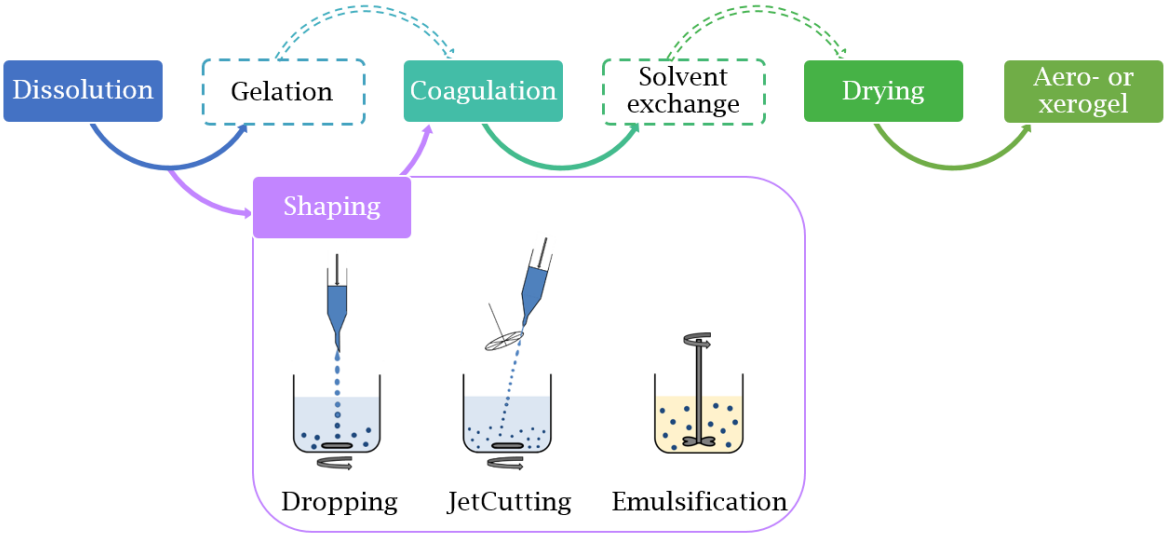


FIGURE 1 – Schematic representation of the pathway used in this work to produce bio-aerogels. Shaping is part of the pathway but was put aside to highlight the different shaping methods used.

First, cellulose needs to be dissolved. Two types of solvents, NaOH based and ionic liquids, as well as two types of cellulose sources, microcrystalline cellulose and pulps, were used. Once cellulose is dissolved, the obtained solution needs to be shaped as desired. In this study we have prepared monoliths and have used three main methods to shape solutions as droplets : the "simple" dropping technique, the JetCutter technology and the emulsification. When cellulose solution is in the desired shape, the latter needs to be fixed. Cellulose solution, depending on the solvent, can undergo gelation with time and temperature, however, when shaped as beads, a direct coagulation turned out to be preferable. To do so, cellulose solutions are placed in a non-solvent. Finally, to proceed to the drying, and especially with supercritical $CO_2$, the coagulated cellulose beads need to be in a fluid miscible with $CO_2$. Hence a step of solvent exchange is often required to replace the non-solvent used for coagulation with a non-solvent of cellulose which is miscible with $CO_2$. After drying the obtained materials must be characterised by multiple means such as analysing their density, morphology, specific surface area and particle size distribution, in the case of beads.

The present manuscript is divided in six chapters giving the context, detailing the materials and methods used and reporting the results obtained by using the pathway described above and by varying different of these steps :

The first chapter, *State of the art*, gives a literature review on the topics broached in this manuscript. It starts with a brief introduction on polysaccharides, wood and pulps. Then it details the structure of cellulose, including an overview of the different existing allomorphs and the way they can be obtained. Cellulose dissolution and solution shaping is then tackled. The two types of solvents (NaOH based and ionic liquids)

used in our study are particularly detailed in terms of dissolution mechanisms. As for shaping, focus is set on dropping, JetCutter and emulsions. Finally, a short introduction on aerogels is given, followed by more details on the preparation and applications of bio-aerogels. Cellulose II aerogels' properties are presented with the emphasis on the influence of processing parameters. In the last part the existing polysaccharide aerogel beads and particles are reviewed with precision given on the methods of their production.

The second chapter, *Materials and methods*, is devoted to the description of the means utilised to conduct this study. The first part details the compounds used in this study, microcrystalline cellulose, pulps prepared and kindly provided by RISE-Innventia, solvents and chemicals such as ionic liquids and non-solvents. All methods used are presented in the second part of this chapter. The preparation pathways and techniques to produce cellulose aerogel and xerogel monoliths and beads are given including descriptions and pictures of the shaping techniques employed. Finally, all techniques of characterisation are specified. Aerogels and xerogels were characterised by measuring their shrinkage during processing, their final bulk density, their specific surface area and morphology. Additional information on the porous materials produced could be obtained with X-ray diffraction, NMR and thermal conductivity measurements. In the case of beads and particles, methods to measure their diameter are also explained. Details on solutions characterisation are given such as the ways to study the rheological properties or surface tension. The parameters and settings that are specific for each study are provided in the corresponding chapters and all concentrations are given in weight percent (%) unless otherwise mentioned.

The third chapter, *Rheology of cellulose-[DBNH][Pr] solutions and shaping into aerogel beads*, is reporting all results that led to the preparation of cellulose aerogel beads with diameters of hundreds of millimetres. For this purpose, microcrystalline cellulose was dissolved in a new ionic liquid : 1,5-diazabicyclo[4.3.0]non-5-enium propionate ([DBNH][Pr]). The obtained solutions were then shaped with the JetCutter technology and the obtained aerogel beads were characterised. A complete study of the rheological properties of these solutions was conducted. The flow and viscoelastic properties of cellulose-[DBNH][Pr] solutions were studied as a function of polymer concentration and solution temperature. Obtained results were compared to the well-known cellulose solutions in 1-ethyl-3-methyl imidazolium acetate ([Emim][OAc]) ionic liquid and it appeared that intrinsic viscosity is higher in the new ionic liquid and the latter shows a better thermodynamic quality toward cellulose at all temperatures studied. These results allowed a selection of solutions viscosity in order to fit into the processing window of the JetCutter.

The properties of the produced cellulose aerogel beads were analysed as a function of

cellulose concentration and coagulation bath. Monolithic counterparts were prepared to study the influence of the size of aerogels on the resulting properties. Cellulose aerogel monoliths showed a surprising structure when coagulated in water. Regarding this peculiar structure obtained, a swift study was conducted to evaluate the potential applications of this material and understand the formation of such a structure.

If the production of cellulose aerogel beads with the JetCutter was successful, more studies are still needed to understand the influence of the coagulation bath on the resulting aerogels' structure.

The fourth chapter, *Micrometric cellulose aerogel beads production from adapted emulsion technique*, deals with the implementation of emulsification method on one type of cellulose solutions. Microcrystalline cellulose was dissolved in NaOH based solvents with the use of different additives. Preliminary studies, including rheological properties, calculation of the viscosity ratio, interfacial tension measurements and rheo-optical observations, were performed. Then a detailed description of how the emulsification method was modified and implemented to make cellulose droplets and beads is given. The different steps that led to this new emulsification technique are explained.

Once the procedure to produce cellulose aerogel particles was established, several parameters were varied to determine their influence on the resulting aerogel particles' properties. It appeared that a lot of parameters have to be taken into account to obtain well shaped and distinct cellulose aerogel particles. Among these parameters, the dissolution state (use of additives or not) and the coagulation mechanisms were key factors.

The diameter of the cellulose aerogel particles obtained was of few tens of microns and their properties were equivalent to the ones of monoliths. This opens a lot of possibilities for application of cellulose aerogel particles in medical or personal care, for instance.

The fifth chapter, *Lightweight and mesoporous cellulose xerogels*, addresses a major economical issue for aerogels, the supercritical drying. In this study, we have demonstrated that we can obviate the $CO_2$ supercritical drying and prepare highly porous, lightweight cellulose materials. Microcrystalline cellulose was dissolved in NaOH-based solvents and the solutions were processed via gelation, coagulation, solvent exchange (when applicable) and vacuum drying. The obtained materials were thus called xerogels. By using specific preparation parameters surface area similar to that of cellulose aerogels was reached. In the first part, the results of different experiments are presented. The aim was to try to sort out the influence of different parameters on the properties of the resulting xerogels and aerogels. Among these parameters, the concentration of additive (ZnO), gelation time and the type of non-solvent were studied. Crystallinity and metal content of xerogels and aerogels were also evaluated. The second part is dis-

cussing all the experimental results obtained and interpretations are given to explain why the obtained xerogels are porous with high specific surface area. In the last part, we found essential to prove that different sizes and shapes of these xerogels could be produced without influencing their properties. For this purpose, cellulose xerogel beads were produced at the lab scale with the dropping technique.

The last chapter, *Pulp based aerogels*, is devoted to the preparation and characterisation of aerogels prepared from pulps. Different types of pulps, with different cellulose degree of polymerisation and cellulose, hemicellulose and lignin content were kindly prepared and provided by RISE-Innventia. These pulps were dissolved in NaOH-ZnO-$H_2O$ solvent, coagulated in different non-solvents which were then exchanged by ethanol to proceed to the supercritical drying. Dissolution efficiency of the solvent was evaluated by optical microscope observations and determination of the non-dissolved fraction. Then the influence on aerogels' properties of several preparation parameters were evaluated, namely, solution gelation time, type of non-solvent and pulp composition. The influence of each parameter was difficult to assess because of their large number but trends could be drawn. In the final part, the production of aerogel particles with the JetCutter technology was evaluated and successfully conducted. Moisture sorption capacity of aerogels and xerogels made from pulp was measured by our partner RISE-Innventia and results were analysed as a function of their preparation conditions.

The final part is devoted to the concluding remarks and perspectives of this work.

# Résumé du travail de thèse

## Introduction générale

Écologie, développement durable, prise de conscience environnementale - ces termes sont maintenant dans l'esprit de tous. En effet, l'utilisation extensive des ressources fossiles pour la production d'énergie, de textiles et d'autres matériaux a conduit à un réchauffement climatique préoccupant et à de multiples problèmes environnementaux. Les gouvernements s'efforcent maintenant de promouvoir le développement de nouveaux matériaux et énergies qui seraient durables et respectueux de l'environnement. La communauté scientifique est pleinement impliquée dans ce processus et beaucoup d'efforts sont déployer pour découvrir et améliorer des produits éco-responsables.

Les aérogels constituent une catégorie de matériaux qui pourraient contribuer à réduire l'impact des activités humaines sur l'environnement. Ils ont été découverts en 1931 par Kistler (Kistler (1931)). Ce dernier a développé une nouvelle méthode pour sécher des matériaux humides sans endommager leur structure : le séchage supercritique. Les aérogels obtenus sont ultra-légers avec un réseau 3D interconnecté, fin et très poreux. Leurs propriétés remarquables en font des matériaux polyvalents à utiliser dans de multiples industries, de la construction au médical. L'un des aérogels les plus célèbres est fait à partir de silice. Les aérogels de silice possèdent des propriétés exceptionnelles en matière d'isolation thermique. Il ont une conductivité thermique qui peut descendre jusqu'à 0,013 W $m^{-1}$ $K^{-1}$. Ces aérogels sont cependant très fragiles et cassants ce qui a conduit au développement d'aérogels à base d'oxydes métalliques ou de polymères synthétiques. Les aérogels de polyuréthane sont maintenant commercialisés par BASF sous forme de panneaux d'isolation thermique (BASF (2019)-https ://www.basf.com) ; cependant, un problème demeure, ces produits impliquent toujours l'industrie pétrochimique.

Il y a une quinzaine d'années, une nouvelle classe d'aérogels a été fabriquée, les bio-aérogels. Composés de polysaccharides, bio-polymères que l'on retrouve dans la nature, ces aérogels ont des propriétés similaires à celles de leurs homologues synthétiques. Cependant, contrairement à eux, ils sont durables et respectueux de l'environnement, sans produits toxiques impliqués dans leur préparation. Cette classe d'aérogels peut être utilisée dans de nouvelles applications qui impliquent directement la santé humaine. Néanmoins, deux problèmes principaux doivent être réglés :

- Le premier est économique ; la production d'aérogels est coûteuse, surtout à cause du séchage supercritique.
- Le deuxième problème est lié à leur forme ; la production d'aérogels en forme de monolithes est maintenant maîtrisée mais d'autres formes, telles que les microsphères, sont nécessaires pour une utilisation dans différents domaines, par exemple, dans les industries pharmaceutique, cosmétique et alimentaire.

Les **objectifs du travail** présenté dans ce manuscrit étaient les suivants :

- Préparation et caractérisation d'aérogels de cellulose sous forme de billes de tailles différentes et contrôlées.
- Utilisation de différentes pâtes à papier afin de rendre la matière première moins chère que la cellulose microcristalline classiquement utilisée.
- Essayer de trouver les moyens d'éviter le séchage dans des conditions supercritiques.

Ce travail a été réalisé dans le cadre du projet européen "NanoHybrids" (Nanohybrids (2019)-https ://nanohybrids.eu/), en concidérant les problématiques cités ci-dessus. Comme son titre l'indique, *"NanoHybrids - Nouvelle génération d'aérogels organiques et hybrides nanoporeux pour applications industrielles : du laboratoire à la production pilote"*, l'objectif principal de ce projet est le développement de méthodes industrialisables pour la production des aérogels. L'accent est mis en particulier sur la production d'aérogels en forme de billes ou de particules et sur l'adaptation de leurs propriétés aux différentes applications. Le consortium de NanoHybrids regroupe plusieurs partenaires académiques et industriels, tous leaders dans leur domaine :

- TUHH, the Hamburg University of Technology, coordinateur du projet.
- DLR, Institute of Materials Research, German aerospace centre.
- KU, Koç University.
- Mines ParisTech (Armines), Center of Material Forming (Cemef) and Centre for Processes, Renewable Energies and Energy Systems (Persée).
- RISE - Innventia AB.
- MUCTR, Mendeleev University of Chemical Technology of Russia.
- The University of Patras.
- The National and Kapodistrian University of Athens.
- BASF, Polyurethanes GMBH.
- Nestlé, Production Technology Centre York.
- Dräger, Safety AG & Co. KGAA
- Arçelik A.Ş.

Les partenaires universitaires se sont concentrés sur le développement de techniques de production industrialisable d'aérogels de différentes sources, aux propriétés versatiles, sous forme de billes. Chaque partenaire industriel testait les aérogels produits pour leurs applications spécifique.

En tant que polysaccharide le plus abondant sur terre, la cellulose est un choix de premier ordre pour la production de bio-aérogels. C'est pourquoi elle a été utilisée dans le but de préparer des billes d'aérogel. Plusieurs étapes doivent être suivies pour leur production. La Figure 2 ci-dessous montre les étapes que nous avons suivi dans le cadre de notre travail pour produire des aérogels de cellulose. Elle inclut également les méthodes utilisées pour les mettre sous forme de billes.

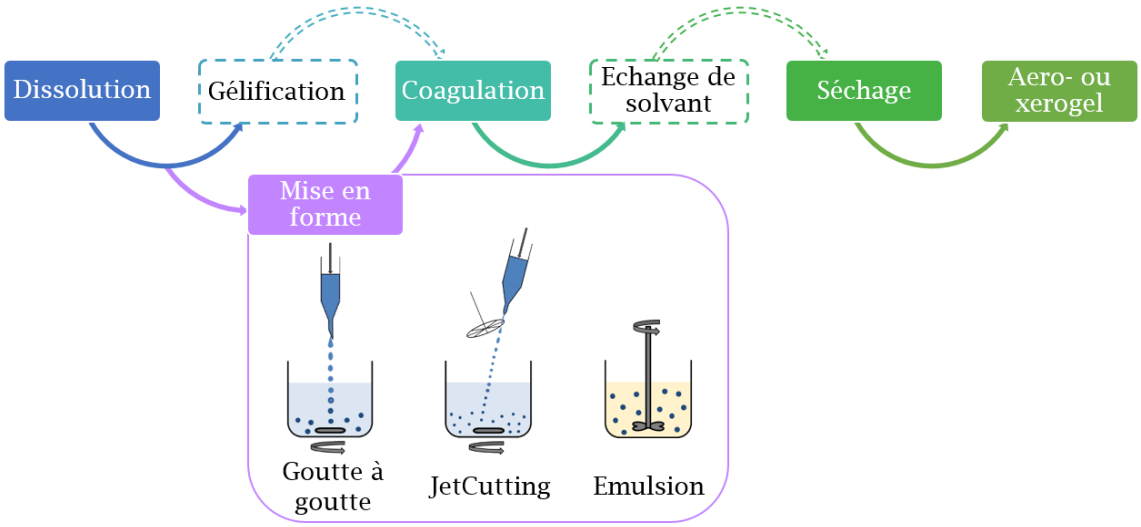


Figure 2 – Representation schématique des étapes de production des bio-aérogel utilisées dans le cadre de ce travail. La mise en forme fait partie du processus mais a été mise de côté pour mettre en évidence les différentes méthodes utilisées.

Premièrement, la cellulose doit être dissoute. Deux types de solvants, à base d'hydroxyde de sodium (NaOH) et de liquides ioniques, ainsi que deux sources différentes de cellulose, la cellulose microcristalline et les pâtes à papier, ont été utilisés. Une fois la cellulose dissoute, la solution obtenue doit être mise en forme comme souhaité. Dans cette étude, nous avons préparé des monolithes et utilisé trois méthodes principales pour produire des gouttelettes de solution : la technique "simple" du goutte à goutte, la technologie "JetCutter" et l'émulsification. Lorsque la solution de cellulose a la forme désirée, cette dernière doit être "fixée". Les solutions de cellulose, selon le solvant utilisé, peuvent subir une gélification spontanée avec le temps et la température. Cependant, lorsqu'elles sont préparées sous forme de billes, une coagulation directe est préférable. Pour ce faire, les solutions de cellulose sont placées dans un non-solvant. Enfin, pour procéder au séchage, en particulier avec le dioxyde de carbone ($CO_2$) supercritique, les billes de cellulose coagulées doivent être dans un fluide miscible avec le $CO_2$. Par conséquent, une étape d'échange de solvant est souvent nécessaire pour remplacer le non-solvant utilisé pour la coagulation par un non-solvant de la cellulose qui est miscible avec le $CO_2$. Après séchage, les matériaux obtenus doivent être caractérisés par de multiples moyens tels que l'analyse de leur densité, de leur morphologie, de leur surface spécifique et de leur distribution de taille, dans le cas des billes.

Le présent manuscrit est divisé en six chapitres donnant le contexte, détaillant les matériaux et les méthodes utilisés et relatant les résultats obtenus en utilisant les étapes de production décrites ci-dessus et en variant les différents paramètres ce processus.

# Chapitre 1 - Etat de l'art

Ce chapitre couvre un large éventail de sujets. Des polysaccharide, à la mise en forme des solutions de cellulose et à la production d'aérogels sous forme de billes, nous pu voir la complexité des problèmes à résoudre en termes de fabrication de billes d'aérogel de cellulose de tailles et morphologies variées et contrôlées.

Tout d'abord, un bref aperçu des différents traitements du bois est présenté pour l'obtenir des pâtes à papier. Selon le traitement reçu (mécanique, chimique ou les deux), la teneur en cellulose, en hémicelluloses et en lignine peut varier. Les propriétés de base de la cellulose ont ensuite été discutées. La cellulose est un polysaccharide linéaire constitué de motifs répétitifs de D-anhydroglucopyranose liés entre eux par des liaisons $\beta$-1,4-glycosidiques. Il existe différentes allomorphes de la cellulose qui correspondent à différentes conformations et interactions des chaînes. Par exemple, la cellulose I est la cellulose native et ses chaînes ont un alignement parallèle conduisant à des liaisons hydrogène intramoléculaires et intermoléculaires à l'intérieur et entre les chaînes. Ces interactions donnent un polymère difficile à dissoudre. La cellulose II est obtenue par mercerisation ou dissolution et régénération ou coagulation de la cellulose I et possède une organisation de chaînes antiparallèles.

Comme les billes d'aérogel de cellulose sont préparées par dissolution de la cellulose, ses solvants ont été présentés en mettant l'accent sur ceux utilisés dans ce travail. Les solvants pour dissoudre la cellulose peuvent être classés en deux catégories : les solvants dérivatisant et les solvants directs (ou non dérivatisant). La première classe implique la formation d'un dérivé de cellulose pour permettre sa dissolution puis sa régénération afin de récupérer de la cellulose pure. Au contraire, les solvants directs dissolvent la cellulose sans aucune modification chimique de cette dernière. Les solvants à base de NaOH-eau et les liquides ioniques font partie des solvents directs et ont été utilisés dans ce travail. Leurs propriétés ainsi que celles des solutions de cellulose obtenues sont donc présentées. Les solvants à base de NaOH font parties des solvants les moins chers, mais la dissolution de la cellulose dans ce milieu est limitée à de faibles concentrations et à des faibles degrés de polymérisation (DP). De plus, la solution cellulose-NaOH-$H_2O$ obtenue gélifie avec le temps et la température, ce qui peut rendre le traitement difficile. Les liquides ioniques sont des sels fondus capablent de dissoudre de la cellulose de différentes sources à diverses concentrations et DP. Ils sont généralement classés comme solvants verts, mais comme une multitude de liquides ioniques différents peuvent être produits, on s'attend à ce que leurs propriétés et leur toxicité varient de l'un à l'autre. La mise en forme des solutions obtenues est une étape importante pour la

production de matériaux à base de cellulose. En effet, une fois régénérée ou coagulée, la cellulose ne peut plus être mise en forme facilement. Dans ce travail, nous nous sommes concentrés sur les matériaux cellulosiques sous forme de billes ou de particules et nous avons vu deux catégories de méthodes pour leur production : la formation de gouttelettes dans une phase gazeuse ou dans une phase liquide non miscible. La première catégorie regroupe la technique simple du goutte-à-goutte et la technique de JetCutter à cadence de production élevée. La deuxième catégorie est la production bien connue d'une émulsion. Ces techniques ont été détaillées dans ce chapitre et nous avons vu que chacune d'elles conduisait à des tailles de gouttelettes différentes.

Dans la dernière partie, la production et les propriétés des matériaux poreux à base de polysaccharides et, plus particulièrement, de cellulose ont été discutées. Il existe différentes méthodes de séchage pour produire des matériaux poreux et dans ce travail, nous avons choisi de classer ces matériaux selon le type de séchage qu'ils ont subi plutôt que selon leurs propriétés finales. Par conséquent, les matériaux obtenus par séchage évaporatif sont appelés xérogels, ceux obtenus par lyophilisation sont appelés cryogels et enfin, lorsque le séchage supercritique est utilisé, les matériaux obtenus sont appelés aérogels. Les propriétés du matériau poreux obtenu sont très dépendantes de la technique de séchage utilisée et nous nous sommes concentrés sur les propriétés des aérogels et leurs applications potentielles. Une vue d'ensemble est donnée sur les aérogels de polysaccharide existants, tels que les aérogels à base d'amidon, de pectine ou d'alginate, et une étude plus détaillée des propriétés des aérogels de cellulose a été réalisée. En particulier, nous avons vu l'influence des paramètres de production sur les propriétés des aérogels qui en résultent ; par exemple, l'augmentation de la densité avec l'augmentation de la concentration en cellulose. Enfin, les aérogels de polysaccharides et de cellulose existants sous forme de billes ont été identifiés et les techniques utilisées pour les produire ont été décrites. Il a été mis en évidence que pour la production de billes d'aérogel de cellulose, la principale technique utilisée jusqu'à présent était le "simple" goutte-à-goutte. Cela ouvre donc de nombreuses possibilités pour notre travail, et l'une d'entre elles est de trouver ou d'adapter de nouvelles méthodes pour produire des billes d'aérogel de cellulose à partir de solvants directs.

# Chapitre 2 - Matériels et méthodes

Les composés et les méthodes utilisés et développés dans cette étude ont été présentés dans ce chapitre. La cellulose microcristalline (MCC) et les pâtes à papier (avec différents DP de la cellulose et différentes teneurs en cellulose, hémicellulose et lignine) fournies par RISE-Innventia ont été utilisées comme matières premières pour produire des aérogels et xérogels. Deux types de solvants ont été utilisés : des solvants à base de NaOH-eau, sans et avec additifs (urée ou ZnO), et des liquides ioniques, à savoir acetate de 1-ethyl-3-methyl imidazolium ([Emim][OAc]) et propionate de 1,5-

diazabicyclo[4.3.0]non-5-enium ([DBNH][Pr]).

La procédure de préparation des monolithes d'aérogel et de xérogel de cellulose et de pâtes à papier a été détaillée. En bref, la MCC est traité pour éliminer l'humidité tandis que la teneur en humidité des pâtes est mesurée et prise en compte pour la dissolution. Les matières premières ont ensuite été dissoutes soit dans des solvants à base de NaOH à basse température et à vitesse d'agitation élevée, soit dans un liquide ionique sous chauffage et agitation douce. En cas de dissolution dans les solvants à base de NaOH, la solution de cellulose pouvait être gélifiée à 50 °C pendant des durées variables. Quand la cellulose est dissoute dans les liquides ioniques, il n'y a pas de gélification et la coagulation a été effectuée en versant doucement le non-solvant sur le dessus de la solution de cellulose. La même procédure de coagulation a été appliquée aux solutions et gels à base de cellulose-NaOH-$H_2O$. Après coagulation, si les monolithes de cellulose coagulés n'étaient pas déjà dans l'éthanol, ils étaient transférés dans ce dernier pour le séchage supercritique ou sous vide primaire.

Les techniques utilisées pour mettre en forme les solutions de cellulose ont été décrites. Trois méthodes différentes ont été employées :

- La technique du goutte-à-goutte, qui consiste à faire tomber les solutions de cellulose directement dans un bain de coagulation à l'aide d'une seringue munie d'une aiguille.
- La technologie de JetCutter avec laquelle la solution de cellulose est extrudée sous pression à travers une buse pour produire un jet de solution qui sera coupé par un outil de tranchant (une roue équipée de fils). Les gouttelettes formées tombent dans un bain de coagulation.
- La dernière méthode utilisée était l'émulsification. Cette technique a été adaptée à nos solutions de cellulose en introduisant le concept d'émulsions séparées. Deux émulsions ont été préparées en mélangeant, dans l'une, de l'huile avec une solution de cellulose et, dans l'autre, de l'huile et du non-solvant. Ensuite, les deux émulsions produites ont été mélangées pour provoquer la coagulation de la cellulose.

Enfin, les méthodes de caractérisation des monolithes et des billes d'aérogel et de xérogel a été décrite. La densité a été mesurée de deux façons, soit par mesure du volume et de la masse des échantillons, soit avec l'appareil Geopyc. La surface spécifique a été calculée en utilisant l'approche BET et la morphologie a été observée par microscopie électronique à balayage. D'autres méthodes de caractérisation utilisées ont été décrites telles que le dispositif de rhéo-optique pour observer les gouttelettes sous cisaillement ou le rhéomètre Gemini de Bohlin pour mesurer la viscosité et le comportement des solutions.

## Chapitre 3 - Rhéologie des solutions de cellulose-[DBNH][Pr] et leur préparation sous forme de billes d'aérogels

Dans ce premier chapitre de résultat, nous avons exploité le liquide ionique récemment développé, [DBNH][Pr], pour produire des aérogels sous forme de billes avec la technologie JetCutter.

Dans ce but, nous avons procédé à une étude approfondie des propriétés rhéologiques des solutions de cellulose-[DBNH][Pr]. Nous avons étudié les propriétés d'écoulement et viscoélastiques de ces solutions en fonction de la concentration en polymère et de la température de la solution. Dans la gamme de conditions étudiées, toutes les solutions ont montré un plateau newtonien avec un début d'amincissement par cisaillement pour des concentrations en cellulose plus élevées et des températures plus basses. Les propriétés viscoélastiques des solutions de cellulose-[DBNH][Pr] peuvent être décrites par les approches classiquement utilisées en physique des polymères. La qualité thermodynamique du [DBNH][Pr] était supérieure à celle de l'[Emim][OAc] à la même température, ce qui implique un gonflement accru des pelotes statistiques de polymère et une concentration seuil plus faible. Ces résultats ont permis de sélectionner des viscosités des solutions afin de les faire correspondre à la fenêtre d'utilisation du JetCutter.

Les billes d'aérogel ont été préparées avec succès à partir de solutions de 2% et 3% de cellulose-[DBNH][Pr] en utilisant de l'eau, de l'éthanol ou de l'isopropanol comme bains de coagulation et par séchage sous conditions supercritiques du $CO_2$.Les réglages du JetCutter ont été adaptés en fonction de la concentration des solutions de cellulose et cette dernière était le principal facteur contrôlant la taille des billes. Les billes de la solution à 2% avaient un diamètre compris entre 0,5 et 0,7 mm et celles de la solution à 3% avaient un diamètre moyen d'environ 1,8 mm. Les propriétés des billes étaient similaires à celles de leurs homologues monolithiques, à l'exception des monolithes coagulés dans $H_2O$ qui avaient une morphologie globulaire particulière. D'autres études sont nécessaires pour bien comprendre ce phénomène. La densité des billes était de 0,04 - 0,07 g $cm^{-3}$ et la surface spécifique variait de 240 $m^2$ $g^{-1}$ à 340 $m^2$ $g^{-1}$.

## Chapitre 4 - Production de billes micrométriques d'aérogel de cellulose à partir d'une technique d'émulsion adaptée

Ce chapitre portait également sur la production d'aérogels de cellulose sous forme de billes. Cependant, dans celui-ci, le diamètre des billes visé était de quelques mi-

crons, cette taille ne peut pas être atteinte avec le JetCutter. Ces petites tailles sont particulièrement requises pour des applications médicales, alimentaires ou cosmétiques et l'utilisation de liquides ioniques n'est pas encore recommandée en toute sécurité. C'est pourquoi, dans notre étude, nous avons utilisé des solvants à base de NaOH-eau et avons mis en œuvre une nouvelle technique d'émulsification pour la production de particules d'aérogel de cellulose.

Des études préliminaires ont été menées pour mettre en évidence les différents prérequis pour l'émulsification des solutions de cellulose. Des mesures rhéologiques et des observations rhéo-optiques ont démontré que l'utilisation d'additifs est nécessaire pour dissoudre efficacement la cellulose et retarder la gélification des solutions. Le rapport de viscosité et la tension superficielle étaient prometteurs pour une bonne émulsification des solutions de cellulose dans l'huile de paraffine.

L'élaboration et la mise en œuvre de la méthode d'émulsification ont ensuite été détaillées. Trois problèmes critiques sont apparus lors de la production des particules : la saponification de l'agent tensioactif (due au pH élevé des solutions de cellulose), l'impossibilité d'obtenir des particules "humides" bien formées en ajoutant le non-solvant directement dans l'émulsion et la formation d'un "blocage interfacial" pendant la séparation des phases. Pour surmonter ces problèmes, nous avons développé une nouvelle technique d'émulsification de deux émulsions distinctes.

- Une émulsion contenant la solution de cellulose dans l'huile, sans surfactant pour éviter la saponification.
- Une autre émulsion de non-solvant dans l'huile, avec surfactant pour avoir plus de contrôle sur la taille des gouttelettes.

Ces deux émulsions ont ensuite été mélangées pour provoquer la coagulation des gouttelettes de cellulose en solution. Cette méthode a permis de surmonter les problèmes de saponification et de coagulation directe. En ce qui concerne le "blocage interfacial", deux approches ont été utilisées : ajouter un fluide miscible à la fois avec la phase aqueuse et avec l'huile juste avant la séparation des phases, comme de l'éthanol, et modifier le mécanisme de coagulation en utilisant un non-solvant soluble dans l'huile. Les deux approches ont été couronnées de succès et des résultats particulièrement concluant ont été obtenus avec le changement de mécanisme de coagulation.

Différents paramètres des émulsions ont été modifiés pour déterminer leur influence sur les propriétés des particules d'aérogel. Comme les solutions à base de cellulose-NaOH-$H_2O$ gélifient avec le temps et la température, nous avons essayé d'induire la gélification de la solution de cellulose dans l'émulsion, avant la coagulation. Il est apparu que la gélification de la solution de cellulose n'est pas assez "rapide" et des débris ont été obtenus. D'autres paramètres ont été testés, comme des concentrations différentes en cellulose, et il semble qu'une solution de cellulose plus concentrée entraîne moins de débris et des particules d'aérogel plus faciles à distinguer. La modification du volume d'acide ou du rapport entre la solution de cellulose et la phase huileuse semble modifier

la forme et l'intégrité des particules d'aérogel résultantes, mais ces paramètres ne sont pas aussi influant que l'un des dernier paramètre modifié : le type d'acide utilisé comme non-solvant. En effet le mécanisme de coagulation, par coalescence ou par diffusion du non-solvant, a été évalué comme le plus important pour obtenir des particules d'aérogel de cellulose bien formées. Lorsque seule la coalescence était impliquée, dans le cas de l'acide chlorhydrique (HCl) comme non-solvant, les particules d'aérogel étaient agglomérées avec un diamètre moyen de 5,4 µm et une surface spécifique d'environ 300 $m^2$ $g^{-1}$. Lors de la coagulation par diffusion, dans le cas de l'acide acétique, les particules d'aérogel étaient bien définies et séparées avec un diamètre moyen de 20,9 µm et une $S_{BET}$ d'environ 350 $m^2$ $g^{-1}$. Enfin, l'influence de l'additif a été vérifiée et il est apparu encore plus clairement que le mécanisme de coagulation, tel que décrit juste avant, était le paramètre le plus influant pour obtenir des particules sphériques et bien définies d'aérogel de cellulose.

## Chapitre 5 - Xérogels de cellulose légers et mésoporeux

A partir de ce chapitre, d'autres problématiques ont été traitées, nous avons développé des xérogels cellulosiques ultra-légers et à surface spécifique élevée. Il a été démontré qu'en utilisant des paramètres de préparation adaptés, nous pouvions éviter le séchage supercritique coûteux et obtenir des matériaux aux propriétés équivalentes à celles des aérogels. La densité des xérogels était comprise entre 0,14 g $cm^{-3}$ et 0,24 g $cm^{-3}$ et la surface spécifique variait de 180 $m^2$ $g^{-1}$ à 275 $m^2$ $g^{-1}$.

Une étude complète a été menée afin de trouver les meilleurs paramètres de préparation et de comprendre pourquoi de telles propriétés exceptionnelles ont été obtenues à partir du simple séchage sous vide primaire de la cellulose coagulées. NaOH-eau a été utilisée comme solvant pour la cellulose microcristalline, avec différentes concentrations en additif, ici ZnO. Différents temps de gélification et types de premiers non-solvants ont été étudiés ainsi que leur influence sur la cristallinité de la cellulose et sur la composition des xérogels obtenus. Plusieurs choses ont tout d'abord été mise en évidence. Les xérogels ultra-légers et à surface spécifique élevée ne sont obtenus que lorsque l'éthanol était utilisé comme premier non-solvant pour la coagulation. Il a été confirmé lors de la préparation des homologues aérogels que ce résultat était spécifique aux xérogels et que les différences dans les propriétés des aérogels coagulés par différents non-solvants n'étaient pas si importantes. L'influence de la concentration de ZnO a ensuite été étudiée. La propriété qui variait le plus en changeant la concentration de ZnO était la surface spécifique : elle décrivait une courbe en U avec l'augmentation de la concentration en ZnO. Cette tendance a également été observée pour les aérogels. De plus, lorsque la concentration de ZnO était égale ou supérieure à 0,5%, des cristaux de Zn pouvaient

être observés au MEB dans la structure des xérogels et aérogels. L'analyse élémentaire a révélé que, ni le Na, ni le Zn n'étaient complètement lavés lors de la coagulation dans l'EtOH, alors qu'ils le sont lors de la coagulation dans le HCl. L'influence du temps gélification et du type de solvant ont également été vérifiés. Le temps de gélification n'a pas eu d'influence significative sur les propriétés des xérogels résultants alors que le type de solvant était critique. Lorsque le liquide ionique était utilisé comme solvant, les xérogels étaient denses, avec une surface spécifique extrêmement faible. Enfin, la cristallinité et l'indice cristallin ont été évalués et les xérogels et aérogels coagulés avec de l'EtOH ont montré une très faible cristallinité par rapport à ceux coagulés avec l'HCl ou l'$H_2O$.

L'ensemble de ces résultats obtenus précédement ont ensuite été analysés en détail. Nous avons formulé des hypothèses pour expliquer pourquoi ces xérogels ont des propriétés exceptionnelles. Nous avons observé que lorsque les solutions de cellulose-NaOH-ZnO-$H_2O$ étaient coagulées et lavées dans l'EtOH, Na et Zn restaient dans leur structure. Notre première suggestion est que les métaux agissent comme "écarteur" entre les chaînes de cellulose empêchant les chaînes de se réarranger pendant la coagulation. Cela expliquerait pourquoi l'indice de cristallinité des aérogels et xérogels coagulés dans l'EtOH est si bas et également pourquoi le réseau ne s'effondre pas pendant le séchage sous vide. Notre deuxième hypothèse est basée sur les travaux de Gunnarsson et al. (2017) qui suggère que des ponts carbonatés se forment entre les chaînes de cellulose lorsque la dissolution est réalisée dans le solvant NaOH-$H_2O$. Lorsque la coagulation est réalisée dans l'EtOH, ces ponts ne sont pas démantelés et empêchent le réseau de cellulose de s'effondrer pendant le séchage sous vide. La question reste ouverte concernant l'influence de la concentration en ZnO sur la $S_{BET}$. Nous avons suggéré que lors de l'ajout de ZnO à la solution cellulose-NaOH-$H_2O$, ZnO joue le rôle d'"écarteur" et la $S_{BET}$ diminue probablement en raison de la formation des macropores. Ensuite, lorsque la limite de solubilité du ZnO est dépassée, les cristaux en "oursin" formés contribuent à la $S_{BET}$ ce qui entraîne une augmentation de cette dernière.

Enfin, nous avons prouvé que la production de billes de xérogel poreuses à haute $S_{BET}$ est possible en utilisant la technique du goutte-à-goutte. Les propriétés des billes sont très similaires à celles des xérogels et aérogels monolithiques. Seul la $S_{BET}$ était plus élevée pour les billes d'aérogel que pour les monolithes, avec les mêmes conditions de préparation.

# Chapitre 6 - Aérogels à base de pâte à papier

Le dernier chapitre de résultats était consacré à la préparation et à la caractérisation d'aérogels préparés à partir de pâtes à papier ayant différentes caractéristiques. Les aérogels de pâtes à papier ont été préparés par dissolution dans des solvants à base de NaOH-ZnO-$H_2O$, gélification, coagulation dans différents non-solvants et séchage dans les conditions supercritique du $CO_2$.

L'efficacité de dissolution du solvant a été évaluée par des observations au microscope optique et la détermination de la fraction non-dissout. La dissolution la plus efficace a été obtenue pour les pâtes à papier à faible degré de polymérisation et faible teneur en lignine. Toutes les pâtes ont été utilisées pour produire des aérogels, quelle que soit leur efficacité de dissolution.

L'influence du temps de gélification, du type de non-solvant et de la composition de la pâtes à papier a été évaluée sur les propriétés des aérogels obtenues. Le type de non-solvant semble être le paramètre qui a le plus d'influence. Tout comme nous l'avions observé pour les xérogels dans le chapitre précédent, les métaux ne sont pas complètement lavés lorsque l'EtOH ou l'eau sont utilisés comme non-solvant alors qu'ils le sont avec HCl ce qui influence la cristallinité de la cellulose, la surface spécifique et la densité des aéogels obtenus. Les aérogels de pâtes à papier coagulés dans l'éthanol montre une densité plus élevée, une $S_{BET}$ plus faible et une cristallinité plus faible que les aérogels coagulés dans l'eau ou dans HCl. L'influence de la composition de la pâtes à papier n'était pas aussi importante que le type de non-solvants, mais des différences ont pu être observées en fonction du degré de polymérisation de la cellulose et de la teneur en hémicellulose. La densité des aérogels augmentait avec l'augmentation du DP de la cellulose et la $S_{BET}$ diminuait légèrement avec l'augmentation de la teneur en hémicellulose. Pour confirmer et comprendre cette dernière tendance, des aérogels d'hémicellulose et des aérogels d'hybrides cellulose-hémicellulose ont été préparés à partir de dissolution dans le [DBNH][Pr] et coagulation dans l'EtOH. Les aérogels d'hémicellulose pure n'ont pu être préparés qu'à partir d'une concentration élevée (30 %) et ont montré une $S_{BET}$ très faible. Les hybrides ont montré une $S_{BET}$ un peu plus basse que celles des aérogels de cellulose pure provenant des mêmes conditions de préparation.

Enfin, après sélection des pâtes à papier appropriées, des billes d'aérogel ont été préparées avec la technologie JetCutter. Le diamètre des billes était de plusieurs centaines de micromètres et leur surface spécifique variant de 300 $m^2\ g^{-1}$ et 350 $m^2\ g^{-1}$, elle était semblable à celle obtenue pour les monolithes. Des xérogels de pâtes à papier ultra-légers ont également été préparés avec succès et la capacité de sorption de l'humidité des xérogels et des aérogels a été testée sur plusieurs cycles. Une augmentation maximale de la masse égale à 18,5 % a été noté dans le meilleur des cas.

# Conclusions et perspectives

Dans l'ensemble, nous avons démontré dans ce travail que par une sélection minutieuse des propriétés de la solution et des paramètres de production, il est possible de produire des billes d'aérogel de cellulose de différentes tailles et, en outre, d'éviter le séchage supercritique au $CO_2$ coûteux. La technologie JetCutter permet d'obtenir des diamètres de centaines de micromètres, alors que l'émulsification produit des particules de seulement quelques microns de diamètre. Ces deux techniques sont potentiellement industrialisables, ce qui apporte beaucoup de valeur et de polyvalence à ces aérogels. La production de xérogels poreux et à haute surface spécifique est d'un grand intérêt économique car les matériaux à haute valeur ajoutée peuvent être produits à moindre coût. Cette valeur ajoutée est également valable pour les aérogels de pâtes à papier, les xérogels de pâtes à papier et les billes d'aérogel de pâtes à papier.

Beaucoup de perspectives et de travaux futurs peuvent être tirés de cette étude. La plus évidente est la production, à l'échelle industrielle, de billes d'aérogel de différentes tailles pour des applications ciblées. Il a été démontré que les solvants à base de [DBNH][Pr] et de NaOH ainsi que la cellulose microcristalline et les pâtes à papier peuvent être utilisés avec la technologie JetCutter. Par conséquent, les travaux ultérieurs portent sur la compréhension et la maîtrise complètes de cette technologie en vue de produire tous les types de billes d'aérogel cellulosiques à partir d'une large gamme de solvants ou d'autres polysaccharidiques. Des possibilités infinies d'applications pourraient ainsi pu être atteintes, du secteur médical à celui de la construction. Les travaux sur l'émulsification ont prouvé qu'une méthode pouvait être appliquée aux solutions à base de cellulose et de NaOH pour la production de microsphères. Maintenant que cette technique est développée, la variation des paramètres d'émulsification pour ajuster et contrôler la taille des particules d'aérogel pourrait conduire à des particules encore plus petites. Les essais de biocompatibilité doivent être réalisés en vue de leur commercialisation et de leur utilisation dans des applications médicales, alimentaires ou cosmétiques.

La littérature rapporte que certaines particules de bio-aérogel, à base de polysaccharides "faciles à gélifier" comme l'amidon ou la pectine, peuvent être utilisées comme supports pour des applications de libération contrôlée de différents médicaments. Les principales conclusions sont que la libération d'un médicament dépend du type de polysaccharide et des propriétés de l'aérogel utilisé. Les propriétés de libération dépendent également du type de médicament. Un seul article de Voon et al. (2017) fait état d'une libération contrôlée par des billes d'aérogel de cellulose. Les propriétés des billes d'aérogel et de xérogel de cellulose peuvent être adaptées et être différentes des autres bio-aérogels car, par exemple, la cellulose n'est pas hydrosoluble. Des aérogels et xérogels hybrides et composites cellulose-organique et cellulose-inorganique peuvent être développés comme supports pour la libération de composés actifs. Cela ouvre une

grande variété d'applications différentes.

De nombreuses perspectives impliquent la production de xérogels poreux. Dans l'état actuel, leur exploitation pourrait être restreinte en raison de leur composition : ils contiennent encore du Na et du Zn. Il est à noter que le Zn est un agent antibactérien et que les xérogels de cellulose peuvent donc avoir des propriétés antibactériennes "naturelles". Les applications impliquant ces métaux peuvent être facilement trouvées en catalyse ou en électrochimie après pyrolyse. De plus, des xérogels à faible densité ont été préparés à partir de pâtes à papier. L'étape suivante consiste à bien comprendre (et confirmer nos hypothèses ou trouver les raisons) pourquoi une surface spécifique élevée et des matériaux légers sont obtenus à partir d'un simple séchage sous vide. Les résultats obtenus pour la cellulose pourraient alors être appliqués à d'autres solvants cellulosiques ou à d'autres bio-polymères.

Enfin, l'utilisation de pâtes à papier, au lieu de cellulose microcristalline purifiée, réduit le coût de production des aérogels. Il a été prouvé que différents types de matériaux, aérogels et xérogels de toute forme, de faible densité et de grande surface spécifique, pouvaient être produits à partir de solutions de pâte à papier-NaOH-ZnO-$H_2O$. Il pourrait donc être très intéressant d'utiliser de moins en moins de traitements du bois, et de comprendre l'évolution correspondante des propriétés des aérogels et des xérogels de "cellulose".

# Articles and communications from this work

In the frame of this work on cellulose aerogels, one article was published in an international peer-reviewed scientific journal, one patent is under submission and four oral communications were given at national and international conferences.

## Article

Druel, L., P. Niemeyer, B. Milow, and T. Budtova

2018. Rheology of cellulose-[DBNH][$CO_2$Et] solutions and shaping into aerogel beads. *Green Chemistry*, 20(17):3993–4002.

## Oral communications

Druel, L., P. Niemeyer, B. Milow, and T. Budtova

Cellulose-[DBNH][$CO_2$Et] rheological properties and aerogel beads made with Jet-Cutting technique. *$5^{th}$ EPNOE International Polysaccharide Conference "Polysaccharides and polysaccharide-based materials: from science to industrial application"*. Jena (Germany). August 20-24, 2017.

Druel, L., A. Kenkel, P. Niemeyer, V. Baudron, B. Milow and T. Budtova

Cellulose aerogels shaping and properties for tailored applications. *$4^{th}$ International Seminar on Aerogels "Properties - Manufacturing - Applications"*. Hamburg (Germany). September 24-26, 2018.

Druel, L. and T. Budtova

Cellulose aerogels: tuning structure and properties. *$4^{th}$ International Conference on Bioinspired and Biobased Chemistry and Materials "Nature Inspires, Creativity Engineers"*. Nice (France). October 14-17, 2018.

Druel, L., P. Niemeyer, B. Milow, and T. Budtova

Rheology of cellulose/1,5-diazabicyclo[4.3.0]non-5-enium propionate solutions and shaping into aerogel beads. *Open seminar of GDR "Liquides Ioniques et Polymeres"*. Lyon (France). October 15-16, 2018.

# Articles and communications outside the topic of the thesis

Formerly to this work, studies on starch aerogels were performed and also resulted in several communications. One article was published in an international peer-reviewed scientific journal, three oral communications were given and two poster presentation were held at internation conferences.

## Article

Druel, L., R. Bardl, W. Vorwerg, and T. Budtova

2017. Starch Aerogels: A Member of the Family of Thermal Superinsulating Materials. *Biomacromolecules*, 18(12):4232–4239.

## Oral communications

Druel, L., R. Bardl, W. Vorwerg, and T. Budtova

Starch aerogels. *Biopolymers 2015*. Nantes (France). December 14-16, 2015.

Druel, L., R. Bardl, W. Vorwerg, and T. Budtova

Starch aerogels – a new member of the family of thermal super-insulating materials. *$5^{th}$ EPNOE International Polysaccharide Conference "Polysaccharides and polysaccharide-based materials: from science to industrial application"*. Jena (Germany). August 20-24, 2017.

Groult, S., L. Druel, C. Rudaz, R. Bardl and T. Budtova

Thermal conductivity of bio-aerogels. *$4^{th}$ International Seminar on Aerogels "Properties - Manufacturing - Applications"*. Hamburg (Germany). September 24-26, 2018.

# Posters

Druel, L., R. Bardl, W. Vorwerg, and T. Budtova

Starch aerogels. *3rd International Seminar on Aerogels "Synthesis - Properties - Applications"*. Sophia-Antipolis (France). September 22-23, 2016.

Druel, L., R. Bardl, W. Vorwerg, and T. Budtova

Starch Aerogels. *2nd International EPNOE Junior Scientists meeting "Future perspectives in polysaccharide research"*. Sophia-Antipolis (France). October 13-14, 2016.

# List of Figures

# List of Tables

# Chapter 1

# State of the art

## Contents

# Abstract

This first chapter gives a large overview on the topics broached in this manuscript. It regroups the state of the art on polysaccharides, more particularly cellulose and its dissolution, bio-aerogels and their shaping as beads.

First, the focus is set on pulp and its main component cellulose. Details are then given on cellulose structure, chains' interaction and conformations.

The second part tackles cellulose dissolution. Cellulose is used in multiple applications but it appears that its dissolution is not easy. Indeed, common solvents for polysaccharides, such as water, are not able to dissolve cellulose, it only swells it. Multiple other solvents are capable to dissolve cellulose at different concentrations and are more or less efficient. Here, attention is given to NaOH based solvents and ionic liquids since they have been used in the frame of this work. These two solvents have very different types of interaction and efficiency toward cellulose dissolution. In addition, the ways to shape cellulose solutions are discussed with more focus on making beads.

Finally in the third and last part, porous materials and more especially aerogels are investigated. Different types of drying are detailed and aerogels are here treated as a porous material obtained from the supercritical drying. Information on aerogels from different polysaccharides is provided with special attention given to cellulose aerogels. A review of the existing methods to produce polysaccharide and cellulose aerogel beads is supplied.

# Résumé

Ce premier chapitre donne un large aperçu des sujets abordés dans ce manuscrit. Il regroupe l'état de l'art sur les polysaccharides et plus particulièrement sur la cellulose et sa dissolution, sur les bio-aérogels et leur production sous forme de billes.

Tout d'abord, l'accent est mis sur la pâte à papier et son principal composant, la cellulose. Des détails sont ensuite donnés sur la structure de la cellulose, les interactions des chaînes et leurs conformations.

La deuxième partie traite de la dissolution de la cellulose. La cellulose est utilisée dans de multiples applications mais sa dissolution n'est pas simple. En effet, les solvants couramment utilisés pour les polysaccharides, comme l'eau, ne sont pas capables de dissoudre la cellulose, ils ne font que la gonfler. Plusieurs autres solvants sont capables de dissoudre la cellulose à différentes concentrations et sont plus ou moins efficaces. Les solvants à base de NaOH et les liquides ioniques font ici l'objet d'une attention particulière puisqu'ils ont été utilisés dans le cadre de ce travail. Ces deux solvants ont des types d'interaction et d'efficacité très différents pour la dissolution de la cellulose. Les façons de mettre en forme les solutions de cellulose sont discutées en mettant davantage l'accent sur la fabrication de billes.

Enfin, dans la troisième et dernière partie, les matériaux poreux et plus particulièrement les aérogels sont étudiés. Différents types de séchage sont détaillés et les aérogels sont ici traités comme des matériaux poreux obtenus à partir du séchage supercritique. Des informations sur les aérogels provenant de différents polysaccharides sont fournies, une attention particulière étant accordée aux aérogels de cellulose. Une revue des méthodes existantes pour produire des billes de polysaccharide et d'aérogel de cellulose est fournie.

# 1.1 Background on cellulose

## 1.1.1 Polysaccharides

Polysaccharides are the most abundant resource on earth as they are natural polymers produced by living species (trees, plants, bacteria, insects...). Also sometimes called biopolymers, they are made of monosaccharides: repetitive units of sugars, linked together by glycosidic bonds. The general formula of polysaccharides is $[C_x(H_2O)_y]_n$ where $n$ is the degree of polymerisation (DP). The repetitive unit can be the same, in the case of homopolysaccharides, such as cellulose, or can change in the case of heteropolysaccharide, such as hemicellulose. The different units and the various linkages between these monosaccharides lead to a wide range of structures and properties (Dumitriu (2004)).

In the frame of this work, the focus will be set on cellulose, one of the main component of wood.

## 1.1.2 Wood and pulp

### Wood

The term "wood" refers to the secondary xylem: the tissue responsible for, among other, water transportation, mechanical support and physiological roles in cell walls of vascular plants. This tissue is present in both types of plants: the angiosperms and the gymnosperms, in which it is named as hardwood and softwood, respectively. Other plants can also produce this secondary xylem such as vines and shrubs (Hon and Shiraishi (2000)).

Hence, wood is a natural organic composite found in most of the "woody plants" such as trees or shrubs and it is composed of:

- Cellulose, the main component, which plays the role of structural polysaccharide. It represents 40% to 50% of wood (Hon and Shiraishi (2000)) and will be described in more details in the following section.

- Lignin can be considered as the cement of wood as it is the encrusting component of cell walls. It brings rigidity, resistance to decomposition, hydrophobicity and gives the brown colour. Lignin is an amorphous cross-linked phenolic polymer which represents from 18% to 35% of wood (Melro et al. (2018)).

- Hemicelluloses, which play various roles such as linking cellulose and lignin in cell walls, are the last main components of wood, representing 20% to 38% of the latter. They are short polysaccharides, classified in four types, each polysaccharide having a different structure: xylans, mannans, xyloglucans and $\beta$-glucans with mixed linkages (Ebringerová et al. (2005)).

- And other extractives such as resins, protein or other polysaccharides, which represent less than 4% of wood content.

Composition of wood varies as a function of source (hardwood or softwood) and geographical region.

### Pulp

The industry devoted to wood processing is called the pulping industry as it leads to the production of pulp, paper, board, and other cellulosic products. The main goal is to separate and extract cellulose for further use; however, in our days "biorefinery concept" started to be applied with all components of wood considered as useful compounds. The treatment of wood starts with a mechanical pretreatment to get chips (small pieces of wood) and is then followed by several chemical and/or mechanical treatments to separate cellulose fibres and to purify it from other components of wood (lignin, hemicellulose and other extractives). The obtained product is called pulp. The treatment is adapted depending on the final composition desired and application of the pulp. Several types of pulps exist and they are sorted as a function of the treatment they received:

- Mechanical pulping consists on disintegrating wood into fibres only by mechanical processing (grinding or refining). This treatment leads to fibres of different sizes from particles to whole or bundle fibres and it has the peculiarity to retain all the wood components. This kind of pulp is typically used for newsprint as it is not bright (due to retained lignin).

- Chemomechanical pulping consists on adding a "chemical" treatment to the mechanical pulping. This leads to a slightly lower pulp yield (lower amount of other components than cellulose in the pulp) inducing a brighter pulp with better mechanical properties.

- Chemical pulping, as its name indicates, uses chemical compounds to separate cellulose fibres. The separation is done by dissolving lignin and part of hemicelluloses under acidic or alkaline conditions. Several types of chemical processes exist. Among them, the kraft pulping is the most used one. Kraft pulping consists on "cooking" the wood chips for 1 to 2 h in a digester with an alkaline, aqueous (aq) mixture of sodium hydroxide (NaOH) and sodium sulphide ($Na_2S$) at temperatures varying from 140 °C to 170 °C, depending on the wood species treated. The kraft pulping leads to brownish pulps with high strength fibres. Another process is the sulphite pulping which is carried in an acidic mixture. This process takes longer than the kraft pulping (6 to 9 h) and is carried out at slightly lower temperatures (120 °C to 150°C) with sulphur dioxide ($SO_2$) and an ion (either calcium ($Ca^{2+}$), sodium ($Na^+$), or magnesium ($Mg^{2+}$)). Sulphite pulping gives brighter pulps but results in weaker fibres.

The last and optional step of the pulps' treatment is bleaching. The beaching is used to get even brighter (white) pulps. It is done with several steps of acidic oxidation and removal of the oxidized lignin.

Pulps, and especially chemical pulps, can also be classified by their quality using the kappa number. This number is obtained by measuring the amount of residual lignin (for a given amount of pulp) in the pulps. The residual lignin is determined by measuring the consumption of potassium permanganate ($KMnO_4$) by the pulp. Higher is the kappa number, the more residual lignin there is in the pulp and lesser is the "pulps' quality" (Hon and Shiraishi (2000)).

### 1.1.3 Cellulose

As one of the main components of wood, cellulose is the most abundant polymer on earth. But woody plants are not the only source of cellulose. The latter can also be found in algae, in cotton (pure cellulose), and it can be produced by bacteria (such as Acetobacter xylinum) resulting in bacterial cellulose. The production of cellulose was estimated around 1.5 $10^{12}$ tons in 2005 (Klemm et al. (2005)). As a comparison, the world production of synthetic plastics was around 3.5 $10^{8}$ in 2017 (PlasticsEurope (2019)-https://www.plasticseurope.org/en).

Cellulose is a linear syndiotactic polysaccharide constituted of repetitive units of D-anhydroglucopyranose linked together through $\beta$-1,4-glycosidic bonds. We can also consider the cellulose as an isotactic polymer if we take the cellobiose as repetitive unit (two D-anhydroglucopyranose unit (AGU)). Indeed, throughout cellulose chain the AGU are rotated by 180 ° each with respect to the other (see Figure 1.1) (Klemm et al. (1998)). The degree of polymerisation of cellulose mainly depends on its source and is decreased during the treatments (such as the pulping).

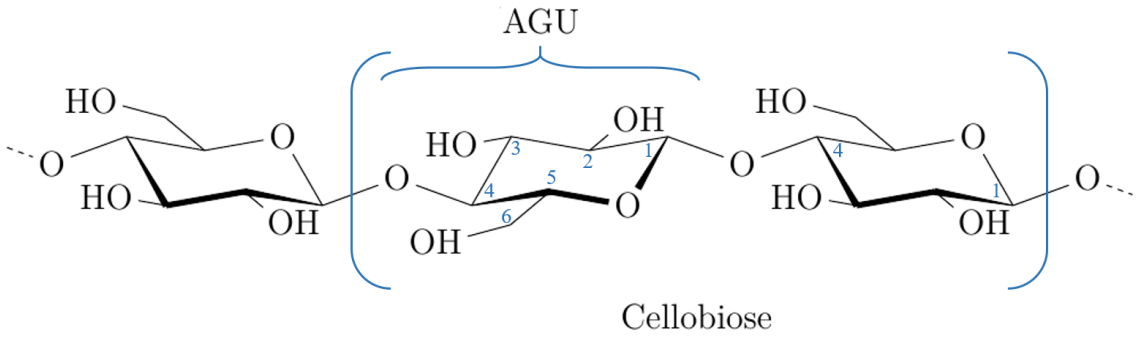


Figure 1.1 – Schematic representation of cellulose chain with three AGU and one cellobiose represented. The numbers stand for the carbon numbers.

Cellulose's hydroxyl groups (-OH) as well as the primary alcohol $CH_2$-OH group are located in the equatorial plane of the glucopyranose rings, while the hydrogens (H) are in the axial plane. These orientations of the groups and atoms allow cellulose chains

to form sheets through intra- and intermolecular hydrophilic bonds: hydrogen bonds. Hydrophobic bonds and Van der Waals forces are linking the sheets together through stacking. This stacking makes cellulose a semi-crystalline polysaccharide composed of amorphous and crystalline regions.

Cellulose has four main allomorphs, namely cellulose I, II, III and IV. Cellulose I is the native cellulose, found in nature, and the other allomorphs are obtained after different treatments of cellulose I.

Cellulose I is metastable and has two different crystalline forms: $I_\alpha$ (triclinic) and $I_\beta$ (monoclinic) which are found alongside but in different ratios depending on the source of the cellulose (see Figure 1.2). Within these two crystalline forms, cellulose has the same backbone, only the hydrogen bonding is different. It was proven by NMR analysis that cellulose from woody plants shows a higher ratio of $I_\beta$ (Atalla and VanderHart (1999)) while cellulose produced by bacteria (bacterial cellulose) results in a high ratio of cellulose $I_\alpha$ (Liebner et al. (2016)).

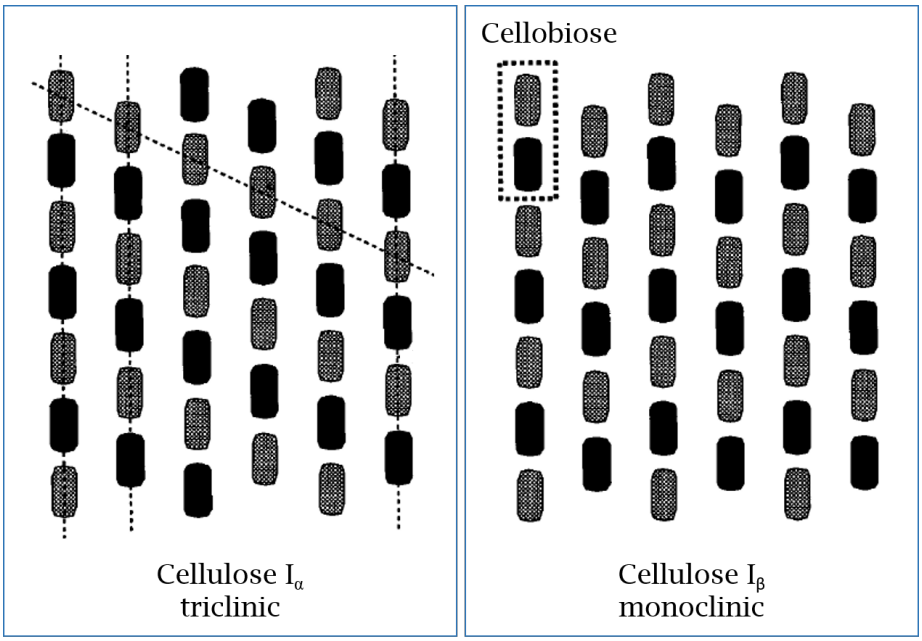


Figure 1.2 – Schematic representation of the $I_\alpha$ (triclinic) and $I_\beta$ (monoclinic) form of cellulose I. Each rectangle represent an AGU. Adapted from Baker et al. (1997).

Cellulose II is obtained after mercerization (treatment with aqueous NaOH) or dissolution and regeneration or coagulation (or precipitation) of the cellulose I. Cellulose II is most stable allomorph with antiparallel organisation of the chains in the sheets, in the a-b plane, in opposition with the parallel organisation of the chains of cellulose I (see Figure 1.3). The $CH_2$-OH group in the backbone has also a different orientation as compared with cellulose I, indeed it goes from a *trans-gauche* position (in cellulose I) to a *gauche-trans* (in cellulose II) with regards to the C5-O5 and C5-C4 bonds, respectively (see, Figure 1.4) (Klemm et al. (1998)). These changes allow hydrogen bondings between the molecular sheets, and not only within the sheet, inducing the

greater stability of this allomorph. One intramolecular hydrogen bonds (within the chain) is present between the O5 atom and the -OH group of C3 and one intermolecular bonds (within the sheet) is present between O6 and -OH of C2 (see Figure 1.3). In addition, a hydrogen bond is formed between the sheets between -OH of C2 and O2 in another sheet (Klemm et al. (1998)).

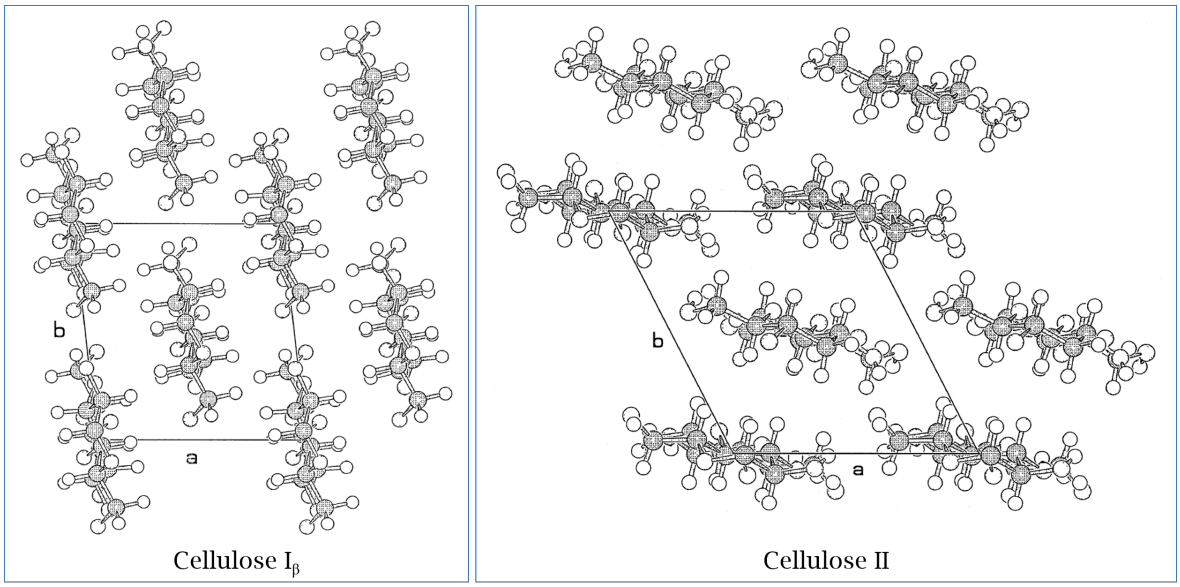


Figure 1.3 – Schematic representation of the cellulose $I_\beta$ and cellulose II in the a-b plan. The sheets and thus cellulose chains are travelling in the c direction. Adapted from Zugenmaier (2001).

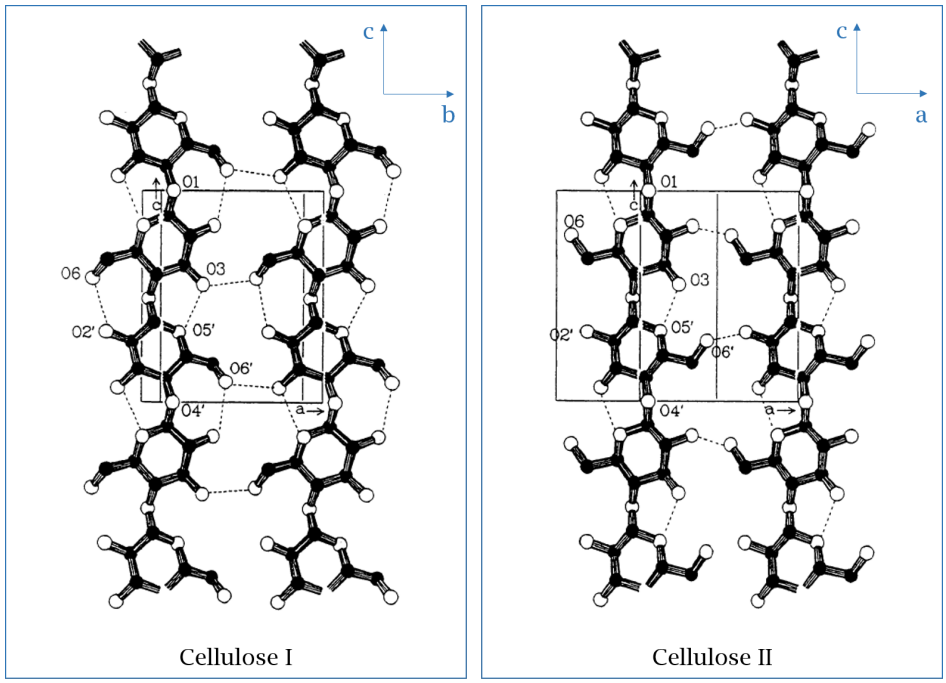


Figure 1.4 – Schematic representation of the cellulose $I_\beta$ and cellulose II in sheets view. Dashed lines represent intra- and intermolecular hydrogen bonds. The coordinate systems are adapted to correspond to Figure 1.3. Adapted from Kroon-Batenburg et al. (1986).

Cellulose III can be obtained from cellulose I (leading to cellulose $III_I$) or cellulose II (leading to cellulose $III_{II}$) by treatment in liquid ammonia (Sarko et al. (1976)). This reaction is reversible.

Cellulose $IV_I$ and $IV_{II}$ can be obtained by treatment in glycerol of cellulose $III_I$ and $III_{II}$, respectively (Gardiner and Sarko (1985)). It was recently demonstrated that *cellulose $IV_I$ is simply cellulose I fragmented into nanocrystals with relatively small cross-sectional dimensions.* (Wada et al. (2004); Newman (2008)).

## 1.2 Cellulose dissolution and solution shaping

Due to its abundance, natural source and properties, cellulose is a key raw material for use in multiple technological fields. However, processing cellulose is not easy. Indeed, cellulose degrades before melting. Its processing and shaping hence follow several "mandatory" steps and the first one is dissolution. We do not consider here cellulose derivatisation which allows obtaining thermoplastic polymers but which is out of the scope of this work. Dissolution of cellulose and the solvents of interest in this work will be presented in the first part of this section. We will consider dissolution only in non-derivatising (direct) solvents. The second step is the shaping of cellulose solutions, it will be detailed in the second part of this section. Afterwards, further processing steps are sometimes needed to obtain the desired final material. Some additional steps will be discussed in the last section of this chapter and more specially the steps needed to obtain porous materials. The Figure 1.5 roughly summarises the main steps of cellulose processing that will be discussed in this section.

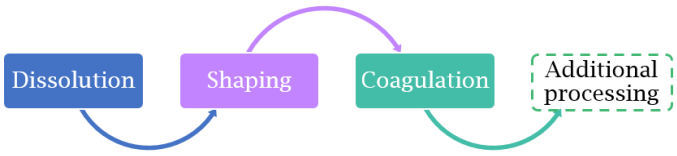


Figure 1.5 – Scheme representing the main steps of cellulose processing excluding viscose and carbamate process.

### 1.2.1 Cellulose and pulp dissolution

We have seen in the previous section that cellulose has intra- and intermolecular hydrophilic bonds (see Figure 1.4) as well as hydrophobic bonds (Van der Waals interaction) between its chains (see Figure 1.6). These two types of bonds give cellulose an amphiphilic nature but also render its dissolution in water and other common solvents impossible (Lindman et al. (2010); Medronho (2015)).

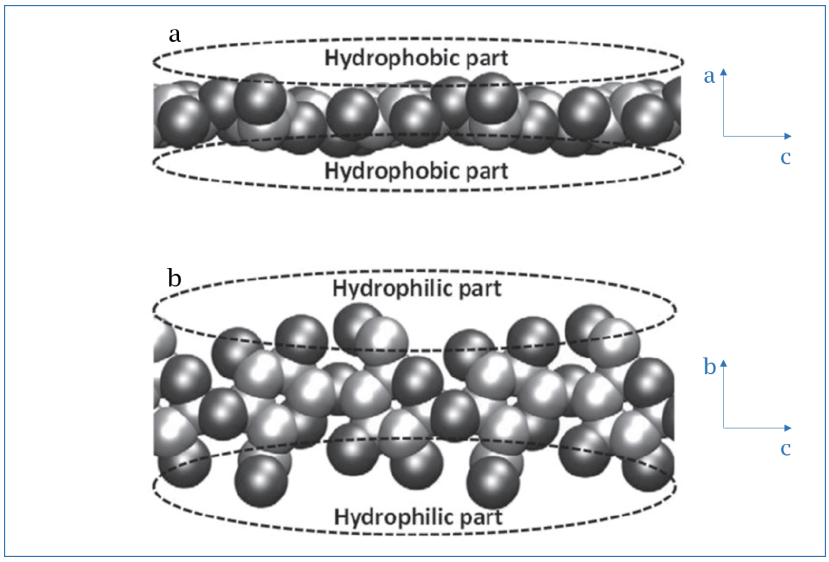


Figure 1.6 – Schematic representation of the cellulose hydrophilic and hydrophobic parts. a: a representation of the cellulose chain seen from the side and b: seen from above. Oxygen atoms are coloured in dark grey and carbon atoms light grey. The hydrophobic and hydrophilic areas are highlighted by the dashed ellipses. The coordinate systems are adapted to correspond to Figure 1.3. Adapted from Medronho and Lindman (2014).

A solvent for cellulose will thus have to efficiently disturb hydrophobic and hydrophilic interactions between cellulose chains. Several types of solvents are known for cellulose. They can be classified in two main categories: indirect (or derivatising) solvents and direct (or non-derivatising) solvents (Klemm et al. (1998, 2005)).

- As their name indicates, indirect solvents are derivatising cellulose prior dissolution. The cellulose derivative is subsequently dissolved in a solvent and then needs to be regenerated to recover pure cellulose.

One of the oldest and commonly used indirect solvent is the viscose process. During this process, cellulose is derivatised with carbon disulphide ($CS_2$) to get cellulose xanthate. This cellulose derivative is then dissolved in NaOH(aq) leading to the viscose solution. Finally, after shaping, cellulose is regenerated in an acid bath, usually based on sulphuric acid.

- On the contrary, direct solvents dissolve cellulose without pre-treatment, by disturbing the hydrogen and hydrophobic bonds.

The Lyocell process is an example of commercialised direct solvent. In this process, N-methylmorpholine N-oxide (NMMO) monohydrate is used as a direct solvent and its polar and non-polar parts efficiently disturb both hydrophilic and hydrophobic interactions of cellulose's chains.
Other direct solvents are heavy metals salts such as cupriethylenediamine (CED) which is used, for instance, as a standard solvent for DP measurement of pulps. These solvents form complexes with cellulose's hydroxyl groups.

Direct solvent are usually more desirable due to their "one-step" and "simple" cellulose dissolution process. Among the direct solvents, NaOH based solutions and ionic liquids (ILs) are of interest in this work and will be described in more details.

### NaOH based solvents

One of the first use of alkaline aqueous solution to process cellulose was for the mercerisation process, which was named and patented by its inventor John Mercer in 1850 (Mercer (1850)). This process consists on treating the native cellulose fibres with concentrated NaOH(aq) at ambient temperature. This treatment leads to improved cellulose fibres' properties, such as better smoothness and mechanical properties. During this process, cellulose swells and its crystalline structure changes from native cellulose I allomorph to cellulose II. This transformation happens through formation of Na-cellulose complexes (Okano and Sarko (1985)). This process is still not entirely understood but is supposed to be a solid-solid phase transition (Budtova and Navard (2016)). Cellulose is not dissolved during mercerisation.

The first time NaOH(aq) was reported to be a solvent for cellulose was by Davidson (1934) who successfully dissolved up to 82.6% "hydrocellulose" (today known as Microcrystalline Cellulose (MCC)) in 2.5 M NaOH at - 5 °C. He also proved that cellulose solubility decreases with increasing chains' length and increasing crystallinity. More investigations were done by Sobue et al. (1939) who established cellulose-NaOH-$H_2O$ phase diagram (Figure 1.7). It can be seen from this diagram that the solubility range of cellulose, referred as *"Na-Cell Q"*, is very small and is comprised between 7% and 10% of NaOH in water at temperature from - 10 °C to 1 °C. The diagram also presents the other forms of alkali-cellulose named *"Na-Cell"* from I to V. Mercerisation is one of the options of cellulose complexes with Na.

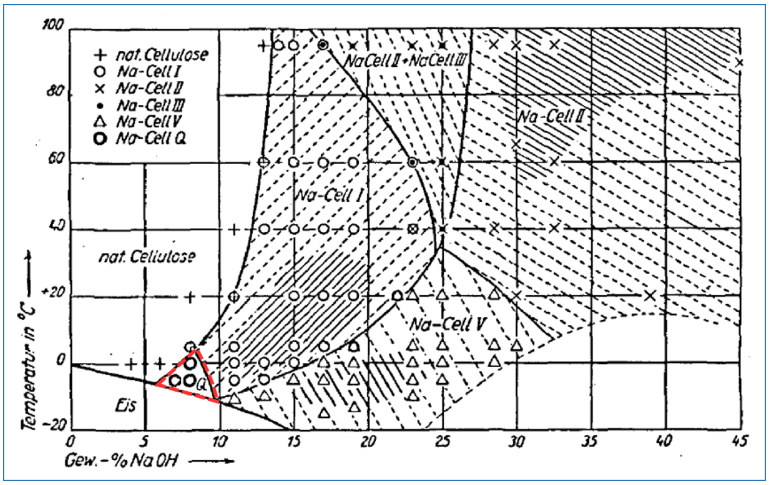


Figure 1.7 – Cellulose-NaOH-$H_2O$ phase diagram. Adapted from Sobue et al. (1939).

The discovery of this solvent (cheap, environmentally friendly, easy to handle) of cellulose attracted a lot of attention in the scientific community. Many researchers

tried to understand the dissolution mechanism and why these particular conditions are needed. This research is still ongoing today.

Several approaches exist. Among them, the Japanese team of Kamide et al. (1984) and Yamashiki et al. (1988) were the first to suggest that for cellulose to be dissolved, hydrogen bonds and more particularly intramolecular bond between the O5 and the hydroxyl group of C3 needed to be weakened. They also stated that the crystallinity of cellulose was not the most influencing parameter on cellulose dissolution efficiency. Later on, they confirmed their hypothesis by efficiently dissolving steam exploded cellulose (cellulose pressurised with steam followed by brutal decompression), even though the crystallinity of the latter is higher, by proving the weakening of hydrogen bonds between O5 and the -OH of C3 but also between O6 and the -OH of C2 (Takahashi et al. (1991); Kamide et al. (1992)).

Later Roy et al. (2001) and Egal et al. (2007) found, with differential scanning calorimetry measurements, the solubility limit of cellulose: they showed that 4 NaOH molecules are required to solvate 1 AGU. This roughly corresponds to 7% to 8% of cellulose in 7% to 8% of NaOH(aq).

More recently, Lindman et al. (2010) made a point on re-evaluating the importance of the influence of the amphiphilic nature of cellulose on dissolution. They stated that it is not cellulose's hydrogen bonds that prevent cellulose dissolution in water. They reminded that more attention is needed to pay on the hydrophobic part of cellulose to find an efficient solvent. To explain the need of low temperature to dissolve cellulose in NaOH(aq), they suggested that this is because of a temperature induced change in cellulose conformation. The segment O-CH2-CH2-O can change its conformation around the C-C bond to a more polar state at low temperature, hence favouring cellulose dissolution (Medronho et al. (2012)). Finally, they reported the work of several researchers, proving the deprotonation of cellulose during dissolution in high pH, which could help to better understand cellulose dissolution mechanism (Lindman et al. (2017)). Hence, a lot of theories exist on cellulose dissolution mechanism in NaOH(aq), sometimes contradictory.

One of the drawbacks of dissolving cellulose in NaOH-$H_2O$ is solution gelation with time and temperature. This phenomenon was widely studied with rheological and X-ray measurements (Roy et al. (2003); Egal (2006); Budtova and Navard (2016); Pereira et al. (2018)). Gelation is a "transformation" of a solution into a more or less elastic "solid". This phenomenon can be observed through the increase of cellulose solution's elastic modulus, accompanied by viscosity increase, and also with the increase of its turbidity, the latter being a sign of microphase separation. Gelation kinetic depends on temperature and cellulose concentration; it is faster at higher temperature and higher cellulose concentration. The gelation mechanism was suggested to be a slow "aggregation" of the cellulose chains into small crystallites of cellulose II (Pereira et al. (2018)). It happens due to hydrogen bonds and hydrophobic associations between cellulose's

chains because of temperature increase (Budtova and Navard (2016)). Another mechanism of cellulose-NaOH-$H_2O$ gelation was recently suggested by Gunnarsson et al. (2017, 2018). They stated that $CO_2$ in the surrounding air can diffuse to deprotonate C6 of the cellulose glucopyranose ring when cellulose is dissolved in NaOH-$H_2O$ based solvent. This chemisorption leads to the creation of carbonates and then carbonate bridges between cellulose's chains (Elschner et al. (2013)) or hydrogen bonds between carbonates and hydrogens from the hydroxyl groups (Gunnarsson (2017)) (See Figure 1.8).

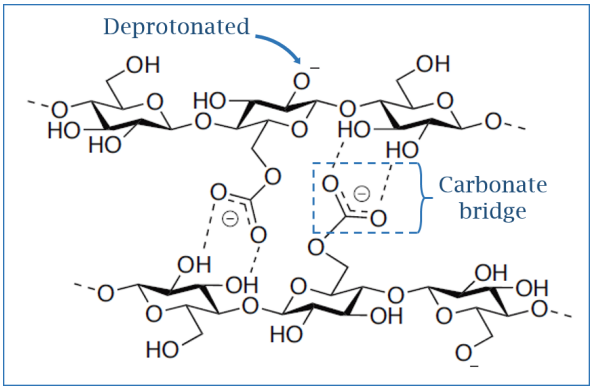


Figure 1.8 – Schematic representation of the mechanism suggested for hydrogen bonding between two chains of cellulose carbonate. Adapted from (Gunnarsson (2017)).

To delay gelation and improve cellulose dissolution various additives were found. Davidson, who discovered NaOH-$H_2O$ as solvent (Davidson (1934)), suggested and studied various additives for improving cellulose dissolution (Davidson (1937)). Nowadays, multiple additives are known and among them urea and zinc oxide (ZnO) where shown to be effective in improving cellulose dissolution and delaying gelation time (Budtova and Navard (2016)).

The team of L. Zhang, China, was one of the first to study in details the influence of urea on cellulose dissolution (Zhou and Zhang (2000)). They proved that NaOH-urea-$H_2O$ is a direct solvent of cellulose and that the addition of 2 - 4% of urea in 6 - 8% NaOH greatly improved the dissolution of cellulose from different sources. More studies were conducted on the mechanism of dissolution and it was suggested by Cai et al. (2008b) that NaOH hydrates were forming hydrogen bonds with cellulose and that the urea would associate to these NaOH hydrates to surround them and form an "inclusion complex" around cellulose's chain. This theory was further supported by Jiang et al. (2014). Finally, Isobe et al. (2013) suggested that the urea might accumulate at the hydrophobic surface of cellulose, preventing the latter to aggregate. In addition, urea would also help NaOH to penetrate the crystalline structure of cellulose.

In the case of zinc oxide, it is supposed that during dissolution, ZnO forms zincate complexes with $H_2O$ ($Zn(OH)_3^-$ and $Zn(OH)_4^{2-}$) which play the role of water "binder". These complexes reduce the amount of free water and prevent the chains from aggregating (Liu et al. (2011)). This would explain why gelation is delayed in the presence

of this additive (Egal (2006)).

Hence, it was proved that neither urea nor ZnO is bound to cellulose during dissolution. What we need to note is that gelation still happens in these solutions and the mechanism seems to be the same as without additives (Isobe et al. (2012)).

In conclusion, NaOH based solvents are cheap, environmentally friendly and easy to handle. These advantages place them as very attractive candidates for cellulose dissolution. However, NaOH based solvents can only dissolve cellulose of low DP and rather low concentrations, the dissolution has to be done at low temperatures, below 0 °C, and the obtained solution gels with time and temperature. The use of additives can enhance cellulose dissolution and delay gelation but solvent recycling with additives becomes more complicated. Even if a lot of researchers who worked in this field have stated various approaches, more studies are needed to fully understand the mechanism of cellulose dissolution and gelation in this type of solvent.

### Ionic liquids

Ionic liquids are organic salts which are liquid at temperatures below 100 °C. A differentiation can be done with the room temperature ionic liquids (RTILs) which have their melting point below 25 °C. RTILs are thus very convenient for use in different applications. More generally, ILs are known to have multiple attractive advantages such as high chemical and thermal stability, low flammability and low vapour pressure. Some of them are also known to be direct solvents for cellulose and are considered as "green solvents". However, they also show some drawbacks such as a high viscosity (which can sometime prevent quick cellulose dissolution), expensive and time consuming production, great sensitivity to impurities, including water, and there are still questions about their recyclability and toxicity. Both their advantages and drawbacks come from their composition and structure (Zhu et al. (2006); El Seoud et al. (2007); Liebert and Heinze (2008)).

ILs are composed of a cation and an anion. The cation is usually large and asymmetric while the anion can be small, sometimes a single anion such as $Cl^-$. The particularity of ILs is that multiple combinations of anions and cations make the number of ILs theoretically infinite. Obviously, depending on the ions coupled, properties can change. This is thus not a surprise that not all ILs are able to dissolve cellulose or that some of them can be considered as toxic.

It is not long ago that the great potential of ILs as cellulose solvent was recognised. Indeed, Graenacher (1934) was the first to dissolve cellulose in what can be considered an IL, but his work did not have a huge impact at his time. It is only in 2002 that Swatloski et al. (2002) studied the dissolution of cellulose in different imidazolium based ILs and opened the field again. ILs as solvents were then extensively studied.

A widely accepted theory suggests that anion plays the major role in cellulose dissolution as hydrogen bond acceptor. The anion breaks cellulose's hydrogen bonds

and form complexes with the cellulose's hydroxyl groups, inducing cellulose dissolution (Wang et al. (2012); Badgujar and Bhanage (2015); Zhang et al. (2017a)). Furthermore, it was proven that the basicity of the anion is positively correlated to cellulose dissolution efficiency. An IL with a "good" hydrogen bond acceptor (anion with high basicity) is a better solvent for cellulose, for the cation being the same (Xu et al. (2010); Wang et al. (2012)). Kamlet-Taft parameters were also demonstrated to be important in predicting cellulose dissolution (Hauru et al. (2012)).

The influence of cation on cellulose dissolution is still a subject of debate. A lot of theories exist, some suggest that the cation does not have any special effect on cellulose dissolution and other suggest the opposite. The fact that the dissolution of cellulose can vary from very efficient to insoluble for the same anion but a different cation clearly demonstrates that the influence of the cation on cellulose dissolution is real. Several theories were given to determine the role of the cation but they will not be detailed in the following, as it is not part of this work. Briefly, interactions of the cation with cellulose's chains were suggested (Zhang et al. (2010); Liu et al. (2010)) and the influence of the nature of the cation was also analysed (Zhao et al. (2012b); Lu et al. (2014)). It is accepted by the scientific community that work needs to be done on the understanding of dissolution mechanism of cellulose in ILs. If one can find the answer, it would help in screening and selecting new and more efficient ILs for cellulose dissolution.

Other parameters influence cellulose solubility in ILs such as viscosity and purity of the IL, cellulose's DP and crystallinity and dissolution conditions. Impurities in the ILs is a very concerning issue. Indeed, impurities, whether they are residues from IL production or water, can completely change ILs' properties: inhibit cellulose dissolution (Seddon et al. (2000); Mazza et al. (2009)) or derivatise cellulose (Karatzos et al. (2012)). Rheological analyses on cellulose-IL solutions were performed. One of the interesting trend observed was the decrease of solvent thermodynamic quality with the increase of temperature (Gericke et al. (2009); Sescousse et al. (2010a)). Temperature increase may increase the kinetic of dissolution but should not help overcoming the dissolution limit. This explains why cellulose "dissolution efficiency" was reported to increase with increasing temperature (Swatloski et al. (2002); Zhao et al. (2012a)). Another way to lower the viscosity of cellulose-IL solutions is to use so-called co-solvents such as dimethyl sulfoxide (DMSO) or dimethylformamide (DMF). These co-solvents were proven to improve cellulose dissolution in ILs by greatly diminishing the viscosity of the media, and hence facilitating mass transport, without significantly interacting with cellulose or the cation and anion of the ILs (Andanson et al. (2014)).

Ionic liquids are very promising cellulose solvents, even if more studies are needed to understand cellulose dissolution mechanism and to better comprehend their "green" quality. A new class of ILs was discovered and one of them demonstrated abilities for industrial production of fibres (Parviainen et al. (2013); Hauru et al. (2016)). This

process is called Ioncell (Michud et al. (2016)).

### Pulp dissolution

In the two previous sections, dissolution of cellulose was discussed. In this section we will focus on the dissolution of pulps. The production of pure cellulose is expensive, time consuming and not environmentally friendly. A challenging task is hence to be able to directly dissolve pulps containing all wood components, in an environmentally friendly media.

Pulps can be more or less dissolved in the same solvents described above. ILs were proved to be good solvents for pulps. For instance, eucalyptus dissolving pulp and organosolv/kraft lignin, mixed in different ratios, were properly dissolved in 1,5-diazabicyclo[4.3.0]non-5-enium acetate and then spun to produce fibres (Ma et al. (2015)). Yet, in this section we will focus on NaOH based solvents.

Due to the other wood components (hemicellulose, lignin) and the high DP of cellulose, the dissolution efficiency is greatly lowered. It should be noted that the dissolution of "real" cellulose fibres is very different from that of "pure" microcrystalline cellulose (often used in laboratories) because of a particular morphology and composition of the fibres. Depending on solvent type, swelling via ballooning or direct dissolution happens. When the solvent is "good" no ballooning effect can be observed, rather, the cellulose fibres break into small spindles and homogeneously dissolve (Cuissinat and Navard (2006a)). Other "less efficient" solvents, whatever the cellulose source, lead to a ballooning effect due to the swelling of fibres' secondary wall followed by either complete or incomplete dissolution. It was demonstrated that plants' fibres are always swelling in NaOH based solvent which means that it is rather bad solvent for cellulose (Cuissinat and Navard (2006b, 2008); Cuissinat et al. (2008)).

Pulp is known to be not well dissolved in NaOH based solvents without pretreatments. Isogai and Atalla (1998) showed that lignin decreased cellulose dissolution efficiency and that hemicellulose did not have any peculiar influence on dissolution. They also concluded that cellulose of high DP was only partially soluble in aqueous NaOH solvents and that a pretreatment of the former is needed to improve dissolution. The influence of the type of pulps, the content on hemicellulose and lignin was investigated (Le Moigne and Navard (2010); Kihlman et al. (2012); Shi et al. (2014)). Le Moigne and Navard (2010) stated that molecular weight of cellulose was not the main parameter influencing cellulose dissolution but rather the macrostructure and the chemical environment of the chains. Kihlman et al. (2012) concluded that only cellulose DP and pulp carbohydrate composition were of important influence on cellulose's fibres dissolution. Influence of hemicellulose and lignin content is still not clear: for example, Isogai and Atalla (1998) stated that hemicellulose did not have any peculiar impact on pulp dissolution efficiency, while Le Moigne and Navard (2010) stated that an increase in hemicellulose content decreased cellulose dissolution ratio. Regarding

lignin content, it was observed by Shi et al. (2014) that decreasing lignin content increased cellulose dissolution ratio, up to a certain extent. Indeed, when the content in lignin was further decreased, cellulose dissolution ratio decreased. They explained that trend by stating that the reduction in lignin content rendered cellulose less accessible for the solvent during dissolution due to the increase of interactions between cellulose's chains and better "packing".

Overall, the dissolution of plants' fibres is not completely understood yet. To improve pulp dissolution in NaOH based solvents, a pre-treatment of the pulp or cellulose is needed (Shi et al. (2018)). The incomplete dissolution of cellulose in this solvent can, however, be exploited. For example, all cellulose composites or self-reinforcing composites are now a current subject of study and the incomplete dissolution of cellulose or pulp in the solvent provides both the matrix (dissolved part) and the reinforcement (non-dissolved fibres). Studies are still on process and show promising outcomes for bio-composites (Nishino et al. (2004); Väisänen et al. (2017); Labidi et al. (2019)).

### 1.2.2 Shaping of cellulose as beads

Several techniques exist and their type will determine the shape and the size of obtained cellulose materials; various shapes are possible such as fibres, films and also beads. The shape needs to be "fixed", this is done through the coagulation step (see Figure 1.5 on page 57). Coagulation is a phase separation (Wijmans et al. (1983, 1984)) which consists on replacing the solvent by a non-solvent of cellulose through diffusion. In opposition with precipitation, and if coagulating cellulose without stretching (case of fibres and films), cellulose 3D network is kept intact after coagulation, only a small shrinkage of the structure can be observed. It should be noted that gelation of cellulose solutions can happen with certain solvents, however, when a particular shape is targeted, gelation is usually avoided.

This work was conducted in the framework of the European project "Nanohybrids". Our goal was the production of cellulose aerogels in form of beads of different sizes, from microns to millimeters, with techniques which can be transformed to the industrial scale. Thus, we will focus on the techniques that can be used to make cellulose particles which potentially can be applied to make aerogels. Note that the words beads, particles and microspheres are sometimes differentiated in literature, depending on their size. The micrometer scaled ones are preferentially called particles or microspheres while millimetre or bigger scaled are called beads. We will try to follow this standard in this work by preferentially using beads and particles as a function of the size.

The techniques to produce droplets applicable for cellulose can be classified in two main categories:

- Formation of droplets in a gaseous phase and subsequently "fixing" the shape by falling in a coagulation (for cellulose) or gelation (for other polysaccharides) bath.

Several techniques are known in this category such as the dropping, atomisation and

spraying.

- Formation of droplets in a non-miscible liquid phase leading to an emulsion and subsequently "fixing" the droplets' size by adding a non-solvent (for cellulose) or a gelling (for other polysaccharides) agent or changing emulsion conditions (temperature, pH).

Both types of techniques are widely used, in particular in the food industry, and will be described thereafter.

### Dropping

Gericke et al. (2013) published a rich review on the production of cellulose beads. Very recently Ganesan et al. (2018) detailed the production of polysaccharide based aerogels shaped as beads. These two reviews agree to present the "simple" dropping (also called dripping) technique as a laboratory scale way to produce beads. It consists on producing a droplet by pushing polysaccharide solution through a thin opening (syringe or pipette, nozzle). The solution pushed will break in air to form droplets as a result of the gravity, pressure, surface tension and capillary forces. The droplets formed will then fall into a coagulation (for cellulose) or a gelation (for other polysaccharides) bath (Gericke et al. (2013)). A schematic representation of the dropping technique is given in Figure 1.9.

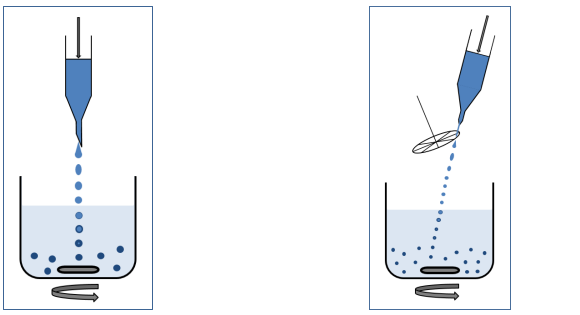

"Simple" dropping JetCutter technique

Figure 1.9 – Schematic representation of two dropping techniques: the "simple" dropping technique and the JetCutter technique.

The size of the droplets obtained with this technique is of few millimetres, and mostly depends on the size of the nozzle used. The shape of the beads depends on ejection speed, the distance from the bath, the viscosity and the surface tension of the two fluids (Sescousse et al. (2011b)). This technique was widely used to produce beads from different polysaccharides, with different solvents and coagulation or gelation baths (De Oliveira and Glasser (1996); Sun et al. (2009); Chan et al. (2009); Trygg et al. (2013); Kamal Mohamed et al. (2015)). The only way to increase the productivity is to multiply the number of nozzles.

Other techniques were developed to increase the production cadence, reduce the beads' size and enhance their regularity. Among them, the addition of a vibrating device or electrostatic forces, the spinning drop atomization and spinning disc atomization were well documented by Ganesan et al. (2018) and Gericke et al. (2013). The JetCutter technique is a sort of dropping but with much higher productivity. A solution is ejected with high pressure through a nozzle to form a jet which is cut with high speed rotating wires to form droplets which progressively become spherical under the influence of surface tension. The droplets fall into a coagulation or gelation bath. Figure 1.9 gives a schematic representation of this technique.

The range of sizes that can be obtained from this technique is very wide. It goes from hundreds of micrometers to few millimetres. Size can be varied by changing the device parameters such as the size of the nozzle or the cutting tool (more or less wires of different diameters). The productivity of this technique is very high but to completely master all the parameters is rather complicated. Furthermore, the size range will not only depend on the parameters of the device, but also on the rheological properties of the solution. This technique was developed and patented by Vorlop and Breford (1996). It is widely exploited by GeniaLab® and only few scientific papers are available using this approach (Prüße et al. (1998b,a); Prüße (2002); Prüße et al. (2003); Prüsse et al. (2008); Pinnow et al. (2008)).

**Emulsions**

The production of micron-size particles is an important matter in a lot of fields of the industry such as cosmetics or food. One of the ways of reaching this size is emulsification. It consists of mixing two non-miscible liquids, here, cellulose or polysaccharide solution and oil, to disperse the first in the second one; the resulting mixture is forming an emulsion (Karbstein and Schubert (1995); Tadros (2013); Ganesan et al. (2018)).

The dispersion of the solution (the dispersed phase) as droplets, in the non-miscible liquid (the continuous phase) will happen because of the disruptive forces produced by mixing. The mixing will increase the interface area between the two fluids. This area depends on the interfacial tension of the system which is expressed as energy per unit area and tends to be as small as possible thanks to the cohesive forces. The interfacial tension thus represents the energy needed to increase the interface area. Therefore, if the input of energy from the disruptive forces is higher than the cohesive forces, droplets will deform above a critical shape and breakup in smaller ones, hence increasing the interface area up to a steady state. This steady state is a balance between cohesive forces and disruptive forces.

The main cohesive forces that are influencing the droplets' shape in emulsion are the Laplace pressure (Equation (1.1)) and the viscosity of the dispersed phase.

$$P_L = \sigma(\frac{1}{r_1} + \frac{1}{r_2}) \tag{1.1}$$

with $\sigma$ the interfacial tension and $r_1$ and $r_2$ the main curvature radii of the interface. For a spherical shape, $r_1 = r_2$. The disruptive forces in emulsion, leading to droplets break up, depend on the flow conditions induced by the emulsification machine and will be detailed later.

During emulsification several phenomena happen:

- Droplet breakage.
- Coalescence: merging of droplets to form a bigger one.
- Flocculation: agglomeration of the droplets.
- Sedimentation: the two liquids separate due to gravitational or centrifugal forces.

In the case of sedimentation, the dispersed phase is denser than the continuous one and droplets sink to the bottom of the emulsion.

- Creaming: same as sedimentation but with the case of a denser continuous phase; droplets float to the top.

Emulsions are consequently metastable colloids that can be classified by type:

- Oil in water (O/W): oil is the dispersed phase, and water the continuous one.
- Water in oil (W/O): water is dispersed in oil. This type is the one we will focus on.

Surfactants can be used to help to "stabilise" the emulsion and reduce droplets' size. A surfactant goes at the interface of two fluids to lower the interfacial tension. This is possible because of their amphiphilic property, they are molecules which possess hydrophilic and hydrophobic (or lipophilic) parts. They exist in many forms (small molecule, proteins...) and can be ionic (charged) or non-ionic, which gives them various properties making them suitable for different types of emulsions. Tools used to help choosing the best surfactant for a given system were developed. The most commonly used one is the Hydrophilic Lipophilic Balance (HLB). It is based on a ranking of surfactant molecules as a function of their hydrophilic over the lipophilic moiety at 25 °C. It goes from 0, for a highly hydrophobic molecule, to 15 for a highly hydrophilic one. Around 7 the molecule is neither more hydrophilic than more lipophilic. As an example, Sorbitan monooleate (Span 80) is a non-ionic surfactant with a HLB of 4.3, describing a rather hydrophobic behaviour, more suitable for use in W/O emulsions.

The mechanisms of droplet breakup have been extensively studied (Karbstein and Schubert (1995); Tadros (2013)). As stated before, the disruptive forces in the emulsions depend on the flow conditions induced by the emulsification machine. These flows can be categorized in two main types: turbulent and laminar. Each flow has regimes which depend on the stresses applied on the droplets. The turbulent flow has two regimes: the turbulent inertial regime, induced by inertial stress and the turbulent viscous with shear stress. The laminar flow has the viscous regime which can be induced by shear or elongational stresses.

The Capillary number (Equation (1.2)) was developed and used by Grace (1982)

and Stone et al. (1986) to characterise the deformation of droplets in laminar flow.

$$C_a = G\frac{\eta_c r}{\sigma} \tag{1.2}$$

with $G$ the deformation gradient, a combination of the elongational and the shear rate, $\eta_c$ the viscosity of the continuous phase, $r$ the radius of the droplet and $\sigma$ the interfacial tension. A given Capillary number corresponds to a given disruptive to cohesive stresses ratio. At a critical deformation, when disruptive stress is equal or higher than cohesive stress, the droplet breaks up. This point is called the Critical Capillary number. This value is used to characterize the droplet breakup in laminar flow for both shear and elongational stresses (Figure 1.10), and depends on the viscosity ratio ($p = \lambda = \frac{\eta_d}{\eta_c}$ with $\eta_d$ the viscosity of the dispersed phase).

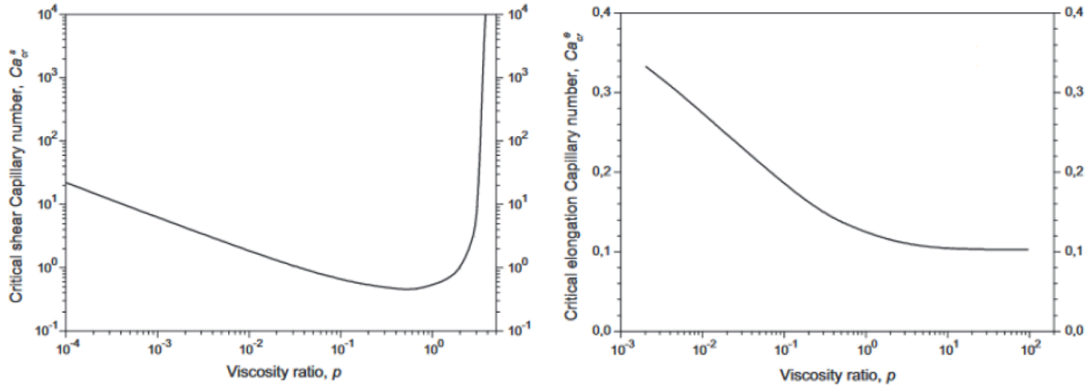


Figure 1.10 – Critical shear capillary number (left) and critical elongational capillary number (right) as a function of viscosity ratio (p). Adapted from Grace (1982) and Stone et al. (1986).

Under shear stress, and for a viscosity ratio higher than 4, there will be rotation of the droplets rather than breakage. At a viscosity ratio of 1, the breakage will be the most efficient. Under elongational stress, breakage will always happen, whatever the viscosity ratios, and the most efficient viscosity ratio are at 5 and higher.

The behaviour of a single droplet under shear flow was extensively studied. This flow was described by Rumscheidt and Mason (1961) as rotational with:

$$u = \dot{\gamma}y; \quad v = 0; \quad w = 0; \tag{1.3}$$

where $u$, $v$ and $w$ are the velocity components along the $x$, $y$ and $z$ axes (Figure 1.11) respectively and $\dot{\gamma}$ is the shear rate. Figure 1.11 gives a schematic representation of the shear flow (left) and the resulting droplet deformation (right) as described by Rumscheidt and Mason (1961).

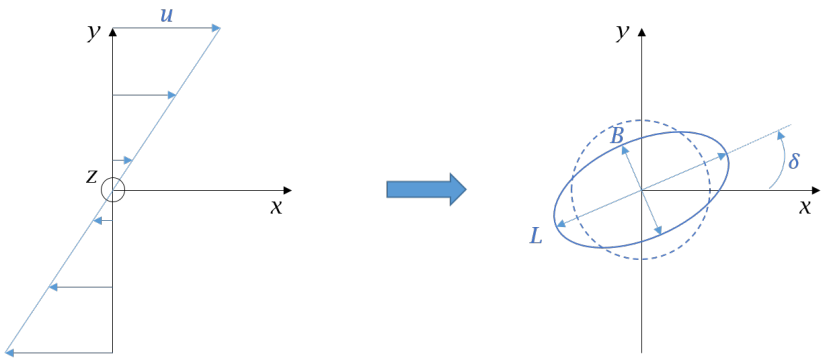


Figure 1.11 – Schematic representation of the shear flow (left) and the resulting droplet deformation (right) as described by Grace (1982). $u$ is the velocity component along $x$ axis, $L$ is the length of the droplet (large axis of the ellipsoid), $B$ the width of the droplet (first small ellipsoid axis) and $\delta$ is the orientation angle of the drop. $W$, which can not be seen here, is the second small axis in the vorticity direction ($z$ axis).

The deformation of the droplet was introduced by Taylor (1934) as:

$$D = \frac{L - B}{L + B} \tag{1.4}$$

with $L$ the length of the droplet (large axis of the ellipsoid) and $B$ the width of the droplet. The small deformation limit was established at D $< 0.2$ in order to derive analytical expressions for the deformation as a function of shear stress.

Literature on the formation of polysaccharide particles with the emulsion technique is numerous (Poncelet et al. (1992); Kim and Pack (2006)). However, the production of cellulose particles with emulsion technique using NaOH-$H_2O$ solvents is less frequent due to its peculiar solution behaviour (very high pH, gelation with time and temperature and thus "unstable" viscoelastic properties). To the best of our knowledge, the group of L. Zhang in China was the only one to report making cellulose particles through emulsification technique (Luo et al. (2009); Luo and Zhang (2010a,b)). The emulsification technique is the same in these three papers, they emulsified cellulose-NaOH-urea-$H_2O$ solution in paraffin oil with addition of Span 80. They coagulated the formed cellulose droplets by adjusting the pH of the emulsion with hydrochloric acid and collected the particles after sedimentation and washing in acetone. They produced a different cellulosic material in each paper. In their first paper they created magnetic $Fe_3O_4$/cellulose particles of few microns. In the second article they varied the size of the produced cellulose microsphere from 5 µm to 1 mm by changing the emulsion's conditions (amount of surfactant, ratio between aqueous and oil phase, stirring speed). Finally, in their third article, they used the same magnetic particles created in their first article to activate them with epoxy for penicillin G acylase immobilisation.

## 1.3 Aerogels

### 1.3.1 Porous materials: drying methods and generalities

In this work, we will mainly focus on aerogels as porous materials. Nowadays, the term aerogel is used to designate all types of foams or porous materials. However, in this study we will make a distinction depending on the drying method used to obtain the porous material concerned.

#### Evaporative drying: xerogel

The evaporative drying is the most simple and the most commonly used drying. Nevertheless, it usually leads to rather dense or non-porous materials. Indeed, during drying of a gel in ambient conditions, the pore walls of a gel are subjected to strong pressures du to the capillary forces (see Figure 1.12). This pressure is developed as described by Young-Laplace Equation (1.5):

$$\Delta p = \frac{2\gamma}{R} = \frac{2\gamma cos\theta}{a} \tag{1.5}$$

with $\Delta p$ the capillary (Laplace) pressure, $\gamma$ the surface tension between the gas and the liquid, $R$ $(= \frac{a}{cos\theta})$ the radius of the formed meniscus and $\theta$ the contact angle which reflects the wettability of pore's walls with the fluid (see Figure 1.12). Higher the surface tension and lower the contact angle (good wettability), higher the capillary pressure. This pressure can be strong enough to induce cracks in the pore's walls or even to provoke pore collapse especially when R is low.

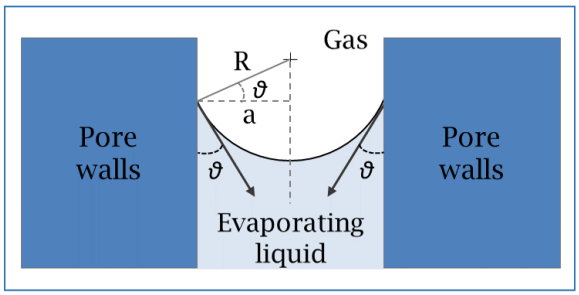


Figure 1.12 – Schematic representation of capillary forces.

Whether they are porous or not, the materials obtained from the evaporative drying (simple ambient evaporation or under low vacuum) will be called xerogels.

#### Supercritical drying: aerogel

To avoid the capillary forces that could lead to an important shrinkage during drying and preserve the gel's structure, the latter can be dried under supercritical (Sc) conditions. The first researcher to use the supercritical drying to evacuate the

liquid from the pores of a gel was Kistler (1931), more details on his discovery will be given later. In the Sc conditions, fluids are neither liquid nor gaseous, there is no meniscus formed and thus capillary pressure is theoretically zero. Figure 1.13 is a schematic representation of a phase diagram with all matter states, including Sc state. Figure 1.13 also shows different possible drying methods and the states the fluid within gel's pores undergoes during these dryings. We can see that during evaporative drying, the fluid goes directly from liquid to gas while during Sc drying, the liquid is firstly brought in the Sc state and then changed into gas.

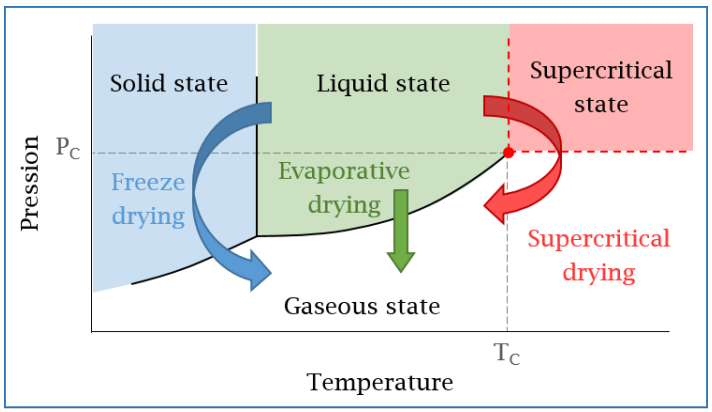


Figure 1.13 – Schematic representation of a phase diagram and possible drying routes. $T_c$ and $P_c$ represent the critical temperature point and critical pressure point, respectively.

Nowadays, carbon dioxide ($CO_2$) is commonly used as Sc fluid because of its non-toxic and non-explosive properties, its low cost and its "soft" Sc conditions: critical pressure point of 72.8 bar and critical temperature point at 31 °C. As a comparison, water critical point is 220 bar and 374 °C and ethyl ether critical point is 36 bar and 194 °C (fluid used by Kistler (1931) for inorganic gels drying).

So far, Sc drying is the main way, especially in the case of polymers, to preserve as much as possible gel's structure when replacing liquid in the pores by gas. The materials obtained from this drying will be called aerogels. They usually show high porosity ($> 90\%$), low density (0.2 g $cm^{-3}$ and lower) and high specific surface area (from 100 $m^2$ $g^{-1}$ up to 1000 $m^2$ $g^{-1}$ and more) (Aegerter et al. (2011)).

### Freeze-drying: cryogel

Another way to get porous materials with a very low density is the freeze drying. As shown in Figure 1.13, during this drying the fluid in gel's pores undergoes solidification and then sublimation. There is no capillary pressure in this case. Water is usually used to perform freeze-drying which results in materials with big pores as they are formed as replica of ice crystals growing during water solidification. Other fluids can be used such as tert-butanol-water mixtures which form smaller crystals (Borisova et al. (2015)). The obtained materials will be called cryogels.

### A bit of history on aerogels

The first aerogel was prepared by Kistler in 1931 and was based on silica (Kistler (1931, 1932)). Kistler was the first to have the idea to place a silica gel in the supercritical conditions of the fluid within its pores (ether) to dry it. He decided to call his invention "aerogel", a gel filled with air, as it was like the liquid was replaced by air. *"The jelly has had no way of 'knowing' that the liquid within its meshes has become a gas"* (from Kistler (1931)). The aerogels were born: porous materials obtained from supercritical drying, mainly constituted of air ($> 90\%$), with an inorganic or organic interconnected open network, showing a very low apparent density and a high specific surface area. Silica aerogels were the first ones to be produced and studied by Kistler (1931), but they were not the only ones. Indeed, in his second article on aerogels preparation, Kistler (1932) reported the preparation of metal oxides based aerogels (such as "tungstic" oxide and ferric oxide) and also cellulose, gelatine, agar and other bio-based aerogels.

In the following years, not all types of aerogels received the same keen interest. As "first born" silica aerogels were extensively studied (Aegerter et al. (2011)) and are now commercialised (CabotCorp (2019)-http://www.cabotcorp.com/). They show outstanding properties such as low density (around 0.1 g $cm^{-3}$) and very high specific surface area (1000 $m^2$ $g^{-1}$ and higher). In addition, silica aerogels demonstrate exceptional thermal insulation properties. Indeed, these aerogels have extremely low thermal conductivity in ambiant conditions, around 0.013 W $m^{-1}$ $K^{-1}$, which is lower than air (0.025 W $m^{-1}$ $K^{-1}$), it is the best insulating material. Silica aerogels can hence be classified as thermal super-insulating materials. However, despite their outstanding properties, silica aerogels are not easy to exploit as they are very brittle. From the 70's of the last century, the interest was therefore focused on other types of aerogels: metal oxides (titanium, zirconium) and synthetic polymers (epoxy, polyurethane) based aerogels. These aerogels showed improved mechanical properties and other potential applications such as in catalysis, in fuel cells and other applications involving high temperatures (Aegerter et al. (2011)).

More recently, around 15 years ago, the interest focused on a completely forgotten class of aerogels: the biomass based aerogels. Also called bio-aerogels, they are, till now, mainly prepared from polysaccharides and have multiple advantages compared to their inorganic based homologues such as bio-compatibility and environmental friendliness. In addition, these aerogels are also mechanically strong as they do not break under compression and some of them also showed thermal super-isolation properties (Rudaz et al. (2014); Druel et al. (2017); Groult and Budtova (2018a)).

### 1.3.2 Bio-aerogels

Generalities on preparation, properties and characterisation methods of bio-aerogels will firstly be presented. Then cellulose II porous materials, including cryogels and xerogels, will be studied in detail with more interest on aerogels. The last part of this section will be dedicated to polysaccharides and especially cellulose aerogels shaped as beads or particles.

#### General pathway for bio-aerogels' preparation

In addition to being made of natural polymers, bio-aerogels involve only non-toxic chemicals for their preparation. The production of bio-aerogels counts 4 main steps as given in Figure 1.14:

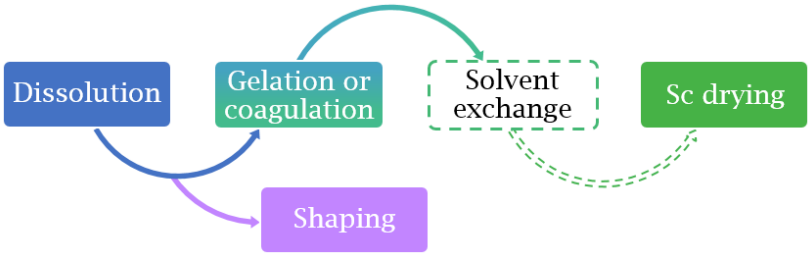


Figure 1.14 – Schematic representation of bio-aerogels' processing steps.

- Dissolution. A polysaccharide is dissolved in a solvent (many are water soluble) and solution properties depend on polysaccharide's type and its concentration.

- Gelation and coagulation. The solution obtained is then shaped as desired (aerogels shaping will be discussed in Section 1.3.4) and gelled and/or coagulated.

Most of polysaccharide solutions have an "easy" gelling pathway by changing solution's conditions such as temperature, pH or by ionic cross-linking with metal ions. Among the temperature dependent gelling polysaccharide solutions we can count starch, carrageenan and agar. The gelation of polyelectrolyte polysaccharide solutions is often triggered by pH or polyvalent metal ions. Cellulose solutions are not easy-gelling, except when dissolved in NaOH(aq) where gelation occurs spontaneously with time and temperature. Cellulose can be chemically cross-linked with epichlorohydrin (Ciolacu et al. (2016)).

Even if gelation is an easy step for most of the polysaccharides, it is possible to "fix" the shape by adding a non-solvent to the polysaccharide solution. It will result in the phase separation also described as "immersion precipitation" (Wijmans et al. (1983, 1984)). It was observed that addition of the pure non-solvent usually leads to a more important shrinkage of a polysaccharide network. A gradual addition of the non-solvent can be performed to reduce the shrinkage (Quignard et al. (2008); Robitzer et al. (2011a); Tkalec et al. (2015)).

• Solvent exchange and supercritical drying. If performing extracting with $CO_2$, the fluid in the gel's pores needs to be miscible with $CO_2$. As most of polysaccharides are usually dissolved in an aqueous solvent and directly gelled in it, a solvent exchange step is required. This step is a "simple" replacement of the solvent by a non-solvent which is miscible with $CO_2$ (commonly ethanol (EtOH) or acetone). As for coagulation, the solvent exchange step is driven by diffusion and thus depends on temperature, polysaccharide concentration and gel's shape (Gavillon and Budtova (2007); Sescousse and Budtova (2009)). In the case when polysaccharide solution was directly coagulated without gelation, if the non-solvent used is miscible with $CO_2$, no further step is needed. It is important to note that when Sc drying is performed, the structure of resulting aerogel was already "fixed" during the gelation or coagulation step. Sc drying is hence a critical step as it can properly preserve this "fixed" polysaccharide gel's structure.

### Characterisation

As for porous materials, there are different ways to characterise aerogels with some particularities for bio-aerogels. Bulk density is one of the most used characteristics to compare aerogels with each other. For regular monoliths, density can be easily measured by recording the weight and measuring the dimensions of the sample. When the size and/or the shape of materials are not "standard", special devices can be used to determine the bulk density; Geopyc, by Micromeritics, is one of them. With the help of a calibrated "chamber" and fine powder (DryFlo), the device will determine the exact volume of the sample. Cautions need to be taken when using this kind of device on bio-aerogels as the latter may be deformable and compressible.

Other characteristics of porous materials are their porosity, specific pore volume ($V_{pores}$) and specific surface area. The porosity is the fraction of gas volume over the total volume of the sample, usually expressed in percent. Knowing that the total mass of the sample is equal to the mass of the skeleton (polysaccharide), porosity can also be determined from the bulk density ($\rho_{bulk}$) and skeletal density ($\rho_{sk}$) of the sample following Equation (1.6).

$$Porosity, \% = \left(1 - \frac{\rho_{bulk}}{\rho_{sk}}\right) \times 100 \tag{1.6}$$

Specific pore volume (often simply called pore volume) is the volume of gas in the sample and is expressed in $cm^3\ g^{-1}$. It can also be calculated from the $\rho_{bulk}$ and $\rho_{sk}$ following Equation (1.7).

$$V_{pores} = \frac{1}{\rho_{bulk}} - \frac{1}{\rho_{sk}} \tag{1.7}$$

Finally, specific surface area is the total surface of pore walls expressed in $m^2\ g^{-1}$. One device using nitrogen adsorption and applying a theory developed by Brunauer, Em-

mett and Teller (BET) is commonly used to measure specific surface area ($S_{BET}$). Pore volume and pore size distribution can also be measured with nitrogen adsorption using the Barrett–Joyner–Halenda (BJH) theory or by mercury porosimetry. It should be noted that these two methods are not applicable to most of bio-aerogels. BJH method only considers small pores, below 200 nm. Yet, most of bio-aerogels have a wide pores' size distribution ranging from tens of nanometers to few microns. The BJH method hence neglects most of the bio-aerogels' porosity (80-90% of the total pore volume) (Rudaz et al. (2014); Jiménez-Saelices et al. (2017); Groult and Budtova (2018a); Robitzer et al. (2011a)). In addition, both BJH method and mercury porosimetry can lead to a compression of the bio-aerogels. In the case of mercury porosimetry, most of the time mercury does not penetrate in the aerogels' pores and only compresses the sample (Rudaz et al. (2014)).

Scanning Electron Microscopy (SEM) is often used for morphological observations. Obtained images do not allow a quantitative measurement of the pores' size distribution but is can give a good indication of the morphology. For example, the morphology of aerogels, xerogels and freeze-dried cryogels from water can easily be differentiated by SEM observations (Buchtová and Budtova (2016)).

Finally, it is important to make a remark on bio-aerogels' ageing. Most of polysaccharide based aerogels and porous materials are very sensitive to moisture, they are highly hygroscopic. It is hence important to consider that some results depend on ageing and measurement conditions (ambient humidity). Water uptake increases with time and can be a really fast process for some bio-aerogels. Aerogels' moisture uptake degrades their properties, it increases density and decreases $S_{BET}$. If an attempt of drying is done, the result will be the same as with evaporative drying and lead to pore collapse. This phenomenon is called "hornification" in the case of drying cellulose.

### Properties and applications

Bio-aerogels were prepared from multiple polysaccharides (alginate, cellulose, pectin, starch, etc). It was observed that their properties are very dependent on the polysaccharide used and on the aerogels' processing steps. Bio-aerogels usually show a low density ($< 0.2$ g cm$^{-3}$) and their specific surface area is usually of few hundreds of m$^2$ g$^{-1}$, allowing a wide range of applications.

As the most abundant polysaccharide on hearth, cellulose based aerogels were extensively studied. The two main types of cellulose used to produce aerogels are cellulose I and II. In this section, only cellulose I aerogels will be briefly discussed as more attention will be given to cellulose II and lignocellulosic aerogels in the next section. Bacterial cellulose can be used as is to make aerogels while various treatments of natural fibres are needed to get nanocellulose. Depending on the treatment, different "sizes" of cellulose's fibres can be obtained: microfibrillated cellulose (MFC), nanofibrillated cellulose (NFC) and cellulose nanocrystals or whiskers (CNC). Above

the percolation concentration, "nanocellulose" can create a network when suspended in water. Probably for easier processing reasons, most of the porous nanocellulose materials are produced with freeze-drying technique (Pääkkö et al. (2008); Chen et al. (2011); Jin et al. (2011); Sehaqui et al. (2011)). When dried in Sc conditions, cellulose I aerogels show remarkable properties. For instance, Heath and Thielemans (2010) obtained cellulose nanowhisker aerogels with a very low density (0.078 g $cm^{-3}$) and still high $S_{BET}$ of more than 500 $m^2$ $g^{-1}$. At the same time, Liebner et al. (2010) prepared bacterial cellulose aerogels with even lower density of 0.008 g $cm^{-3}$ and a still relatively high $S_{BET}$ of 200 $m^2$ $g^{-1}$. The same team demonstrated the suitability of the produced bacterial cellulose aerogel for use in drug controlled release (Haimer et al. (2010)). Nanocellulose aerogels are the only cellulose based aerogels to show thermal super-insulation properties with thermal conductivity $\approx$ 0.022 W $m^{-1}$ $K^{-1}$ for a density of $\approx$ 0.01 g $cm^{-3}$ (Sakai et al. (2016)). A wide range of applications can be targeted by these aerogels in biomedical fields (Lavoine and Bergström (2017)) or thermal insulation materials (Kobayashi et al. (2014); Jiménez-Saelices et al. (2017)).

Starch is a "mixture" of polysaccharides found in plants, fruits or tubers. It is composed of amylose (linear 1,4 linked $\alpha$-D-Glucopyranose polysaccharide) and amylopectine (ramified 1,4 linked $\alpha$-D-Glucopyranose), present in different ratios depending on the starch's source. It was observed that this ratio had a huge influence on the aerogels' properties (García-González and Smirnova (2013); Druel et al. (2017)) which makes this polysaccharide a very good example of the influence of source on the final material's properties. Starch aerogels show a "standard" density but a rather low $S_{BET}$ as compared to some other bio-aerogels (50 - 250 $m^2$ $g^{-1}$). They have been particularly studied for their properties as matrix for drug delivery systems (Mehling et al. (2009); García-González and Smirnova (2013); De Marco et al. (2015); Ubeyitogullari and Ciftci (2016)). Studies also report their thermal super-insulation properties (Glenn and Irving (1995); Druel et al. (2017)) and their potential use in food industry (Ubeyitogullari et al. (2019)). Research is still ongoing and corn starch aerogels were, for example, used as template to study the influence of Sc drying parameters on the resulting aerogels' properties (García-González et al. (2012a)) or for a life cycle assessment (De Marco et al. (2019)).

Pectin also comes from plants, vegetables and especially from fruits and is composed of 1,4 linked $\alpha$-D-anhydrogalacturonic acid with different degrees of methyl esterification of carboxyl groups, depending on the source. Pectin aerogels are becoming an important field of research as they are bio-aerogels with fully tunable properties depending on their preparation process (Groult and Budtova (2018b)). They showed one of the highest $S_{BET}$ for bio-aerogels, up to 600 $m^2$ $g^{-1}$ (Tkalec et al. (2015); Groult and Budtova (2018b)), and demonstrated impressive thermal super-insulation properties, with thermal conductivity as low as 0.015 W $m^{-1}$ $K^{-1}$ (Rudaz et al. (2014); Groult and Budtova (2018a)). Just like starch, pectin aerogels are also studied as potential carriers

for drug delivery systems (García-González et al. (2011); Veronovski et al. (2014)) and for catalytic and electrochemical applications when pyrolysed (White et al. (2010)).

Marine polysaccharides are usually regrouped as one class of bio-aerogels obtained from seaweeds, fungi and shell of crustaceans. Among these polysaccharides we can find alginate, carrageenan, chitin and chitosan. Aerogels from marine polysaccharides were more particularly studied by Quignard and co-workers as well as Smirnova and co-workers (Quignard et al. (2010); García-González et al. (2011)). Alginate mainly comes from brown algae and is constituted of 1,4 linked $\beta$-D-mannuronic acid and $\alpha$-L-guluronic acid in varying composition and sequence. One of the first alginate aerogel was produced by Valentin et al. (2005). Recently, Gurikov et al. (2015) demonstrated that alginate concentration and gelation method can be adapted to reach $S_{BET}$ of 538 $m^2$ $g^{-1}$ for a density of 0.021 g $cm^{-3}$. In addition, Tkalec et al. (2016) showed that a wide range of properties were achievable by changing gelation time and the non-solvent for direct coagulation of alginate. Chitin can be extracted from shell of crustaceans or fungi and is a linear 1,4 linked poly-$\beta$-acetylglucosamine. Chitosan can be obtained by deacetylation of chitin (degree of deacetylation beyond 50%) to get a 1,4 linked $\beta$-glucosamine copolymer. Chang et al. (2008) demonstrated that different cross-linked chitosan aerogels had good adsorption capacity of an anionic surfactant (sodium dodecylbenzene-sulfonate). Chitosan cryogels and aerogels were also showing suitable performances as catalysts (Tsutsumi et al. (2014)) and in biomedical applications (Terzić et al. (2018); López-Iglesias et al. (2019)). Very recently, outstanding properties were discovered for chitosan aerogels: they can be hydrophobic after modification with alkyl aldehyde (Takeshita et al. (2017)), with extremely high $S_{BET}$ of 973 $m^2$ $g^{-1}$ (Zhang et al. (2017b)), and with thermal super-insulation properties (thermal conductivity of 0.016 - 0.017 W $m^{-1}$ $K^{-1}$) (Takeshita and Yoda (2018)). These discoveries open a new range of applications. As for chitin, it was also proven to be biocompatible (Ding et al. (2012)), suitable for medical application, when dissolved or extracted in/from IL (Silva et al. (2011); Shen et al. (2016)) and be used as carbon aerogels precursor after pyrolysis (Tsioptsias et al. (2009)). Finally, carrageenans are a family of polysaccharides that come from red algae. $\kappa$-carrageenan is more often used for its good gelation properties. It is made of linear chains of 1,3 linked $\alpha$-galactose-4-sulfate and 1,4 linked 3,6-$\beta$-anhydrogalactose. $\kappa$-carrageenan aerogels were prepared and studied by Quignard et al. (2008) and also by Ganesan and Ratke (2014). Latter reported density between 0.04 g $cm^{-3}$ and 0.16 g $cm^{-3}$ and $S_{BET}$ around 230 $m^2$ $g^{-1}$. Later, Manzocco et al. (2017) demonstrated good properties of oil absorption by $\kappa$-carrageenan.

### 1.3.3 Cellulose II porous materials

#### Cellulose II aerogels

Cellulose II aerogels are obtained following the same pathway as presented in Figure 1.14 on page 74. Preparation of cellulose II aerogels was reported in literature from different solvents (derivatising and direct), from liquid, crystallised or gelled solutions, with various coagulation media (water, ethanol, acetone...) and from numerous cellulose sources (pulp, MCC, cotton...) of different concentrations. All these variations in the processing parameters influence the resulting aerogels properties which will be in the focus of our discussion in this section. Yet, in view of all the parameters variation, it is very hard to make a "correct" comparison so only trends will be exposed.

Various solvents were used to produce cellulose II aerogels, the first used were the derivatising ones (Ookuma et al. (1993); Pinnow et al. (2008)) but not a lot of aerogels were produced from them. For a matter of simplicity, direct solvents are preferred. Alkali based solvents, aqueous NaOH and LiOH, are the most popular. A lot of studies were performed on cellulose aerogels from these solvents (Cai et al. (2008a); Gavillon and Budtova (2008); Sescousse and Budtova (2009)). Since the outbreak of ionic liquids, several ones were used to produce aerogels (Aaltonen and Jauhiainen (2009); Rudaz (2013); Wang et al. (2013); Buchtová and Budtova (2016); Sescousse et al. (2011a); Mi et al. (2016)). Cellulose aerogels were also produced from NMMO (Innerlohinger et al. (2006); Liebner et al. (2008, 2009)), molten salt hydrates solvent such as zinc chloride based (Rege et al. (2016); Schestakow et al. (2016); Ganesan et al. (2016)) or calcium thiocyanate based (Hoepfner et al. (2008); Karadagli et al. (2015); Rege et al. (2016)) and tetrabutylammonium fluoride (Pircher et al. (2016)). The influence of solvents on aerogels' properties was studied by several authors (Gavillon and Budtova (2008); Sescousse et al. (2011a); Rege et al. (2016); Pircher et al. (2016)) and the main observation concerned samples' morphology. When cellulose solutions are coagulated from the liquid state, morphology is different than when coagulated from the "solid" state. This was firstly observed with NMMO as solvent as both molten and solid states are possible before coagulation (Gavillon and Budtova (2008)). The result was confirmed by different authors reporting aerogels obtained from coagulation of "solid" solutions (gelled cellulose-NaOH-$H_2O$ and solidified cellulose-molten salt hydrates) and coagulation of liquid solutions (liquid cellulose-IL and liquid cellulose-tetrabutylammonium fluoride trihydrate) (Gavillon and Budtova (2008); Sescousse et al. (2011a); Rege et al. (2016); Pircher et al. (2016)). Two types of morphologies were obtained depending on the state of the solution before coagulation. Liquid coagulated solutions show aerogels with a globular morphology while solid coagulated solutions show aerogels with a fibrous morphology (see Figure 1.15). The authors suggested that this may be due to spinodal decomposition happening during phase separation of the solutions in the liquid state with NMMO and IL as solvents.

This theory was originally suggested by Biganska and Navard (2008). A recent study by Pircher et al. (2016) focused more particularly on the influence of solvent on the aerogels' properties and they confirmed the importance of the state of cellulose solution before coagulation.

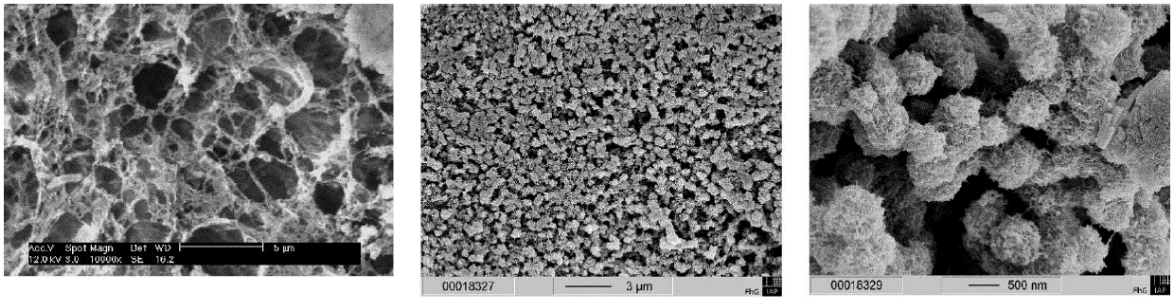


a b c

Figure 1.15 – Morphology of cellulose aerogels depending on solution state before coagulation from NMMO dissolution. Aerocellulose prepared from solid (a) and molten (b, c) Solucell950/NMMO solution regenerated in water at 25 °C with further water to acetone exchange and dried in supercritical conditions. Reprinted with permission from Gavillon and Budtova (2008). Copyright (2008) American Chemical Society.

Gelation of cellulose-NaOH-$H_2O$ solutions was studied with regards to its influence on coagulation kinetic and aerogels' properties. It was demonstrated that the diffusion kinetic only depended on the state of the solution: diffusion was three times slower when solution were coagulated rather than gels. This phenomenon was explained by the more homogeneous cellulose concentration in solution than in gels that induced a higher medium viscosity in solution than in gels, decreasing diffusion speed (Sescousse and Budtova (2009)). Regarding aerogels' properties, no particular influence of the gelation conditions was observed (Gavillon and Budtova (2008)).

Coagulation conditions and non-solvent used for this purpose seem to have a primordial influence on the resulting aerogels' properties. The influence of coagulation bath was firstly reported by Innerlohinger et al. (2006) and they stated that when cellulose is dissolved in NMMO, no influence was observed on the resulting aerogels properties when coagulated in EtOH, water or methanol, but when water-NMMO mixture was used as coagulation bath, a decrease of the $S_{BET}$ was observed. They also demonstrated that when coagulated in a cold water bath, the $S_{BET}$ was higher. Cai et al. (2008a) reported a slight increase of porosity with increasing coagulation bath temperature. The influence of temperature of coagulation bath was studied in more details. It was demonstrated that with increasing coagulation bath temperature, the diffusion is faster (Sescousse and Budtova (2009)) inducing a lower density of the resulting aerogels (Gavillon and Budtova (2008)). The same authors also reported an increase in density with increasing coagulation bath acidity (Gavillon and Budtova (2008)), even if no influence was observed on the diffusion kinetic (Sescousse and Budtova (2009)). Recently Schestakow et al. (2016) reported an influence of coagulation bath on shrink-

age, stating that the latter was dependent on bath polarity and solubility of solvent and non-solvent. The influence of coagulation bath hydrophilicity was observed by Isobe et al. (2011) who reported that aqueous non-solvents led to higher crystallinity because of a different orientation of the cellulose chains during coagulation. Finally, the second non-solvent for solvent exchange to proceed to Sc drying seems not to have any particular influence on the resulting aerogels' properties (Gavillon and Budtova (2008)).

The influence of cellulose source on the resulting aerogels' properties was reported not to be significant by several authors (Innerlohinger et al. (2006); Gavillon and Budtova (2008)). Only longer dissolution for higher DP and molecular weight was reported by Liebner et al. (2009) without further interpretation on the resulting aerogels' properties. However, the presence of lignin decreases aerogels' density (Innerlohinger et al. (2006); Aaltonen and Jauhiainen (2009)). The reasons were suggested by Sescousse et al. (2010b) who observed that organosolv lignin was not bound to cellulose during dissolution in NaOH-$H_2O$ solvent and that it was partly washed out during coagulation depending on the non-solvent used leading to bigger pores and lower density. This was in agreement with the results of Aaltonen and Jauhiainen (2009) which showed aerogels with lower density and lower $S_{BET}$ in the presence of lignin and for wood.

It is now well accepted that with increasing cellulose concentration, with all other conditions kept constant, the aerogels' density increases (Innerlohinger et al. (2006); Cai et al. (2008a); Gavillon and Budtova (2008); Liebner et al. (2008); Sescousse et al. (2011a); Rege et al. (2016); Pircher et al. (2016); Schestakow et al. (2016)). This is an expected trend as with increasing concentration, the mass increases for the same volume of sample, inducing a density increase. This phenomenon was very well exposed by Schestakow et al. (2016) when different cellulose concentrations were dissolved in calcium thiocyanate based solvent, coagulated in water, exchanged to EtOH and Sc dried (see Figure 1.16). The opposite effect is observed for shrinkage as it decreases with cellulose concentration increase (Innerlohinger et al. (2006); Gavillon and Budtova (2008); Sescousse et al. (2011a); Schestakow et al. (2016)). The effect of cellulose concentration on $S_{BET}$ is still not clear as all the previously cited authors reported a decrease of $S_{BET}$ with increasing concentration while the opposite effect was reported by Liebner et al. (2008) and Buchtová and Budtova (2016) (with NMMO/DMSO and IL as solvents, respectively and EtOH as coagulation bath). A constant $S_{BET}$ was observed by Hoepfner et al. (2008) and Cai et al. (2008a) reported an increase from 1% to 3% cellulose concentration and then a decrease of $S_{BET}$.

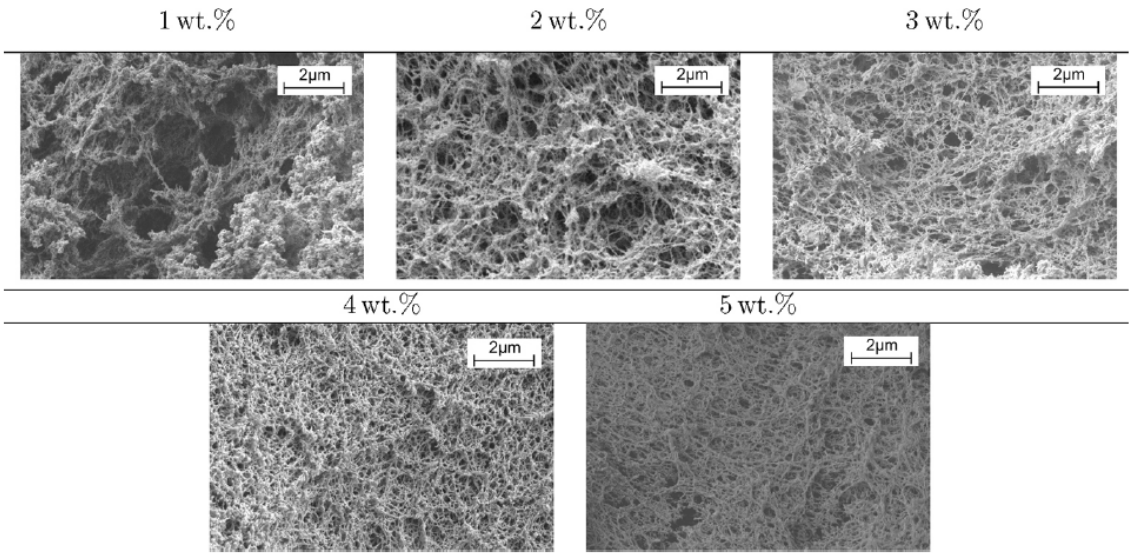


Figure 1.16 – Morphology of cellulose aerogels as a function of concentration when dissolved in calcium thiocyanate based solvent, coagulated in water, exchanged to EtOH and Sc dried. Reprinted from Schestakow et al. (2016), Copyright (2015), with permission from Elsevier.

Cellulosic aerogels' mechanical properties where extensively analysed but will not be detailed in this work as it was not in the focus of the study. The same concerns cellulose aerogels composites. For more information readers can refer to Budtova (2019).

### Cellulose II xerogels and cryogels

We have seen that Sc drying is not the only way to obtain porous materials. For example, cryogels can be obtained through freeze-drying. Two main fluids are usually employed for this type of drying: water or tert-butanol-water mixtures. It was observed that these fluids had a critical influence on the resulting cryogels' properties. Gels dried from water usually lead to very low density but with low $S_{BET}$ while tert-butanol dried cryogels show higher $S_{BET}$ (Cai et al. (2008a)). As compared to aerogels, in most of the cases, cryogels show a lower density (induced by a lower shrinkage) and a lower $S_{BET}$ (Hoepfner et al. (2008); Buchtová and Budtova (2016)). These tendencies are obvious when taking a look at the morphology of cryogels and aerogels from the same preparation procedure (see Figure 1.17). Water crystals growth during samples freezing induces large pores (Figure 1.17 A and B) and low shrinkage while tert-butanol dried cryogels (C and D) and aerogels (E and F) have better preserved structure with smaller pores and thinner pores' walls. Cryogels are not in the topic of our study so no further details will be given on this subject.

Several researchers attempted the preparation of porous cellulose II xerogels from different solvents and preparations (Cai et al. (2008a); Liebner et al. (2008); Buchtová and Budtova (2016)). However, without any particular treatment or modification of cellulose, shrinkage and collapse of the structure due to capillary forces is inevitable

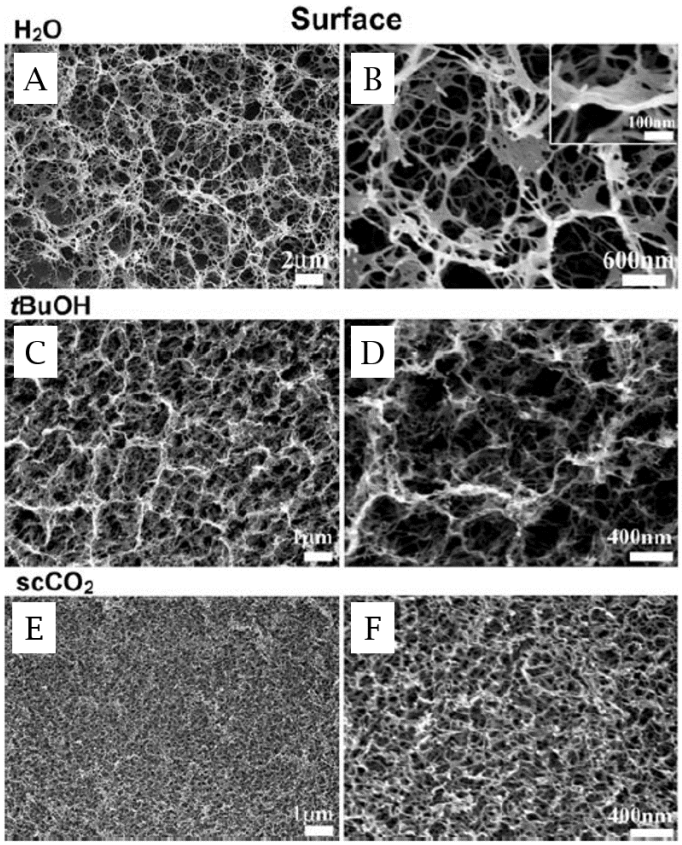


Figure 1.17 – Morphology of the surface of cellulose cryogels and aerogel as a function of drying. Cryogels from water freeze-drying (A and B), from tert-butanol (C and D) and aerogel from Sc drying (E and F). Adapted From Cai et al. (2008a).

during drying. Cai et al. (2008a) reported the formation of *"solid cellulose films, essentially without porosity"* from filter paper dissolved in NaOH-urea-$H_2O$ and LiOH-urea-$H_2O$, followed by coagulation in water and ambient drying from water or EtOH. Ganesan et al. (2016) demonstrated that it was possible to produce cellulose xerogels with a $S_{BET}$ of around 100 $m^2$ $g^{-1}$. Cellulose was dissolved in calcium thiocyanate hydrate and then emulsified with oil and surfactant to create cellulose scaffolds. The obtained gels were dried from isopropanol. These xerogels are the only "pure" cellulose xerogels showing noticeable $S_{BET}$.

### 1.3.4 Polysaccharide and cellulose aerogels shaped as beads

Shaping of bio-aerogels as beads opens a lot of different applications in food and pharma industry. An example of this interest is the European project "Nanohybrids" which started in 2015 and had as objective the production and optimisation, for future industrial exploitation, of polysaccharide aerogels shaped as beads and particles. In this section, we will focus on the existing bio-aerogel beads, their production and properties with a special interest on cellulose II aerogel beads.

### Bio-aerogel beads

Cellulose I aerogel beads were produced by Wang et al. (2016) from nanocrystalline cellulose dispersed in water and dropped in calcium chloride solutions. The obtained beads had diameter of around 0.3 mm and a $S_{BET}$ up to 354 $m^2$ $g^{-1}$, with a very low shrinkage (4%).

Starch aerogel particles were prepared with the emulsion technique through thermal gelation as developed by García-González et al. (2011). Typical size of the obtained particles ranged from 200 to 1200 µm (García-González et al. (2012b); Starbird et al. (2014)), see Figure 1.18. Properties are very similar to monolith starch aerogels with $S_{BET}$ around 100 $m^2$ $g^{-1}$. Drug release properties from the particles obtained with emulsion technique were tested and showed promising results (García-González et al. (2015); Lovskaya et al. (2015)). Dropping technique was used to produce starch aerogel beads by Kenar et al. (2014) from starch–sodium palmitate inclusion complexes. As expected from this technique, aerogel beads diameter was bigger (3.88 mm) and they showed high $S_{BET}$ of 362 $m^2$ $g^{-1}$.

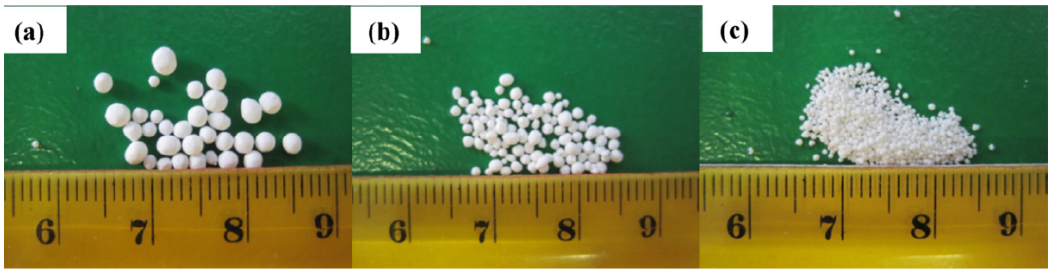


Figure 1.18 – Picture of starch aerogel particles of different sizes, obtained from emulsion-gelation method. Reprinted from García-González et al. (2012b), Copyright (2012), with permission from Elsevier.

Unlike starch aerogel, pectin aerogel beads were produced from several techniques including dropping (Veronovski et al. (2014)), emulsion (García-González et al. (2012c, 2015)), prilling (core pectin and shell alginate from De Cicco et al. (2016)) and Jet-Cutter (Preibisch et al. (2018)). All these techniques resulted in a very wide range of bead diameters from 200 µm (with emulsion) to 9.8 mm (with dropping). $S_{BET}$ seemed not to depend on the technique and varied from 440 $m^2$ $g^{-1}$ to 595 $m^2$ $g^{-1}$. Bio-medical applications were targeted in the study of pectin aerogel particles with regards to bio-compatibility, drug delivery and wound healing (García-González et al. (2012c); Veronovski et al. (2014); García-González et al. (2015)).

If one polysaccharide is famous for its "easy" shaping properties, it is alginate. Multiple methods were used to produce alginate aerogel beads and it almost always results in perfectly spherical particles. Marine polysaccharide, more broadly, were usually produced as beads. Dropping technique was the first and most used method to produce alginate, chitosan, chitin and carrageenan aerogel beads. There is a lot of literature reporting the use of dropping technique for these polysaccharides, Quignard

et al. (2008); Robitzer et al. (2008); Quignard et al. (2010); Ricci et al. (2010); Robitzer et al. (2011b,a); Kayser et al. (2012); Silva et al. (2013)). An example of marine polysaccharide beads obtained by dropping is given in Figure 1.19. Emulsion technique was also used for alginate and carrageenan polysaccharides leading to aerogel size ranging from 8 µm to 1400 µm (Alnaief et al. (2011); García-González et al. (2015); Menshutina et al. (2017); Alnaief et al. (2018)). The $S_{BET}$ was up to 680 $m^2$ $g^{-1}$ and 174 $m^2$ $g^{-1}$ for alginate and carrageenan, respectively. JetCutter technique was also used to produce alginate and carrageenan aerogel beads, along with the pectin aerogel beads (Preibisch et al. (2018)). As for other bio-aerogels, medical application were tested (Veronovski et al. (2013); García-González et al. (2015); Lovskaya et al. (2015); Obaidat et al. (2018)) and chitosan aerogels were most particularly exploited as catalyst (Valentin et al. (2003); Kayser et al. (2012)). Finally, a recent study proved the production of alginate aerogel particles to be possible at the industrial scale with emulsification technique which is a promising insight for the future of bio-aerogels (Baudron et al. (2019)).

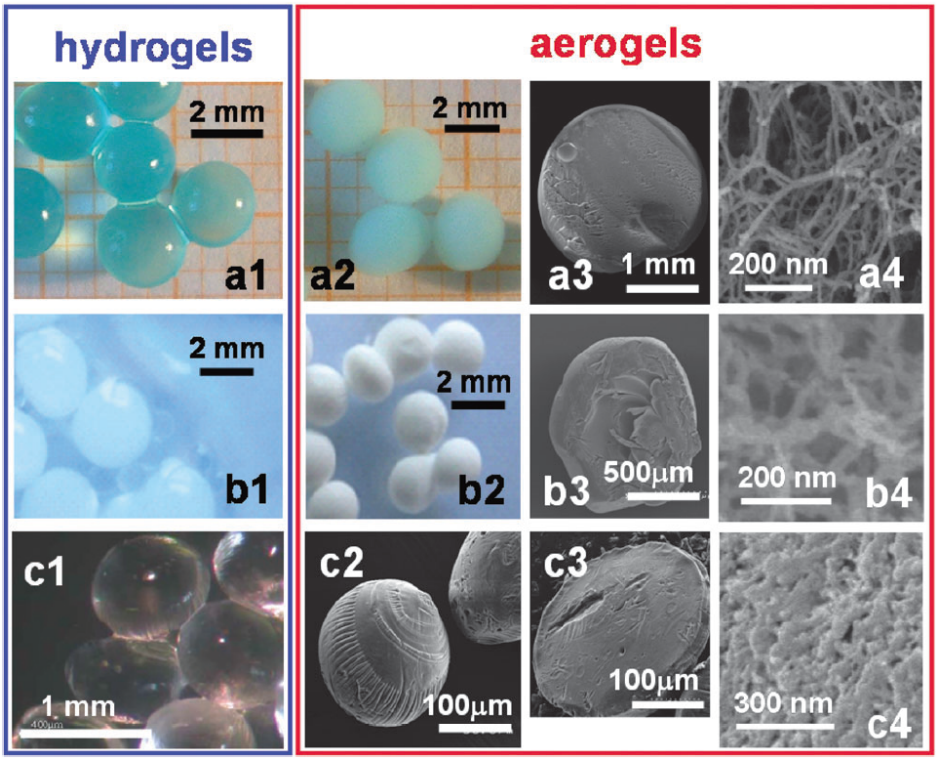


Figure 1.19 – Picture and morphology of hydrogel and aerogel beads from (a) alginate, (b) chitosan and (c) carrageenan, obtained from dropping technique. Reproduced from Quignard et al. (2008) with permission from the Centre National de la Recherche Scientifique (CNRS) and The Royal Society of Chemistry.

### Cellulose II aerogel beads

The first cellulose aerogel particles produced were made from cellulose xanthate (viscose) by dispersing the latter in a water soluble polymer solution (Ookuma et al.

(1993)). The obtained particles were then regenerated in acid and the latter was washed in water, exchanged for ethanol and then isoamyl acetate to proceed to Sc drying. Particles' size was below 500 µm, $S_{BET}$ was not measured but pores' diameter (measured with mercury porosimetry) ranged from 6 nm to 1 µm.

The second and most used technique for cellulose II aerogel beads production was the dropping technique. Innerlohinger et al. (2006) were the first to report the production of cellulose beads from a direct solvent with this technique. They used NMMO as solvent and water as coagulation bath, and obtained beads with diameter between 2 mm and 4 mm and $S_{BET}$ of beads were demonstrated to be higher than that of their monolithic counterparts. In the same article, authors reported using JetCutter to produce smaller beads (400 – 1200 µm diameter) but no further information was given.

Other solvents were used for the production of cellulose II aerogel beads by dropping. Sescousse et al. (2011b) demonstrated the importance of the dropping parameters (solution state, distance to coagulation bath, bath temperature) for the production of aerogels from NaOH-$H_2O$ solvents. The main conclusion was that the solution should withstand the "shock" with the coagulation bath when falling into it. Several parameters needed to be adjusted to improve beads' shape such as a higher viscosity of the solution, by slightly gelling the latter, or a higher coagulation bath temperature. The production of particles of aerogel precursor was performed by GeniaLab (most probably with the JetCutter) and studied in the work of Gavillon (2007). NaOH-$H_2O$ solvent was used to dissolve cellulose and sulphuric acid ($H_2SO_4$) was used as coagulation bath before replacing it by water and then acetone for Sc drying. The morphology of beads revealed the formation of a denser skin at their surface (see Figure 1.20).

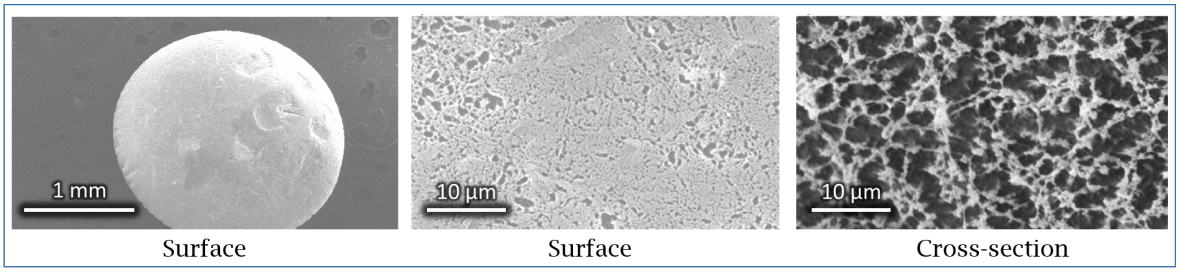


Figure 1.20 – Morphology of cellulose aerogel beads produced from the JetCutter technique. Different morphology can be observed between the surface and the cross-section. From Gavillon (2007).

Production of beads was also proven successful using additives in cellulose-NaOH-$H_2O$ solutions. Urea was used by Trygg et al. (2013, 2014) and urea-ZnO by Kamal Mohamed et al. (2015). In their first article, Trygg et al. (2013) varied cellulose concentration, coagulation bath acidity and temperature. They reported a decreasing shrinkage and increasing circularity with higher coagulation bath temperature and higher acid concentration. They also reported the decrease of $S_{BET}$ when decreasing

cellulose concentration and also when increasing bath temperature and acidity up to a certain concentration. Then, due to competing coagulation mechanism when acid is stronger, the $S_{BET}$ increases with further increase of the acid concentration. Kamal Mohamed et al. (2015) used ZnO of different concentrations in addition to urea. With increasing ZnO concentration, beads diameter was slightly decreasing (from 0.1% to 0.3% ZnO) and then increasing, overall beads' size varied from 2 mm to 2.5 mm. Density was following this trend with an increase from 0.082 g $cm^{-3}$ to 0.250 g $cm^{-3}$ between 0% and 0.4% ZnO and then density was relatively stable around 0.09 g $cm^{-3}$. $S_{BET}$ was reported to range from 323 $m^2$ $g^{-1}$ up to 407 $m^2$ $g^{-1}$ and also influenced by ZnO concentration, increasing up to 0.5% ZnO and then slightly decreasing. Maximum solubility of ZnO in 8% NaOH was given as the reason for the change in trends. The presence of non-dissolved ZnO would lead to less free zincate reducing the solubility of cellulose in the solvent.

Finally, IL was used as solvent for dropping cellulose solution in water coagulation bath (Voon et al. (2016)). The author reported using different nozzles inner diameter to obtain aerogel beads of diameter size varying from 0.4 mm to 2.2 mm. Interestingly, they also reported a decrease of the $S_{BET}$ from 498 $m^2$ $g^{-1}$ to 107 $m^2$ $g^{-1}$ with an increase of the beads size from 0.41 mm to 2.14 mm. The lower $S_{BET}$ for bigger beads was attributed to a *"higher packing density of their 3D nanofibrillar networks microstructure"* as compared to smaller beads (see Figure 1.21). This explanation still needs to be further confirmed but a similar behaviour was already observed earlier by Innerlohinger et al. (2006) between beads and monoliths. In a second article, Voon et al. (2017) tested the potential application of these beads as drug delivery systems.

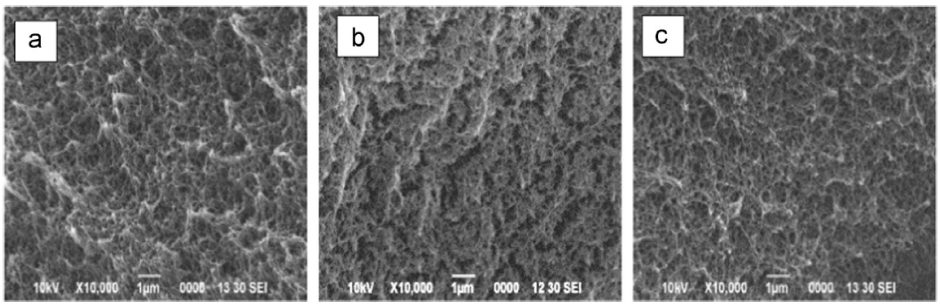


Figure 1.21 – Morphology of cellulose aerogel beads produced from dropping of cellulose-IL solutions in water coagulation bath. Different mean diameter of beads were obtained: (a) 0.41 ± 0.03 mm, (b) 0.83 ± 0.11 mm, and (c) 2.14 ± 0.08 mm. Reprinted from Voon et al. (2016), Copyright (2015), with permission from Elsevier.

Hence, as can be seen from this state of the art, research on the production of cellulose II aerogel beads is still at the beginning and a lot of efforts are needed to bring this material to a potential industrialisation.

# Conclusions

This chapter covered a wide range of topics. From polysaccharide to cellulose solution shaping and aerogel production as beads, we have seen the complexity of the problems to tackle in terms of making cellulose aerogel beads with various and controlled sizes and morphology.

First a brief overview of various treatments of wood are presented in the view of obtaining pulps. Depending on the treatment received (mechanical, chemical or both) pulps can have different content in cellulose, hemicelluloses and lignin. Then the background properties of cellulose are discussed. Cellulose is linear polysaccharide constituted of repetitive units of D-anhydroglucopyranose linked together through $\beta$-1,4-glycosidic bonds. Different allomorphs of cellulose exist which correspond to different chain arrangement and interactions. As an example, cellulose I is the native cellulose and its chains have a parallel alignment leading to intramolecular and intermolecular hydrogen bonds within and between chains. These interactions result in a polymer which is hard to dissolve. Cellulose II is obtained from mercerisation or dissolution and regeneration or coagulation of cellulose I and has an antiparallel chains' organisation.

Because cellulose aerogel beads are prepared via cellulose dissolution, cellulose solvents were presented focusing on those that will be used in this work. Solvents to dissolve cellulose can be categorised in two classes: derivatising ones and direct solvents (or non-derivatising). The first class implies the formation of cellulose derivative to enable its dissolution and then regeneration of the latter to recover pure cellulose. The famous viscose process is a member of this first class as cellulose xanthate derivative is produced and dissolved to finally be regenerated. On the contrary, direct solvents are dissolving cellulose without any chemical modification of cellulose. NaOH-$H_2O$ based solvent and ionic liquids will be used in this work and thus cellulose dissolution and solutions' properties in these two solvents are overviewed. NaOH based solvents are among the cheapest direct solvents but dissolution of cellulose in this media is limited to low concentrations and low degree of polymerisation. In addition, the obtained cellulose-NaOH-$H_2O$ solution is gelling with time and temperature which can make processing challenging. Other examples of direct solvents are ionic liquids. They are molten salts known to be able to dissolve a wide range of cellulose at various concentrations and DP. They are usually classified as green solvents but since a multitude of different ionic liquids can be produced, their properties and toxicity are expected to vary from one to the other. Shaping of the obtained cellulose solutions is an important step for the production of cellulose based materials. Indeed, once regenerated or coagulated, cellulose can no longer be easily shaped as desired. In this work we focused on cellulose materials shaped as beads or particles and we have seen two main methods

for their production: the formation of droplets in a gas phase or in an immiscible liquid phase. The first category regroups the simple laboratory scale dropping technique and the high production rate JetCutter technique. The second category is the well-known production of an emulsion. These techniques were detailed in this chapter and we have seen that each of them led to different droplets' sizes.

In the final section, the production and properties of porous materials based on polysaccharides and, more especially, cellulose were discussed. Different drying methods exist to produce porous materials and in this work we chose to classify materials by the type of drying they underwent rather than by their final properties. Hence, materials obtained from evaporative drying were called xerogels, the ones from freeze-drying were referred to as cryogels and finally, when supercritical drying was performed, the resulting materials were called aerogels. The properties of the obtained porous materials are very dependent on the drying technique used and we focused on aerogels' properties and potential applications. A broad overview was given on existing polysaccharide aerogels, such as starch, pectin or alginate based aerogels and a more detailed study of the properties of cellulose aerogels was performed. In particular, we have seen the influence of processing parameters on the resulting aerogels' properties; for example, the increase of density with increasing cellulose concentration. Finally, existing polysaccharide and cellulose aerogels shaped as beads were identified and the techniques used to produce them were described. It was obvious that for cellulose aerogel beads, the main technique used so far was the simple dropping. This opens a lot of possibilities for our work, and one of them is finding or adapting new methods to successfully produce cellulose aerogel beads from direct solvents.

# Chapter 2

# Materials and methods

## Contents

# Abstract

This chapter lists the products used in this work and gives global descriptions of methods and characterisation techniques used through this study. It should be noted that only the main principles are given here. For the sake of clarity, the particular chemicals used, their concentrations as well as the techniques developed and their setups are specified at the beginning of each corresponding chapter. Furthermore, it should be noted that all concentrations are given in weight percent (%) unless otherwise mentioned.

The first part of this chapter details the compounds used in this study such as the type of cellulose or the pulps prepared and kindly provided by RISE-Innventia. The solvents and chemicals are also listed together with their origin and purity.

The second part is dedicated to all methods used in the frame of this work. First the preparation techniques to produce cellulose aerogel and xerogel monoliths are given. Details on cellulose and pulps pre-treatments and their dissolution conditions in each solvent are provided. Gelation conditions, if relevant, and coagulation procedures are explained. The two types of drying, vacuum and supercritical drying are exhibited. Then, main descriptions and pictures of the shaping techniques that were used to produce aerogel beads and particles are given.

Finally, all techniques of characterisation are specified. Aerogels and xerogels are characterised by measuring their shrinkage during processing, their final bulk density, their specific surface area and morphology. Additional information on the porous materials produced could be obtained with X-ray diffraction, NMR and thermal conductivity measurements. In the case of beads and particles, methods to determine their diameter are also explained. Details on characterisation of solutions are given such as the rheological properties and surface tension. Final chemical composition of the aerogels and xerogels are also investigated and the methods used are provided at the end of the chapter.

# Résumé

Ce chapitre énumère les produits utilisés dans ce travail et donne une description globale des méthodes et des techniques de caractérisation utilisées tout au long de cette étude. Il convient de souligner que seuls les grands principes sont exposés ci-après. Dans un souci de clarté, les produits chimiques utilisés, leurs concentrations ainsi que les techniques développées et leurs réglages seront précisés au début de chaque chapitre correspondant. De plus, il est à noter que toutes les concentrations sont exprimées en pourcentage en poids (%), sauf indication contraire.

La première partie de ce chapitre détaille les composés utilisés dans cette étude tels que le type de cellulose ou les pâtes à papier préparées et aimablement fournies par RISE-Innventia. Les solvants et les produits chimiques sont également répertoriés avec des précisions sur l'origine et la pureté de chacun.

La deuxième partie est consacrée l'ensemble des méthodes utilisées dans le cadre de ce travail. Tout d'abord, les techniques de préparation pour produire les aérogels et les xérogels de cellulose sous forme de monolithes sont présentées. Des détails sur les prétraitements de la cellulose et des pâtes à bois ainsi que leurs conditions de dissolution dans chaque solvant sont fournis. Les conditions de gélification, si applicable, et les procédures de coagulation sont expliquées. Les deux types de séchage, le séchage sous vide et le séchage supercritique, sont présentés. Ensuite, les principales descriptions et images des techniques de mise en forme qui ont été utilisées pour produire des billes et des particules d'aérogels sont données.

Enfin, toutes les techniques de caractérisation sont précisées. Les aérogels et les xérogels sont caractérisés par la mesure de leur retrait pendant leur fabrication, leur densité apparente finale, leur surface spécifique et leur morphologie. Des informations complémentaires sur les matériaux poreux produits ont été obtenues par diffraction de rayons X, RMN et mesures de conductivité thermique. Dans le cas des billes et des particules, les méthodes de détermination de leur diamètre sont également expliquées. Des détails sur la caractérisation des solutions sont donnés, comme les propriétés rhéologiques et de tension superficielle. La composition chimique finale des aérogels et des xérogels est également étudiée et les méthodes utilisées sont données en fin de chapitre.

# 2.1 Materials

## 2.1.1 Polysaccharides

### Microcrystalline cellulose

Microcrystalline cellulose (MCC) Avicel®PH-101 was purchased from Sigma-Aldrich.

Avicel is obtained from wood (either hardwood or softwood) pulps by acid hydrolysis treatment. During this treatment the amorphous parts are hydrolysed and cellulose molecular weight is decreased. This results in a purified, more crystalline and partially depolymerised cellulose: the so-called microcrystalline cellulose. MCC degree of polymerisation (DP) thus depends on the treatment: the type of acid used, the time and the temperature. Avicel PH-101 obtained is a purified white powder with about 50 µm particles' size. Our MCC lot DP was 348. It was measured following the method described in Section 2.2.4 on page 109.

### Pulps

Softwood kraft pulps were kindly prepared, characterised and provided by RISE-Innventia (Stockholm, Sweden) and will simply be called "pulps" in the following.

Eight different pulps, with varying cellulose DP, hemicellulose and lignin contents were used to prepare pulp based aerogels. Table 2.1 on page 97 shows the different pulps' characteristics as well as the specific treatments they received to get these properties. The pulping method is described thereafter and the matter obtained at each stage, from the chips (left), to the unbleached pulp (middle) and to the bleached pulp (right), are given in Figure 2.1.

Figure 2.1 – Photo of the pulps after treatments: chips (left), unbleached pulp (middle) and bleached pulp (right). Photo taken by RISE-Innventia.

Cellulose DP was calculated from pulp intrinsic viscosity ($[\eta]$), measured by RISE-Innventia, following the same calculation as for MCC (see Section 2.2.4 on page 109). As hemicellulose and lignin also influence the viscosity, this calculated DP should be considered as an approximation of the actual DP of cellulose in the pulp.

Note that the names of pulps are composed of a number and letters. The number under brackets was given to differentiate the pulps from each other by "type" and the letters were chosen as a function of cellulose DP, hemicellulose and lignin contents. In this code, "h" stands for high and "l" for low. These letters are then ordered in the same way as the pulps' characteristics. For example, the first pulp described, (1)h-h-h, means that it's a type 1 pulp with (h) high cellulose DP, (h) high hemicellulose and (h) high lignin content. Another example could be the pulp (2)l-h-l which is a type 2 pulp with low cellulose DP, high hemicellulose and low lignin content. Abbreviation letters in the treatment stand for oxygen delignification (O), chlorine dioxide bleaching (D) and alkaline extraction stage (E). They are explained later in this section on pulp preparation process.

Table 2.1 – Pulps' characteristics and treatments.

| | | | | Pulp treatments | |
|---|---|---|---|---|---|
| **Pulp** | **DP** | **Hemicellulose (%)** | **Lignin (%)** | **Pulping process** | **Treatments** |
| **(1)h-h-h** | 1452 | 12.8 | 5 | Kraft cook to kappa no. 32<br>Pulp viscosity 950 mL/g | HCl 0.7 M, 90 °C, 70 min |
| **(1)l-h-h** | 755 | | | | HCl 1.0 M, 90 °C, 410 min |
| **(2)h-h-l** | 1328 | 16.5 | 0.9 | Kraft cook to kappa no. 28<br>Pulp viscosity 1180 mL/g | ODED, HCl 0.3 M, 90 °C, 60 min |
| **(2)l-h-l** | 770 | 7.4 | | | ODED, HCl 0.7 M, 90 °C, 420 min |
| **(3)h-l-h** | 1384 | 4.8 | 7 | Prehydrolysis and kraft cook kappa no. 45 Pulp viscosity 900 mL/g | HCl 0.6 M, 90 °C, 70 min |
| **(3)l-l-h** | 657 | | | | HCl 0.9 M, 90 °C, 180 min |
| **(4)h-l-l** | 986 | 2.1 | 0.8 | Prehydrolysis+kraft cook kappa no. 12 Pulp viscosity 630 mL/g | OODED |
| **(4)l-l-l** | 608 | | | | OODED, HCl 0.3 M, 90 °C, 90 min |

Pulps were treated and prepared at RISE-Innventia using kraft process. Spruce wood was firstly chipped. The chips, air-dried to a solids content of 93%, were screened and the fraction with a thickness of 2 to 8 mm was selected. The composition of the wood chips is given in Table 2.2. Note that "total lignin" is equal to the sum of "acid insoluble residue" and "acid soluble residue". Wood chips contained 10 mg $g^{-1}$ of extracts (extraction by acetone). The content of inorganic components was 0.33% (ash content, obtained at 525°C). The metals content is presented in Table 2.3.

Table 2.2 – Chemical composition of wood, in relative % of dry solids.

| Arabinose | Galactose | Glucose | Xylose | Mannose | Acid insoluble residue | Acid soluble residue | Total lignin |
|---|---|---|---|---|---|---|---|
| 1.1% | 1.9% | 46.4% | 5.3% | 12.5% | 32.0% | 0.7% | 32.7% |

Table 2.3 – Metal content in chips, in mg/kg of dry wood.

| Al | Ba | Ca | Cu | Fe | K | Mg | Mn | Na | P | S | Si | Zn |
|---|---|---|---|---|---|---|---|---|---|---|---|---|
| 2.3 | 14.1 | 1005 | 1.7 | 3.7 | 315 | 83 | 60 | 6.7 | 25 | 38 | 10.0 | 8.3 |

Chips in 500 g batches (given as dry weight) were subjected to cooking in steel digester with forced liquor circulation, heated by indirect heating in steam heat exchangers. The air within the digester and chips was evacuated by vacuum suction for 30 min.

The procedure of the pre-hydrolysis kraft cooking was started by adding water to the chips by suction to the digester. A pressure of 5 bar was applied by nitrogen gas over-night. The following day, the water-to-wood ratio was adjusted to 6:1 and the circulation of water and heating was started, increasing the temperature from room temperature to 170 °C by 5 °C $min^{-1}$. Temperature was maintained at 170 °C for 60 min, after which heating was stopped and the hydrolysate removed when the digester reached a temperature of 120 °C. Kraft cooking liquor with 25% effective alkali and 30% sulfidity was pumped into the digester to reach a liquor-to-wood ratio of 5:1. The cooking liquor was allowed to impregnate the chips for 30 min at 120 °C, then temperature was increased by 5 °C $min^{-1}$ to 160 °C remaining for 2 h (for type "3" pulps) or 3.5 h (for type "4" pulps).

The procedure of kraft cooking was started by removing excess water from the chips and adding kraft cooking liquor with 18% effective alkali and 35% sulfidity to reach a liquor-to-wood ratio of 4:1. The temperature was increased by 1 °C $min^{-1}$ to 160 °C and remained at this level for 3 h.

After completing kraft cooking, both with and without pre-hydrolysis stage, the delignified chips were washed in deionized water over-night and subsequently defibrillated in a water-jet defibrillator and screened in a Wennberg screen with 0.2 mm slits.

Oxygen delignification (O), was performed in Teflon-coated steel autoclaves adding oxygen gas to a pressure of 0.7 bar and 3.5% NaOH. Temperature was 120 °C and treatment time was 60 min.

Chlorine dioxide bleaching (D) was performed in plastic bags. Charge of chlorine dioxide was 2% in first stage and 1% in second D-stage (calculated as active chlorine). Temperature and time were 40 °C for 45 min and 75 °C for 120 min in first and second D-stages, respectively. The alkaline extraction stage (E) between the D-stages was performed at 90 °C for 90 min with a NaOH charge of 0.7%. The pulps were washed with deionized water between each bleaching stage.

#### Hemicellulose

Hemicellulose from softwood was kindly provided by RISE-Innventia. It contained approximately 60% glucomannan, 10% xylan and 3% lignin. It is a galactoglucomannan and arabinoxylan, probably with methyl uronic acid groups. Lignin is guaiacyl lignin.

### 2.1.2 Solvents, non-solvents and chemicals

As detailed in Chapter 1, Section 1.2.1 on page 57, cellulose can be dissolved in different solvents. Each solvent has its advantages and drawbacks and was chosen accordingly. In the following work, we have used two categories of solvents: aqueous based, i.e. NaOH based, and non-aqueous, i.e. ionic liquids (ILs).

#### NaOH based solvents

NaOH pellets with a purity > 98 % were purchased from Fischer Scientific. It was dissolved in distilled water prepared in Cemef - Mines ParisTech.

Two types of additives were used: ZnO with a ReagentPlus purity > 99.9 % purchased from Sigma Aldrich and urea with a purity > 99.5 % purchased from Fisher Scientific.

#### Ionic liquids

1-ethyl-3-methyl imidazolium acetate (Figure 2.2), called [Emim][OAc] in the following, was purchased from BASF. Dimethyl sulfoxide (DMSO), used as co-solvent, was purchased from Fischer Scientific (purity > 99.7%).

The ionic liquid, 1,5-diazabicyclo[4.3.0]non-5-enium propionate ([DBNH][Pr]), shown in Figure 2.3, was prepared in Cemef - Mines ParisTech from 1,5-Diazabicyclo[4.3.0]non-5-ene (DBN), purchased from Fluorochem, and propionic acid ($EtCO_2H$) with purity > 99%, purchased from Fisher Scientific. The synthesis is described in Chapter 3, Section 3.1.2 on page 117.

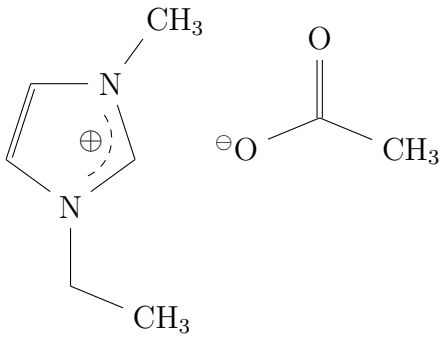

Figure 2.2 – Chemical representation of [Emim][OAc].

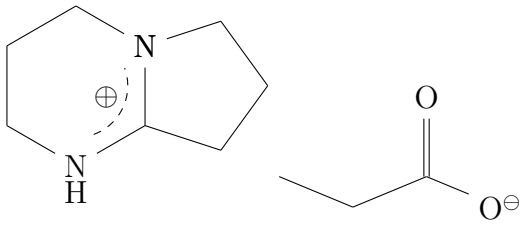

Figure 2.3 – Chemical representation of [DBNH][Pr].

### Coagulation bathes (non-solvents)

Cellulose was coagulated in the following non-solvents:

- Distilled water ($H_2O$), prepared in Cemef - Mines ParisTech.
- Absolute ethanol (EtOH) (purity > 99%).
- Propan-2-ol (isopropanol) (purity > 99.5%).
- Propan-2-one (acetone) (purity > 99%).
- Diluted to different extents 32% hydrochloric acid (HCl).
- Diluted to different extents glacial acetic acid (AA) (purity > 99%).

All chemicals were purchased from Fisher Scientific.

### Other chemicals

The emulsion continuous phase, paraffin liquid, was purchased from Fisher Scientific. Surfactant, sorbitane monooleate (Span 80) (Figure 2.4), was purchased from Alfa Aesar.

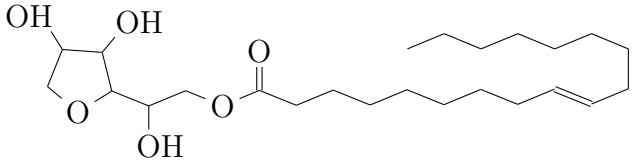

Figure 2.4 – Chemical representation of Span 80.

The cupriethylenediamine (CED), for cellulose dissolution and DP determination, was purchased from Merck.

## 2.2 Methods

### 2.2.1 Preparation of cellulose aerogel and xerogel monoliths

Figure 2.5 gives a schematic representation of the aerogel and xerogel preparation, from dissolution to the final aero- or xerogel, including the shaping methods. This figure will help to understand the following parts and will serve as a reference in the descriptions below.

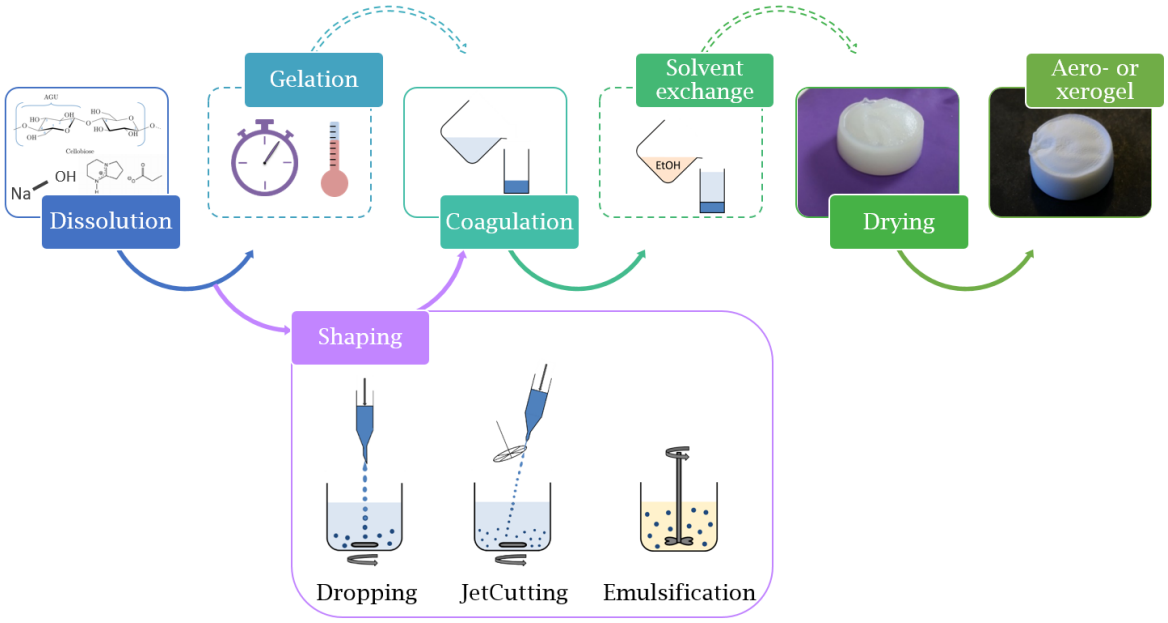


Figure 2.5 – Schematic representation of the process of aero- or xerogel preparation, from dissolution to the final material, including shaping methods.

#### Microcrystalline cellulose and pulp pre-treatment

Before use, MCC was dried at 50 °C under vacuum for at least 2 h to get rid of the moisture.

Pulps' moisture content was measured and taken into account in the concentration calculations for dissolution.

#### Dissolution in NaOH based solvents

MCC or pulp were placed in water at 5 °C for 2 h swelling. At the same time, NaOH was dissolved in water to get 20% solution concentration. If an additive was used, it was added to the NaOH solution while it was still warm from the exothermal reaction. Once all was dissolved, the produced solution was stored at -6 °C. Swollen cellulose and NaOH based solution were finally mixed together at 1000 rpm and -6 °C

for 2 h. The final cellulose and additive concentrations were varied and will be given in each case. NaOH concentration in water was always 8%.

### Dissolution in ionic liquids

Polysaccharides were dissolved in [DBNH][Pr] at 40 °C and 400 rpm stirring with a Heidolph RZR 50 overhead mixer for 24 h.

The same conditions were used for the [Emim][OAc] dissolution only the temperature was 75 °C. DMSO was added at room temperature to adjust solution viscosity.

### Solution gelation and coagulation

Only cellulose dissolved in NaOH based solvents can gel with time and temperature. If needed, gelation was carried out in a thermo-regulated Heraeus oven at 50 °C. Gelation times, i.e. time during which solution was kept at 50 °C, will be given for each case.

Coagulation of cellulose was induced by carefully pouring the desired non-solvent on the top of the solution or gel. The volume of non-solvent exceeded solution's volume for at least 5 times and it was kept for diffusion for at least 24 h. The coagulated sample was then washed several times (at least 5 times every 12 h) to remove cellulose solvent. In the case when cellulose was dissolved in ionic liquid, the electrical conductivity of the bath was checked to insure a complete washing of the ionic liquid.

When it was required, the non-solvent was replaced by EtOH with multiple solvent exchanges (at least 5).

### Supercritical drying

$CO_2$ supercritical (Sc) drying was performed in PERSEE Mines ParisTech.

The samples in EtOH were placed in the 1 L autoclave (Figure 2.6 on the following page). The latter was filled with EtOH to avoid drying of the samples during the Sc drying preparation.

Firstly, the system was pressurized at 50 bar and 37 °C with gaseous $CO_2$ while the EtOH was slowly drained from the autoclave. Afterwards, the pressure in the autoclave was increased to 80 bar to be above the $CO_2$ critical point (72.8 bar at 31.1°C) so the Sc $CO_2$ can solubilise the residual non-solvent inside samples' pores. Two dynamic washing steps were then performed for 1 h and 2 h at 80 bar and 37 °C with a $CO_2$ output of 5 kg $h^{-1}$. In between the dynamic washing steps a static mode was used, with no $CO_2$ output, of 1 to 2 h in the same conditions of pressure and temperature. Finally, the system was slowly depressurised at 4 bar $h^{-1}$ and 37 °C, and cooled down to room temperature before being opened to collect the samples.

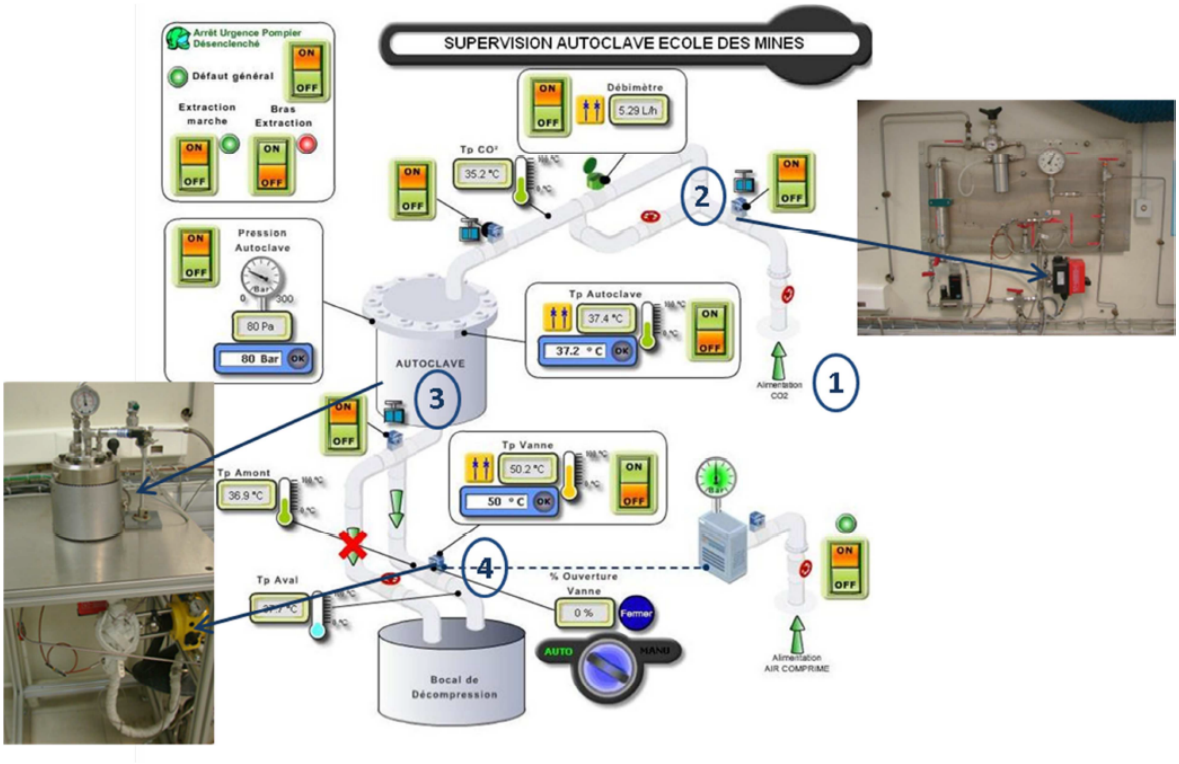


Figure 2.6 – Laboratory-scale supercritical $CO_2$ drying device in PERSEE Mines ParisTech. (1) $CO_2$ supply, (2) Feeding valve, (3) autoclave, (4) depressurisation valve. Courtesy of Pierre Ilbizian, PERSEE Mines ParisTech.

#### Vacuum drying

To ensure homogeneous drying under low vacuum, the samples were disposed on a regularly perforated grid. It was then directly placed in an oven at 50 °C, under primary vacuum for 24 h.

### 2.2.2 Cellulose aerogel shaping as beads

Shaping as beads and particles was done before coagulation of cellulose with different methods, as represented in Figure 2.5. All detailed parameters of the device for bead preparation will be provided in the corresponding chapters. Below, only general information is given.

#### Dropping technique

The dropping technique is a laboratory scale technique to produce beads. The principle is to simply drop cellulose solution into a coagulation bath. A schematic representation of the dropping technique as well as a picture of the device built in Cemef Mines ParisTech is given in Figure 2.7.

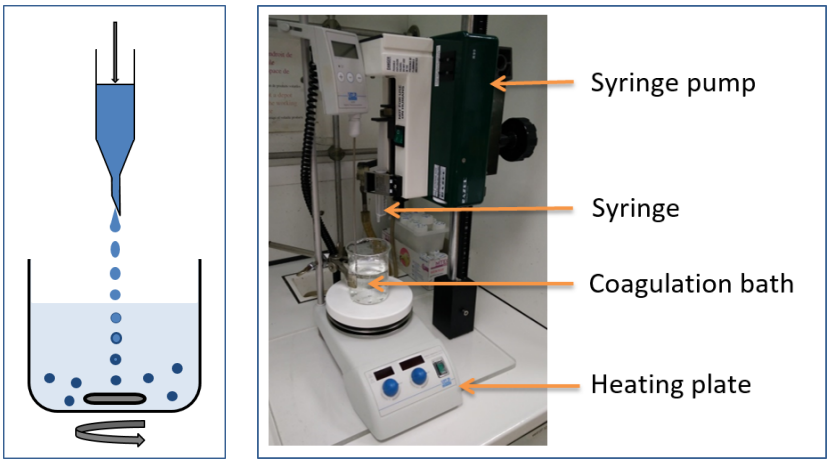


Figure 2.7 – Schematic representation (left) and picture (right) of the dropping device built in Cemef Mines ParisTech.

### JetCutter technology

JetCutter Type S from GeniaLab®, Germany, was used for the shaping of beads with diameters of few hundreds of micrometers. JetCutter was used at the location of DLR (Aerogel department, German Aerospace Center, Institute for Materials Research, Cologne, Germany) and RISE-Innventia (Stockholm, Sweden). Schematic representation and pictures of the JetCutter and its tools are shown in Figure 2.8.

As explained in Chapter 1, the principle of the JetCutter consists of cutting a jet of solution with high speed rotating wires. The jet cut into "cylinders" form spheres which are collected in a bath (here, different cellulose non-solvents were used).

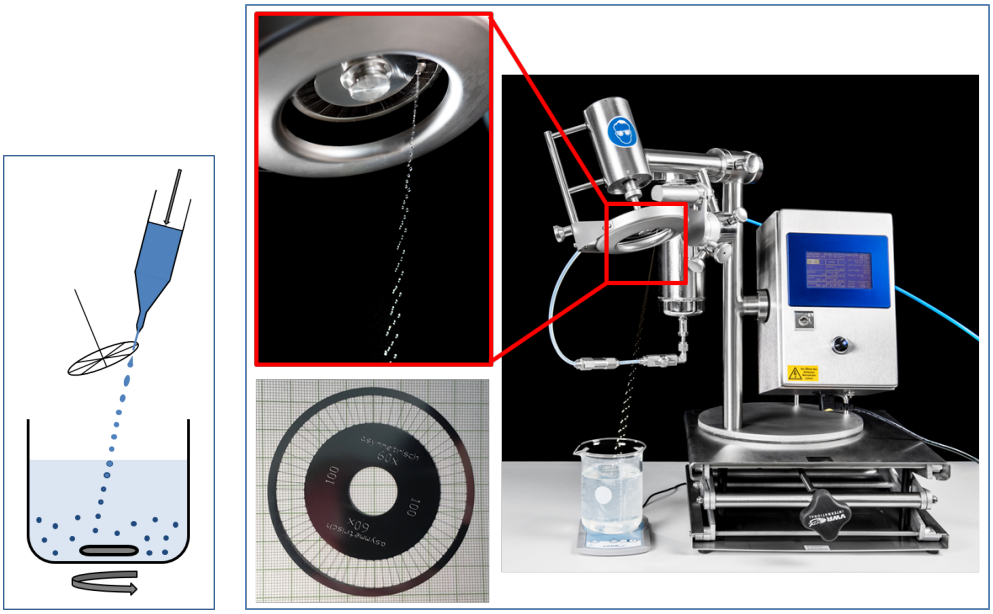

Figure 2.8 – Schematic representation (left) and pictures of the JetCutter (right) and one of the cutting tools used (bottom middle). Pictures provided by GeniaLab (Germany).

### Emulsification technique

The emulsification technique was used to produce cellulose aerogel beads in micrometer scale. This technique consists of dispersing a solution in a non-miscible continuous phase by high stirring speed. The dispersed phase will form droplets of a given size once the emulsion is stable. Surfactants can be used to help to stabilise the emulsion and reduce the size of the droplets.

The emulsification technique was adapted to answer the requirements of the cellulose aerogel beads production. Figure 2.9 shows the schematic representation of the emulsion technique developed.

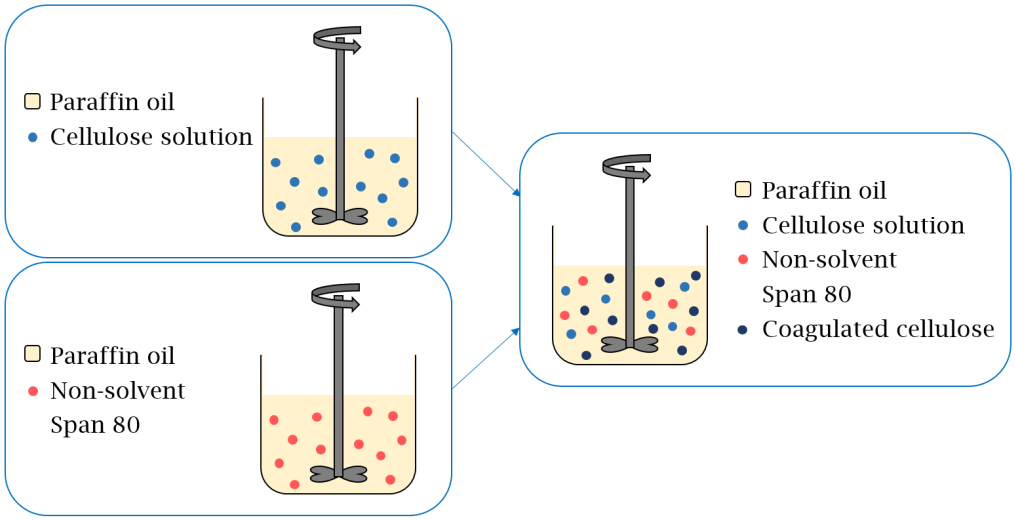


Figure 2.9 – Schematic representation of the adapted emulsion technique used for cellulose beads production.

First, cellulose solution and non-solvent were mixed with oil in two separate emulsions and stabilized separately. Then, the two emulsions were mixed together to trigger cellulose coagulation. Finally, cellulose wet beads were separated from the continuous phase by centrifugation, washed in EtOH and dried under Sc $CO_2$ conditions. All details of the process will be described in the corresponding Chapter 4 on page 139.

## 2.2.3 Aerogels and xerogels characterisation

### Shrinkage

The shrinkage of aerogels and xerogels represents the loss in volume between the cellulose solution and the dried matter. Shrinkage happens during the coagulation and the Sc or vacuum drying. In this work, we will only consider the overall shrinkage, which is the difference between the volume of solution and the final aero- or xerogel's volume. The shrinkage can be expressed as stated in the following Equation (2.1):

$$Shrinkage = \frac{V_{ini} - V_{final}}{V_{ini}} \tag{2.1}$$

with $V_{ini}$ the volume of the solution, and $V_{final}$ the volume of the resulting aero- or xerogel.

### Density

The bulk density ($\rho_{bulk}$) is defined as the ratio of mass to volume:

$$\rho_{bulk} = \frac{m}{V} \tag{2.2}$$

with $m$ being sample mass and $V$ its volume. When the samples had a regular size, their density was calculated from Equation (2.2) by measuring their mass and volume. However, when samples' shape was not well defined or when they were shaped as beads or particles the measurement uncertainty was too high and power densitometer Micromeritics Geopyc 1360, with DryFlo powder was used. The chamber was 19.1 mm diameter, and the force applied was 25 N. The error was less than 10%.

### Porosity and pore volume

Porosity (Equation (1.6) on page 75) and theoretical specific pore volume ($V_{pores}$, Equation (1.7) on page 75) can be calculated using bulk density ($\rho_{bulk}$) and cellulose skeletal density ($\rho_{sk}$), which is equal to 1.5 g cm$^{-3}$ for neat cellulose (Kamal Mohamed et al. (2015); Rudaz (2013)).

### Morphological observations

The morphology of aerogels was studied by with Scanning Electron Microscopy (SEM) using a Supra40 Zeiss microscope with a Field Emission Gun (Figure 2.10). The observations were done with diaphragms from 7.5 µm to 20 µm diameter and the acceleration voltage was set between 1 kV and 3 kV. Prior to the observations, a 7 nm layer of platinum was applied on the surface of the samples with a Q150T Quarum metalliser (Figure 2.10) to prevent the accumulation of electrostatic charges.

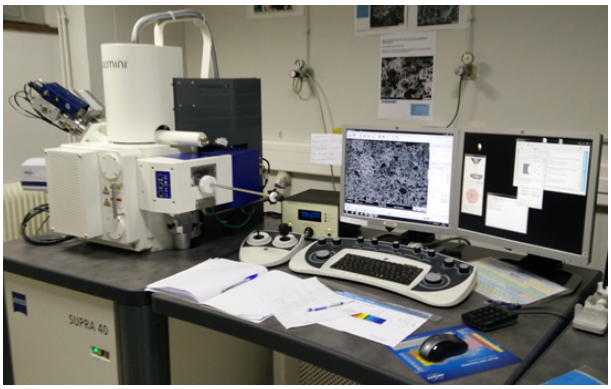

Supra40 Zeiss microscope

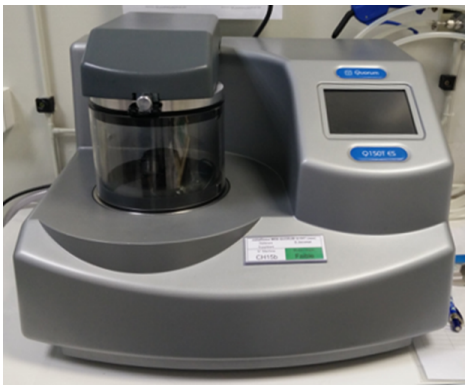

Q150T Quarum metalliser

Figure 2.10 – Scanning electron microscope and metalliser.

### Specific surface area measurements

The specific surface area ($S_{BET}$) was measured with an ASAP 2020 from Micromeritics using nitrogen adsorption and BET method. The samples were degassed under high vacuum at 70 °C for 10 h prior to measurements. The error was within ± 20 $m^2$ $g^{-1}$ .

### Beads measurements

Beads' size distribution was built by image analysis. Images of the beads were taken with an Epson Perfection V550 Photo Color Scanner in transmission mode, in 8-bits greyscales with a 6400 dpi resolution (4 µm $pixel^{-1}$). The images obtained were then analysed with the ImageJ software: the segmentation of the image was adjusted manually with a fixed grey level threshold to differentiate each bead from the background. Using "Analyse particles" tool of ImageJ, the beads were labelled, and their surface area measured. The beads were considered spherical in the first approximation and their diameter was calculated from the area. For each formulation at least 100 beads were analysed.

When the size was below 100 µm, particles were measured from SEM images.

### X-ray diffraction

Wide-angle X-ray diffraction (XRD) was measured with a XPERT-PRO diffractometer system with ScanPixcel measurement program, both from PANalytical. Measurements were performed at electron voltage of 45 kV and current of 30 mA with a Cu anticathode ($K_{\alpha 1}$ $\lambda = 1.5406$ $\mathring{A}$). The diffraction patterns were recorded in a continuous single scan from 4° to 70° with 0.08° steps in the $2\theta$ range.

Spectra were analysed with HighScore software from PANalytical. Peaks were deconvoluted between $2\theta = 10°$ and 30° to avoid the low angle uncertainty and to exclude Zn peaks, as shown on the example of Figure 2.11.

The crystallinity Index (Cr.I.) was estimated using the Hermas-Weidinger method as in Ciolacu et al. (2011), with the following Equation (2.3):

$$Cr.I.(\%) = \frac{I_c}{I_a + I_c} * 100 \tag{2.3}$$

with $I_c$ the integrated area of the crystalline phase and $I_a$ the integrated area of the amorphous phase.

Solid samples were ground to fine powder before analysis and placed on the sample holder, leading to random orientation of the particles. Surface had to be very smooth and aligned with the sample holder's borders. Irregular sample surface can lead to peak shift and incertitude in the resulting analysis.

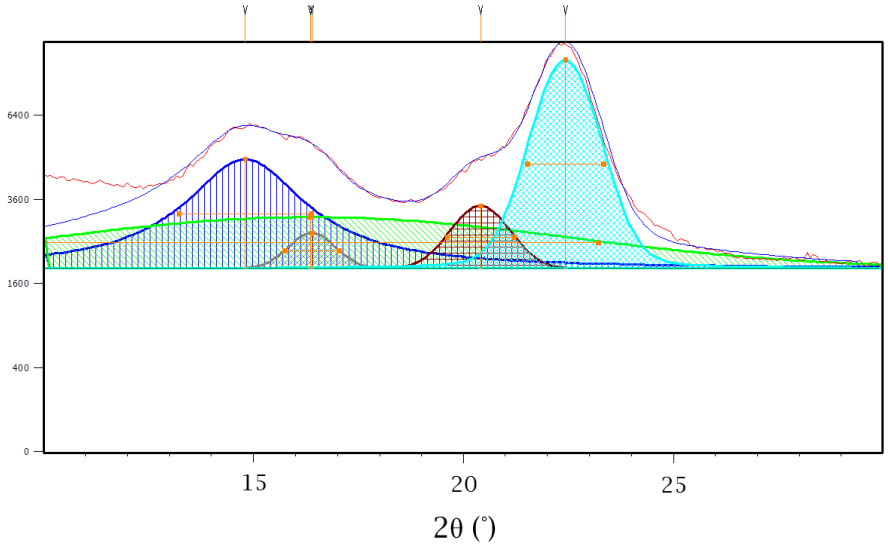


Figure 2.11 – Example of peaks' deconvolution with the HighScore software for MCC.

### NMR spectroscopy

Pulp aerogels' crystallinity was measured by solid state NMR analysis in RISE-Innventia. CP/MAS $^{13}$C-NMR spectra were recorded with a Bruker Avance III AQS 400 SB instrument operating at 9.4 T, filled with a double air-bearing two-channel probe head. Samples were packed uniformly in a 4 mm zirconium oxide rotor. All measurements were performed at 296 (± 1) K. The MAS rate was 10 kHz. Acquisition was performed with a CP pulse sequence using a 2.95 µs proton 90° pulse, an 800 µs ramped (100 - 50%) falling contact pulse and a 2.5 s delay between repetitions. A SPINAL64 pulse sequence was used for $^{1}$H decoupling. Hartman-Hahn matching procedure was performed on glycine and the chemical shift scale was calibrated to TMS ($(CH_3)_4Si$) by assigning the data point of maximum intensity in alfa-glycine carbonyl signal a chemical shift of 176.03 ppm (Larsson et al. (1997); Wickholm et al. (1998)).

### Moisture sorption

The moisture sorption isotherms were measured with a Dynamic Vapor Sorption (DVS) equipment from Surface Measurement Systems Ltd by RISE-Innventia. It was equipped with a microbalance to register the mass of sample throughout the sorption process.

Samples used were powders of aero- or xerogels of about 10 mg. Samples were dried at 0% RH until no weight loss was detected before being tested.

Relative humidity (RH) was varied between 0% and 80% at 30 °C for 3 cycles. The duration of each step was 500 minutes for a total of 50 hours.

Equation (2.4) gives the change in mass (in percent) with $m_t$ the sample mass at

time t, and $m_{dry}$ the mass of the dry sample.

$$Change\ in\ mass\ (\%) = \frac{m_t - m_{dry}}{m_{dry}} * 100 \tag{2.4}$$

**Thermal conductivity**

A Fox150 thermal conductivity meter (Laser Comp) equipped with a custom "micro flow meter cell" developed for small samples by CSTB (Grenoble, France) was used to measure thermal conductivity in PERSEE Mines ParisTech (see details in Rudaz et al. (2014)). Calibration was performed in accordance with the European Norm EN 12667 using Spaceloft® aerogel from Aspen (thickness: 3.70 mm, thermal conductivity: 13.3 mW $m^{-1}$ $K^{-1}$ at 20 °C).

### 2.2.4 Other characterisation techniques

**Viscosity measurement and determination of cellulose degree of polymerisation**

The MCC intrinsic viscosity ($[\eta]$) was measured by dissolution in cupriethylenediamine (CED) following the SCAN-CM standard 15:88 which complies with the requirements of the ISO 5351. Viscosity of solvent and cellulose solutions was measured with a LAUDA iVisc viscometer equipped with an Ubbelohde-type viscometer.

DP can be deduced from intrinsic viscosity thanks to Mark-Houwink-Sakurada equation (Equation (2.5)) which gives an estimation of the viscosity average DP (shortened in DP in the following), as a function of the intrinsic viscosity ($[\eta]$) and two empirical constants, $K'$ and $a$, which depend on the solvent used to dissolve cellulose (Evans and Wallis (1989); Scandinavian Pulp (1988)).

$$(DP)^a = K' * [\eta] \tag{2.5}$$

Different values for $K'$ and $a$ are proposed in the literature. Table 2.4 on the next page presents four suggestions for these constants and examples of DP for each.

Most of the standards suggest to use the Mark-Houwink equation for the DP calculation with, among others, the constants K' = 0.75 and a = 0.905. However, according to Van Heiningen et al. (2004), the cellulose DP values of pulps calculated from most of the equations given in the "Tests Method SCAN-CM" (Scandinavian Pulp (1988)), and especially from the constants K' = 0.75 and a = 0.905, are underestimating the cellulose DP because of the degradation in the solvent used (CED). The constants proposed by Evans and Wallis (1989) seem to give the closest values of DP compared to DP calculated from solvent which does not degrade the cellulose.

This is why, in this work, all cellulose DP were calculated from the Evans and Wallis (1989) constants ($(DP)^{0.90} = 1.65 * [\eta]$).

Table 2.4 – Different constants in Equation (2.5) for DP calculation (Evans and Wallis (1989); Scandinavian Pulp (1988)) and the corresponding DP.

| **Method** | Evans-Wallis (1989) | SCAN C15:62 | Marx-Figini DP < 950 | Marx-Figini DP > 950 |
|---|---|---|---|---|
| **K'** | 1.65 | 0.75 | 2.38 | 0.44 |
| **a** | 0.90 | 0.905 | 1 | 0.76 |
| **DP for $[\eta]$=100** | 291 | 118 | 238 | - |
| **DP for $[\eta]$=250** | 805 | 325 | 595 | - |
| **DP for $[\eta]$=450** | 1548 | 622 | - | 1047 |

### Rheological measurements

All rheological measurements were performed on a Bohlin Gemini rheometer. The geometry was adapted as a function of solutions and measurements and will be detailed in the corresponding chapters. The temperature was controlled with a Peltier temperature control system.

### Rheo-optical observations

A rheo-optical device was used to observe droplets under shear in a continuous phase. Cemef Mines ParisTech developed counter-rotating rheo-optical device consisting of a shear cell with transparent plates and a microscope (Metallux 3, Leitz) equipped with a camera (Sony DXC 107 AP), to record images. A schematic representation of the device is given in Figure 2.12. More details can be found elsewhere: Desse et al. (2009); Le Duc et al. (2011).

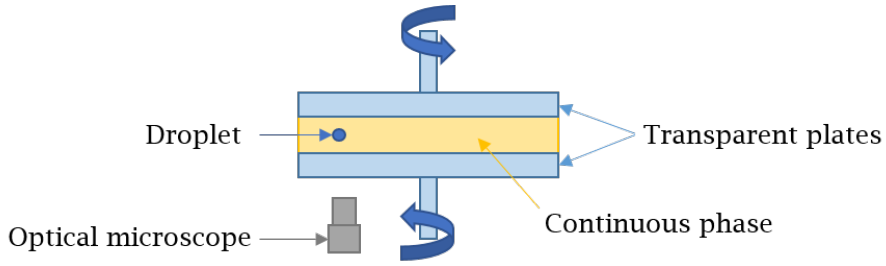


Figure 2.12 – Schematic representation of the rheo-optical device developed and used in Cemef Mines ParisTech.

Plates had a diameter of 40 mm and their rotation speed was controlled individually. The image recorder took around 25 pictures per second allowing an accurate analysis of the droplet movements and deformations all through the experiment. Details on the droplet, continuous phase and rheo-optical settings will be given in the corresponding chapter (Chapter 4, Section 4.1.2 on page 145).

### Interfacial tension measurements

The interfacial tension of liquids was measured using the pendant drop method with a Drop Shape Analyzer (DSA100B). The drop analyser software was DSA v 1.92 Drop Shape Analysis (Krüss GmbH, Hamburg, Germany). The values of the interfacial tension were taken after an equilibration time of 5 minutes maximum for each drop. Interfacial tension was measured several times per droplet.

### Determination of carbohydrates and lignin composition in the pulps

Samples were kindly analysed by RISE-Innventia according to the SCAN-CM 71:09. Briefly, the samples were hydrolysed at 121°C in an autoclave with 0.4 M $H_2SO_4$. The solubilised monosaccharides were quantified using an high-performance anion exchange chromatography coupled to a pulsed amperometric detector (IC-PAD). Acid-insoluble residue was determined gravimetrically according to TAPPI T222 om-11. The acid-soluble residue was measured by UV spectrophotometry at 205 nm according to TAPPI UM 250. MilliQ water was used as blank and for the dilution of hydrolysate. The content of acid-soluble residue was calculated using the absorptivity coefficient 110 L $g^{-1}$ $cm^{-1}$.

### Metal content measurements

Two methods based on elemental analysis were used to measure the concentration of metals in aerogels and xerogels.

In Chapter 5, *Lightweight and mesoporous cellulose xerogels*, metals content in xerogels was measured by Nestlé Quality Assurance Centre Nunspeet using method "HI00.1500.120".

In Chapter 6, *Pulp based aerogels*, the content of inorganics (metals) in pulp aerogels was measured from ash content, obtained at 525°C by RISE-Innventia.

# Conclusions

Compounds and methods used and developed in this study were presented in this chapter. Microcrystalline cellulose and pulps (with different cellulose content and DP, hemicellulose and lignin contents) provided by RISE-Innventia were used as starting material to produce aerogels and xerogels. Two types of solvents were employed: NaOH-water solvent without and with additives (urea or ZnO), and ionic liquids, namely, [Emim][OAc] and [DBNH][Pr].

The procedure to prepare cellulose and pulp aerogel and xerogel monoliths was detailed. Briefly, MCC is treated to get rid of moisture while pulps moisture content was measured and taken into account for dissolution. The raw materials were then dissolved either in NaOH-based solvents at low temperature and high stirring rate, or in ionic liquid under mild heating and stirring. In the case of dissolution in NaOH-based solvents, cellulose solution was gelled at 50 °C for different periods of time. When dissolved in ionic liquids, no gelation occurs and coagulation was performed by gently pouring the non-solvent on the top of cellulose solution. The same coagulation procedure was applied to both cellulose-NaOH-$H_2O$ based solutions and gels. After coagulation, if the coagulated cellulose monoliths were not already in ethanol they were transferred in the latter for the subsequent supercritical or vacuum drying.

The techniques used to shape cellulose solutions were described. Three different methods were employed:

- The simple dropping technique, which consists on dropping cellulose solution, through a syringe equipped with a needle, directly into a coagulation bath.
- The up-scalable JetCutting technology, with which the cellulose solution is extruded under pressure through a nozzle to produce a jet of solution that is cut by a cutting tool (high-speed rotating wires). The droplets of cellulose solutions fall in a coagulation bath.
- The last method used was the emulsification. This technique was adapted to our cellulose solutions by introducing the concept of separate emulsions. Two emulsions were prepared by mixing oil with cellulose solution in one, and with non-solvent in the other. Then the two emulsion produced were mixed together to get cellulose coagulated particles.

Finally, the way the obtained aerogel and xerogel monoliths and beads were characterised was described. Density was measured in two ways, either with simple volume and mass measurement or with the Geopyc device. Specific surface area was calculated using BET approach and morphology was observed by scanning electron microscopy. Other characterisation methods used were described such as the rheo-optical device to observe droplets under shear in oil continuous phase or the Bohlin Gemini rheometer to measure the viscosity of solutions and their gelling properties.

# Chapter 3

# Rheology of cellulose-[DBNH][Pr] solutions and shaping into aerogel beads

## Contents

# Abstract

Until now, cellulose aerogels were produced in the form of monoliths mostly because of the ease of preparation on laboratory scale. However, for many practical applications (food, cosmetics, medical...) the shape of particles is preferable. The shaping into particles also greatly reduces the time and costs of each processing step (solvent exchange, drying). Making cellulose beads is known since a long time for various applications. However, in most of the cases they are used either in the “wet state” (never dried) or, if dried, this is done, at ambient conditions which results in a non-porous material.

Multiple techniques are used to make beads from cellulose solutions, from the classical dropping of solution with a syringe (Sescousse et al. (2011b); Trygg et al. (2013, 2014); Kamal Mohamed et al. (2015); Voon et al. (2016)) to the emulsion method (Luo and Zhang (2010a); Zhang et al. (2018); Lin et al. (2009)). A review summarises various ways to produce cellulose beads (Gericke et al. (2013)). Yet, very few is reported on the whole production “chain” from the cellulose dissolution to the bead shaping and to the resulting aerogel properties. The majority of publications use "simple" dropping method to obtain beads. Even less is known on using ionic liquids for making cellulose aerogels in the form of beads. It seems there is only two publications, by the same authors, reporting making cellulose aerogel beads from ionic liquid (1-allyl-3-methylimidozoium chloride solution), and this was done by dropping (Voon et al. (2016, 2017)). Ionic liquids are powerful cellulose solvents, with negligible vapour pressure, allowing cellulose derivatisation in homogeneous conditions (El Seoud et al. (2007)) and spinning fibers from dissolved lignocellulose (Ma et al. (2015)). Ionic liquids have strong advantages against NaOH-water based solvents: they allow the dissolution of high molecular weight cellulose and no gelation occurs with time and temperature increase (Budtova and Navard (2016)).

The goal of this work was to demonstrate the feasibility of making cellulose II aerogel beads from cellulose-ionic liquid solutions using a processing method which can be easily up-scaled: the JetCutter.

In the results section, first, the rheological properties of cellulose-[DBNH][Pr] solutions were investigated in details to validate the selection of this IL to be used in JetCutter processing conditions. Classical polymer physics principles are used to interpret the results obtained. Finally, cellulose aerogel beads were prepared using the JetCutter technology and characterised by aerogel standards. The properties and morphology of beads were compared with those for cellulose aerogel monoliths made from the same solutions.

# Résumé

Jusqu'à présent, pour des raisons de facilité de préparation à l'échelle du laboratoire, les aérogels de cellulose étaient produits sous forme de monolithes. Cependant, pour de nombreuses applications (alimentaire, cosmétique, médicale...), il est préférable de les produire sous forme de particules. De plus, la préparation d'aérogels sous forme de particules réduit considérablement le temps et les coûts de chaque étape de production (échange de solvant, séchage...). La fabrication de billes de cellulose est connue depuis longtemps pour diverses applications, cependant, dans la plupart des cas, les billes sont utilisées soit à l'état "mouillé" (jamais séché), soit si elles sont séchées, elles le sont dans des conditions ambiantes, ce qui donnent un matériau non poreux.

De multiples techniques sont utilisées pour fabriquer des billes à partir de solutions de cellulose, allant du "goutte-à-goutte" classique avec une seringue (Sescousse et al. (2011b); Trygg et al. (2013, 2014); Kamal Mohamed et al. (2015); Voon et al. (2016)) au procédé d'émulsification (Luo and Zhang (2010a); Zhang et al. (2018); Lin et al. (2009)). Une étude par Gericke et al. (2013) résume les différentes façons de produire des billes de cellulose. Pourtant, très peu de choses sont rapportées sur l'ensemble de la "chaîne" de production, de la dissolution à la mise en forme des billes pour finir par les propriétés des aérogels qui en résultent. La majorité des publications utilisent la méthode simple du "goutte-à-goutte" pour obtenir des billes et on en sait encore moins sur l'utilisation des liquides ioniques pour la fabrication de billes d'aérogels de cellulose. Il semble qu'il n'y ait que deux publications faisant état de la fabrication de billes d'aérogel de cellulose à partir de liquide ionique (chlorure de 1-allyl-3-méthylimidozoium), et elles ont été faites par goute-à-goute avec une seringue (Voon et al. (2016, 2017)). Les liquides ioniques sont des solvants très efficassent pour la cellulose, avec une pression de vapeur négligeable, permettant la dérivatisation de la cellulose dans des conditions homogènes (El Seoud et al. (2007)) et le filage de fibres à partir de lignocellulose dissoute (Ma et al. (2015)). Les liquides ioniques présentent d'importants avantages par rapport aux solvants à base de NaOH-eau : ils permettent la dissolution de cellulose à haute masse moléculaire sans qu'aucune gélification ne se produise (Budtova and Navard (2016)).

L'objectif de ces travaux était de démontrer la faisabilité de la fabrication de billes d'aérogel de cellulose à partir de liquide ionique en utilisant une méthode de production qui peut être facilement industrialisée : le "JetCutter". Les propriétés rhéologiques des solutions de cellulose-[DBNH][Pr] ont été étudiées en détail pour valider la sélection de ce liquide ionique pour son utilisation dans les conditions de production du JetCutter. Les principes classiques de la physique des polymères sont utilisés pour interpréter les résultats obtenus. Enfin, des billes d'aérogel de cellulose ont été préparées à l'aide de la technologie JetCutter et caractérisées en suivant les standards des aérogels. Les propriétés et la morphologie des billes d'aérogel ont été comparées à celles des aérogels de cellulose sous forme de monolithe, issus des même solutions.

# 3.1 Materials and methods

## 3.1.1 Materials

MCC, Avicel®PH-101, was dissolved in two different ionic liquids: [Emim][OAc] and [DBNH][Pr]. Both MCC and ILs were described in Section 2.1.1 on page 95 and Section 2.1.2 on page 99, respectively.

We used three different non-solvents: $H_2O$, EtOH and isopropanol. All were described in Section 2.1.2 on page 100.

## 3.1.2 Methods

### Ionic liquid synthesis

The ionic liquid, 1,5-Diazabicyclo[4.3.0]non-5-enium propionate ([DBNH][Pr]), was prepared before each experiment to prevent any influence of ageing. $EtCO_2H$ and DBN were mixed at a 1:1 molar ratio according to procedure described by Parviainen et al. (2013): $EtCO_2H$ was slowly added to DBN under nitrogen atmosphere and 400 rpm magnetic stirring, in an ice bath, as far as the reaction is exothermal. Temperature was controlled throughout the reaction so that it did not exceed 30 °C. Stirring was maintained at least 30 min after all $EtCO_2H$ was added to insure a complete reaction. The ionic liquid obtained was transparent and slightly yellowish.

[DBNH][Pr] was characterised with $^1$H NMR in DMSO-$d_6$ using a Varian 300 MHz Unity spectrometer (Department of Chemistry, University of Helsinki). Full and expanded spectra are shown in Figure 3.1 on the next page together with assigned peaks. The $^1$H NMR data are consistent with those reported previously by Parviainen et al. (2013, 2015):
$^1$H NMR (600 MHz, DMSO-$d_6$, 27 °C): $\delta$ 0.90 (t, $J$ = 7.6 Hz, 3H), 1.83 (m, 2H), 1.89 (q, $J$ = 7.6 Hz, 2H), 1.97 (m, 2H), 2.72 (t, $J$ = 7.9 Hz, 2H), 3.24 (t, $J$ = 5.7 Hz, 2H), 3.31 (t, $J$ = 5.8 Hz, 2H), 3.49 (t, $J$ = 7.1 Hz, 2H), 12.66 (br s, 1H).

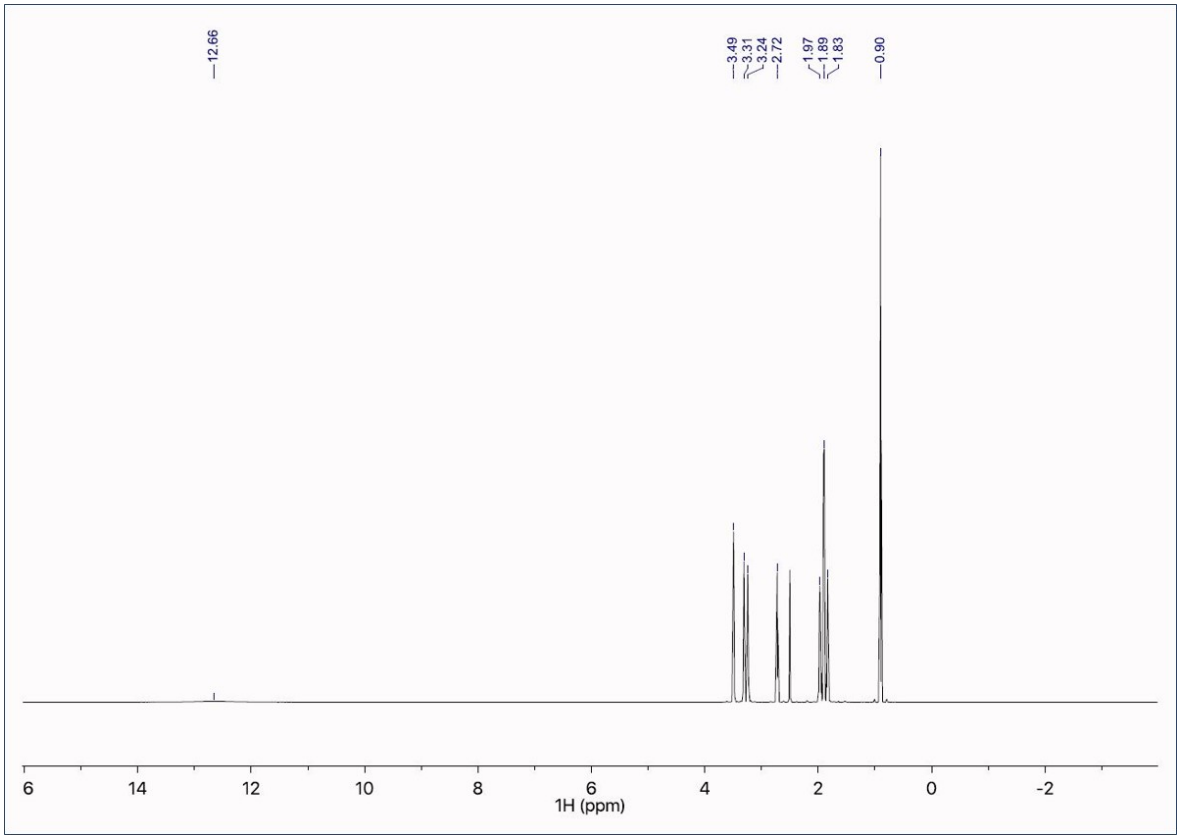


Full spectrum with main peak assignments in ppm

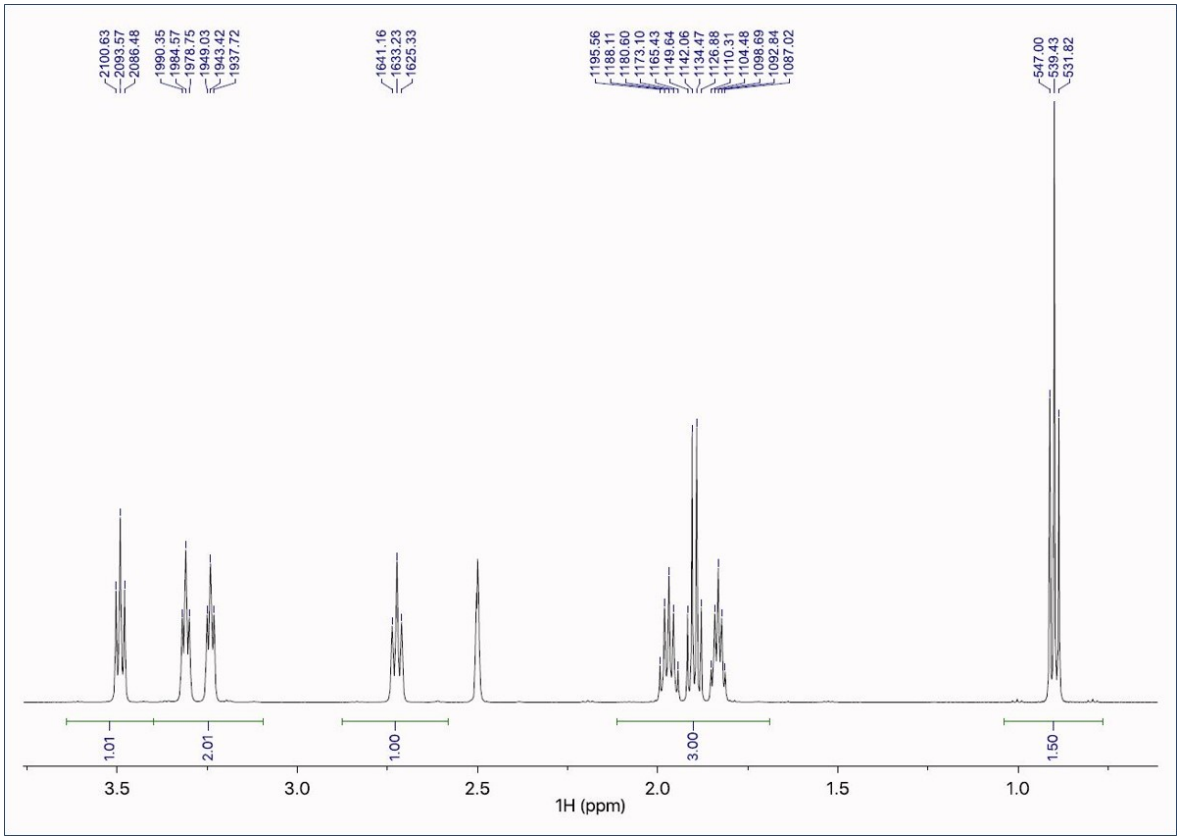


Expanded spectrum with all peak assignments in Hz

Figure 3.1 – $^{1}$H NMR in DMSO-d$_6$ spectra of [DBNH][Pr] with main peak assignments.

### Solutions preparation

MCC dissolution in [DBNH][Pr] was already described in Section 2.2.1 on page 102. Briefly, MCC was dried overnight under vacuum at 50 °C prior to use. It was then dissolved at various concentrations in [DBNH][Pr] at 40 °C and 400 rpm stirring for 24 h.

Dried MCC was also dissolved in [Emim][OAc] at 75 °C and 400 rpm stirring for 24 h. The viscosity of this solution was adjusted by adding DMSO.

All solutions were kept at room temperature, under nitrogen atmosphere, to prevent moisture and oxygen uptake.

### Aerogel beads preparation

Cellulose aerogel beads were prepared from the fresh cellulose-IL solutions with the JetCutter technology, described in Section 2.2.2 on page 104. Cellulose concentrations in [DBNH][Pr] matching the JetCutter processing window were 2% and 3%. 5% cellulose-[Emim][OAc] solution was diluted with DMSO to match the JetCutter parameters to reach the final concentrations of 3.5% cellulose, 65.8% [Emim][OAc] and 30.7% DMSO.

The droplets produced from the JetCutter fell into three different bathes: $H_2O$, EtOH and isopropanol. Solvent in cellulose beads was washed out with non-solvent by several exchanges with the fresh one leading to non-solvent induced phase separation (or coagulation) of cellulose. The goal was to stabilise the shape of cellulose beads. If the non-solvent of the coagulation bath was not EtOH, it was then exchanged to it and washed several times until the electrical conductivity of the EtOH bath was below 8.1 µS $cm^{-1}$. Cellulose coagulated beads in EtOH were then dried in a custom made 12 L autoclave from Eurotechnika, Germany at the German Aerospace Center (DLR) Koln, Germany. Process conditions for the Sc $CO_2$ drying were 115 bar and 60 °C. Dynamic washing with Sc $CO_2$ was performed at flow rates around 15 kg $h^{-1}$ for 2 h before the extractor was depressurised at rates not lower than 1.5 bar $min^{-1}$ and not higher than 3 bar $min^{-1}$.

### Aerogel monoliths preparation

Cellulose aerogel monoliths were produced as described in Section 2.2.1 on page 101: Freshly prepared cellulose-[DBNH][Pr] solutions, of concentration ranging from 2% to 5% were poured un cylindrical moulds. When the solution was particularly viscous, it was stand still until the bubbles from the dissolution had vanished. Coagulation was induced by carefully pouring $H_2O$, EtOH or isopropanol on the top of the solutions. At least 5 times the solution's volume was added and it was kept for diffusion for at least 24 h. The coagulated sample was then washed several times (at least 5 times every 12 h) until a clear solution was obtained. The non-solvent of coagulation was

then replaced by EtOH, if not already in it, to proceed to the Sc drying described in Section 2.2.1 on page 102.

**Rheological measurement**

All rheological measurements were performed within 3 days after solution preparation with a cone-plate geometry (4 ° - 40 mm) on the rheometer described on Section 2.2.4 on page 110. For steady state, shear rate was varied from 0.01 $s^{-1}$ to 300 $s^{-1}$ and temperature from 10 °C to 60 °C. For dynamic mode, frequency sweeps were performed between 0.01 Hz and 10 Hz at 5 Pa which corresponds to the linear viscoelastic regime, with temperature also varying from 10 °C to 60 °C. To prevent moisture and oxygen uptake, a thin layer of low-viscosity silicon oil ($\eta_{(20°C)}$ = 9.5 mPa s) was disposed on the edge of the measuring cell.

## 3.2 Results and discussions

The first part of this section is devoted to the rheological study of cellulose-[DBNH][Pr] solutions, and the second to the preparation of cellulose aerogel beads made with JetCutter technology and their characterisation. A complementary study was also conducted on monoliths to widen the range of concentrations.

The understanding of the viscoelastic properties of cellulose solutions is dictated by two main parameters:

- The use of the JetCutter, which has a certain processing window in terms of solution viscosity.
- And the need in using cellulose solutions of concentration which is at least 3 times higher than the overlap concentration (C*).

The latter criterion is somehow evident as far as a self-standing cellulose network should be formed, and it was confirmed when making monolithic cellulose aerogels from cellulose-[Emim][OAc] (Sescousse et al. (2011b); Buchtová and Budtova (2016)) and cellulose-8%NaOH-water solutions (Gavillon (2007)).

Cellulose-[Emim][OAc] solutions of viscosities around and above 5 to 10 Pa s turned out to be difficult to process with the JetCutter. This was the case of 5% cellulose-[Emim][OAc] which is a typical low concentration for making aerogels when using microcrystalline cellulose (Buchtová and Budtova (2016)). There are several ways to overcome the problem of "too high" viscosity. One is simply to decrease cellulose concentration. However, when microcrystalline cellulose is dissolved in [Emim][OAc] at 2 - 3%, the network formed upon coagulation in non-solvent is very weak, and the beads are either not intact or highly deformed. The reason is that these concentrations are too close to cellulose C* which in [Emim][OAc] is around 1% at room temperature (Gericke et al. (2009)) (the same cellulose was used in the present work as by Gericke et al. (2009)).

A compromise between not too high solution viscosity and not too low cellulose concentration (not too close to C*) is thus needed. To decrease the overlap concentration can be possible by using cellulose of higher molecular weight but viscosity increase will be more pronounced than the decrease in C*. The second way to decrease viscosity is to increase temperature but the JetCutter Type S is not adapted to this option. The third way is to use so-called co-solvents, for example, dimethylsulfoxide as it is known for [Emim][OAc] (Gericke et al. (2011); Le et al. (2014)). The results on cellulose aerogel beads from [Emim][OAc]-DMSO solutions will be presented in Section 3.2.2 on page 129. However, the use of "co-solvents" has several drawbacks such as complications during solvent recovery and presence of undesirable traces. The "ideal" solvent should be with:

- A lower viscosity than [Emim][OAc], to decrease the overall solution viscosity.
- If possible, better thermodynamic quality as compared to [Emim][OAc], to de-

crease C* allowing having stable cellulose network at lower polymer concentrations.

Below we shall demonstrate that this is the case of [DBNH][Pr]. Based on the results obtained with the rheological study, the preparation and properties of cellulose aerogel beads are then described.

### 3.2.1 Cellulose-[DBNH][Pr] rheological properties

#### Solvent and solution ageing

First of all, we examined the influence of ageing on solvent and solution viscosity as far as visual observations showed the darkening of solutions with time and temperature increase (Figure 3.2).

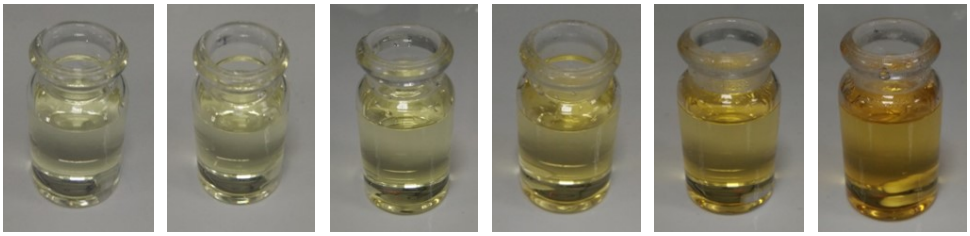


Figure 3.2 – Pictures of [DBNH][Pr] ageing with temperature increase.

To do so, the evolution of viscosity of [DBNH][Pr] at 20 °C was followed after shearing from 0.01 $s^{-1}$ to 300 $s^{-1}$ for 7 min at 40 °C and at 60 °C. The viscosity slightly increased but was within the 10% experimental errors. Yet, the influence of ageing on cellulose-[DBNH][Pr] solutions was considerable: the viscosity of a 5% solution at 20 °C was 27.7 Pa s and it doubled to 53.2 Pa s after 2 months of storing at ambient conditions. The ageing of the pure ionic liquid was not so important but still noticeable: the viscosity increased from 0.146 Pa s to 0.165 Pa s after 1.5 months and to 0.210 Pa s after 3 months of storage at room temperature. We suppose that the reason is hydrolysis of ionic liquid, as suggested by Parviainen et al. (2015). Taking this ageing into account, all rheological experiments and preparations of cellulose beads were performed on freshly made solutions.

#### Flow curves

The flow of [DBNH][Pr] and cellulose-[DBNH][Pr] solutions at different concentrations and temperatures was investigated in steady state and in dynamic mode. The examples of steady state viscosity ($\eta$) as a function of shear rate and of elastic ($G$') and viscous ($G$") moduli as well as complex viscosity ($\eta^*$) as a function of frequency are shown in Figure 3.3 and Figure 3.4, respectively.

Figure 3.3 shows that the solvent and solutions have a Newtonian plateau for at least one or two decades of shear rates. Higher concentration and lower temperature

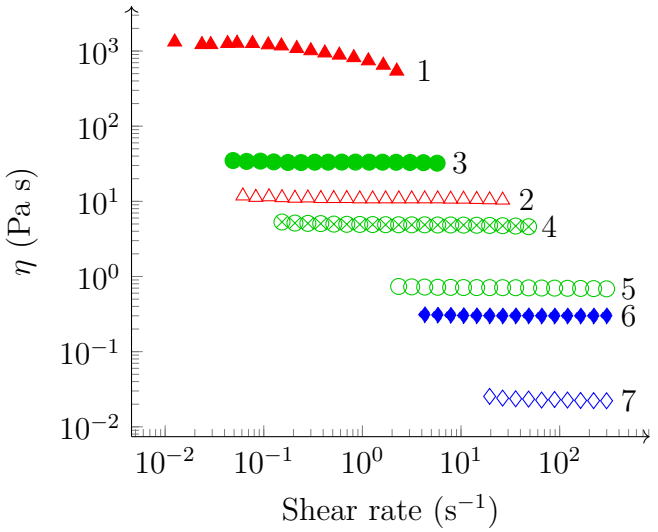


Figure 3.3 – Examples of flow curves for [DBNH][Pr] and cellulose-[DBNH][Pr] solutions at different concentrations and temperatures: 8% cellulose at 10 °C (1) and 60 °C (2), 4% cellulose at 10 °C (3), 30 °C (4) and 60 °C (5), neat [DBNH][Pr] at 10 °C (6) and 60 °C (7). Adapted from Druel et al. (2018).

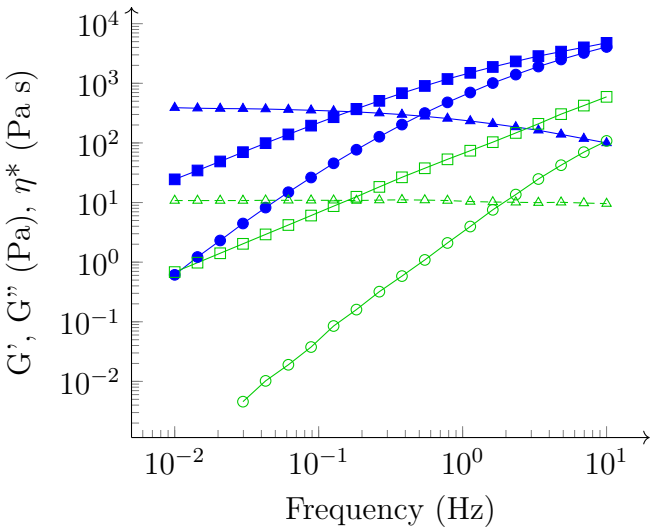


Figure 3.4 – Examples of $G'$ (circles), $G''$ (squares) and $\eta^*$ (triangles) as a function of frequency. Filled points are measurements of 8% cellulose-[DBNH][Pr] at 20 °C, open points are at 60 °C. Lines are given to guide the eye. Adapted from Druel et al. (2018).

lead to higher viscosity and a beginning of shear thinning. These results correlate with the behaviour of a classical polymer solution. The value of viscosity at the Newtonian plateau, the zero shear rate viscosity, will be used for the following analysis and referred as $\eta_N$. It should be noted that the viscosity of the neat solvent [DBNH][Pr] at 20 °C is 0.145 Pa s (not shown) and of [Emim][OAc] at the same temperature is 0.161 Pa s (Gericke et al. (2009)). Lower solvent viscosity is more favourable for processing with the JetCutter. Figure 3.4 also shows typical behaviour of an un-entangled viscoelastic polymer solution, with $G' < G''$ over three decades of frequencies, from 0.01 to 10 Hz.

Because cellulose-[DBNH][Pr] solutions show a classical polymer solution behaviour, we checked if Cox-Merz rule (which postulates the equality of steady state and dynamic viscosities) is obeyed (Cox and Merz (1958)). An example at 20 °C and 60 °C is presented in Figure 3.5 for three cellulose concentrations. It shows a very good match of $\eta$ and $\eta^*$; Cox-Merz rule can consequently be applied to cellulose-[DBNH][Pr] solutions.

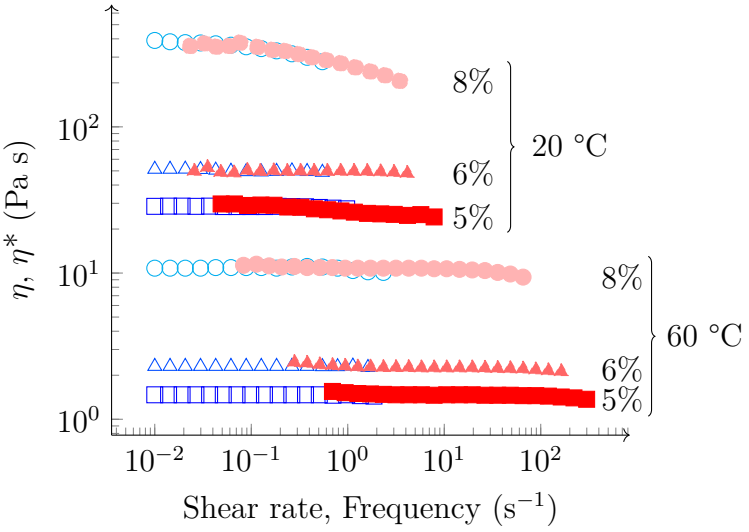


Figure 3.5 – Example of steady state viscosity (open points) and complex viscosity (filled points) curves of cellulose-[DBNH][Pr] solutions at 20 and 60 °C and different concentrations, illustrating the Cox-Merz rule. Adapted from Druel et al. (2018).

### Activation energy and master curves

Arrhenius approach was used to correlate zero shear rate viscosity $\eta_N$ and temperature $T$ and calculate the activation energy $E_a$ of viscous flow:

$$\eta_N \sim \exp\left(\frac{E_a}{RT}\right) \tag{3.1}$$

where $R$ is the ideal gas constant and temperature is expressed in $K$. The dependences of $\eta_N$ of the solvent and cellulose solutions on inverse temperature are shown in Figure 3.6. They all show linear trends ($R^2 > 0.99$) allowing calculation of $E_a$ at each cellulose concentration. It was reported in previous studies (Gericke et al. (2009); Sescousse et al. (2010a)) that $\ln(\eta_N)$ vs $1/T$ for [Emim][OAc] and cellulose-[Emim][OAc]

solutions showed a concave shape, this being "dictated" by the ionic liquid. Even if a very weak trend can also be guessed for [DBNH][Pr] and low concentrated cellulose-[DBNH][Pr] solutions (Figure 3.6), the deviation from the linear dependence is within the experimental errors in the temperature interval studied.

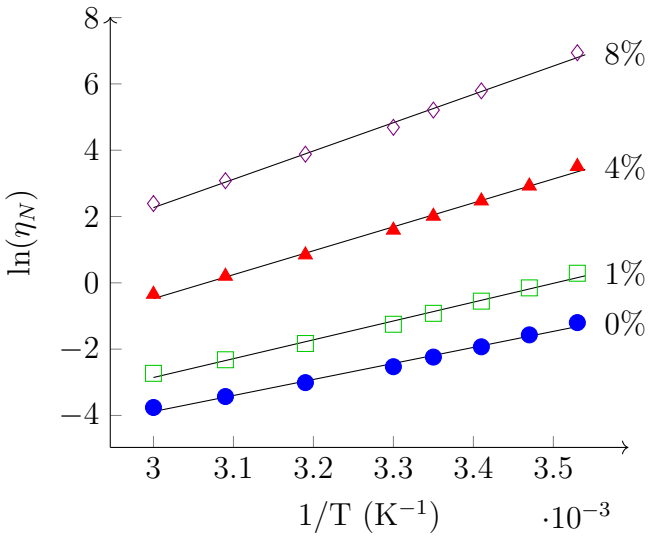


Figure 3.6 – Arrhenius plots of [DBNH][Pr] and cellulose-[DBNH][Pr] solutions of 1%, 4% and 8%. Lines are linear approximations. Adapted from Druel et al. (2018).

The activation energies calculated using Equation (3.1) and data in Figure 3.6 are plotted as a function of cellulose concentration in Figure 3.7 and are shown together with the values for cellulose-[Emim][OAc] system taken from Gericke et al. (2009). The power law approximations, given by Equation (3.2) which describes the activation energy as a function of polymer concentration, are also shown in Figure 3.7 with $p = 8.22$ and $k = 0.60$ for cellulose-[DBNH][Pr] solutions and $p = 3.21$ and $k = 0.83$ for cellulose-[Emim][OAc] solutions.

$$E_a = E_a(0) + pC^k \tag{3.2}$$

While the activation energy of the neat solvents are almost the same, $E_a$ of cellulose-[DBNH][Pr] solutions is higher than that of cellulose-[Emim][OAc] solutions at all concentrations. This shows that the viscosity of cellulose-[DBNH][Pr] solutions is more temperature sensitive and slightly more energy is needed to flow these solutions as compared to cellulose-[Emim][OAc].

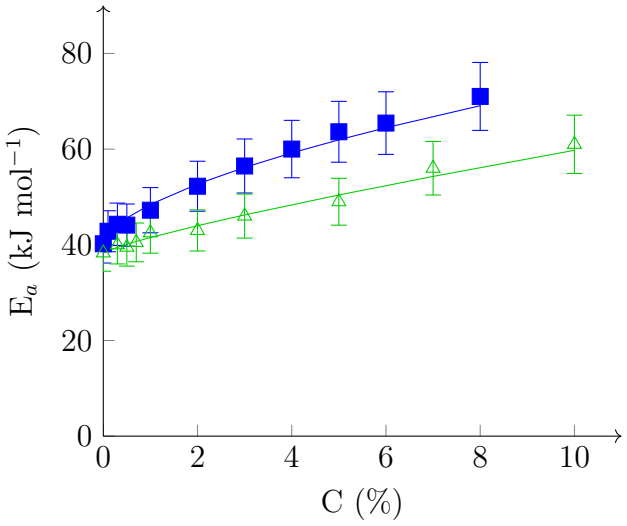


Figure 3.7 – Activation energy as a function of cellulose concentration for cellulose-[DBNH][Pr] solutions (filled points) and cellulose-[Emim][OAc] solutions (open points). Solid lines correspond to approximations calculated with Equation (3.2).Adapted from Druel et al. (2018).

Time-temperature superposition principle was applied to build master curves by shifting the experimental data of $G'$, $G''$ and $\eta^*$ by the corresponding $a_T$ shift factor. The latter was calculated from Equation (3.3) with $T_{ref}$ as the reference temperature, here 20 °C.

$$a_T = \exp\left(\frac{E_a}{R}\left(\frac{1}{T} - \frac{1}{T_{ref}}\right)\right) \tag{3.3}$$

Examples of master plots for 8% and 5% cellulose-[DBNH][Pr] solutions, with all data reduced to the reference temperature of 20 °C, are shown in Figure 3.8. $G''$ is higher than $G'$ for both concentrations for five decades of frequency; these solutions behave as a classical un-entangled polymer solution. For a monodispersed flexible polymer at low frequencies Maxwell model predicts power law exponents in $G' \sim \omega^x$ and $G'' \sim \omega^y$ with $x = 2$ and $y = 1$. For 8% solutions $x_{exp} = 1.85$ and $y_{exp} = 0.94$, and for 5% solutions $x_{exp} = 1.63$ and $y_{exp} = 0.99$. The values obtained show the applicability of Maxwell model in the terminal zone; a deviation for 5% solution may be due to the fact that terminal zone cannot be reached because of too low $G'$ values.

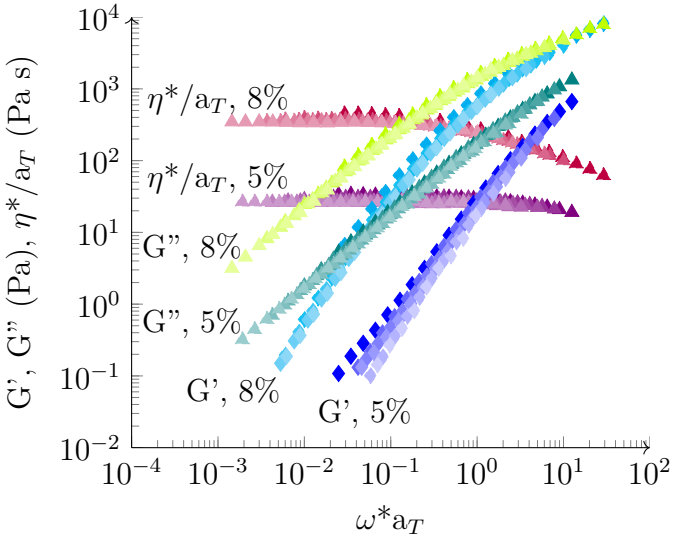


Figure 3.8 – Master curves for $G'$, $G''$ and complex viscosity of 5% and 8% cellulose-[DBNH][Pr] solutions at temperature ranging from 10 °C to 60 °C, with 20 °C as reference temperature. Adapted from Druel et al. (2018).

### Concentration dependences, intrinsic viscosity and overlap concentration

Figure 3.9 shows the influence of cellulose concentration on the Newtonian viscosity of solutions at different temperatures. Two different regions can be distinguished: the dilute region, with linear viscosity-concentration dependence, and the semi-dilute region that obeys the power law $\eta_N \sim C^n$. The power law coefficient $n$ decreases with increasing temperature from 3.78 at 10 °C to 2.93 at 50 °C. Similar values and tendencies were already reported for cellulose in different ionic liquids and in other solvents (Blachot et al. (1998); Matsumoto et al. (2001); Gericke et al. (2009); Sescousse et al. (2010a)).

The intrinsic viscosity $[\eta]$ is an important parameter that describes the volume of macromolecule depending on temperature and thermodynamic quality of the solvent. Cellulose intrinsic viscosity in [DBNH][Pr] was calculated using the Wolf approach (Wolf (2007); Eckelt et al. (2011)). This method was preferred over the classical Huggins approach for two main reasons: firstly, measurements in a capillary Ubbelohde viscometer were not possible because of the too high viscosity of our solutions and because of the solvent sensitivity to moisture and oxygen. Secondly, when using the zero shear rate viscosity values calculated above, the Huggins plots where scattered and did not allow an adequate determination of the intrinsic viscosity. In Wolf approach (Wolf (2007)), according to phenomenological considerations, the calculation of the limiting slope of the logarithm of the relative viscosity ($\eta_{rel}$) versus concentration is identical to the intrinsic viscosity, where $\eta_{rel} = \eta_{sol}/\eta_{solv}$ with $\eta_{sol}$ and $\eta_{solv}$ being solution and solvent viscosities, respectively. This approach was developed for polyelectrolyte solutions but it was also successfully used for uncharged polymer solutions as shown by Eckelt et al. for cellulose dissolved in NMMO monohydrate (Eckelt et al. (2011)). This

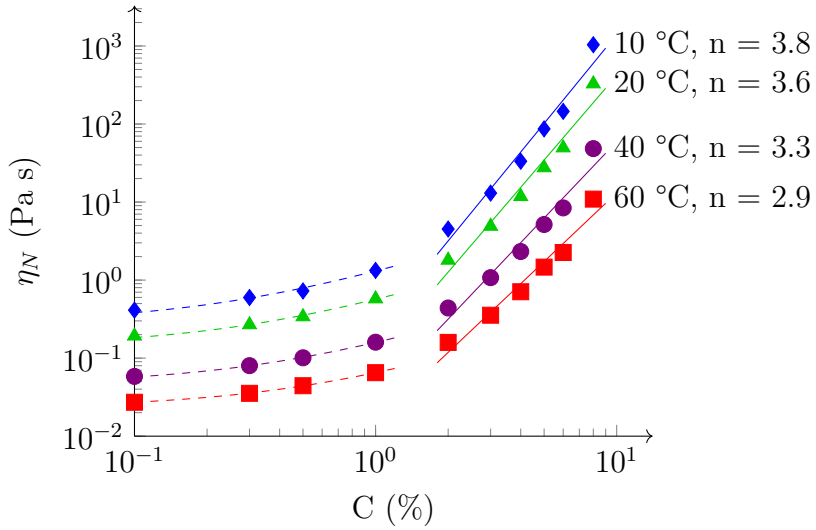


Figure 3.9 – Newtonian viscosity as a function of cellulose concentration at different temperatures. Dashed lines correspond to the linear dependence in dilute region and solids lines correspond to the power-law approximation above the overlap concentration, $n$ is power law coefficient. Adapted from Druel et al. (2018).

approach was also used to determine amylopectin intrinsic viscosity (Liu and Budtova (2013)) and cellulose acetate intrinsic viscosity (Rudaz and Budtova (2013)), both in [Emim][OAc]. Cellulose concentrations were recalculated in mL g$^{-1}$, with mean value of [DBNH][Pr] density taken for all solution concentrations as 1.1 g cm$^{-3}$. It was shown that [DBNH][Pr] density-temperature dependence is very weak (Green (2017)) and may not be taken into account within experimental errors.

Figure 3.10 demonstrates the intrinsic viscosity of cellulose in [DBNH][Pr] and in [Emim][OAc] as a function of temperature, the latter taken from Gericke et al. (2009). Both intrinsic viscosities decrease with temperature increase. This shows that cellulose macromolecules are sensitive to temperature variations, and that thermodynamic quality of both solvents is decreasing with the increase of temperature. The intrinsic viscosity of cellulose in [DBNH][Pr] is more than two times higher than that in [Emim][OAc], indicating that in this temperature range [DBNH][Pr] is thermodynamically much better solvent of cellulose. For example, $[\eta]$ at 20 °C is 237 mL g$^{-1}$ in [DBNH][Pr] against 101 mL g$^{-1}$ in [Emim][OAc].

As mentioned above, cellulose overlap concentration is an important parameter which reflects the end of dilute regime; it can be roughly estimated as $C^* = 1/[\eta]$. According to results presented in Figure 3.10, cellulose overlap concentration in [DBNH][Pr] is much lower than that in [Emim][OAc] in the temperature interval studied. For example, at 20 °C in [DBNH][Pr] $C^* = 4.2\ 10^{-3}$ g mL$^{-1}$ (0.38%) and in [Emim][OAc] $C^* = 9.9\ 10^{-3}$ g mL$^{-1}$ (0.9%). This is an important result to take into account for processing because it means that cellulose network can be formed at lower cellulose concentrations when dissolved in [DBNH][Pr]. It means that in order to make intact beads with JetCutter, cellulose concentration in [DBNH][Pr] should be at least 1%.

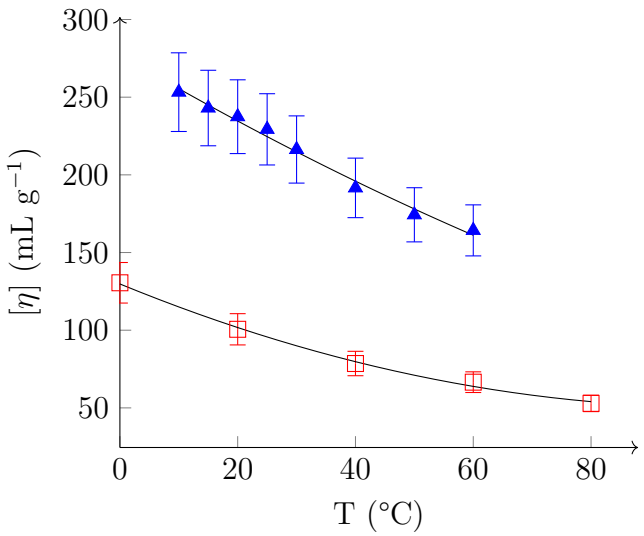


Figure 3.10 – Intrinsic viscosities of cellulose in [DBNH][Pr] (filled points) and in [Emim][OAc] (open points, data taken from Gericke et al. (2009)) as a function of temperature. Lines are given to guide the eye. Adapted from Druel et al. (2018).

The results on the beads obtained with JetCutter technology are presented in the next section.

### 3.2.2 Cellulose aerogel beads

#### Preliminary tests with [Emim][OAc] solutions

[Emim][OAc] is a commonly used and well known cellulose solvent (Gericke et al. (2011); Le et al. (2014)). However the viscosity of resulting cellulose solutions, even at low cellulose concentration, is too high to be processed with the JetCutter. We thus used a co-solvent to reduce cellulose solution viscosity: dimethylsulfoxide (DMSO). By adding DMSO to 5% cellulose-[Emim][OAc] solution (final concentration: 3.5% cellulose, 65.8% [Emim][OAc] and 30.7% DMSO), we could adequately reduce solution viscosity to be able to use it with the JetCutter technology. From this solution, we could successfully produce porous cellulose beads, as shown in Figure 3.11 with specific surface area of 330 $m^2$ $g^{-1}$. These beads had a mono-dispersed size distribution with a mean diameter of 0.57 mm and a standard deviation of 0.25 mm (Figure 3.11). This relatively large standard deviation is a proof of the non-regularity of the produced beads. They were, for some of them, deformed and not round which is a sign that the JetCutter parameters were not optimal for this solution. Moreover, the use of an additional reagent (DMSO) and the limited processing windows of the JetCutter led us to consider another solvent for cellulose dissolution: [DBNH][Pr].

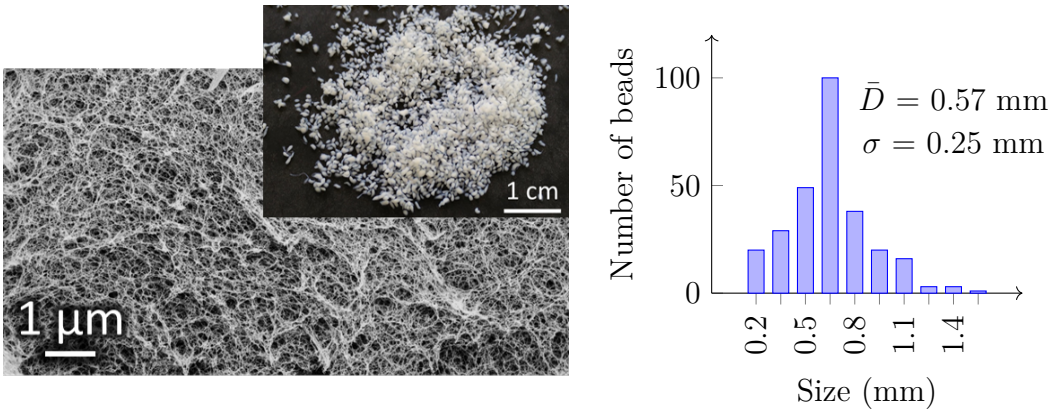


Figure 3.11 – Picture, morphology and size distribution of cellulose beads prepared with the JetCutter from 3.5% cellulose-65.8% [Emim][OAc]-30.7% DMSO. $\bar{D}$ stands for the mean diameter and $\sigma$ for the standard deviation.

### Visual observations and size distribution

The images of cellulose aerogel beads made from 2% and 3% cellulose-[DBNH][Pr] coagulated in water, ethanol and isopropanol are shown in Figure 3.12. Their size distribution together with mean arithmetic values of diameter ($\bar{D}$) and standard deviation ($\sigma$) are shown in Figure 3.13. Cellulose concentration plays the main role in the size and shape of the beads: mean diameter from 2% cellulose-[DBNH][Pr] solution, whatever the coagulation bath, varies from 0.5 to 0.7 mm (Figure 3.13), and from 3% solution it is around 1.8 mm (Figure 3.13). The reason is that viscosity of 3% solution is more than two times higher than that of 2% solution at 20 °C: 1.8 Pa s *vs.* 4.9 Pa s, respectively (Figure 3.9). These concentrations are in semi-dilute region with viscosity proportional to polymer concentration in power 3.6 at room temperature (Figure 3.9).

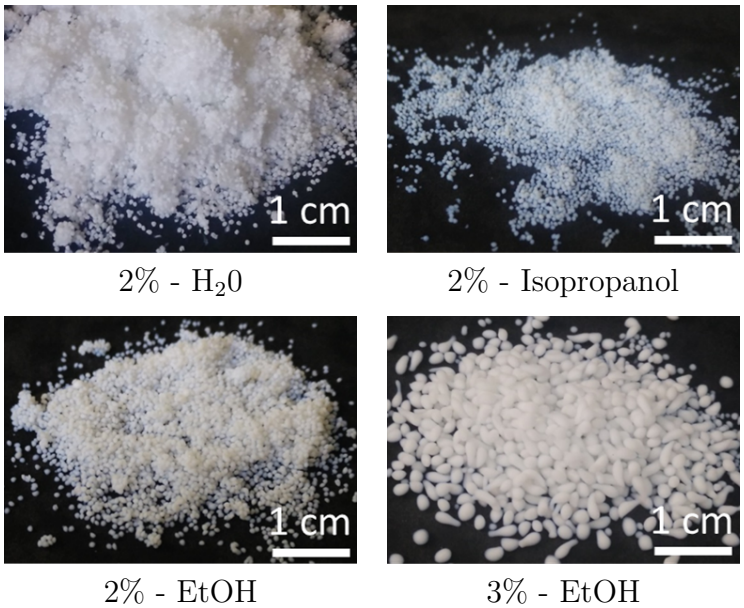


Figure 3.12 – Cellulose aerogel beads from various cellulose-[DBNH][Pr] solution concentrations and coagulation bathes. Adapted from Druel et al. (2018).

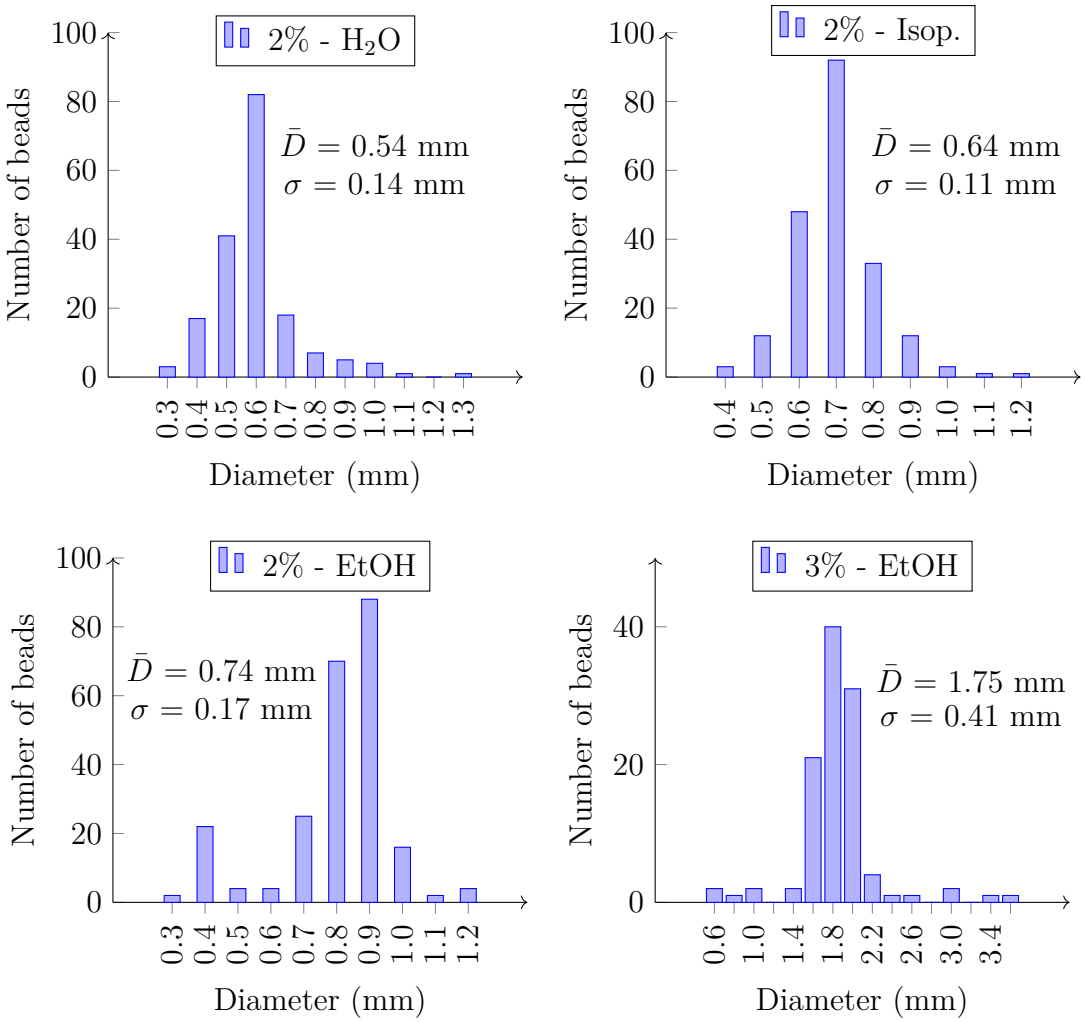


Figure 3.13 – Size distribution, mean diameter ($\bar{D}$) and standard deviation ($\sigma$) for aerogel beads as shown in Figure 3.12: from 2% and 3% cellulose-[DBNH][Pr] solutions coagulated in $H_2O$, isopropanol and EtOH. Adapted from Druel et al. (2018).

### Bulk density, specific surface area and morphology

The main characteristics of aerogels such as bulk density, porosity, pore volume and specific surface area are shown in Table 3.1 for beads made from 2% and 3% cellulose-[DBNH][Pr] solutions and coagulated in water, isopropanol and ethanol. Bulk densities are very low, 0.04 – 0.05 g $cm^{-3}$ for samples from 2% solutions, and 0.07 g $cm^{-3}$ for samples from 3% solutions, but are still higher than what could be expected for the case of no volume change during all processing steps (0.022 g $cm^{-3}$ and 0.033 g $cm^{-3}$ for 2% and 3%, respectively). The reason is shrinkage during solvent exchange which leads to non-solvent induced phase separation and also during drying (large difference between the solubility parameters of cellulose and $CO_2$). For the low cellulose concentrations used, shrinkage is around 60 – 70 vol.% corresponding to previously reported results on aerogel monoliths from cellulose-[Emim][OAc] solutions (Buchtová and Budtova (2016)). It seems that the type of coagulation bath does not influence much the density

within the interval of conditions studied.

Table 3.1 – Bulk density ($\rho_{bulk}$), porosity, specific surface area ($S_{BET}$) and specific pore volume ($V_{pores}$) of cellulose aerogel beads made from 2% and 3% solutions and coagulated in water, isopropanol and ethanol. Adapted from Druel et al. (2018).

| **Cellulose concentration (%)** | **Coagulation bath** | $\boldsymbol{\rho_{bulk}}$ **(g cm$^{-3}$)** | **Porosity (%)** | $\mathbf{S_{BET}}$ **(m$^2$ g$^{-1}$)** | $\boldsymbol{V_{pores}}$ **(cm$^3$ g$^{-1}$)** |
|---|---|---|---|---|---|
| 2 | $H_2O$ | 0.04 | 97.3 | 238 | 24.3 |
| 2 | isopropanol | 0.04 | 97.3 | 302 | 24.3 |
| 2 | EtOH | 0.05 | 96.7 | 295 | 19.3 |
| 3 | EtOH | 0.07 | 95.3 | 257 | 13.6 |

Porosity was calculated with Equation (1.6) on page 75, using the values of bulk density ($\rho_{bulk}$, Table 3.1), and cellulose skeletal density, which is the same as for neat cellulose, $\rho_{sk} = 1.5$ g cm$^{-3}$ (Kamal Mohamed et al. (2015); Rudaz (2013)). As expected from low values of bulk density, porosity is very high, from 95% to 97% (Table 3.1). Specific surface area ($S_{BET}$) is within 240 – 300 m$^2$ g$^{-1}$ for all aerogel beads, which reflects certain mesoporosity. Overall, density and specific surface area of cellulose aerogel beads are very similar to those obtained for aerogel monoliths from ionic liquids, NMMO monohydrate and NaOH-water based solvents (Innerlohinger et al. (2006); Gavillon and Budtova (2007); Tsioptsias et al. (2008); Liebner et al. (2008); Aaltonen and Jauhiainen (2009); Sescousse et al. (2011b)). The JetCutter technology preserves the main characteristics of cellulose aerogels.

The experimental results presented in Table 3.1 allowed a rough estimation of the theoretical specific pore volume $V_{pores}$, using Equation (1.7) on page 75. The results are shown in Table 3.1. Pore volume is high and comparable with that of other bio-aerogels (Rudaz et al. (2014)). As seen in Chapter 1, *State of the art*, it should be noted that pore volume and pore size distribution of bio-aerogels with "mixed" meso- and macro-porosity cannot be measured with nitrogen adsorption and BJH approach: the experimental data take into account only 10 - 20% of the real volume. This was demonstrated for several bio-aerogels (Robitzer et al. (2011a); Rudaz (2013); Rudaz et al. (2014); Jiménez-Saelices et al. (2017); Groult and Budtova (2018a)). Mercury porosimetry also does not allow measuring pore size distribution as far as sample is compressed and mercury does not penetrate the pores (Rudaz (2013); Rudaz et al. (2014)).

The internal morphology of aerogel beads is presented in Figure 3.14. All samples are with small and large macropores and some mesoporosity as reflected by specific surface area.

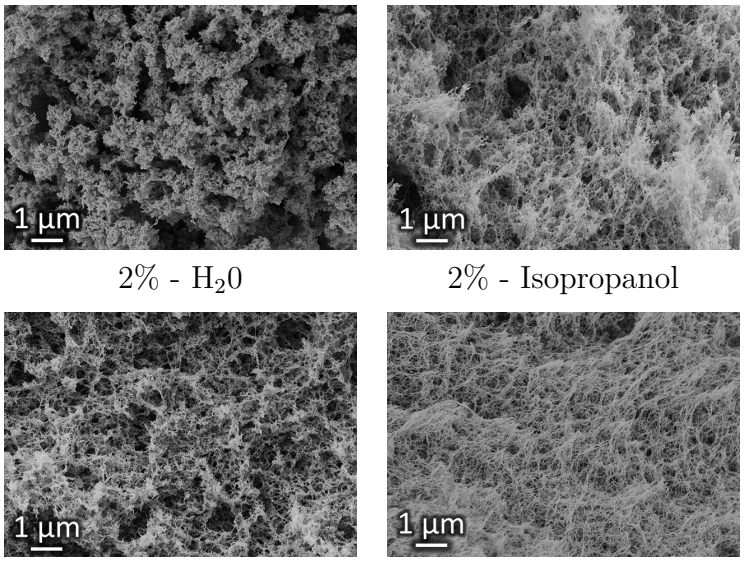


Figure 3.14 – Morphology of aerogel beads from cellulose-[DBNH][Pr] solutions of 2% and 3% cellulose coagulated in water, isopropanol and ethanol. Adapted from Druel et al. (2018).

### 3.2.3 Cellulose aerogel monoliths

The majority of bio-aerogels are made as monoliths of $\approx 6$ cm$^3$. Does the change of the size of aerogel, from classical monoliths to beads (0.013 cm$^3$), influence aerogel morphology and properties? For example, Voon et al. (2016) reported the decrease of specific surface, from 498 m$^2$ g$^{-1}$ to 107 m$^2$ g$^{-1}$, with the increase of particles' mean diameter from 0.41 $\pm$ 0.03 mm to 2.14 $\pm$ 0.08 mm. Thus we found essential to check if the same properties and morphology are obtained for monolithic and bead samples prepared from the same cellulose-[DBNH][Pr] solutions.

Aerogel monoliths with cellulose concentration of 3% and 5% were prepared with [DBNH][Pr] as solvent and $H_2O$, EtOH and isopropanol as non-solvents. Figure 3.15 on the next page shows the resulting aerogel monoliths' morphology and pictures of 5% cellulose, $H_2O$ and EtOH coagulated aerogel monoliths, as examples. Figure 3.16 summarises aerogel monoliths and beads' properties as a function of concentration and coagulation bath.

When comparing Figure 3.14, Figure 3.15 and Figure 3.16 we can firstly see that morphology and properties of the monoliths and the beads are very similar, except in the case of monoliths when cellulose-[DBNH][Pr] solutions were coagulated in $H_2O$. Monolithic aerogels have low density, similar to beads. It is lower compared to what is known in the literature for cellulose aerogels made from cellulose dissolved in other solvents at similar polymer concentration (Gavillon and Budtova (2008); Sescousse et al. (2011a); Kamal Mohamed et al. (2015)). At the same densities, specific surface area is similar for monoliths and beads and is higher than when cellulose is dissolved in NaOH based solvents. The reason is the better dissolution of cellulose in ionic liquids.

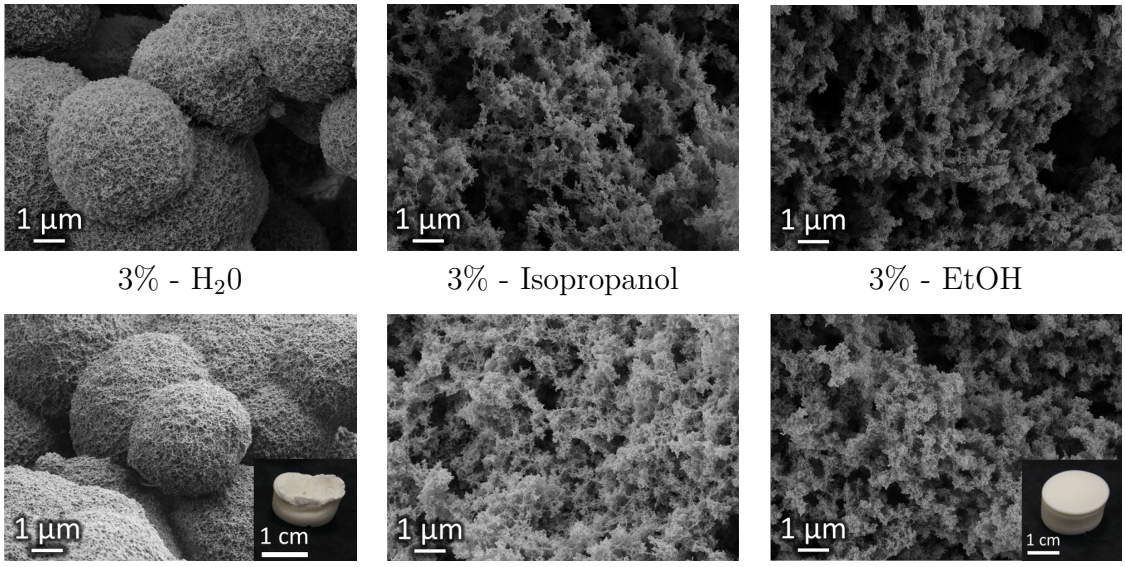


Figure 3.15 – Morphology of aerogel monoliths from cellulose-[DBNH][Pr] solutions of 3% and 5% cellulose coagulated in water, isopropanol and ethanol.

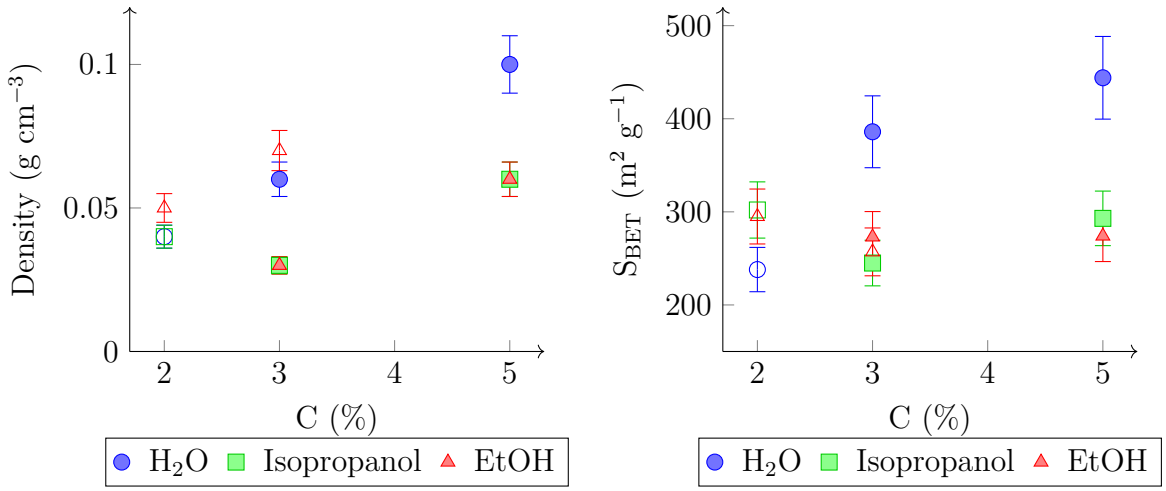


Figure 3.16 – Properties of aerogel monoliths from cellulose-[DBNH][Pr] solutions of 3% and 5% cellulose (filled points) and beads (open points) from 2% cellulose-[DBNH][Pr] coagulated in water, isopropanol and EtOH and 3% cellulose-[DBNH][Pr] coagulated in EtOH.

In addition, an increase of both the density and the specific surface area with increasing concentration can be noted. This also complies with what was reported for some other bio-aerogels (based on cellulose, Buchtová and Budtova (2016) and based on pectin: Groult and Budtova (2018a)).

One considerable difference can, however, be noted for monolithic aerogels made from cellulose-[DBNH][Pr] coagulated in $H_2O$ as compared to beads. The formers show higher specific surface area (Figure 3.16) and a peculiar globular morphology. More images of their micro-structure, at different magnification, are given in Figure 3.17.

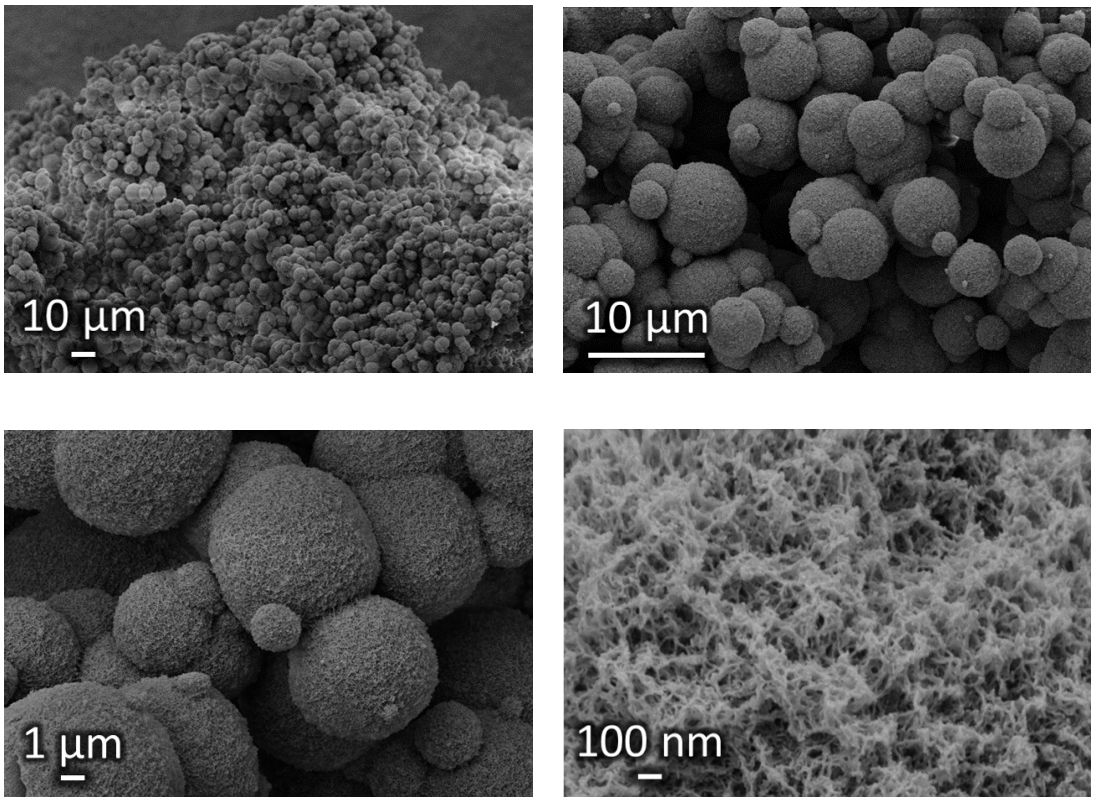


Figure 3.17 – Morphology of aerogel monoliths from 3% cellulose-[DBNH][Pr] solution coagulated in water at different magnifications.

Globular morphology was already observed for cellulose aerogels from Solucell(DP 950)-NMMO solution, also coagulated in $H_2O$, by Gavillon and Budtova (2008), and for aerogels from MCC or cotton dissolved in Emimac/DMSO solution coagulated in EtOH (Buchtová and Budtova (2016); Pircher et al. (2016)). However, the "hairy beads" observed previously were of much smaller size, around 1 µm. Hairy beads that are similar to what was observed previously, all in diameter of about half a micron, can be seen on Figure 3.15 for aerogel coagulated in EtOH, and less clearly when coagulated in isopropanol. The formation of these hairy beads is a result of phase separation via spinodal decomposition which is taking place when cellulose solution is in contact with non-solvent. Why large spheres of approximately two different diameters (5 - 7 µm and around 1 µm, see Figure 3.15 and Figure 3.17), are formed when cellulose-[DBNH][Pr]

was coagulated in $H_2O$, is not clear. Sphere of different sizes is not typical to spinodal decomposition. The interactions between the solvent and $H_2O$, the miscibility of all three components (cellulose, IL and $H_2O$) and the kinetics of phase separation and coagulation should be considered to better understand the phenomenon observed. In the case of monoliths, cellulose is in contact with IL/$H_2O$ mixture much longer than in the case of beads; hydrolysis of cellulose might happen. To test this hypothesis, the molecular weight of cellulose in $H_2O$ coagulated aerogel was determined and compared to the one of MCC precursor. The DP of MCC was measured to be 348 while the one of cellulose aerogel coagulated in $H_2O$ was 302. This difference is larger than the 10% incertitude measurement, which means that some hydrolysis of cellulose dissolved in [DBNH][Pr] happens during coagulation in $H_2O$, however, it is not so strong to completely change aerogels' morphology.

With this kind of "big" spheres in the monolith aerogels' structure, we could expect a very low specific surface area. However, if we take a closer look at the spheres on the SEM pictures of Figure 3.17, we can see that they are made a network of cellulose strands with pores of few tens of nanometres. Pores of this size are not usually observed in cellulose II aerogels, neither the very high (for cellulose II aerogels) specific surface area that they produced (up to 445 $m^2\ g^{-1}$). These peculiar properties make these cellulose II aerogels interesting candidates for different applications such as drug delivery matrix, for encapsulation or as catalyst/catalyst support.

The thermal conductivity of these aerogels was also tested. It was the same as of the "regular" cellulose aerogels, around 35 $mW\ m^{-1}\ K^{-1}$, which can be explained by large pores between the spheres that do not participate to Knudsen effect but increase the porosity.

Further study and especially on $H_2O$ coagulated aerogels should be conducted to completely understand the peculiar morphology observed. Varying the coagulation kinetic and/or the temperature during coagulation could allow us to tailor the final aerogels' properties.

# Conclusions

This work is an extended investigation of the rheological properties of cellulose-[DBNH][Pr] solutions in the view of using these results for making cellulose aerogel beads with the JetCutter technology and drying with supercritical $CO_2$. The flow and viscoelastic properties of cellulose-[DBNH][Pr] solutions were studied as a function of polymer concentration and solution temperature. In the range of conditions used all solutions show Newtonian plateau with a beginning of shear thinning regime for higher cellulose concentrations and lower temperatures. Viscoelastic properties of cellulose-[DBNH][Pr] solutions can be described by classical approaches used in polymer physics. Cellulose intrinsic viscosity in [DBNH][Pr] turned out to be more than two times higher than that in previously studied [Emim][OAc] solutions for the same cellulose, and also decreases with temperature increase. Thermodynamic quality of [DBNH][Pr] is thus higher at the same temperature leading to more swollen polymer coils and lower overlap concentration. The latter allowed fitting into the processing window of the JetCutter in terms of not too high viscosity but high enough cellulose concentration to make intact beads.

Aerogel beads were prepared from 2% and 3% of cellulose-[DBNH][Pr] solutions by replacing ionic liquid by water, ethanol or isopropanol followed by drying with supercritical $CO_2$. Cellulose concentration was the major factor controlling beads' size which varied from 0.5 - 0.7 mm when made from 2% solutions to 1.8 mm from 3% solution. The density of beads was 0.04 – 0.07 g $cm^{-3}$ and specific surface area 240 – 340 $m^2$ $g^{-1}$. We demonstrated that by a careful selection of solution properties it is possible to obtain with the JetCutter technology intact cellulose aerogel beads with properties similar to those known for monolithic cellulose aerogels made using other solvents. The results can be extended for making other bio-aerogels in the form of beads.

The preparation of cellulose aerogel monoliths showed that properties were the same as beads, except for the morphology when coagulated in $H_2O$. These last ones showed a peculiar globular morphology, most probably because of partial cellulose hydrolysis during coagulation and potential interactions between ionic liquid and water. Further studies are needed to completely understand and control this phenomenon.

Overall, the possibility to make cellulose aerogels beads with the up-scalable JetCutter process, opens numerous opportunities for using bio-aerogels, and in particular cellulose aerogel beads, as carriers for controlled release applications in cosmetics, food and pharma.

# Chapter 4

# Micrometric cellulose aerogel beads production from adapted emulsion technique

## Contents

# Abstract

We have seen in the previous chapter that it was possible to prepare cellulose aerogel beads from cellulose dissolved in ionic liquids with the up-scalable JetCutter technology. This is a very good result, however, still several questions remain.

The first one concerns the size of the beads obtained: the smallest ones were in the range of hundreds of micrometres. Unfortunately, to be used in pharma or food, these beads are too large. As an example, if these beads are to be used in food, and for human tongue not to feel the particles, they have to be smaller than 30 µm in diameter because of the sensitivity threshold. Hence, another technique to produce cellulose particles in the range of maximum few tens of micrometres in diameter maximum is needed. The emulsification method is widely used in the cosmetic industry and allows the production of "wet" particles with diameter of few micrometres. This technique can be an option if applicable to our system. It was proved to be successful for the production of different polysaccharide based aerogels (García-González et al. (2015)), which makes it very promising for cellulose.

The second question concerns the solvent we used in the previous chapter. Ionic liquids are said to be "green solvents", however, their bio-compatibility and toxicity still need to be tested for each new ionic liquid. For the time being, this makes them unusable in medical or food applications. One option would be to use a different solvent such as NaOH-water with or without additives.

In the view of all these requirements, this study was aiming at finding a way to make emulsions applicable for "unstable" cellulose solutions like cellulose-NaOH-water in order to produce aerogel particles of few microns diameter. The work presented in this chapter was achieved thanks to the help of Amelie Kenkel (Master student from TUHH, Germany, who performed her work in our laboratories) and the expert advices of Pavel Gurikov and Victor Baudron, both from TUHH, Germany.

The chapter starts with presenting particular materials and methods used in this study. Then, the preliminary studies and measurements realised for emulsification method to be successful are presented. The different steps and findings that led to the implementation of the new emulsification technique, adapted for cellulose-NaOH-water based solutions, are then explained. Finally, several parameters were tested and their influence on the resulting cellulose aerogel particle properties are analysed.

# Résumé

Nous avons vu dans le chapitre précédent qu'il était possible de préparer des billes d'aérogel de cellulose à partir de cellulose dissoute dans des liquides ioniques avec la technologie industriable du JetCutter. Ce résultat est très bon, cependant, plusieurs questions subsistent encore.

La première concerne la taille des billes obtenues, les plus petites étaient de l'ordre d'une centaines de micromètres. Malheureusement, pour une utilisation dans l'industrie pharmaceutique ou alimentaire, ces billes sont trop grosses. Par exemple, si ces billes devaient être utilisées dans les aliments, pour que la langue humaine ne puisse pas les sentir, elles doivent avoir un diamètre inférieur à 30 µm à cause du seuil de sensibilité. Par conséquent, une autre technique pour produire des particules de cellulose de l'ordre de quelques dizaines de micromètre de diamètre maximum est nécessaire. La méthode d'émulsification est largement utilisée dans l'industrie cosmétique et permet la production de particules "humides" de quelques micromètres de diamètre. Cette technique pourrait être une bonne alternative si elle s'applique à notre système. Elle s'est avérée efficace pour la production d'aérogels à base de différents polysaccharidiques (García-González et al. (2015)), ce qui la rend très prometteuse pour la cellulose.

La deuxième question concerne le solvant que nous avons utilisé dans le chapitre précédent. Les liquides ioniques sont dit être des "solvants verts", mais leur biocompatibilité et leur toxicité doivent encore être testées pour chaque nouveau liquide ionique. Pour l'instant, cela les rend inutilisables dans des applications médicales ou alimentaires. Une option serait d'utiliser un solvant différent tel que NaOH-eau avec ou sans additifs.

Au vu de tous ces exigences, cette étude visait à trouver un moyen de rendre les émulsions applicables à des solutions de cellulose "instables" comme l'est cellulose-NaOH-eau afin de produire des particules d'aérogel de quelques microns de diamètre. Le travail présenté dans ce chapitre a été réalisé grâce à l'aide d'Amélie Kenkel (étudiante en Master à TUHH, Allemagne, qui a effectué son travail dans nos laboratoires) et aux conseils d'experts de Pavel Gurikov et Victor Baudron, tous les deux de TUHH, Allemagne.

Ce chapitre commence par la présentation des matériaux et méthodes particuliers utilisés dans cette étude. Ensuite, les études préliminaires et les mesures réalisées pour que la méthode d'émulsification soit un succès sont présentées. Les différentes étapes et découvertes qui ont conduit à la mise en œuvre de la nouvelle technique d'émulsification, adaptée aux solutions à base de cellulose, de NaOH et d'eau, sont ensuite expliquées. Enfin, plusieurs paramètres ont été testés et leur influence sur les propriétés des particules d'aérogel de cellulose obtenues sont analysé.

# 4.1 Materials and methods

## 4.1.1 Materials

MCC, Avicel®PH-101, was dissolved in 8% NaOH based solvents, without additive, with urea or with 0.5% ZnO. MCC, NaOH based solvents and its additives were described in Section 2.1.1 on page 95 and Section 2.1.2 on page 99, respectively.

We used two different acids as non-solvents, 0.5 M HCl and 8.6 M acetic acid (AA) as well as EtOH, for coagulation and washing. All non-solvents were described in Section 2.1.2 on page 100.

Paraffin oil as continuous phase and Span 80 as non-ionic surfactant were used to emulsify cellulose solutions and non-solvents.

## 4.1.2 Methods

### Cellulose dissolution

In this chapter, we used a different method for cellulose dissolution, inspired by Cai and Zhang (2005). MCC was dried under vacuum at 50 °C for at least 3 h and swelled in distilled water at 5 °C for 3 h. At the same time, NaOH was dissolved in water to get 20% solution. If urea or ZnO was used, it was added to the NaOH solution while it was still warm because of the exothermal reaction. Once all was dissolved, the produced NaOH based solvent was cooled down at -12.3 °C. Swollen cellulose and NaOH based solvent were finally mixed together at 1000 rpm and -3 °C for 3 min.
The final concentrations were:

- 3.8% or 5% cellulose.
- No additive or 11.5% urea or 0.5% ZnO.
- NaOH concentration in $H_2O$ was 8%.

### Emulsification technique

Emulsification principle was described in Section 2.2.2 on page 105. In more details, cellulose solution was added drop wise in paraffin oil and was emulsified with a marine impeller for 30 min at 700 rpm. At the same time, non-solvent (HCl or AA) was emulsified separately in paraffin oil with 1 vol.% of Span80, with a flat impeller, for 30 min to 45 min at 700 rpm. Cellulose solution emulsion and non-solvent emulsion were thus stabilized separately. Finally, the two emulsions were mixed together at 1000 rpm for 2 h in order to trigger cellulose coagulation. A schematic representation of this process was given in Figure 2.9 on page 105. After 2 h the stirring was stopped and the resulting emulsified suspension was let stand still at room temperature for particles sedimentation.

Several parameters were varied:

- Cellulose solution concentration.
- Gelation state of cellulose solution.
- Non-solvent: 0.5 M HCl or 8.6 M AA.
- Cellulose solution to oil ratio in the first emulsion was 1:10 or 1:3.
- Non-solvent to oil ratio was kept constant at 1:2.
- The volume ratio of non-solvent to cellulose solution was varied from 4:1 to 8:1.

Emulsion parameters will be specified for each case.

### Particles separation and drying

After a short sedimentation time, the emulsion was centrifuged with addition of twice its volume of 50% EtOH in $H_2O$, at 9000 rpm for 5 min to 10 min. 50% EtOH was added before the centrifugation to prevent the interface jamming which will be described later. Cellulose particles and aqueous liquid sedimented on the bottom while oil floated on the top due to density difference. The floating oil was progressively removed and replaced by 50% EtOH throughout several centrifugation steps. Once most of the oil was washed away, particles were washed at least 6 times in pure EtOH for the subsequent supercritical drying (described in Section 2.2.1 on page 102). In some cases, before washing in pure EtOH, particles were washed in 0.5 M HCl to completely get rid of the remaining NaOH, urea and ZnO.

### Monolith counterparts preparation

Monolith aerogel counterparts were prepared to be compared with the particles made via emulsification. Cellulose was dissolved following the same procedure as described for particles production (Section 4.1.2 on the previous page). Solution was then poured in cylindrical containers and gelled 2 h at 50 °C before coagulation in 0.5 M HCl. The non-solvent was replaced by washing with $H_2O$, at least 5 times every 24 h. Then, $H_2O$ was exchanged for EtOH, also washed at least 5 times, and dried under $CO_2$ Sc conditions.

### Rheological measurements

All rheological measurements were performed with a cone-plate geometry (2 ° - 60 mm) with the device described in Section 2.2.4 on page 110.

Paraffin oil viscosity was measured in steady state mode with shear rate varying from 0.05 $s^{-1}$ to 200 $s^{-1}$ and temperature from 10 °C to 50 °C.

Storage modulus (G'), loss modulus (G") and complex viscosity ($\eta^*$) of cellulose solutions were measured as a function of time. Frequency and stress were set at 1 Hz and 0.01 Pa, respectively, and temperature was varied from 5 °C to 50 °C. Initial complex viscosity ($\eta^*$) of the solutions was recorded before gelation, at the very beginning of the measurement ($\approx$ 12 sec). Gelation time was taken when G' and G" intersect.

### Interfacial tension measurements

Using the method described in Section 2.2.4, interfacial tension was measured for the systems used to make emulsions (values were taken within 5 minutes):

- 3.8% and 5% cellulose-6.7% NaOH-urea-$H_2O$ solutions in oil, without surfactant.
- 0.5 M HCl in oil, with 1.5 vol.% and 0.66 vol.% Span 80.
- 8.6 M AA in oil with 0.66 vol.% Span 80.

### Rheo-optical observations

The rheo-optical device described in Section 2.2.4 on page 110 was used to observe our system, with cellulose solution being the droplet, paraffin oil with Span 80 being the continuous phase. The gap between the transparent plates was set at 1.2 mm. Shear was applied by rotation of the plates in opposite directions. It was increased by steps to observe droplets deformation, stabilisation of the shape and break-up. The images presented were taken after stabilization of the droplet at the targeted shear rate.

## 4.2 Results and discussions

In regards to gelation and coagulation, cellulose is a particular polymer compared to other polysaccharides such as the "easy gelling" solutions of alginate or pectin. While other biopolymers can have a reversible and/or chemically triggered quick gelation, cellulose solutions do not gel when dissolved in ionic liquids, or irreversibly and spontaneously gel with time and temperature increase when dissolved in NaOH based solvents. Because of this property, cellulose solutions' gelation is very hard to control. A lot of parameters influencing gelation, not always well understood, are to be taken into account. In the case of no gelation, when dissolved in ionic liquids, cellulose has to be directly coagulated for aerogel production to be possible. That is why only few is known on cellulose solution emulsions.

In this work, we implemented a new technique for the production of cellulose aerogel particles using emulsion approach. This section starts with the preliminary studies performed to select emulsion's components and conditions as well as their characterisation. Then, different methods were tested, including the one reported by Luo and Zhang (2010a), and the encountered problems are described. Finally, the study done on the influence of the emulsification parameters on aerogels' properties is presented.

### 4.2.1 Preliminary studies to determine emulsification parameters

The selection of emulsion components and conditions were based on application requirements, our background knowledge and on Luo and Zhang (2010a) article. NaOH based solvents were selected for cellulose dissolution because of the final applications: food and potentially medical/pharma. Two different concentrations of cellulose were tested to find the most suitable one within the possible options of cellulose dissolution in NaOH base solvents. On one hand, cellulose concentration should be at least two times higher than the overlap concentration to get "self-standing" beads. It was demonstrated by Roy et al. (2003) that for microcrystalline cellulose, the overlap concentration in NaOH based solvent is around 1%. On the other hand the possible maximum concentration of cellulose to be dissolved in NaOH based solvents, without immediate gelation, is around 6%. The interval of cellulose concentrations is thus within 2% and 5%. Paraffin oil was chosen as continuous phase as it is known to be chemically stable and it was already used to emulsify polysaccharide solutions (Luo and Zhang (2010a); Alnaief et al. (2011)). Finally, Span 80 is a large molecule with a HLB of 4.3, which makes it suitable for using in W/O emulsions. All these components are coherent with what was done by Luo and Zhang (2010a) as they also used them to produce cellulose particles from emulsification technique.

### Rheological measurements

Rheological study of cellulose solutions and paraffin oil is a required step before emulsion preparation as it gives us the gelation time of cellulose solutions as well as their viscosity. With this information we will be able to have more control on gelation of cellulose solutions and we will be able to determine the viscosity ratio between cellulose solution and oil. The latter will give a good indication on emulsion's feasibility.

Figure 4.1 presents gelation time as a function of temperature of cellulose solutions:

- with urea as additive: 3.8% and 5% cellulose-6.7% NaOH-11.5% urea-$H_2O$,
- with ZnO as additive: 5% cellulose-7.56% NaOH-0.5% ZnO-$H_2O$,
- and without any additive: 5% cellulose-7.6% NaOH-$H_2O$.

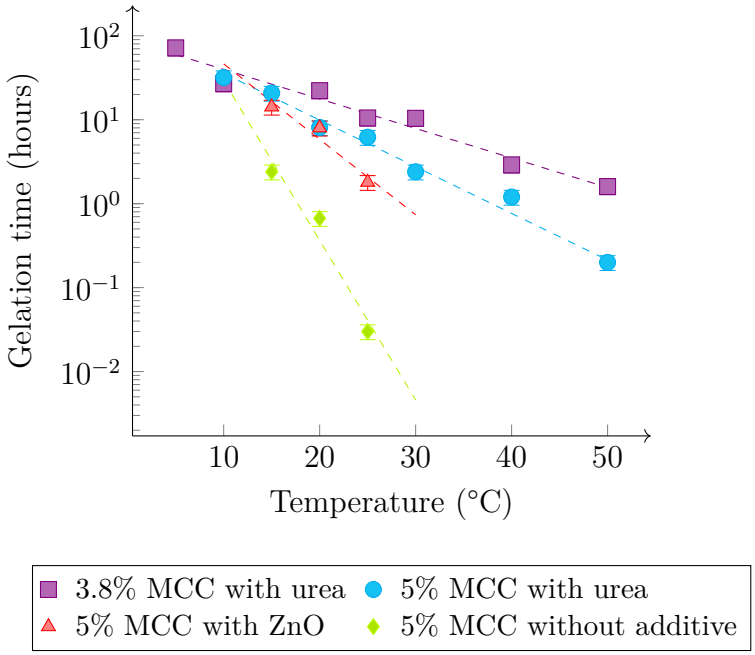


Figure 4.1 – Gelation time of cellulose solutions as a function of temperature. Dashed lines are exponential approximation curves.

The results are in accordance with what was already reported in literature (Roy et al. (2003); Egal (2006); Cai and Zhang (2006); Liu et al. (2011)): with increasing temperature, gelation is quicker and with an additive (urea or ZnO), gelation is delayed. In addition, lower cellulose concentration leads to delayed gelation time and 11.5% urea seems to delay the gelation more efficiently than 0.5% ZnO.

The graph in Figure 4.1 helps us to select the emulsion's conditions in both cases: when cellulose solution gelation is desired and when it is not. At room temperature (25 °C), we can see that gelation time of 5% cellulose solutions with additive is longer than 1 h 30 min while it is less than 1 h without additives. Also, gelation time is further delayed in the presence of urea than with ZnO (6.2 h against 1.5 h) and it could even be delayed to 10.5 h with lower cellulose concentration. Thus, in the case of non-desired gelation, using an additive is the best option. The emulsification would, however, need

to be shorter than 1 h, otherwise only urea as additive is recommended. In the case of desired gelation, multiple combinations are possible. We could use cellulose solution without additive but the not complete dissolution will disturb the formation of stable cellulose droplets (it will be demonstrated in the rheo-optical part and later in this chapter). The use of an additive is thus essential to have a homogeneous solution resulting in spherical droplets in the emulsion. In this case, to trigger gelation in a reasonable time, temperature will need to be increased.

Regarding emulsion's feasibility, viscosity of the cellulose solutions, as well as paraffin oil viscosity, need to be investigated to determine the viscosity ratio. As paraffin oil shows a Newtonian behaviour, it is possible to plot it as a function of temperature. As plotted in Figure 4.2, paraffin oil follows the Arrhenius law.

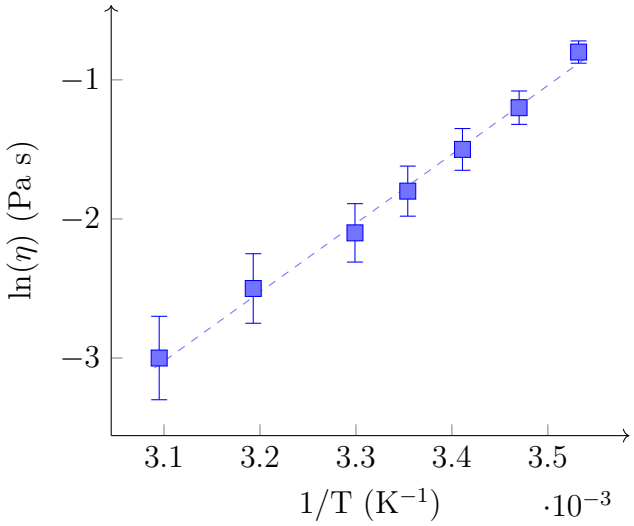


Figure 4.2 – Arrhenius plot of viscosity for paraffin oil. Dashed line is linear approximation.

Table 4.1 summarises the initial complex viscosity ($\eta^*$) of different cellulose solutions with the additives used in this study as well as the paraffin oil viscosity at 20 °C and 25 °C.

Table 4.1 – Initial complex viscosity ($\eta^*$) of the different cellulose solutions and viscosity ($\eta$) of paraffin oil at 20 °C and 25 °C.

| Tested Fluid | 3.8% MCC with urea | 5% MCC with urea | 5% MCC with ZnO | Paraffin oil |
|---|---|---|---|---|
| $\eta^*$ or $\eta$ at 20 °C | 0.06 | 0.14 | 0.16 | 0.22 |
| $\eta^*$ or $\eta$ at 25 °C | 0.04 | 0.12 | 0.15 | 0.16 |

### Viscosity ratio

As seen in the *State of the art*, Section 1.2.2 on page 67, viscosity ratio ($p = \lambda = \frac{\eta_d}{\eta_c}$ with $\eta_d$ and $\eta_c$ the viscosity of the dispersed and the continuous phases, respectively),

together with the Critical Capillary Number ($C_a^{Crit}$), can be used to determine if droplet break-up will happen and at what size of droplet. For simplicity we will consider, in the first approximation, that the flow in the emulsion is laminar with a shear regime. In this type of regime, the critical capillary number reaches a minimum for a viscosity ratio of 1. To calculate viscosity ratio, we use viscosity of cellulose solutions at the very beginning of shearing (i.e. no gelation). For our solution droplets to break-up in paraffin oil, the viscosity ratio will have to preferably be less than 1. Table 4.2 presents the viscosity ratios of paraffin oil to different cellulose solutions at 20 °C and 25 °C.

Table 4.2 – Viscosity ratios ($\lambda$) of cellulose solutions and paraffin oil used at 20 °C and 25 °C.

| cellulose solution | 3.8% MCC with urea | 5% MCC with urea | 5% MCC with ZnO |
|---|---|---|---|
| $\lambda$ at 20 °C | 0.27 | 0.64 | 0.73 |
| $\lambda$ at 25 °C | 0.25 | 0.75 | 0.94 |

We can see that for all cases viscosity ratio is lower than 1. From these results we can conclude that the breakage of droplets should happen, whatever the solution used. Elongational component of flow which is present when using marine impeller should help the breakage.

### Interfacial tension

Interfacial tension is, as the viscosity ratio, an important parameter to take into account for the emulsification of our solutions. As it was seen before in Chapter 1, the Laplace forces, which describe the cohesive forces, are a function of the surface tension. Also, the capillary number is calculated depending on the interfacial tension between the two fluids. With a low interfacial tension, breakage will be more likely to happen than with a higher one. Surfactant can also be used to lower the interface tension.

Interfacial tension ($\sigma$) of cellulose solutions in paraffin oil was measured at the macroscopic scale. Interfacial tension of 3.8% cellulose solution with urea was measured without surfactant as the latter is degrading in strong alkaline media. The interfacial tension between acid non-solvents, 0.5 M HCl and 8.6 M AA, and paraffin oil was measured with two concentrations of Span 80: 1.5 vol.% and 0.66 vol.% (volume in oil). These correspond to the concentrations used in the emulsions of this work. Table 4.3 gives the results obtained. Cellulose solutions' density did not significantly vary and was around 1.25 g $cm^{-3}$. 0.5 M HCl density was taken as 1.01 g $cm^{-3}$ and 8.6 M AA one was 1.058 g $cm^{-3}$ (density were calculated from measuring the mass and volume of fluids).

Table 4.3 – Interfacial tension between cellulose solution, 0.5 HCl, 8.6 M AA and paraffin oil at 20 °C.

| | 3.8% MCC with urea | 0.5 M HCl 1.5 vol.% Span 80 | 0.5 M HCl 0.66 vol.% Span 80 | 8.6 M AA 0.66 vol.% Span 80 |
|---|---|---|---|---|
| $\sigma$ (mN m$^{-1}$) | 35 | 3.2 | 6.9 | 4.1 |

Cellulose solution shows really higher surface tension with paraffin oil as compared to the non-solvents. The presence of surfactant in the continuous phase of systems with non-solvents can explain this important difference. We considered that the surface tension between cellulose solution concentration of 3.8% and 5% was the same within the experimental errors.

The results of interfacial tension obtained for the non-solvents allow us to conclude on two aspects: the influence of surfactant concentration and the type of acid on the interfacial tension. As expected, with increasing Span 80 concentration, the surface tension decreases. If we compare 0.5 M HCl with 8.6 M AA, for the same Span 80 concentration, we can see that AA has a lower interfacial tension with oil than HCl. This can be due to two main reasons: the first one is the molecular structure of AA compared to HCl, and the second is the solubility of the acids in paraffin oil. Firstly, AA and HCl are two very different molecules, both of them are polar, but AA also possesses a non-polar group (more lypophilic). AA can thus act like a "surfactant" and more interactions will happen between AA and oil than between HCl and oil. Secondly, the partial solubility of AA in paraffin oil can also increase the interactions at the interface of the two fluids. These two reasons are both leading to a lower interfacial tension for 8.6 M acetic acid with paraffin oil than for 0.5 M HCl with paraffin oil.

**Visualisation of droplet behaviour with rheo-optics**

Rheo-optical technique was used to illustrate the behaviour of a droplet of cellulose-NaOH-$H_2O$ solution (without and with additives) placed in paraffin oil and submitted to shear.

We started with the analysis of a droplet of 5% cellulose-8% NaOH without additive. As demonstrated in Figure 4.3, cellulose was not fully dissolved in 8% NaOH-$H_2O$ without additive (Figure 4.3 a). It is clear that the swollen cellulose particles are disturbing the break-up mechanism of the droplet which may then influence the homogeneity of the emulsion. Under shear, non-dissolved cellulose particles stay agglomerated in the centre of the droplet while low concentrated cellulose solution is progressively expelled from it (Figure 4.3 b, c and d). There is hence formation of highly concentrated cellulose particle droplets on one side and formation of low concentrated cellulose solution on the other side. This inhomogeneous emulsion will lead to different sizes and shapes of the droplets with irregular properties. The use of an additive during cellulose dissolution was thus proven to be necessary.

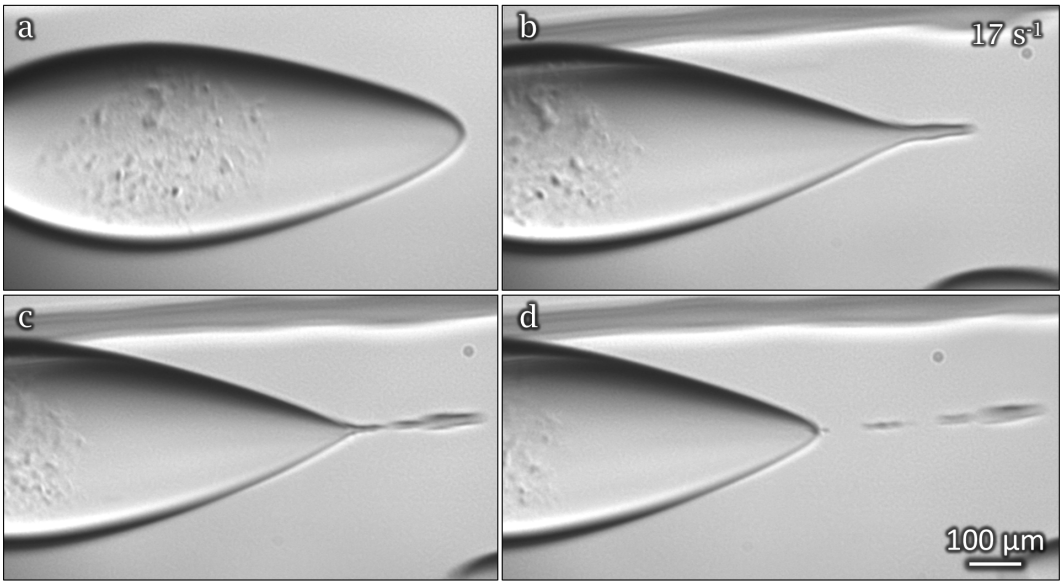


Figure 4.3 – Pictures illustrating the evolution in time (deformation and break-up) of 5% cellulose-8% NaOH-water solution droplet placed in paraffin oil at 17 $s^{-1}$ shear rate. Shear rate and scale are the same for all pictures.

The deformation of a droplet of 3.8% cellulose-8% NaOH-11.5% urea-$H_2O$ in paraffin oil was then studied. As it will be observed later, Span 80 decomposes in the presence of NaOH solutions. We thus added a very small quantity of Span 80, $\approx$ 0.15 vol.%, to facilitate droplet break-up on one hand, but to decrease the influence of surfactant decomposition on the other. Figure 4.4 shows the deformation of a cellulose solution droplet in paraffin oil at different shear rates, until break-up.

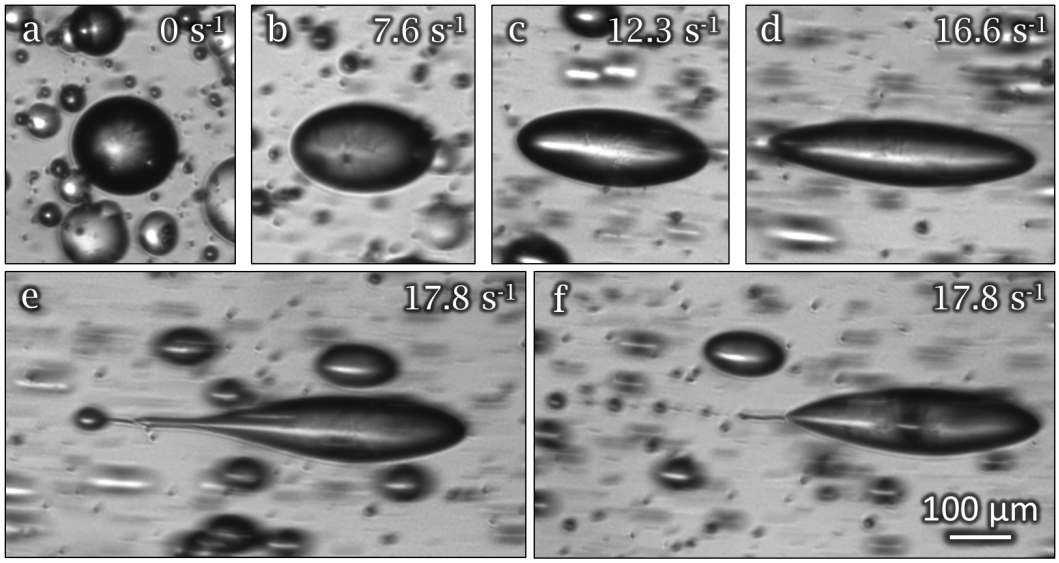


Figure 4.4 – Pictures illustrating the deformation and breakage of a droplet of 3.8% cellulose-6.7% NaOH-11.5% urea-water placed in paraffin oil with 0.15 vol.% of Span 80 with increasing shear rate. Shear rates are given on the top right corner of each picture and the scale is the same for all pictures.

We can observe multiple phenomena on this figure, among them the droplet deformation and the droplet break-up. At rest (Figure 4.4 a) the droplet is spherical with a diameter of 171 µm. With increasing shear rate, the droplet gradually deforms into an ellipsoid with a small orientation angle towards flow direction (Figure 4.4 b, c and d). The small deformation limit of the droplet, as established by Taylor (1934) ($D = \frac{L-B}{L+B} < 0.2$, see Equation (1.4) on page 70), was already exceeded for a shear rate of 7.6 $s^{-1}$ with $D = 0.23$. Upon reaching the critical deformation at 17.8 $s^{-1}$ (Figure 4.4 e and f), the droplet breaks-up from one side by tipstreaming. This break-up mechanism was reported several times in the past (Taylor (1934); Rumscheidt and Mason (1961); Grace (1982); De Bruijn (1993)) and De Bruijn (1993) described it as *"Tipstreaming in simple shear flows is a mode of droplet break-up in which the droplet develops a sigmoidal shape and a stream of tiny droplets is ruptured off the tips of the drop"*. He suggested that this type of break-up mechanism occurred because of the development of a gradient of interfacial tension at the surface of the droplet, leading to lower surface tension at the tips of the droplet. The fact that break-up occurs only on one tip may be due to the non-homogeneous environment in which the droplet is: other droplets are present and may perturb shear stress distribution around the droplet.

The other observable phenomena from the rheo-optical analysis were the short time needed for the droplet to reach the steady state deformation (when no further deformation can be observed at a constant shear rate) and the very fast relaxation time (the time needed for the droplet to return to its spherical shape when shear is stopped). The graph on Figure 4.5 shows D, the Taylor's droplet deformation parameter, as a function of strain ($shear\ rate * time$), representing the number of strain units for the droplet to reach the steady state deformation. This graph was obtained by measuring the deformation of a droplet at a constant shear rate, over time, just after the shear rate was increased from 13 $s^{-1}$ to 15 $s^{-1}$. The droplet was thus already deformed from the previous stress before we started the measurement, this explains why D does not start from 0 but from 0.46. We can see that the stabilisation of the shape of the droplet is relatively fast, it takes less than 2 s, corresponding to a strain of less than 30. This is due to the low cohesive forces and the low viscosity ratio ($\lambda = 0.25$). Figure 4.6 represents the relaxation of the droplet to undeformed state plotted for D as a function of time. The size of the droplet at 0 second was recorded when the shear rate of 17.5 $s^{-1}$ was stopped and the relaxation was observed over time. We can see that the droplet needs only around half a second to go back to its spherical shape and no break-up of the droplet was observed during relaxation. Based on the study of Tjahjadi et al. (1994), it is no surprise as the critical aspect ratio ($AR_{crit} = \frac{L}{B}$) at which the droplet will break-up during relaxation for our viscosity ratio ($\approx 0.25$) is around 15 and the aspect ratio of the droplet before stopping the shear was 3.4.

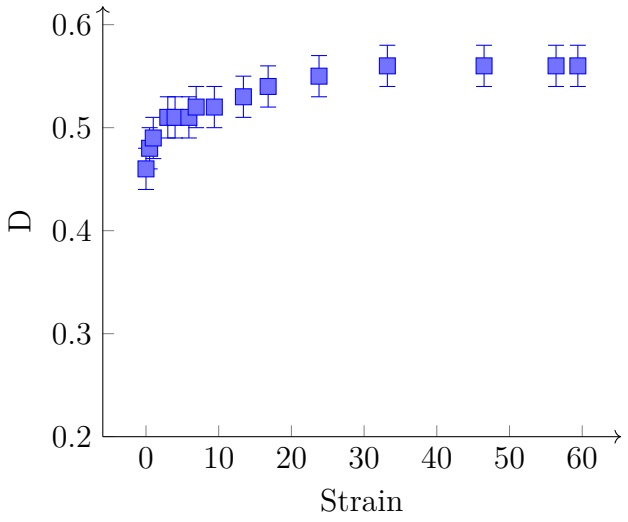


Figure 4.5 – D (the Taylor's droplet deformation parameter) as a function of strain (*shear rate* $*$ *time*) for a droplet of 3.8% cellulose-6.7% NaOH-11.5% urea-$H_2O$ in paraffin oil with 0.15 vol.% Span 80 just after shear rate was increased from 13 $s^{-1}$ to 15 $s^{-1}$ (shear rate constant at 15 $s^{-1}$ during observation).

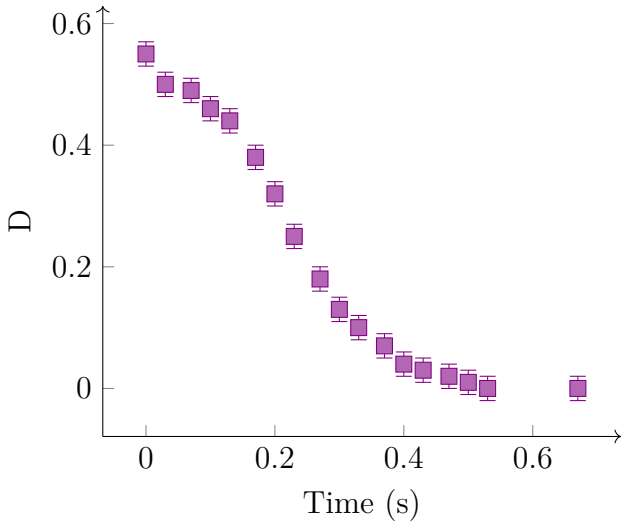


Figure 4.6 – D as a function of time representing relaxation of a droplet of 3.8% cellulose-6.7% NaOH-11.5% urea-water in paraffin oil with 0.15 vol.% Span 80 when shear rate was stopped from 17.5 $s^{-1}$ (shear rate null during observation).

### 4.2.2 Implementation of cellulose solutions' emulsification method

The preliminary studies, described above, show that we can theoretically emulsify cellulose solutions in paraffin oil, with droplet break-up demonstrated by rheo-optics. This section will give a chronological overview of different approaches tested to make cellulose solution droplets via emulsion method, with a description of the problems encountered and solutions found. It should be noted (and it will be demonstrated) that classical approaches used to make gelled polysaccharide particles via emulsion method cannot be directly applied to cellulose solutions. The results presented below are only the beginning of the long way in the understanding of making stable cellulose droplets and aerogel particles via emulsion method.

#### Direct emulsification

Following the protocol described in the article of Luo and Zhang (2010a), we emulsified 3.8% MCC-6.7% NaOH-11.5% urea-$H_2O$ in paraffin oil, with the addition of 1 vol.% Span 80. However, when checking under the optical microscope the evolution of the cellulose solution droplets after 30 min and 2 h stirring (Figure 4.7), we clearly saw that they got deformed over time with the appearance of a rough "skin" on their surface.

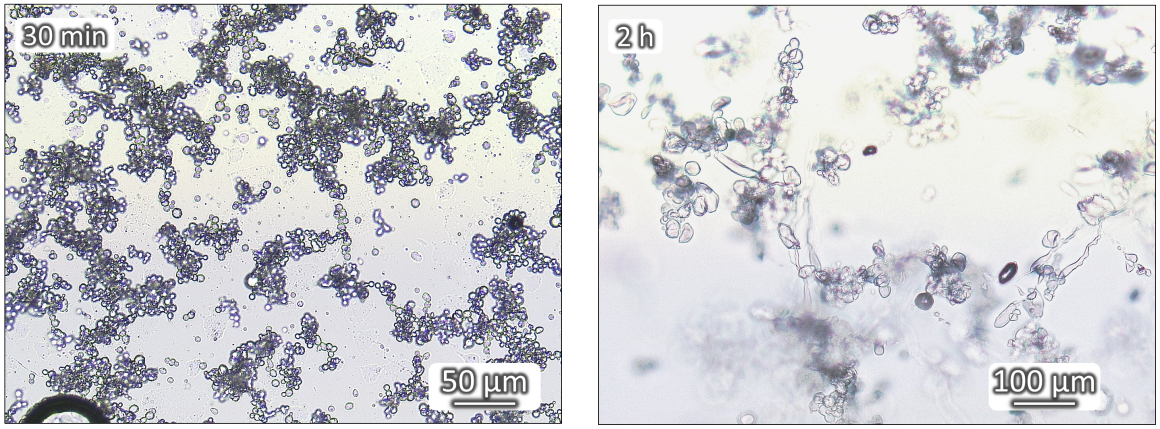


After 30 min stirring | After 2 h stirring

Figure 4.7 – Picture of 3.8% MCC-6.7% NaOH-11.5% urea-$H_2O$ solution emulsified in paraffin oil with 1 vol.% Span 80, after 30 min and 2 h.

Cellulose is dissolved in a solvent of very high pH (more than 14), we suppose that the reason of the formation of this skin and of irregular shape of the droplets is saponification of the surfactant. Hydrolysis of the ester of the Span 80 could happen in contact with the basic cellulose solution (see Span 80 chemical representation in Figure 2.4 on page 100).

To validate this hypothesis, we emulsified only the solvent, 6.7% NaOH-12% urea-$H_2O$, in paraffin oil with 1 vol.% Span 80. The same "skin" appeared on the surface of

the solvent droplets after mixing, as shown in Figure 4.8; this was never reported in literature. The surfactant is losing its properties and cannot be used in this way.

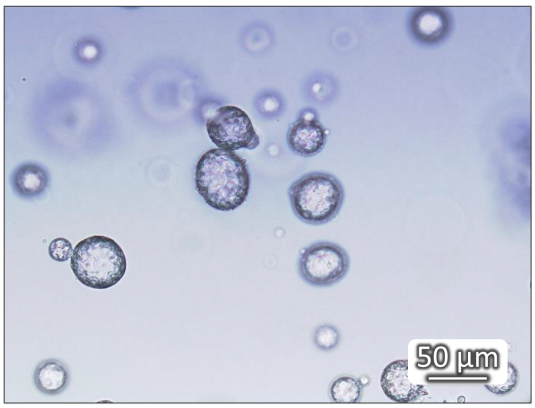


Figure 4.8 – Picture illustrating the formation of a "skin" on the surface of 6.7% NaOH-11.5% urea-$H_2O$ droplets dispersed in paraffin oil with 1 vol.% Span 80, after 2 h mixing.

To avoid surfactant saponification, we decided to emulsify the cellulose solutions without it. As Figure 4.9 demonstrates, even if the obtained droplets were rather big and with a bimodal size distribution (around 250 µm and from 30 to 50 µm diameter), the emulsification worked out in a reasonable way.

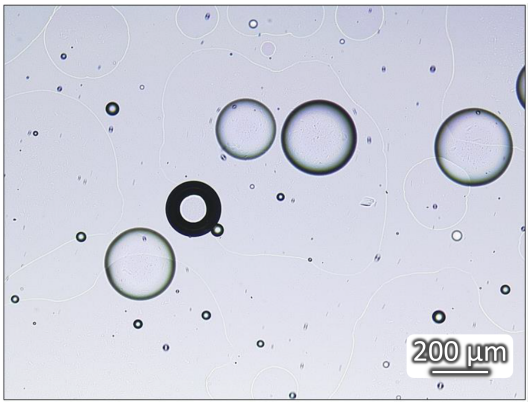


Figure 4.9 – Picture of the 5% cellulose-6.7% NaOH-11.5% urea-$H_2O$ droplets in paraffin without surfactant, after 30 min mixing at 700 rpm.

### Cellulose coagulation from the emulsion

Following the procedure suggested by Luo and Zhang (2010a), we directly coagulated the cellulose droplets by addition of 0.5 M HCl in the emulsion. The acid was added drop wise with a syringe equipped of a needle with a diameter of 0.8 mm. Once again, this procedure did not work as we expected and we obtained deformed and broken cellulose particles. Two hypotheses are possible to explain this result:

- The addition of acid droplets, directly in the emulsion, may have disturbed the stability of the latter.

- The diameter of acid droplets may be too big compared to the cellulose droplets in emulsion, leading to deformed or broken coagulated cellulose particles.

In view of these results, a completely different approach needed to be found.

### Implementation of the "separated" emulsions technique

In the previous section, we have seen that the saponification of the surfactant with the basic cellulose solvent prevented us from using Span 80 for cellulose solution emulsification. Furthermore, a dropwise addition of the non-solvent in cellulose solution emulsion was not possible as it also led to broken and deformed particles. Therefore, we decided to try a new approach by mixing two separate emulsions:

- one emulsion of the cellulose solution in paraffin oil without surfactant,
- and the other of the non-solvent in paraffin oil with Span 80.

We have seen previously that the emulsification of cellulose solutions in paraffin oil without surfactant worked properly (Figure 4.9). However, surfactant had to be added to non-solvent dispersed in paraffin oil as coalescence rate of the acid droplets was too high to get a relatively stable second emulsion. Figure 4.10 shows HCl droplets dispersed in paraffin oil with 1 vol.% Span 80: the droplets were quite small (mean diameter of $\approx 17$ µm) with a wide mono-dispersed size distribution (size between 10 µm and 30 µm, measured from microscope images) but somehow they were agglomerated. The reason why the acid droplets are agglomerating may be due to a beginning of coalescence, because of the not stable emulsion, and it should be taken into account that hydrolysis of the surfactant may occur due to strong acid medium of the dispersed phase (0.5 M HCl).

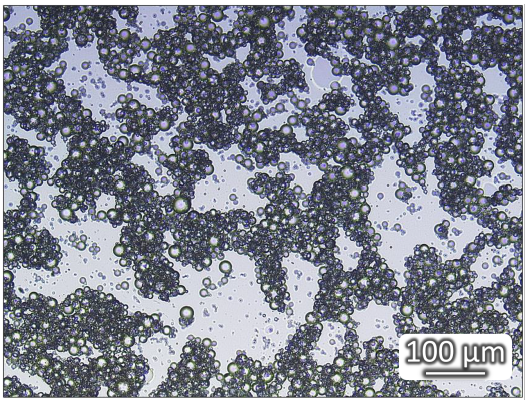


Figure 4.10 – Picture of the 0.5 M HCl emulsion with 1 vol.% Span 80 after 30 min of mechanical stirring at 700 rpm.

Once the two emulsions were prepared, we mixed them together to trigger cellulose coagulation by coalescence of the cellulose solution droplets with the acid droplets (a schematic representation of the process implemented was already given in Figure 2.9 on page 105). Figure 4.11 shows the resulting mixed emulsions. We can see on Figure 4.11 a that the observable droplets seem to be spherical and well shaped even though their

size distribution is wide. However, as shown on Figure 4.11 b, it seems that droplets are composed of sort of particles.

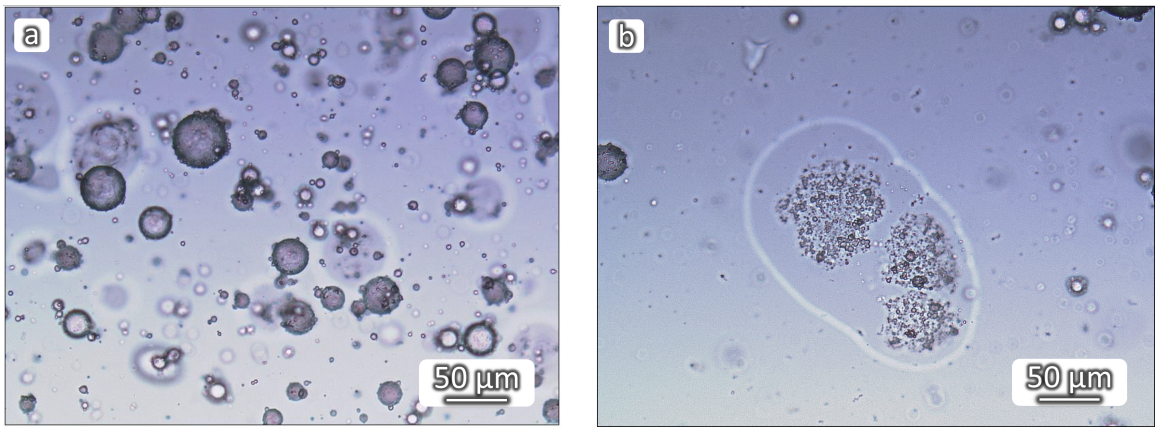


Figure 4.11 – a: Picture of the cellulose solution emulsion and the 0.5 M HCl emulsion mixed together for 2 h at 1000 rpm. b: picture was taken after HCl droplets met with the microscope slide, revealing cellulose particles.

We assume that the droplets seen in Figure 4.11 a are heterogeneous and are made of coagulated cellulose particles that are inside big acid droplets. But, knowing that the cellulose droplets (Figure 4.9) were bigger than the acid ones (Figure 4.10) before mixing of the two emulsions together, how did this size ratio reversed? Before mixing of the two separate emulsions together, there was no Span 80 in the cellulose solution emulsion while there was 1 vol.% in the acid emulsion. When we mixed the two emulsions together, we increased the stirring speed from 700 rpm to 1000 rpm to ensure an efficient stirring of the larger volume of liquid, but we hereby increased the shear rate. In addition, the overall Span 80 concentration decreased to 0.52 vol.%. Thus, with a higher stirring speed and the presence of surfactant, we can assume that the cellulose droplets' size decreased as compared to their size in the separate cellulose solution-oil emulsion. On the other side, as the concentration of Span 80 decreased this could lead to an increase of coalescence of HCl droplets.

It will be shown later that the size of obtained cellulose aerogel particles is similar to the one of the small particles observed in Figure 4.11 b.

### Particles separation

The separation of cellulose particles and aqueous phase from the oil was done by centrifugation. However, an important phenomenon happened: the formation of a layer of coagulated cellulose at the interface between the oil and the aqueous phase after centrifugation (see Figure 4.12 a). This phenomenon is called "interface jamming".

The most probable reasons for the appearance of an "interface jamming" are:

- the presence of Span 80 at the interface of the two phase during separation,
- and the probable incomplete coagulation of cellulose.

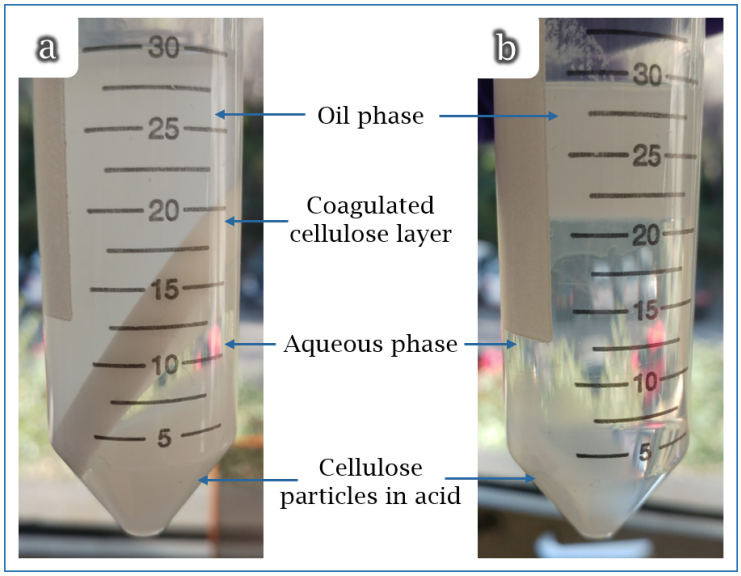


Figure 4.12 – a: picture of the interface jamming after centrifugation. b: example of a proper phase separation after centrifugation.

Indeed, during centrifugation, because of density difference, cellulose particles as well as the aqueous phase will sediment while the oil will float. During centrifugation, the reduction of the surface area between the two phases occurs and a concentrated layer of Span 80 is formed at the interface between the oil and the aqueous phase. Non-coagulated (or partly coagulated) cellulose will sediment and "settle" at the interface between the two fluids during phase separation, because of the concentrated layer of Span 80. Coagulation of the non-coagulated cellulose will start as the centrifugation continues, hence forming this coagulated cellulose layer: the interface jamming.

To avoid this interface jamming, two main approaches are possible:

- to adapt the centrifugation process in order to avoid jamming during the phase separation,
- or to change the system, and more particularly the non-solvent, to ensure a complete coagulation of the cellulose before centrifugation.

To avoid the jamming during the phase separation, we had to find a way to let the non-coagulated cellulose droplets pass through the Span 80 interface between the oil and the aqueous phase while still keeping their size. The addition of another cellulose non-solvent, just before centrifugation, which is soluble in both oil and aqueous phase, would help avoiding the formation of a "solid" layer of cellulose at the interface. Ethanol, that will be used later for the supercritical drying, is an excellent candidate as it is soluble in both paraffin oil and the aqueous phase. Yet, the density of neat EtOH is lower than the one of paraffin oil. If added "as is" to the mixed emulsions, it will float above the paraffin oil after centrifugation. We thus decided to add 50% of EtOH in $H_2O$, before centrifugation. The result was successful and led to a proper phase separation as shown on Figure 4.12 b.

The second approach would be to change the system to ensure a better coagulation of cellulose before centrifugation. The most efficient way to do so would consist of changing the non-solvent used by the one which is soluble (or partly soluble) in paraffin oil and which would trigger a "fast" cellulose coagulation. In this case, the coagulation mechanism in the mixed emulsions would change: it would not be a simple coagulation by coalescence (Figure 4.13) but coagulation by both diffusion (Figure 4.14) and coalescence. With the coagulation induced only by coalescence, for example in the case of 0.5 M HCl, cellulose coagulates only if solution droplet meets and coalesces with a non-solvent droplet. If we add the mechanism of diffusion to the coalescence, cellulose will start to coagulate at the moment we mix the non-solvent emulsion with the cellulose solution emulsion. A skin of coagulated cellulose will form on the surface of the cellulose solution droplet helping to fix droplet's shape. Then, with diffusion continuation or/and with coalescence with a non-solvent droplet, coagulation of the cellulose droplet will be completed.

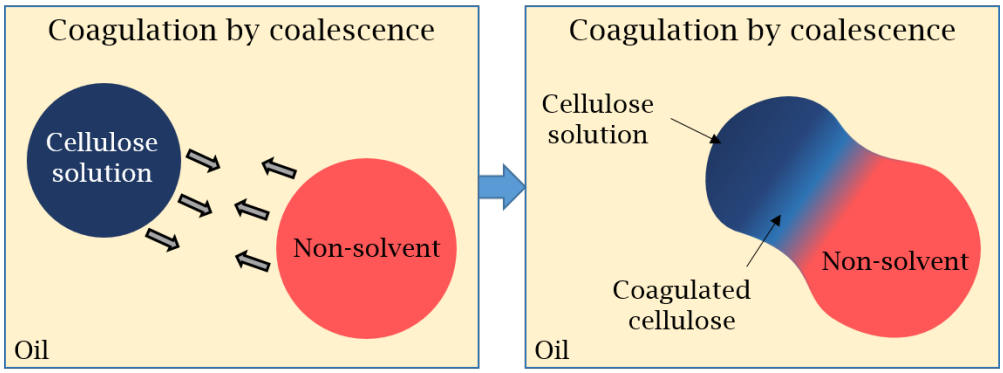


Figure 4.13 – Schematic representation of the coagulation of cellulose due to droplets' coalescence.

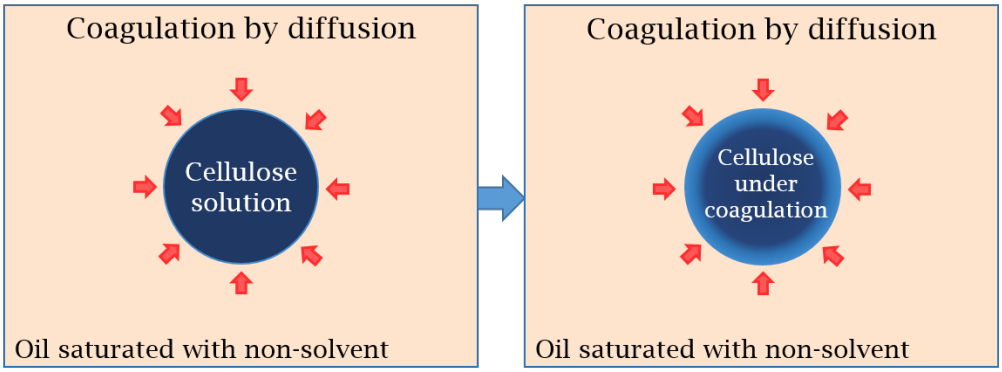


Figure 4.14 – Schematic representation of the coagulation of cellulose by diffusion of non-solvent from oil.

This idea was tested using ethanol as non-solvent to trigger coagulation by diffusion as it is partly soluble in paraffin oil. However, it appeared that urea is not soluble in ethanol and urea crystals formed during cellulose coagulation, making the formation of

spherical and regular cellulose particles impossible. Finally, we selected aqueous acetic acid (AA) which is well known to coagulated cellulose, but also to be partly soluble in paraffin oil. 8.6 M AA was emulsified in paraffin oil with 1 vol.% of Span 80 in the same way as 0.5 M HCl was. As shown in Figure 4.15, the emulsification was successful, with AA droplets of around 8 µm mean diameter. The lower interfacial tension of 8.6 M AA compared to 0.5 M HCl with paraffin oil can explain the smaller mean diameter of AA droplets compared to HCl droplets (≈ 17 µm). Furthermore, in opposition to HCl, AA droplets were not agglomerated. AA being a weak acid, the hydrolysis of Span 80 was less likely to happen.

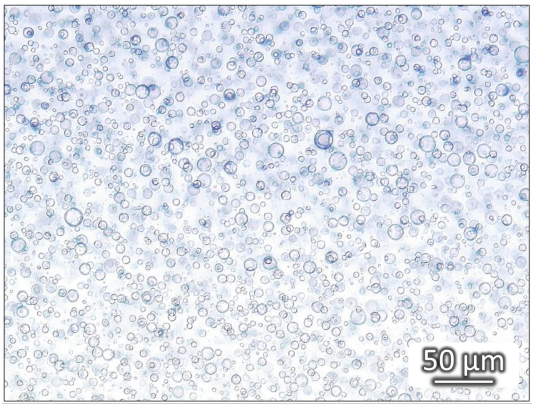


Figure 4.15 – Picture of the 8.6 M AA emulsion with 1 vol.% of Span 80 after 30 min of mechanical stirring at 700 rpm.

Cellulose solution emulsion and AA emulsion were then mixed together to trigger cellulose coagulation by diffusion and by coalescence. The obtained mixed emulsions was then centrifuged with addition of 50% EtOH for phase separation. This led to a proper phase separation, similar to the one shown in Figure 4.12 b.

After separation and washing from the oil, the particles were washed in pure ethanol for the subsequent supercritical drying. Figure 4.16 shows pictures of HCl coagulated cellulose particles (a) and the AA coagulated cellulose particles (b), in pure ethanol, just before Sc drying.

With the two non-solvents used, and hence with the two approaches, cellulose particles were successfully obtained. Cellulose particles coagulated with AA were more regular in size and shape as well as bigger than the ones coagulated with HCl (mean diameter 35 µm against 18 µm, respectively), the latter looked somehow agglomerated. The reasons for these differences will be discussed later (Section 4.2.3 on page 168).

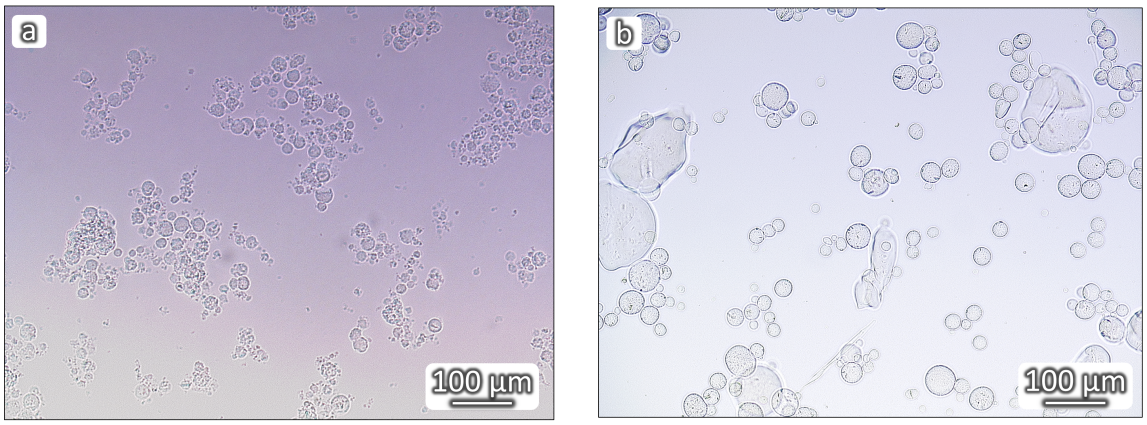


HCl coagulated cellulose particles AA coagulated cellulose particles

Figure 4.16 – Optical microscopy images of cellulose particles after coagulation with (a) HCl and (b) AA, in suspension in pure ethanol, before drying.

Emulsification and coagulation of cellulose solution droplets, as well as separation of the resulting cellulose particles was done successfully with two methods, implying two non-solvents. The particles were washed in ethanol to proceed to the supercritical drying. The following section will focus on the characterisation of obtained cellulose aerogel particles as a function of emulsion parameters.

### 4.2.3 Influence of emulsion parameters on cellulose aerogel particles' properties

A new method to produce cellulose particles from emulsions was implemented as described above. How different parameters of this method influence the properties of resulting aerogel particles is still unknown. In this section, we will tackle this question by varying several parameters of emulsions such as cellulose solution concentration, non-solvent volume or coagulation mechanism.

The emulsification procedure will always be the one as described in Section 4.2.1, with standard parameters as:

- 5% MCC-11.5% urea-6.7% NaOH-water solution.
- No gelation of the cellulose solution before coagulation.
- HCl as non-solvent.
- Cellulose solution to oil volume ratio in the first emulsion of 1:10, without surfactant.
- Non-solvent to oil volume ratio of 1:2, with 1 vol.% Span 80.
- Non-solvent to cellulose solution volume ratio of 4:1.

Changes of these parameters will be stated in each case.

### Cellulose solution concentration

Two cellulose concentrations in solution were tested for the production of aerogel particles: 3.8% and 5%. As it was demonstrated in Section 4.2.1, higher cellulose concentration (5%) should lead to a more viscous solution which should be favourable for the droplets' stability. The obtained aerogel particles are presented in Figure 4.17.

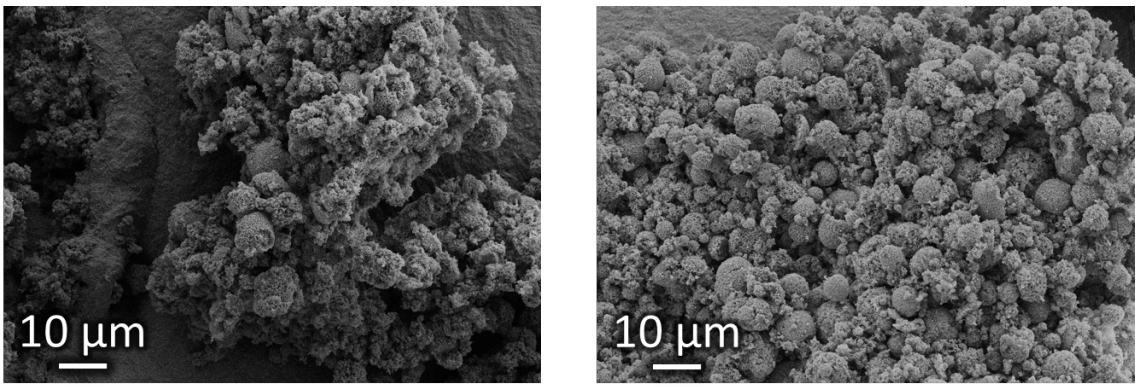


From 3.8% cellulose solution From 5% cellulose solution

Figure 4.17 – SEM pictures of HCl coagulated cellulose aerogel particles from 3.8% and 5% cellulose-6.7% NaOH-11.5% urea-water solutions.

From these SEM pictures, we can see that in both cases, cellulose aerogel particles are agglomerated and a lot of them are broken or surrounded by debris. For a 3.8% cellulose concentration, particles are hard to distinguish. The presented agglomerates are mostly constituted of broken particles and debris. If comparing them with the ones from the 5% cellulose solution, it seems that round particles are more distinguishable, even if they are also surrounded by a lot of debris. The debris are probably coming from the phase separation stage and also from particles breakage during mixing at coagulation stage.

### Gelation

It is known that many aerogel particles based on polysaccharides are made via gelation of polymer solution droplets. Thus the idea here was that gelation should help droplet shape stabilisation. It is very well known that cellulose solutions in 8% NaOH are gelling with time and temperature. The rheological study presented in Section 4.2.1 on page 147 allowed us to accurately determine the gelation time of our cellulose solutions. We thus added a heating step (3 h at 50 °C) to our emulsion process to trigger gelation of cellulose solution droplets before mixing the two emulsions together. Figure 4.18 gives an updated version of the emulsion process we are using in this particular case.

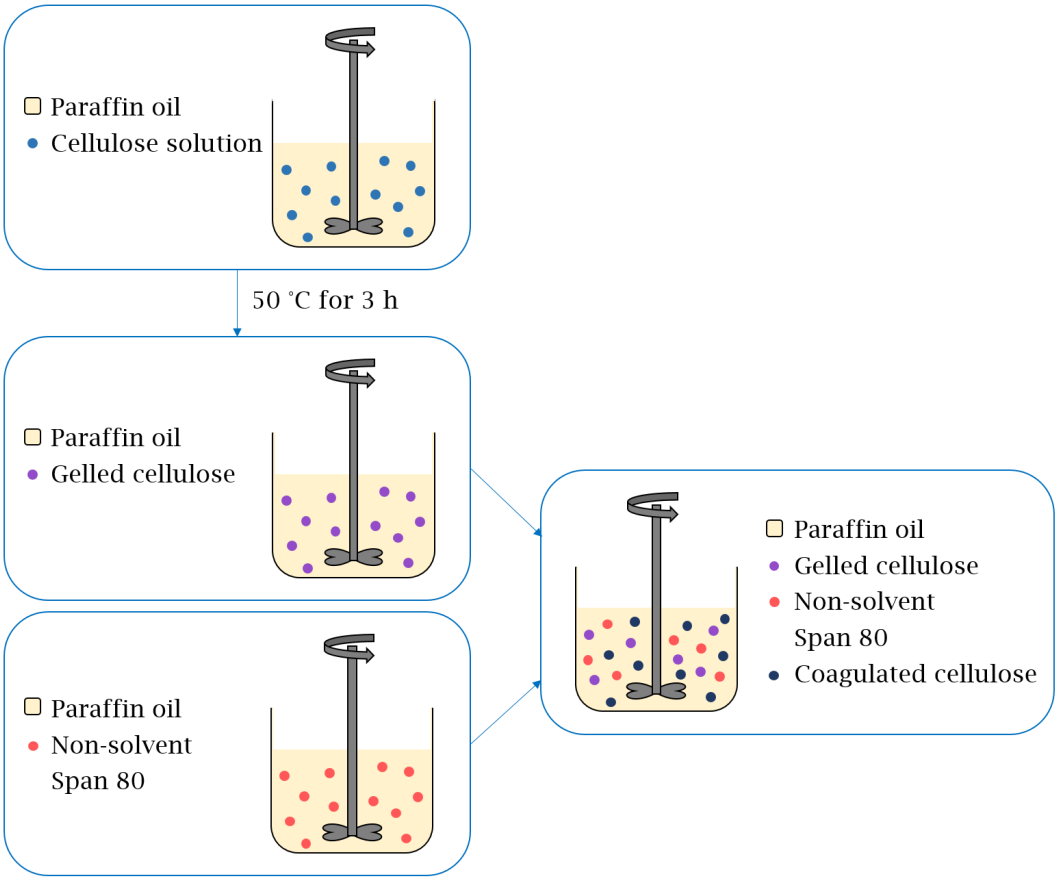


Figure 4.18 – Schematic representation of the "separated" emulsion technique with gelation of the cellulose solution before coagulation.

SEM pictures of the resulting aerogel particles are presented in Figure 4.19 on the next page. Unexpectedly almost no particles can be distinguished from these pictures; the only one that can be seen on the left picture had a rather large diameter ($\approx 47$ µm). Cellulose solution gelation happens in time, forming a weak gel. During emulsification and heating process, breakage and coalescence of the droplets happen. On one hand, because gels are weak they were broken, and on the other hand, gelled droplets were not able to "reshape" and to coalesce because they were gelled. This leads to the formation of debris instead of the expected spherical particles. Only a very small number of particles could "survive" the whole process. The fact that the stirring speed was increased from 700 rpm to 1000 rpm during mixing of the two emulsions could also be the cause of further breakage and debris production.

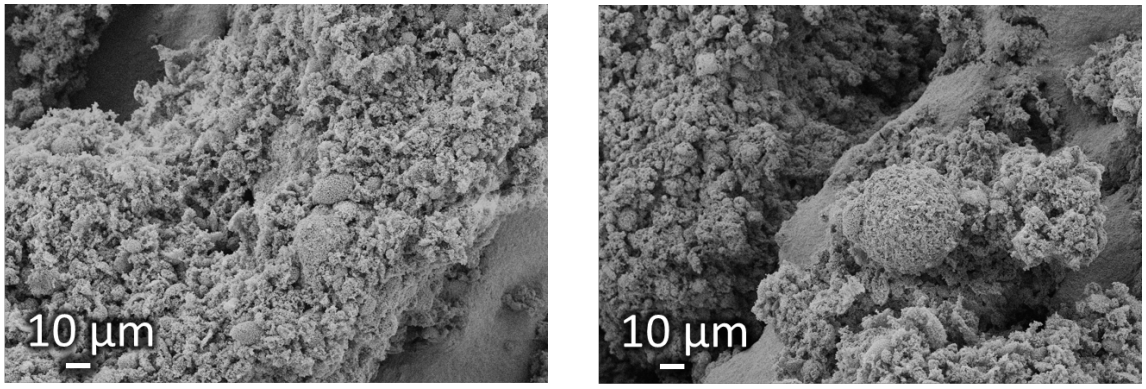


Figure 4.19 – SEM pictures of cellulose aerogel particles obtained from emulsion technique with pre-gelation of the cellulose, before coagulation.

In the view of these non-successful results, it was decided not to put more efforts on gelation of cellulose solution droplets during emulsification.

**Ratio of cellulose solution to paraffin oil**

The influence of the phase ratio in the cellulose solution emulsion (the volume of cellulose solution to the volume of oil) on the resulting particles' size and shape was studied. Two different phase ratios were tested: 1:10 and 1:3 (cellulose solution:oil). To ensure a complete cellulose coagulation and neutralisation of NaOH, the volume of acid was always four times the volume of cellulose solution. The volume ratio of cellulose non-solvent to oil in the acid emulsion was always 1:2 (acid:oil) with a constant concentration of surfactant of 1 vol.%. Only the amount of oil and non-solvent in the acid emulsion was adapted to fit the preceding requirements. When the two emulsions were mixed together the overall volume ratio of dispersed phases (cellulose solution + acid) to oil and the surfactant concentration were:

- For the initial 1:10 (cellulose solution:oil), the final ratio was 1:4:18 (cellulose solution:acid:oil) and the overall ratio was 1:3.6 (dispersed phases:oil), with 0.52 vol.% of surfactant concentration (towards total volume).
- For the initial 1:3, the final ratio was 1:4:11 and the overall ratio was 1:2.2, with 0.75 vol.% of surfactant.

As an example of calculation, with the initial ratio of 1:10 (cellulose solution:oil) we have:
For the cellulose solution emulsion:

- Cellulose = 1.
- Oil = 10.

The ratio is 1:10.

For the non-solvent emulsion:

- Acid = 1.

- Oil = 2.

But the volume of non-solvent is always four times the volume of cellulose solution, hence:

- Acid = $1 * 4 = 4$.
- Oil = $2 * 4 = 8$.

The ratio is 4:8.

Finally, we have in the mixed emulsions:

- cellulose = 1.
- acid = 4.
- oil = $10 + 8 = 18$.

The final ratio is 1:4:18.

The overall ratio corresponds to the volume of dispersed phases (= cellulose solution + acid) to the volume of oil, hence we have:

- Dispersed phase = $1 + 4 = 5$.
- Oil = 18.

which gives:

- Dispersed phase = $5/5 = 1$.
- Oil = $18/5 = 3.6$.

The overall ratio is 1:3.6.

Figure 4.20 shows the resulting particles, as a function of initial cellulose solution to oil volume ratio. With a lower quantity of cellulose solution as compared to oil (initial volume ratio 1:10), the particles are more distinguished and less debris are present. Three main reasons can explain this phenomenon:

- The lower volume ratio (1:10 compared to 1:3) led to less coalescence during emulsification of the cellulose solution.
- The total dispersed phase volume as compared to oil volume in the mixed emulsions (1:3.6 against 1:2.2). When the initial cellulose solution to oil ratio is 1:10, the overall volume of oil when the two emulsions are mixed together is greater that when the initial cellulose solution to oil ratio is 1:3 (1:4:18 against 1:4:11 or in volume of oil; 18 against only 11). This higher volume of oil led to less coalescence events between the droplets of the dispersed phase (cellulose solution and non-solvent). Cellulose solution droplets had then more time to stabilize in the new conditions of the mixed emulsions because of less coalescence events and this led to more regular shaped particles.
- The higher surfactant concentration in the mixed emulsion (0.75 vol.% against 0.52 vol.%) for initial cellulose solution to oil ratio of 1:3 should be favourable for preserving the shape and the integrity of the cellulose droplets when they were not coagulated yet. However, it may be possible that the higher coalescence rate between cellulose solution droplets and acid droplets (as discussed before) counterbalance this

effect. Coalescence happens more often after mixing of the emulsions, leading to irregular and broken particles.

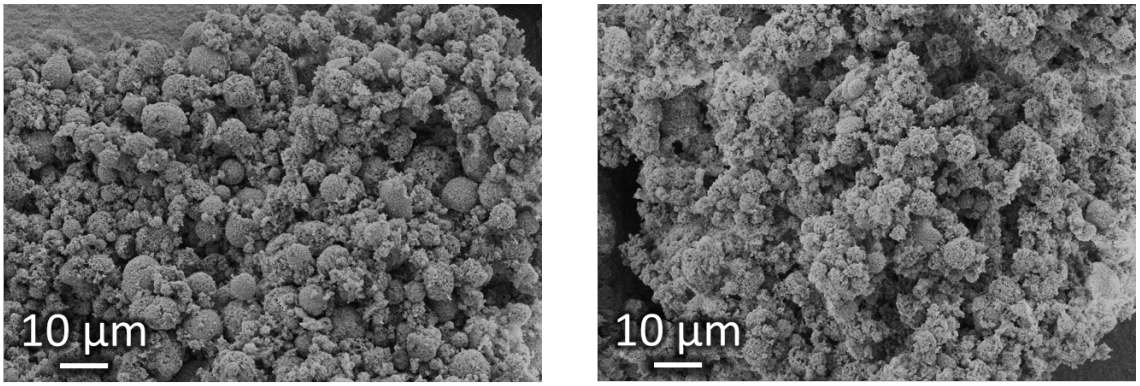


Initial volume ratio 1:10 Initial volume ratio 1:3

Figure 4.20 – SEM pictures of cellulose aerogel particles obtained from emulsion technique as a function of the initial cellulose solution to oil volume ratio.

In conclusion, increasing the volume ratio of cellulose solution to oil in the initial emulsion (from 1:10 to 1:3) should increase the coalescence rate and lower the stability of the final emulsion. With a smaller quantity of oil in the mixed emulsions, coalescence between cellulose solution droplets and non-solvent droplets, and thus coagulation, should happen faster leading to deformed and broken particles because the droplets were not stable yet with regards to the new emulsification conditions.

**Volume of acid**

Next, the volume of non-solvent added to the mixed emulsions was changed, without changing the initial phase ratios (1:10 for cellulose solution to oil emulsion and 1:2 for acid to oil emulsion) and surfactant concentration in the acid emulsion (1 vol.%).

- In the first case, the volume of acid added was 4 times the volume of cellulose solution. This led to a final ratio of 1:4:18 (cellulose solution:non-solvent:oil) and an overall ratio of 1:3.6 (dispersed phase:oil), with surfactant concentration of 0.52 vol.% (towards total volume).
- In the second case, the volume of acid added was 8 times the volume of cellulose solution. This led to a final ratio of 1:8:26 (cellulose solution:non-solvent:oil), an overall ratio of 1:2.9 (dispersed phase:oil) and surfactant concentration of 0.69 vol.% (towards total volume).

With a larger volume of acid, a lower volume of oil and a higher surfactant concentration in the mixed emulsions (second case), coalescence of cellulose solution droplets with acid droplets should happen more frequently. In addition, the higher concentration of surfactant, for a lower oil volume, should enhance the diffusion of surfactant to the cellulose solutions droplets during mixing of the two emulsions leading to smaller droplets' size.

Figure 4.21 presents pictures of the mixed emulsions after 2 h mixing for the lower quantity of acid (final volume ratios 1:4:18) and for the higher quantity of acid (final volume ratio 1:8:26). Figure 4.22 presents the resulting aerogel particles.

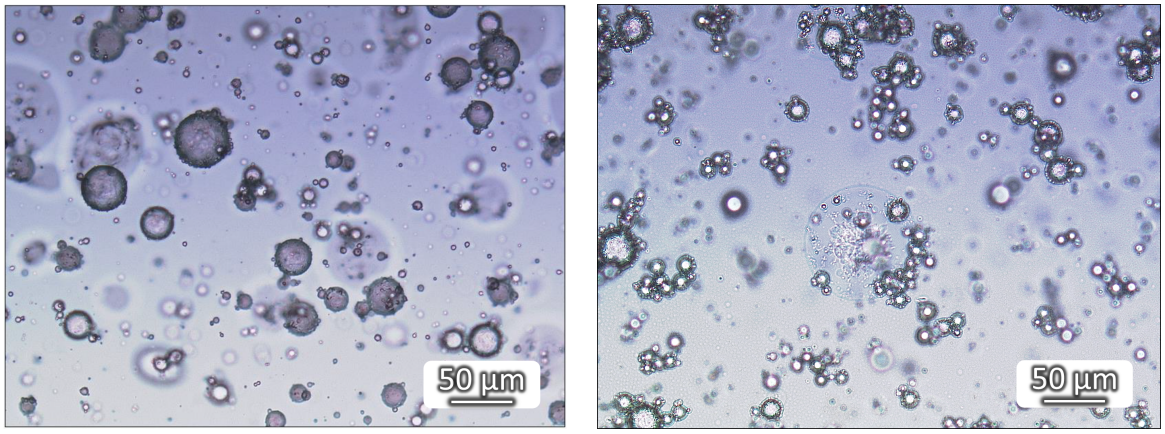


Final volume ratio 1:4:18 Final volume ratio 1:8:26

Figure 4.21 – Pictures of the mixed emulsions (5% cellulose solution:0.5 M HCl acid:paraffin oi), after 2 h mixing, as a function of their final volume ratio.

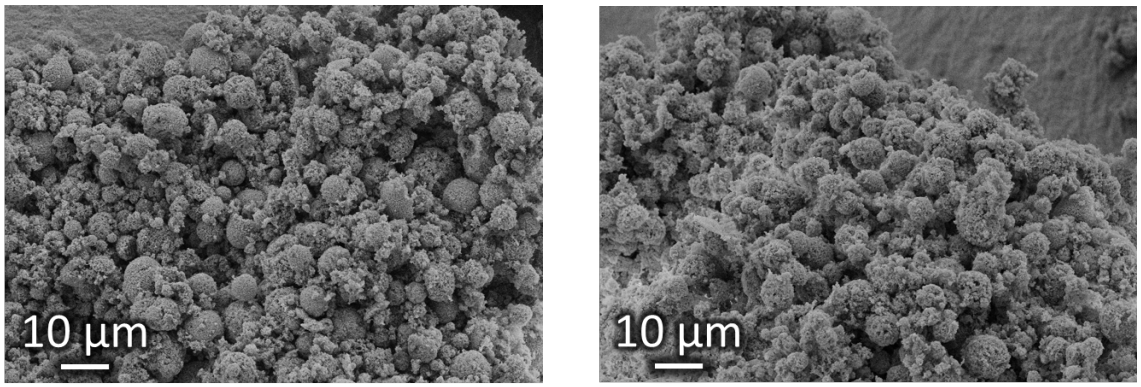


Final volume ratio 1:4:18 Overall volume ratio 1:8:26

Figure 4.22 – SEM pictures of cellulose aerogel particles obtained from emulsion technique as a function of the final volume ratio.

The most important differences that can be noticed from pictures a and b of Figure 4.21 are the smaller size of the particles and that they are more agglomerated when the volume of acid was higher (second case, final volume ratio 1:8:26). The reason can be the higher surfactant concentration (0.69 vol.%). The fact that they are more agglomerated can come from the surfactant hydrolysis by the acid, which may have happened faster as the acid quantity and acid droplet surface area were more important.

Not much difference can be seen for aerogel particles made from these two cases (Figure 4.22). It looks like their size is similar but the particles from a lower quantity of acid (first case, final volume ratio 1:4:18) seem more spherical and regular, with less debris. It can be because of the smaller final volume of oil: the coagulation may have

happened faster as the coalescence rate of a cellulose solution droplet with an acid droplet should be higher. Another explanation could be that the higher concentration of surfactant have prevented cellulose and non-solvent droplets from coalescing, leading to more non-coagulated cellulose solution droplets. These non-coagulated cellulose solution droplets got coagulated during phase separation, leading to irregular particles or debris.

The volume of acid and the size of droplets produced during mixing of the emulsions did not seem to have a significant impact on the resulting aerogel particles. On the other hand, the surfactant concentration and thus the amount of non-coagulated cellulose solution droplets before phase separation seem to be the most influencing parameters.

### Type of acid

Multiple parameters were varied in the previous sections without successfully contributing to the improvement of the cellulose aerogel particles shape and integrity. A completely different approach was thus used and, instead of changing the parameters of the emulsions, we decided to change the mechanism of coagulation as described in Section 4.2.2 and Figure 4.14 on page 159. 8.6 M acetic acid (AA) was used instead of 0.5 M HCl. The obtained aerogel particles are presented in Figure 4.23.

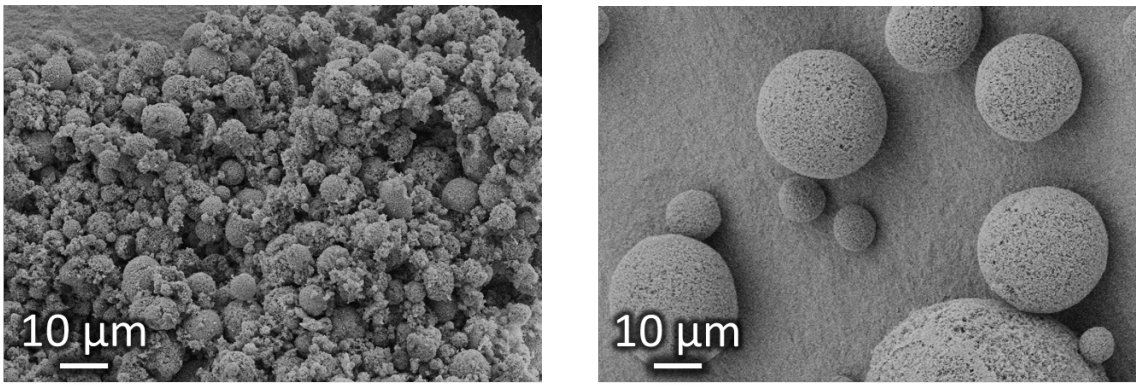


HCl coagulation - Coalescence mechanism

AA coagulation - Diffusion and coalescence mechanism

Figure 4.23 – SEM pictures of cellulose aerogel particles obtained from emulsion technique as a function of non-solvent.

As it was observed from Figure 4.16 on page 161 before drying of the particles, the difference between the two coagulation mechanisms is remarkable. When using AA as a non-solvent, aerogel particles are bigger, well defined and separated from each other. Size distribution and particles' mean diameter were measured from SEM pictures and are given in Figure 4.24. Particles from AA coagulation are at least 3 times bigger than the ones from HCl coagulation.

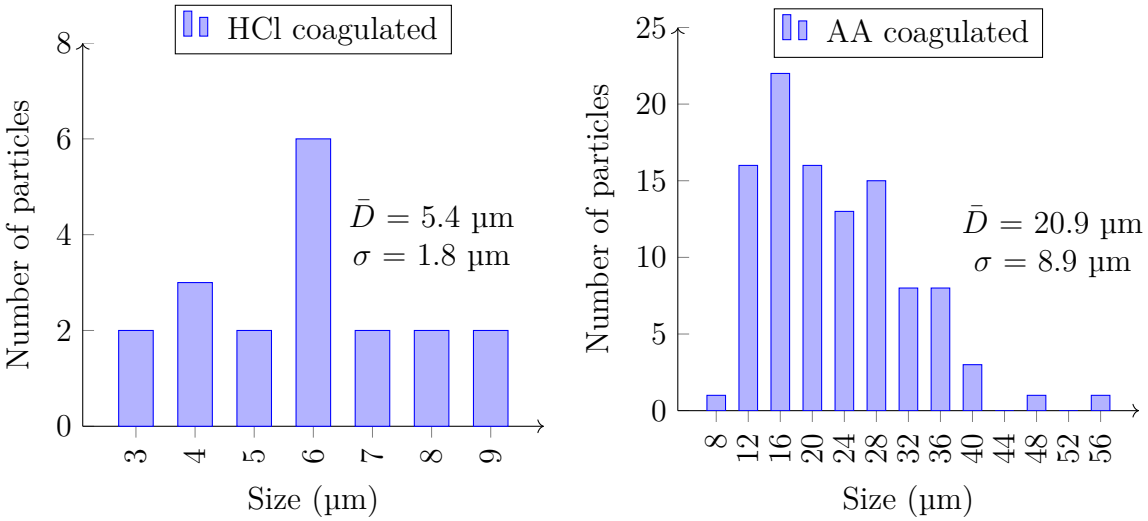


Figure 4.24 – Size distribution of cellulose aerogel particles from emulsion technique with HCl (left) and AA (right) as non-solvent. Debris in the case of HCl were not taken into account.

When coagulated in AA, as compared to HCl coagulation, we obtained:

- Bigger particles,
- well defined and separated from each other (no agglomeration),
- slightly deformed and/or elongated rather than broken (as seen in Figure 4.16 on page 161).
- No debris.

These differences are resulting from the mechanism of coagulation. As it was already mentioned earlier, when mixing the acetic acid in oil, the former diffuses in the latter. Then, when mixing the AA:oil emulsion with the cellulose solution:oil emulsion, the AA solubilised in the oil is diluted but AA is still present in enough quantity. Thus cellulose solution droplets will immediately start to coagulate in contact with the oil containing AA, while the mixing continues. Hence a shell of coagulated cellulose will form around cellulose solution droplets while the AA from the oil diffuses inside (see schematic representation on Figure 4.14 on page 159). If a cellulose solution droplet is not stable yet or if it is under shear, it will create an elongated or deformed particle, fixing the current shape. Upon meeting an AA droplet, the coagulation of the cellulose will be complete.

With coagulation starting at the same time as the two emulsions are mixed together, cellulose solution droplets do not have enough time to break-up to smaller ones. As a result, they are coagulated at the size that they had in the cellulose solution:oil emulsion, around 30 µm to 50 µm diameter (Figure 4.9 on page 155).

In view of these promising results, SEM pictures of the particles' microstructure as well as their specific surface area were measured (Figure 4.25 and Table 4.4, respectively). Figure 4.25 shows the particles' microstructure when coagulated with HCl (left) and with AA (right). They both have a porous structure, with small pores. A

small difference in the morphology between the particles coagulated from HCl and the ones coagulated from AA can be seen: the surface of HCl coagulated particles is slightly denser than that of AA coagulated ones. Stronger is the acid, denser is surface morphology. With HCl as non-solvent, during the coagulation, cellulose solution droplets are in direct contact with this strong acid. With AA as a non-solvent, the coagulation is gently done through diffusion of the weak acid from the oil.

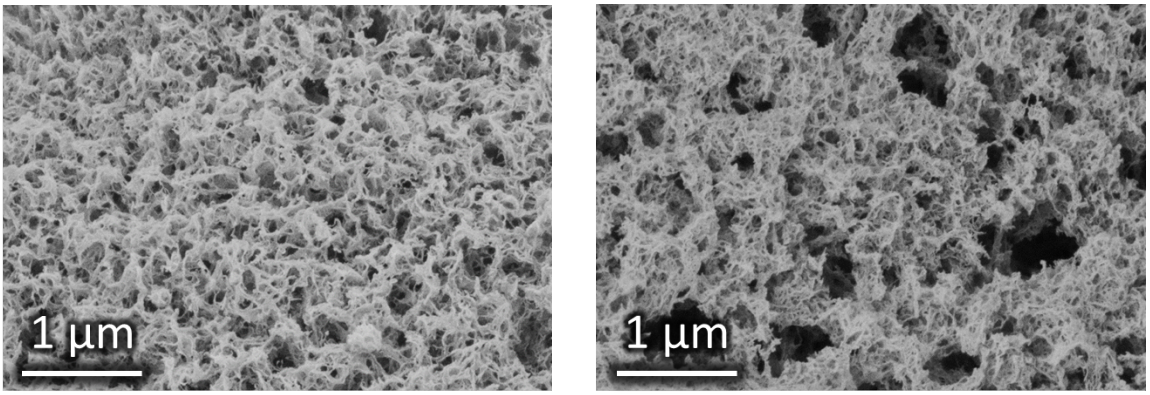


HCl coagulation AA coagulation

Figure 4.25 – SEM pictures of cellulose aerogel particles microstructure obtained from emulsion technique as a function of non-solvent.

Table 4.4 – $S_{BET}$ of particles and monoliths from 3.8% and 5% cellulose solutions and from HCl and AA coagulation.

| Shape | Cellulose concentration (%) | Non-solvent | $S_{BET}$ ($m^2$ $g^{-1}$) |
|---|---|---|---|
| Particles | 5 | 0.5 M HCl | 307 ± 34 |
| | | 8.6 M AA | 356 ± 50 |
| Monolith | 3.8 | 0.5 M HCl | 420 ± 7 |

As discussed in the previous chapter, Voon et al. (2016) reported the decrease of specific surface, from 498 $m^2$ $g^{-1}$ to 107 $m^2$ $g^{-1}$, with the increase of particles' mean diameter from 0.41 ± 0.03 mm to 2.14 ± 0.08 mm. In the case of our monoliths made from 3.8% cellulose-6.7% NaOH-11.5% urea-water solutions, even if the concentration of cellulose in solution is lower and sample volume higher, for the same non-solvent, their specific surface area is larger than the one of the particles (420 $m^2$ $g^{-1}$ against 307 $m^2$ $g^{-1}$ for HCl as coagulating media). The reason can be as follows. As it was demonstrated before (Section 4.2.2 on page 157), to avoid the interface jamming when HCl was used, 50% EtOH-$H_2O$ had to be added to complete cellulose coagulation. However, as it will be demonstrated in the two following chapters, coagulation in EtOH usually leads to lower specific surface area when the solvent was NaOH-based. Hence, as the cellulose particles were partly coagulated in 50% EtOH-$H_2O$ during phase separation (and not only by HCl, as it was the case for monoliths), the $S_{BET}$ is lower.

In the case of emulsifications with acetic acid, the specific surface area of aerogels was slightly higher as compared to the HCl coagulated particles. The coagulation with AA should be more complete before phase separation than with HCl, leading to higher specific surface area (because the cellulose was partly coagulated by EtOH when the acid used for the emulsion was HCl).

The coagulation mechanism appears to be the main influencing parameter on the resulting aerogels particle shape and integrity. With AA as non-solvent, the particles are distinct and well-shaped with a mean diameter of around 21 µm and a high (for cellulose aerogels) specific surface area of around 356 $m^2\ g^{-1}$. The final particles' size seems to depend on the size of the cellulose solution droplets in the first cellulose solution:paraffin oil emulsion. By varying the conditions of this emulsion, for instance changing the stirring speed, using a suitable surfactant or using a different additive for cellulose dissolution, we may adapt the size of the particles to suit different applications.

### Type of additive

With regards to our previous very successful result, we chose to keep the same coagulation mechanism by using 8.6 M AA as non-solvent. The focus was set on the type of additive used for cellulose dissolution. We dissolved 5% MCC in 8% NaOH-$H_2O$ with addition of 11.5% urea, or 0.5% ZnO, or no additive. Figure 4.26 presents SEM images of aerogel particles obtained and Table 4.5 gives their specific surface area.

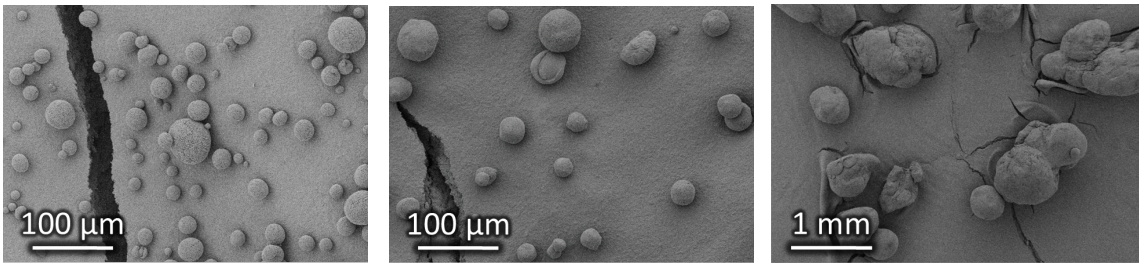


11.5% urea 0.5% ZnO No additive

Figure 4.26 – SEM pictures of aerogel particles obtained from cellulose solutions prepared with different additives or no additive.

Table 4.5 – $S_{BET}$ of particles from 5% cellulose solutions with 11.5% urea, or with 0.5% ZnO or without additive, all coagulated with AA.

| | 11.5% urea | 0.5% ZnO | No additive |
|---|---|---|---|
| $S_{BET}$ ($m^2\ g^{-1}$) | 356 ± 50 | 346 ± 35 | 279 ± 28 |

As expected, when no additive was used for cellulose dissolution, the particles are bigger and deformed, and they show a lower specific surface area. Their bigger size is a result of the higher viscosity ratio between cellulose solution and oil. Without additive, the cellulose solution has a higher viscosity and gelation starts during the

emulsification. Their irregular shape and size are due to the non-dissolved cellulose parts in the solution which created instability and non-homogeneous cellulose concentration droplets during the emulsification. This phenomenon was observed earlier with the rheo-optics (see Figure 4.3 on page 151). Finally, the lower $S_{BET}$ is also a cause of the incomplete dissolution of the cellulose. Indeed, the non-dissolved cellulose parts do not contribute to the surface area of the resulting aerogel leading to a lower specific surface area than if all was well dissolved.

When an additive is added to the cellulose solution during dissolution, either urea or ZnO, the aerogel particles obtained are well shaped and smaller. Both formulations resulted in very similar particles' size and high specific surface area, as shown in Figure 4.27.

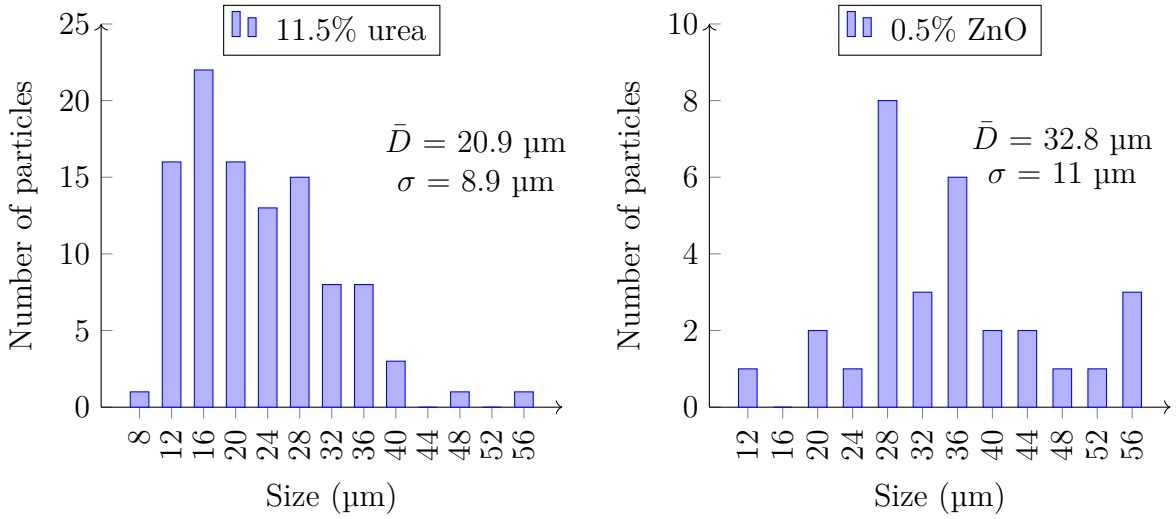


Figure 4.27 – Size distribution of cellulose aerogel particles from emulsion technique with two types of additives.

We can conclude that, when using the diffusion mechanism for coagulation, as long as cellulose dissolution is complete, the particles have regular and distinct shape. Numerous questions still need to be solved to better understand the influence of various parameters, and especially of the type of non-solvent, on cellulose emulsification and aerogel particles' properties. It would also be interesting to try this process with ionic liquids as solvent. However, the toxicity of ionic liquids should be first clarified even if they remain in ppm traces, which is crucial for life science applications.

# Conclusions

This chapter was dealing with the development and implementation of a new emulsification technique for aerogel particle production that was adapted to cellulose-NaOH based solutions. This led to the successful production of cellulose aerogel particles with diameters from few microns to few tens of microns.

The preliminary studies highlighted different requirements for cellulose solutions. One of the most important was the necessity of using additives. Indeed, without additive, cellulose solution gelation would occur too fast during emulsification. In addition, additives improve cellulose dissolution which is here an imperative. As it was observed with rheo-optics, the behaviour of cellulose solution during shear is critically influenced by impurities, namely, non-dissolved cellulose particles. A complete dissolution of cellulose in NaOH-water based solvent was thus a number one priority, rendering additives the best option. Viscosity of cellulose solutions and paraffin oil, as well as the viscosity ratio calculated from them was proved to be optimal for 5% cellulose solution concentration. Other parameters were also promising for a good emulsification of the cellulose solutions in paraffin oil.

The development and implementation of the emulsification method was then detailed. Several problems appeared to be critical during the procedure. The first one was the saponification of the surfactant used (span 80), due to the high pH of cellulose solutions. Secondly, coagulation of emulsified cellulose solutions by adding non-solvent directly in the emulsion did not lead to spherical particles. One solution hence appeared relevant in our case, preparing two separate emulsions:

- One emulsion containing cellulose solution in oil, without surfactant to avoid saponification.
- And the other emulsion made of non-solvent in oil, with surfactant to have more control on droplet size.

After mixing of these two emulsions together, cellulose particles seemed to be properly formed as shown by optical microscope. Finally, the last issue appeared when performing the separation of particles and oil. An "interface jamming" was observed, probably due to accumulation of non-dissolved and coagulated cellulose droplets at the interface between the oil and the aqueous phase. Two approaches were used to avoid this interface jamming: adding a fluid miscible in both aqueous phase and oil, such as ethanol, to disturb the formed interface and help particles to go through. The other approach was the use of another non-solvent for cellulose which would also be soluble in oil and ensure a complete coagulation of all cellulose in the droplets, before separation. Both techniques were proven successful in separating particles from oil.

In the final part, the influence of different parameters on the properties and shape of aerogel particles were analysed. As cellulose-NaOH-water based solutions are gelling with time and temperature, we tried to induce cellulose solution gelation in the emul-

sion, before coagulation. It appeared that gelation of cellulose solution is not "fast" enough and many debris were obtained. Other parameters were tested such as different cellulose concentration in solution and it seemed that more concentrated cellulose solution lead to less debris and more distinguishable aerogel particles. Changing the volume of acid or the ratio between cellulose solution and oil phase seemed to change the shape and integrity of resulting aerogel particles but was not as significant as the last changed parameter: the type of acid. When replacing hydrochloric acid by acetic acid for coagulation of cellulose, it notably improved the integrity, size and shape of the particles. When using acetic acid as non-solvent, the latter is partially solubilised in oil during emulsification. Hence when mixing acid emulsion with cellulose emulsion, the cellulose droplets are coagulated by diffusion of the acid from the oil rather than by coalescence. This leads to the formation of a shell around cellulose solution droplet and then complete coagulation. Particles are thus well shaped and separated from each other. Their size ranged from 10 µm to 50 µm and they had a high specific surface area of $\approx 350$ $m^2$ $g^{-1}$. Finally, the influence of additive was checked and it appeared even clearer that coagulation mechanism, as described just before, was the main influencing parameter to get spherical and well defined cellulose aerogel particles.

These results are very promising for future work for the production of cellulose aerogel particles with diameter of few micrometres. It revealed the importance of a complete dissolution of cellulose and that the most important factor to get separated and well shaped particles was the coagulation mechanism. Coagulation of cellulose solution droplet should be done by diffusion rather than coalescence. This work gives a good starting point in further development of the method, for instance to control particle size.

# Chapter 5

# Lightweight and mesoporous cellulose xerogels

## Contents

# Abstract

In the past decades, cellulose based, and more widely, bio-based aerogels, were extensively studied and showed high porosity (> 90%), high specific surface area (200 – 600 $m^2$ $g^{-1}$) and low density (around 0.1 g $cm^{-3}$). Up to now, these outstanding properties were reached thanks to drying with supercritical $CO_2$. During this drying, the capillary pressure, that leads to the collapse of the gel pore walls, is theoretically zero, and the structure is kept intact. Despite the remarkable aerogels' properties, this drying is time consuming, it uses a lot of $CO_2$ and it is rather expensive.

In this study, we have demonstrated that by using selected preparation parameters, we can obviate the $CO_2$ supercritical drying and prepare highly porous, lightweight cellulose "xerogels" with specific surface area similar to that of cellulose aerogels.

In this chapter, cellulose xerogels were prepared from microcrystalline cellulose via dissolution-solvent exchange and vacuum drying. The influence of cellulose solvent, additive and its concentration, solution gelation or not and non-solvent type was studied and correlated with xerogels' properties. These properties were compared to those of their aerogel counterparts and the use of supercritical $CO_2$ for the drying was proven not to be necessary to obtain cellulose aerogel-like materials. In addition, rheology of cellulose solutions as well as X-Ray diffraction and elemental analysis measurements of the final xerogels were performed. Finally, we found interesting to study the influence of the size and shape of these xerogels on their properties. We thus produced cellulose xerogel beads by dropping technique.

# Résumé

Au cours des dernières décennies, les aérogels à base de cellulose, et plus largement les aérogels bio-sourcés, ont fait l'objet d'études approfondies. Ils ont montré une porosité élevée (> 90%), une surface spécifique élevée (200 - 600 $m^2$ $g^{-1}$) et une faible densité (environ 0,1 g $cm^{-3}$). Jusqu'à présent, ces propriétés exceptionnelles étaient atteintes grâce au séchage dans les conditions supercritiques du $CO_2$. Pendant ce séchage, la pression capillaire, qui conduirait à l'effondrement des parois des pores du gel, est théoriquement nulle et la structure est maintenue intacte. Malgré les propriétés remarquables des aérogels, ce séchage est long, utilise beaucoup de $CO_2$ et est assez coûteux.

Dans cette étude, nous avons démontré qu'en utilisant des paramètres de préparation particuliers, nous pouvons éviter le séchage supercritique au $CO_2$ et préparer des "xérogels" de cellulose très poreux, légers et à la surface spécifique comparable à celle d'aérogels de cellulose.

Dans ce chapitre, des xérogels de cellulose ont été préparés à partir de cellulose microcristalline par dissolution-échange de solvants et séchage sous vide. L'influence du solvant, d'un additif et sa concentration, de la gélification de la solution ou non, et du type de non-solvant a été étudiée et corrélée aux propriétés des xérogels. Ces propriétés ont été comparées à celles de leurs homologues aérogels et l'utilisation de $CO_2$ supercritique pour le séchage s'est avérée inutile pour obtenir des matériaux de cellulose aux propriétés similaires à celles des aérogels. De plus, la rhéologie des solutions, la diffraction de rayons X ainsi que des mesures d'analyse élémentaire ont été réalisées sur les xérogels finaux. Enfin, nous avons trouvé intéressant d'étudier l'influence de la taille et de la forme de ces xérogels sur leurs propriétés. Nous avons donc produit des billes de xérogel de cellulose avec la technique du "goutte-à-goutte".

## 5.1 Materials and methods

### 5.1.1 Materials

In this chapter, MCC was used as cellulose precursor (described in Section 2.1.1 on page 95).
Two solvents were used to prepare cellulose aerogels and xerogels:

- 8% NaOH-$H_2O$ solution with addition of ZnO at various concentrations,
- and [DBNH][Pr].

Five different non-solvents were used:

- EtOH,
- $H_2O$,
- 2 M HCl ,
- Isopropanol,
- Acetone.

All these components were already listed and described in Section 2.1.2 on page 99.

### 5.1.2 Methods

#### Xerogel and aerogel monoliths preparation

Xerogel and aerogel monoliths were prepared from cellulose dissolved in NaOH based solvent following the dissolution process described in Section 2.2.1 on page 101. The final solution concentrations were:

- 5% cellulose,
- from 0 to 1% ZnO,
- and from 7.5% to 7.6% NaOH depending on ZnO concentration (NaOH concentration is always so that there is 8% NaOH in $H_2O$).

After cellulose dissolution, 6 mL of solution was poured in cylindrical containers. Solutions in containers were gelled at 50 °C for 1 h, 4 h, 8 h or 20 h before coagulation in one of the five different coagulation baths used:

- When the first non-solvent was HCl, it was then washed out (at least 4 times) with $H_2O$ and the latter was replaced by EtOH for the subsequent drying.
- When the first non-solvent was $H_2O$, it was washed several times (at least 5 times) with $H_2O$ and then exchanged for EtOH.
- When the first non-solvent was EtOH, isopropanol or acetone, samples were directly dried after washing from cellulose solvent.

Xerogels and aerogels prepared from [DBNH][Pr] solvent followed the dissolution described in Section 2.2.1 on page 102. MCC was dissolved in [DBNH][Pr] at 40 °C and 400 rpm stirring for 24 h, with and without addition of 0.8% ZnO. When the first non-solvent was $H_2O$, it was washed several times (at least 5 times) with $H_2O$

and then exchanged for EtOH. When the first non-solvent was EtOH, samples were directly dried after washing from cellulose solvent.

Drying under $CO_2$ supercritical conditions resulted in aerogels. Drying under vacuum at 50 °C resulted in xerogels. Both dryings were described in Section 2.2.1 on page 102.

### Xerogel and aerogel beads production

Xerogel and aerogel beads were prepared from NaOH based solvents without and with addition of 0.5% ZnO, following the same dissolution procedure as for monoliths preparation. The final solution concentrations were:

- 5% cellulose,
- 0% or 0.5% ZnO,
- and 7.6% or 7.56% NaOH depending on ZnO concentration (NaOH concentration is always such that there is 8% NaOH in $H_2O$).

The obtained solutions were then put in 10 mL syringes equipped with a 0.8 mm diameter needle and dropped into an EtOH coagulation bath with the automatic piston at room temperature. The dropping technique principle was described in Section 2.2.2 on page 103. The coagulated beads were washed in EtOH and dried under vacuum or under Sc $CO_2$ conditions (described in Section 2.2.1 on page 102).

### Rheological measurements

All rheological measurements were performed with a cone-plate geometry (2 ° - 60 mm), in oscillatory mode with frequency and stress set at 1 Hz and 0.1 Pa, respectively. Solutions were prepared and maintained steady at 5 °C for 1 h before measurement to let the bubbles produced by the dissolution to escape. To prevent possible evaporation of the solvent, a thin layer of low-viscosity silicon oil ($\eta_{(20°C)} = 9.5$ mPa s) was disposed on the edge of the measuring cell. Temperature was varied from 15 °C to 25 °C for each solution.

Gelation time was recorded when the storage modulus G' and the loss modulus G" intersect.

## 5.2 Results and discussions

In a first part, all experimental results will be presented. In a second part, they will be discussed by analysing and putting together all the results obtained. Finally, cellulose xerogel beads will be presented and their properties will be compared to the ones of monoliths.

### 5.2.1 Properties of cellulose xerogels: experimental results

All results obtained in this work are presented in this section as a function of the various parameters.

#### Influence of the type of the first non-solvent

The influence of the type of non-solvent on xerogels' and aerogels' properties was studied on 5% MCC, dissolved in 8% NaOH-$H_2O$ based solvent, with and without addition of 0.5% ZnO and gelled 8 h at 50 °C. At this temperature cellulose solutions are gelling within few minutes at any ZnO concentration (Liu et al. (2011)). Three non-solvents were used for the first coagulation bath:

- EtOH,
- $H_2O$,
- and 2 M HCl.

Each non-solvent was then exchanged by EtOH, if not already in it, for both vacuum and Sc drying. It is important to underline that non-solvent in the pores of cellulose before drying was always the same (EtOH) in order to exclude the influence of the type of evaporating fluid, for the case of vacuum drying, on cellulose xerogels' properties.

Figure 5.1 and Figure 5.2 demonstrate pictures of xerogels and aerogels as well as their morphology as a function of the type of the first coagulation bath, for 8% NaOH-$H_2O$ solvent with no additives and with 0.5% ZnO, respectively. Figure 5.3 and Figure 5.4 on page 182 show their density and specific surface area, respectively.

The first striking result seen on these figures is low density and high specific surface area of cellulose xerogels when the first and all further non-solvent bathes were EtOH. This is not the case when cellulose was coagulated in $H_2O$ or 2 M HCl despite that they were then exchanged to EtOH and vacuum-dried from the latter. It is thus clear that it is not (or not only) capillary pressure which controls the morphology and properties of cellulose low-vacuum dried materials.

As it can be seen from the pictures, when the first non-solvent was EtOH, shrinkage was much lower and cellulose morphology was preserved as compared to the cases when first coagulation medium was $H_2O$ or HCl. As shown in Figure 5.3, EtOH coagulated xerogels even have density comparable to their aerogel counterparts when the solvent was with 0.5% ZnO: 0.15 g $cm^{-3}$ for the xerogels and 0.14 g $cm^{-3}$ for the aerogels. In

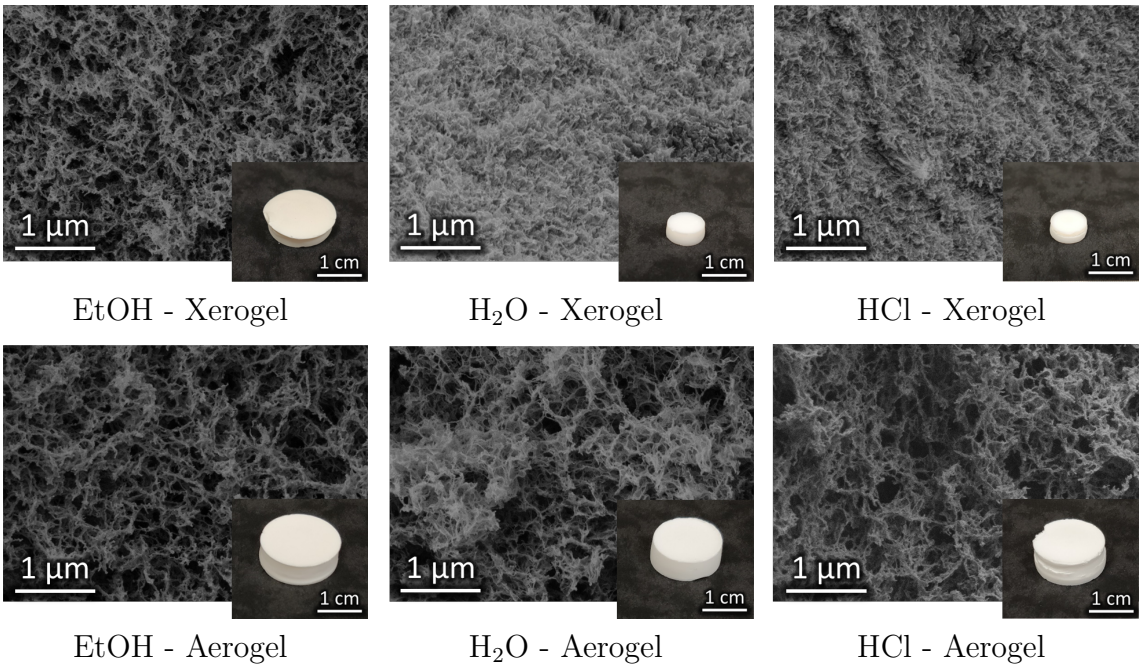


Figure 5.1 – Pictures of cellulose xerogels (top) and aerogels (bottom) from 5% cellulose-8% NaOH-$H_2O$ **(0% ZnO)** solution, gelled for 8h at 50 °C as a function of non-solvent's type in the first coagulation bath.

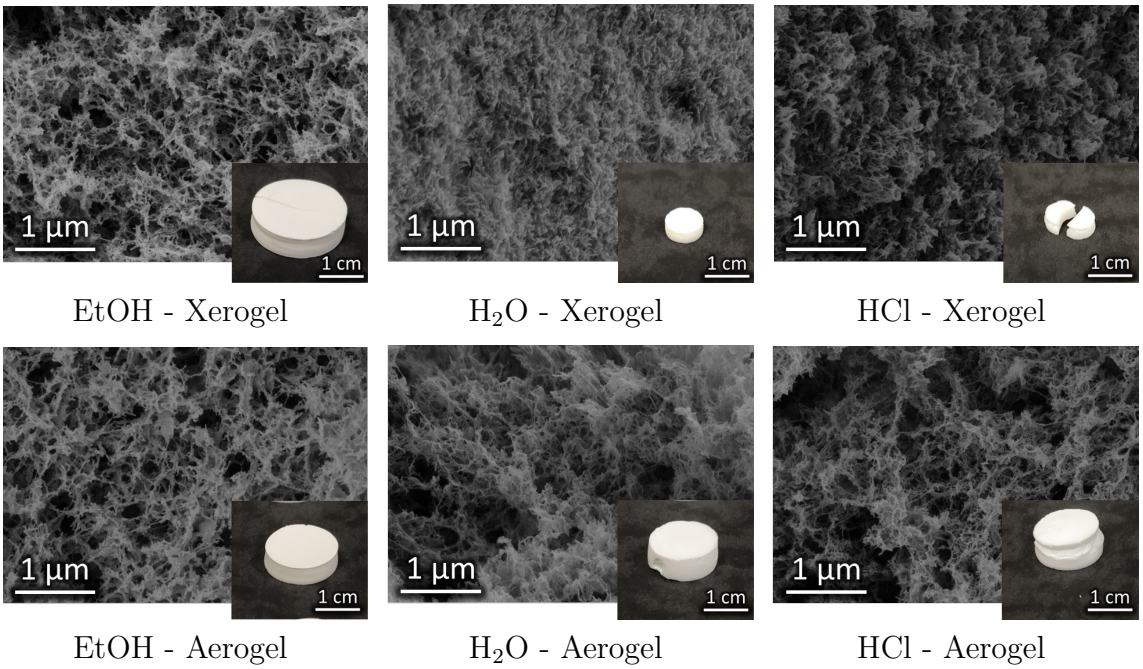


Figure 5.2 – Pictures of cellulose xerogels (top) and aerogels (bottom) from 5% cellulose-8% NaOH-**0.5% ZnO**-$H_2O$ gelled for 8 h at 50 °C as a function of non-solvent's type in the first coagulation bath.

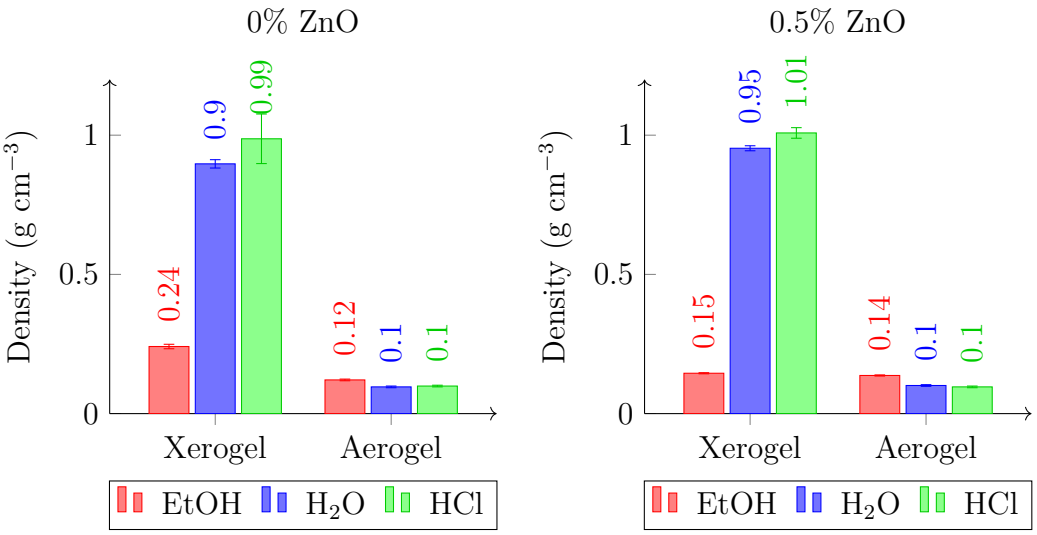


Figure 5.3 – Xerogels' and aerogels' **density** as a function of the first coagulation bath without ZnO in the solvent and with 0.5% ZnO.

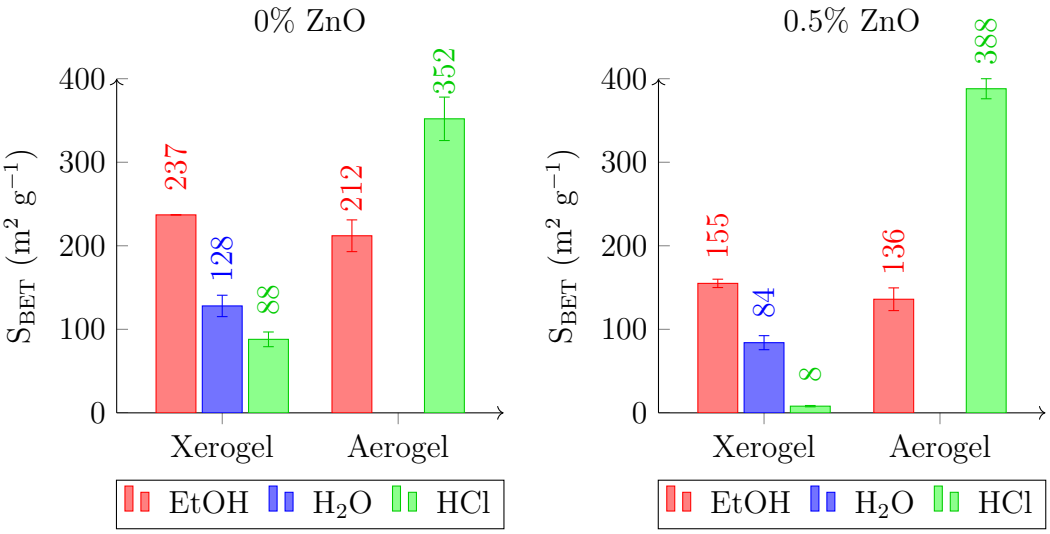


Figure 5.4 – Xerogels' and aerogels' $\mathbf{S_{BET}}$ as a function of the first coagulation bath without ZnO in the solvent and with 0.5% ZnO.

both cases, with or without ZnO, $S_{BET}$ of EtOH coagulated xerogels is comparable to the one of their aerogel homologues, as shown in Figure 5.4.

$H_2O$ and HCl coagulated xerogels are a perfect representation of what vacuum drying usually leads to (Buchtová and Budtova (2016)) despite that drying was performed from EtOH in all cases. Compared to their aerogel counterparts, xerogels have high density, around ten times higher ($\approx$ 1 g cm$^{-3}$ against 0.1 g cm$^{-3}$ for the aerogels) which denotes a great densification of the structure during vacuum drying. However, xerogels' density is still lower than the one of xerogels obtained when cellulose was coagulated in EtOH but then dried from $H_2O$ ($\approx$ 1.4 g cm$^{-3}$, see Buchtová and Budtova (2016)) or of cellulose crystals (1.5 – 1.6 g cm$^{-3}$). In addition to their high density, xerogels coagulated in $H_2O$ and in HCl show low specific surface area. $S_{BET}$ of $H_2O$ coagulated aerogels was not measured in the exact conditions used in this study. But, as examples to compare xerogels and aerogels coagulated in $H_2O$, an aerogel without ZnO, aged 24 h at ambient temperature (different from our study: 8 h at 50 °C) has a $S_{BET}$ of 324 m$^2$ g$^{-1}$ while an aerogel with 0.8% ZnO, aged 4 h at 50 °C (different from our study: 0.5% ZnO and aged 8 h at 50 °C) gives a $S_{BET}$ of 332 m$^2$ g$^{-1}$.

As far as aerogels are concerned, the difference in properties when coagulated in different non-solvents is not significant and trends seem to be reversed as compared to xerogels. When $H_2O$ and HCl were used as first non-solvent for coagulation, and then exchanged by EtOH for the Sc drying, aerogels showed a density of 0.1 g cm$^{-3}$ whatever the ZnO concentration in cellulose solution. When EtOH was used as non-solvent, density was slightly higher and dependent of the concentration in additive (0.12 - 0.14 g cm$^{-3}$). Regarding $S_{BET}$, EtOH coagulated aerogels show a really lower specific surface area than HCl coagulated ones (212 m$^2$ g$^{-1}$ against 352 m$^2$ g$^{-1}$) especially when 0.5% ZnO was added to cellulose dissolution (136 m$^2$ g$^{-1}$ against 388 m$^2$ g$^{-1}$). The influence of ZnO concentration will be studied in more details in the following section.

It is well known that during evaporative drying capillary pressure is developed as described by Young-Laplace equation (see Equation (1.5) on page 71 of the *State of the art* chapter). This pressure usually leads to collapse of pores of cellulose network and great densification of resulting xerogels.

In the view of the interesting results obtained when xerogels were coagulated and dried only from EtOH, two other non-solvents with a similar surface tension were tested: acetone and isopropanol. Table 5.1 summarises non-solvent properties used for this study. They were chosen:

- Acetone, because its higher vapour pressure, its lower relative polarity and its similar surface tension with air compared to EtOH (see Table 5.1).
- And isopropanol, because it is chemically closer to EtOH than the other previously studied non-solvents, the same surface tension, slightly lower polarity and vapour pressure.

The same conditions of preparation were applied as before, except that the non-solvents

were not exchanged by EtOH before vacuum drying.

Table 5.1 – Cellulose non-solvents' characteristics (Reichardt (2006)). The values for relative polarity are normalized from measurements of solvent shifts of absorption spectra and were extracted from Reichardt (2006).

| **Cellulose non-solvent** | **Relative polarity** | **Surface tension with air at 20 °C, mN m$^{-1}$** | **Vapour pressure at 20 °C, hPa** |
|---|---|---|---|
| $H_2O$ | 1 | 72.9 | 23 |
| EtOH | 0.654 | 22.1 | 59 |
| Isopropanol | 0.546 | 22 | 44 |
| Acetone | 0.355 | 24 | 240 |

Figure 5.5 presents acetone and isopropanol coagulated xerogels' pictures and morphology when 0.5% ZnO was present in cellulose solvent. For these two xerogels, density was around 1.1 g cm$^{-3}$ and $S_{BET}$ was lower than 10 m$^2$ g$^{-1}$.

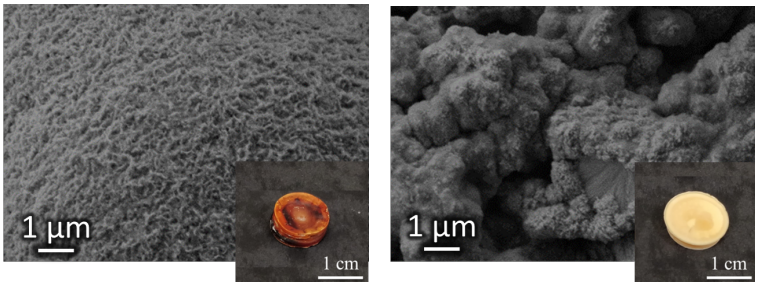


Acetone - Xerogel Isopropanol - Xerogel

Figure 5.5 – Pictures of xerogels from 5% cellulose-NaOH-0.5% ZnO-water solution, aged 8 h at 50 °C, coagulated in acetone or in isopropanol and vacuum dried from these non-solvents.

For both acetone and isopropanol coagulated xerogels, we obtained samples densified during vacuum drying because of shrinkage, with a high density and a very low specific surface area. Considering these results, we decided not to continue the study with these non-solvents but to rather focus on the process with EtOH as non-solvent.

These results led us to the conclusion that it is the type of the first non-solvent which is the main parameter influencing xerogels' properties. In the range of non-solvents studied, only EtOH as first and only coagulation bath leads to low density and high specific surface area xerogels. Their properties are even comparable to the ones of their aerogel homologues.

### Influence of ZnO concentration

The previous section was devoted to the analysis of the influence of non-solvent in the first coagulation bath on xerogels' and aerogels' properties. Only little attention was given to ZnO concentration. However, it seems that ZnO is also playing a significant role on cellulose aerogels' and xerogels' properties.

Thus we dissolved 5% of MCC in solutions of 8% NaOH-$H_2O$ with ZnO concentration varying from 0% to 1%. The resulting solutions were gelled for 4 h at 50 °C, coagulated and washed in EtOH only and dried under vacuum and under Sc $CO_2$ conditions.

Figure 5.6 shows examples of xerogels' and aerogels' pictures and morphologies for 0%, 0.5% and 1% ZnO. For the same ZnO concentration, both the aspect and the morphology of xerogels are very similar to the ones of aerogels. Their texture is porous with pores' size varying from few tens to few hundreds of nanometres as deduced from SEM images. Figure 5.7 on the next page shows density and $S_{BET}$ and Figure 5.8 shows shrinkage (calculated from Equation (2.1) on page 105) and mass (always the same initial concentration and initial mass of solution was prepared for each sample) of xerogels and aerogels as a function of ZnO concentration. These figures further emphasise the similarities between these porous materials.

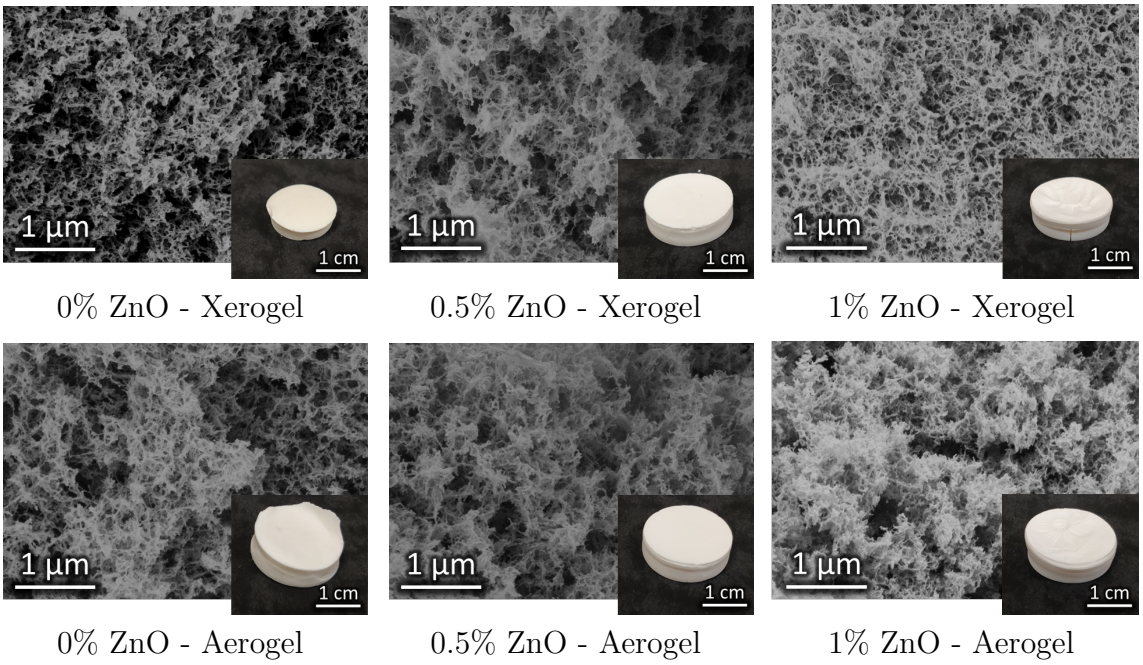


Figure 5.6 – Pictures of cellulose xerogels (top) and aerogels (bottom) from 5% cellulose-NaOH-ZnO-$H_2O$ solutions, as a function of ZnO concentration. Solution were aged for 4 h at 50 °C, coagulated and washed in EtOH.

Except for 0% ZnO, the characteristics of the materials are very similar for the xerogels and the aerogels: the density of aerogels and xerogels is almost the same (with almost the same shrinkage and mass) and it slightly increases with the increase of ZnO concentration in cellulose solution. When no ZnO is added to cellulose solvent, shrinkage and density of xerogels are higher than those of aerogels. As for specific surface area, it follows a "U" shaped curve for xerogels and aerogels as a function of ZnO concentration. The reasons will be discussed later in Section 5.2.2 on page 200, when analysing the role of ZnO on the morphology and properties of cellulose aerogels and xerogels.

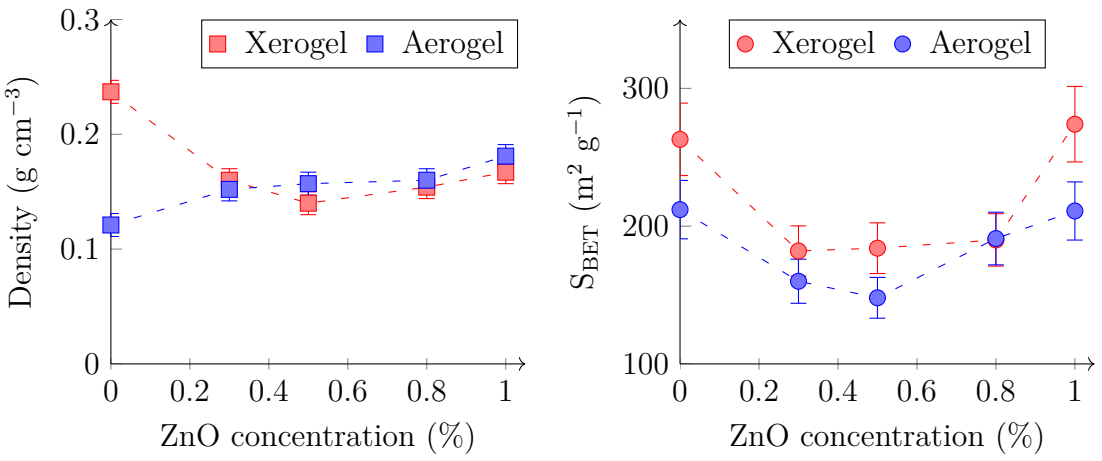


Figure 5.7 – Xerogels' and aerogels' density and $S_{BET}$ as a function of ZnO concentration. Dashed lines are to guide the eye.

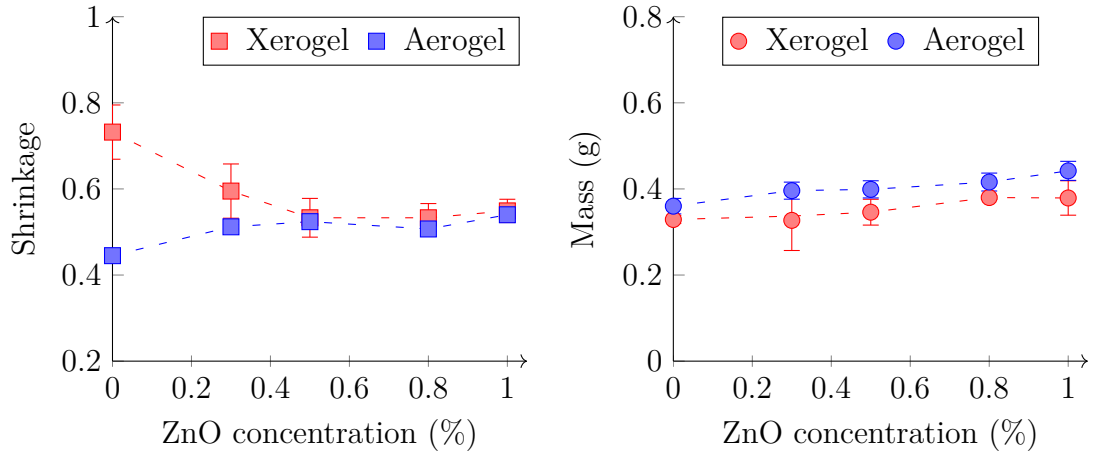


Figure 5.8 – Xerogels' and aerogels' shrinkage and mass as a function of ZnO concentration. Dashed lines are to guide the eye.

The fact that the mass increases with increasing ZnO concentration means that Zn and/or Na are not washed out when cellulose is coagulated in EtOH. When observing the morphology of the porous materials prepared with ZnO concentration of 0.5% and higher, the presence of crystals confirmed that there is remaining Zn or/and Na in the final materials (see in Figure 5.9, examples of crystals in xerogels from cellulose dissolved at different concentrations of ZnO).

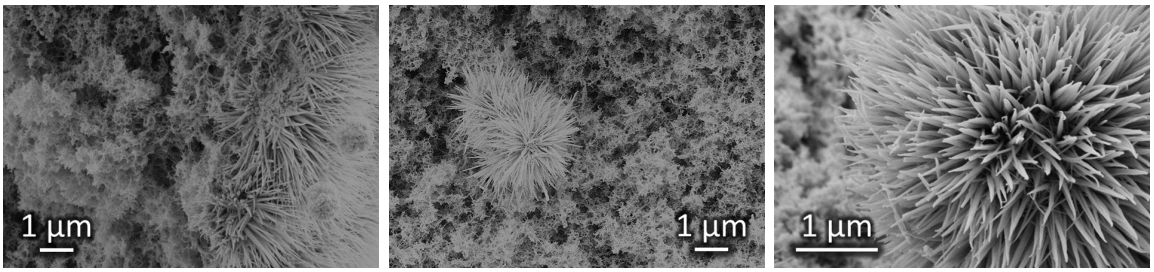


0.5% ZnO 0.8% ZnO 1% ZnO

Figure 5.9 – Morphology of cellulose xerogels made from 5% MCC dissolved in 8% NaOH-$H_2O$ solutions with addition of 0.5%, 0.8% or 1% ZnO, gelled 4 h at 50 °C, coagulated and dried from EtOH.

To understand this behaviour, it is important to learn more about ZnO solubility in the solvent and different non-solvents used. The solubility of ZnO strongly depends on pH, as demonstrated by Liu (1998): it is soluble only at very low and very high pH. ZnO can only be dissolved up to 4 g $L^{-1}$ in 8% NaOH-$H_2O$ (Liu (1998)), which corresponds to around 0.4% of ZnO in our cellulose solutions. This means that at ZnO concentrations higher that 0.4% ZnO, the ZnO is not dissolved anymore. It may be possible that two "types" of ZnO are present in the cellulose-8% NaOH-$H_2O$ solutions (as also demonstrated in Liu et al. (2011)), which would behave differently and result in different structures during coagulation in EtOH: ZnO that was dissolved in 8% NaOH-$H_2O$ and that will precipitate upon addition of EtOH and ZnO that was not dissolved in 8% NaOH-$H_2O$. Because at ZnO concentrations below 0.5% no crystals were seen on SEM images of xerogels or aerogels, we hypothesise that these crystals are not of "Na origin" (sodium is not soluble in EtOH) and are not dissolved-precipitated Zn from ZnO; the crystals shown in Figure 5.9 are from non-dissolved ZnO in 8% NaOH-$H_2O$.

In cellulose non-solvents used, ZnO is not soluble in EtOH and in $H_2O$ while it is soluble in HCl solutions of very low pH (Liu (1998)). To check the influence of ZnO on aerogels when the former is washed away, we prepared aerogels coagulated in 2 M HCl. Figure 5.10 and Figure 5.11 show density and $S_{BET}$ as well as shrinkage and mass of HCl coagulated aerogels for different ZnO concentrations, respectively. We can clearly see that the initial ZnO concentration does not influence the resulting aerogels' shrinkage, mass or density. Furthermore, no Zn crystals were detected during SEM observations. The $S_{BET}$ however, is slightly increasing until reaching a plateau. These results will be analysed in *Analysis and discussions* Section 5.2.2 on page 200.

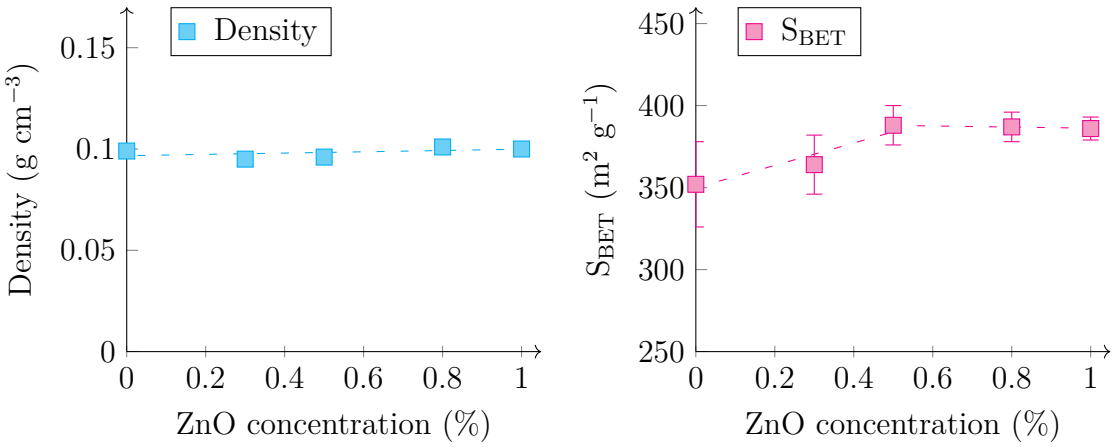


Figure 5.10 – HCl coagulated aerogels' density and $S_{BET}$ as function of ZnO concentration. Dashed lines are to guide the eye.

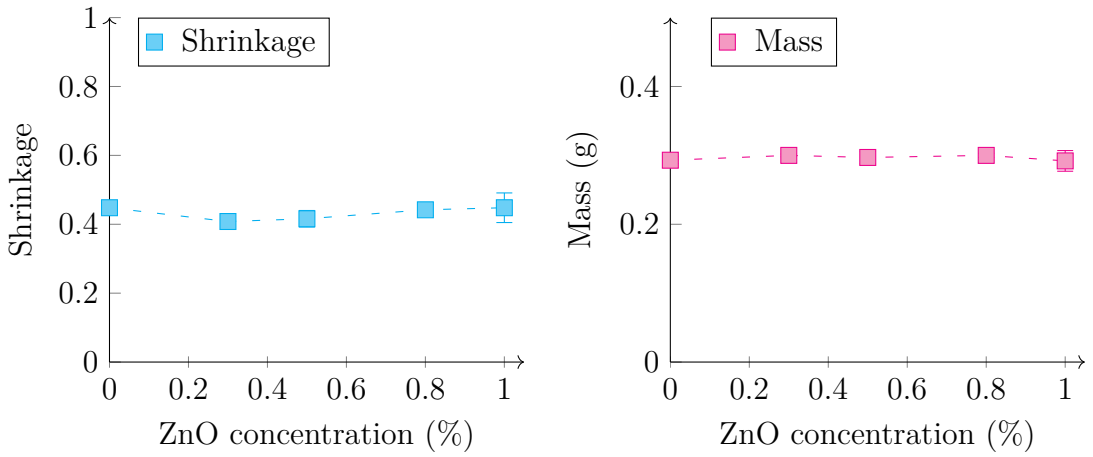


Figure 5.11 – HCl coagulated aerogels shrinkage and mass as a function of ZnO concentration. Dashed lines are to guide the eye.

### Elemental analysis of cellulose xerogels

To identify the presence and the quantity of the metals remaining in the xerogels and aerogels could help us to better understand the trends described above. If Na and/or Zn are not well washed out during coagulation and washing, they can represent the "heaviest" part in cellulose aerogels or xerogels and thus influence their properties. Consequently, elemental analysis and more particularly, metal content measurements[1] were conducted on xerogels coagulated in EtOH and also when the first coagulation bath was either 2 M HCl or $H_2O$ (then all dried from EtOH) for different ZnO concentrations in the solvent. The results are given in Table 5.2.

Table 5.2 – Metal content in cellulose xerogels as a function of ZnO concentration in cellulose solutions and first coagulation bath.

| **Initial composition in dry matter (%)** | **Non-solvent of the first bath** | **Final composition measured (%)** | **Loss (%)** |
|---|---|---|---|
| **Case 0% ZnO**<br>Cellulose: 53.4<br>Na:46.6<br>ZnO: 0 | EtOH | Na: 5.13<br>Zn: - | 93.8<br>- |
| | 2 M HCl | Na: 0.02<br>Zn: - | 100<br>- |
| **Case 0.3% ZnO**<br>Cellulose: 52.1<br>Na:45.4<br>Zn:2.5 | EtOH | Na: 5.55<br>Zn: 2.61 | 93.1<br>40.9 |
| | 2 M HCl | Na: 0.02<br>Zn: 0.01 | 100<br>99.8 |
| **Case 0.5% ZnO**<br>Cellulose: 51.3<br>Na:44.6<br>Zn:4.1 | EtOH | Na: 4.53<br>ZnO: 4.38 | 94.2<br>39 |
| | 2 M HCl | Na: 0.02<br>Zn: 0.01 | 100<br>99.8 |
| **Case 0.8% ZnO**<br>Cellulose: 50.2<br>Na:43.4<br>Zn:6.4 | EtOH | Na: 4.9<br>Zn: 6.47 | 93.7<br>43.2 |
| | 2 M HCl | Na: 0.02<br>Zn: 0.01 | 100<br>99.9 |
| | $H_2O$ | Na: 0.04<br>Zn: 6.4 | 100<br>46.8 |
| **Case 1% ZnO**<br>Cellulose: 49.4<br>Na:42.7<br>Zn:7.9 | EtOH | Na: 5.48<br>Zn: 8.33 | 92.7<br>40.7 |
| | 2 M HCl | Na: 0.21<br>Zn: 0.001 | 99.8<br>100 |

An example of calculation of the initial composition of dry matter is given for the following initial concentrations: 5% MCC-7.56% NaOH-0.5% ZnO-$H_2O$ (NaOH concentration in $H_2O$ is always 8%):
As only Na and Zn were taken into account in the metal content measurements in cellulose xerogels, we need to subtract the OH and O from the initial composition:

[1]We are grateful to Nestlé for the determination of metal content. The details on the method used are given in Section 2.2.4 on page 111.

- Na represents 57.48% of the NaOH mass and
- Zn represents 80.36% of the ZnO mass.

We thus have the following initial composition:

- 5% cellulose,
- 4.35% Na ($7.56 * 0.5748 = 4.35$) and 3.21% OH,
- 0.40% Zn ($0.5 * 0.8036 = 0.40$) and 0.10% O,
- 86.94% $H_2O$.

Knowing that the total mass in dry matter is: $5\ g + 4.35\ g + 0.40\ g = 9.75\ g$, we can now calculate the initial composition in dry matter:

- Cellulose initial content: $5/9.75 = 51.3\%$,
- Na initial content: $4.35/9.75 = 44.6\%$,
- Zn initial content: $0.4/9.75 = 4.1\%$.

Similar calculations were performed for matter composition at all the other ZnO concentrations.

The "loss" (or the mass of metal washed out in percent) is calculated as follows. Let us take the case of 0.5% ZnO in the solvent as mentioned above, and the experimental data obtained when the first and all baths were EtOH (Table 5.2):

- Na final content: 4.53%,
- Zn final content: 4.38%,
- cellulose final content: $100 - 4.53 - 4.38 = 91.1\%$.

Knowing that there is no loss in cellulose mass, we can now calculate the final mass of the xerogel sample: $(51.3\ g * 100)/91.1\% = 56.3\ g$. Hence, in mass:

- Na represent 4.53% of the final total mass: $56.3 * 0.0453 = 2.6\ g$
- and Zn represent 4.38% of the final total mass: $56.3 * 0.0438 = 2.5\ g$.

Now that we know the initial and final mass of all components, we can calculate the loss in metals, in percent:

- Loss in Na: $(44.6 - 2.6)/(44.6) * 100 = 94.2\%$
- and loss in Zn: $(4.1 - 2.5)/(4.1) * 100 = 39\%$.

Similar calculations were performed for the loss in metal at all the other ZnO concentrations.

We can see from Table 5.2 that the quantity of metals remaining in the xerogels mainly depends on the type of the first coagulation bath. When the first non-solvent was 2 M HCl, all metals were washed out because both ZnO and NaOH are very well soluble at this very low pH. On the contrary, when cellulose was coagulated in EtOH, only 40 - 45% of Zn was washed and around 93 - 94% of Na. When the first coagulation bath was water, all sodium was washed out but only around 47% of ZnO. As mentioned above, this is due to the solubility of NaOH and ZnO in the corresponding fluids.

### Influence of gelation time

It is well known that cellulose-8% NaOH-$H_2O$ solutions are gelling with time and temperature increase. All results presented above were performed on solutions aged for 4 h or 8 h. The next question is: "is there any influence of gelation time on cellulose aerogels' and xerogels' morphology and properties"?

First, the rheological properties of cellulose-8%NaOH-$H_2O$ solutions were studied for concentrations of ZnO from 0% to 1% and for temperatures varying from 15 °C to 25 °C. Figure 5.12 and Figure 5.13 on the next page show gelation time as a function of temperature and the ZnO concentration, respectively.

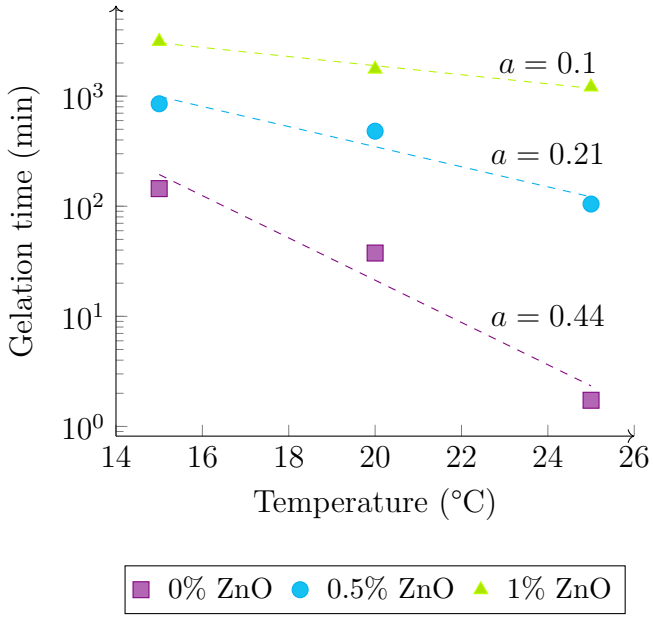


Figure 5.12 – 5% cellulose-8% NaOH-$H_2O$ solutions' gelation time as a function of temperature, for three different ZnO concentrations. Dashed lines are exponential approximation and $a$ is the corresponding constant as seen in Equation (5.1).

Figure 5.12 and Figure 5.13 are in accordance with what was already reported by Liu et al. (2011): with increasing temperature gel time is shorter and with increasing ZnO concentration, gelation is delayed. It was suggested (Liu et al. (2011)) that gelation time depends on cellulose and ZnO concentration and solution temperature as follows:

$$t_{gel} = \left( \frac{A}{C^n_{Avicel}} + B * C^m_{ZnO} \right) e^{-a*T} \tag{5.1}$$

with $A$, $B$, $n$, $m$ and $a$ being constants. $A$ and $n$ were determined from the power law approximations by plotting the 1/(gelation time) as a function of cellulose concentration in log-log scale. As gelation time was measured for only one cellulose concentration, we are not able to obtain these parameters. $a$, $B$ and $m$ were determined in Figure 5.12 and Figure 5.13 which show that the slopes ($a$ and $m$ in Equation (5.1)) depend on solution temperature and ZnO concentration, respectively.

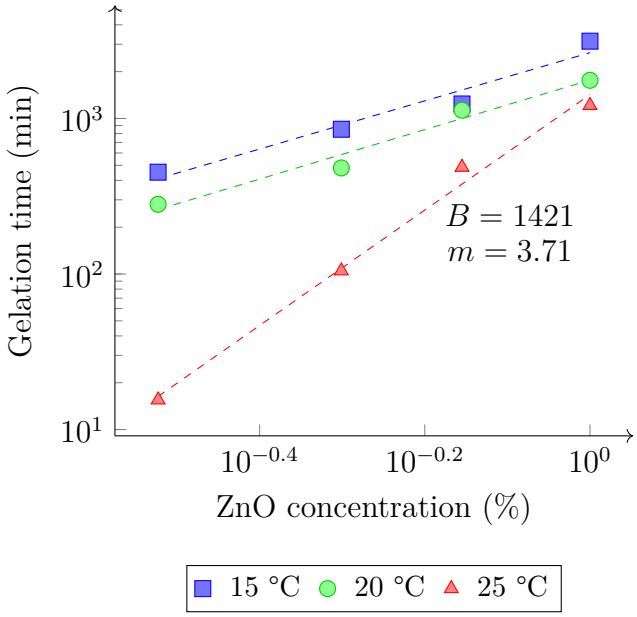


Figure 5.13 – 5% cellulose-8% NaOH-$H_2O$ solutions' gelation time as a function of ZnO concentration, for three different temperatures. Dashed lines are power law approximation and $B$ and $m$ are the constants according to Equation (5.1) for the 25 °C curve.

If comparing the constants obtained in this work with the ones of Liu et al. (2011), we can see that, in the latter, when no additive was added to 4% and 6% cellulose-NaOH-$H_2O$ solutions, $a$ was equal to 0.46 and 0.43 respectively. Our result is similar as we obtained $a = 0.44$ for a 5% cellulose-NaOH-$H_2O$ solution. It is harder to compare the $a$ constants from the slopes of Figure 5.12 with the work of Liu et al. (2011) as cellulose and ZnO concentrations are different. But we can see that, as reported by Liu et al. (2011), with increasing ZnO concentration, $a$ is decreasing. Hence higher is ZnO concentration less important is the temperature influence on gelation time (Figure 5.12).

To compare the $B$ and $m$ constants, we need to follow the limitation that gelation occurs instantaneously for a 0% ZnO concentration. Our closest value is for 25 °C, with a gelation time of 1.73 min. From Figure 5.13, we obtained $B = 1421$ (against $10^{9.13}$ in Liu et al. (2011)) and $m = 3.71$ (against 3.53 in Liu et al. (2011)). The difference in the $B$ constant can come from the not accurate approximation on the gelation time at 0% ZnO. The values of slopes $m$ are, however, very similar, demonstrating the same influence of the ZnO concentration: at lower temperature, less influence of ZnO concentration on gelation time (Figure 5.13). As cellulose-NaOH based solutions are very complex systems, more data are needed to clarify the influence of various parameters on gelation time.

It is interesting to note that, even if not all the ZnO is dissolved in cellulose solutions (solubility limit $\approx 0.4\%$), ZnO still has a strong impact on gelation time. It seems that, even if ZnO limit of solubility in 8% NaOH-$H_2O$ is exceeded, the trends of the influence of ZnO concentration on gelation of cellulose solutions stay the same.

The influence of gelation time (time of storage of cellulose solution at a given temperature) on the properties of cellulose xerogels was then studied. 5% of MCC was dissolved in 8% NaOH-$H_2O$ without and with 0.5% of ZnO. The resulting solutions were then kept for 1 h, 8 h and 20 h at 50 °C for gelation, coagulated and washed in EtOH and dried under vacuum or under Sc conditions.

Figure 5.14 shows density and $S_{BET}$ and Figure 5.15 shows shrinkage and mass of xerogels and aerogels as a function of gelation time for 0% and 0.5% of ZnO.

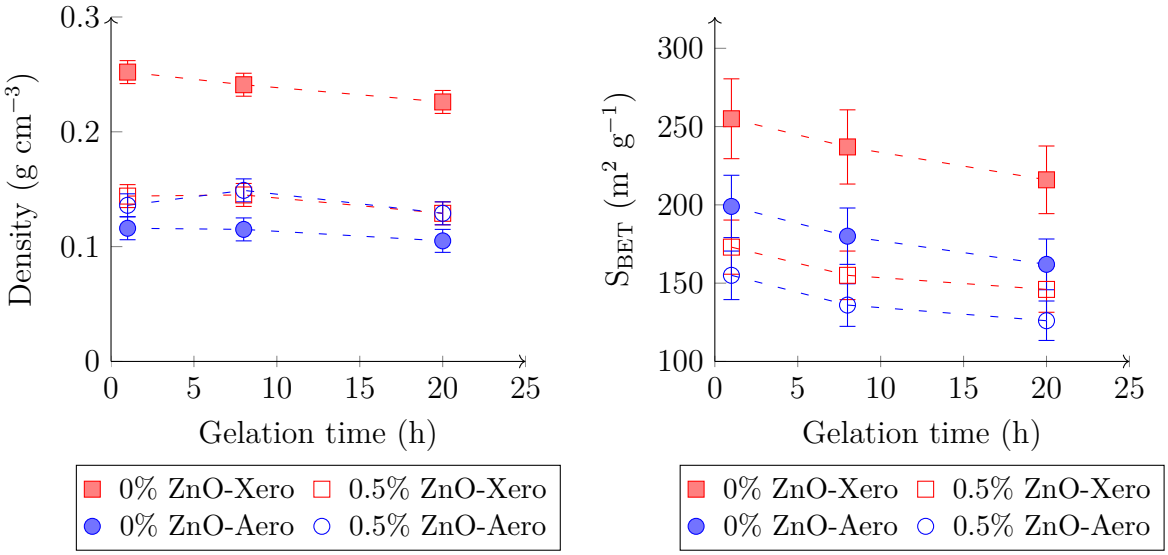


Figure 5.14 – Xerogels' and aerogels' density and $S_{BET}$ as a function of gelation time. Dashed lines are to guide the eye.

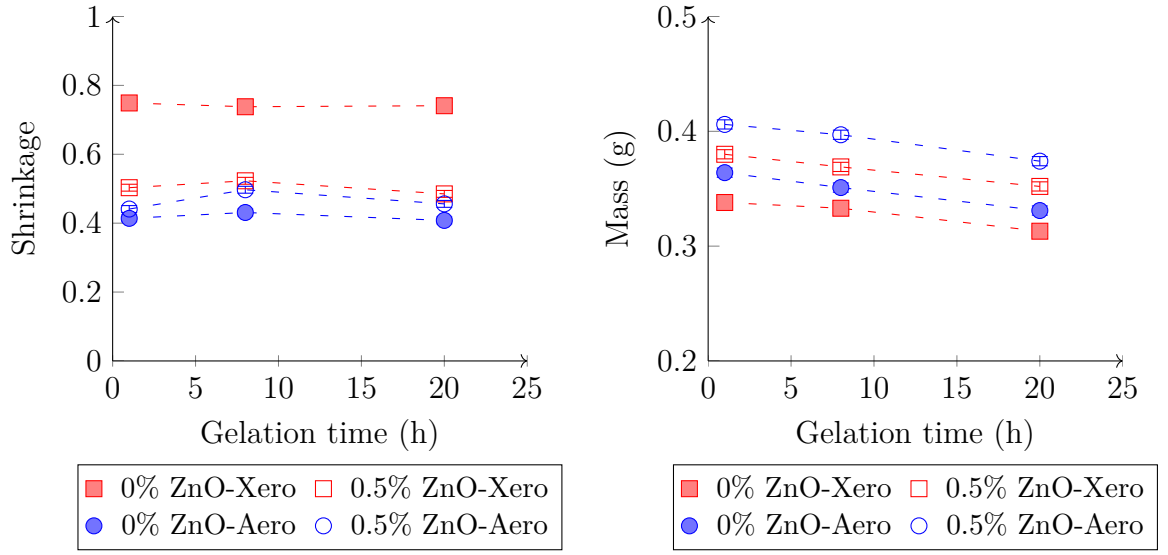


Figure 5.15 – Xerogels' and aerogels' shrinkage and mass as a function of gelation time. Dashed lines are to guide the eye.

When no ZnO was added to the solvent for cellulose dissolution, density of xerogels is twice higher than the one of aerogels (Figure 5.14). Specific surface area as well as shrinkage are also higher compared to aerogels. This is logic: high shrinkage induces higher density and potentially lower number of macropores, thus increasing $S_{BET}$. Similar trend was obtained for pectin aerogels by Groult and Budtova (2018b). When 0.5% ZnO was added, xerogels and aerogels have the same density, but $S_{BET}$ of xerogels is slightly higher than the one of aerogels. All these results are coherent with the one obtained in the previous section on the influence of ZnO concentration. Overall, we can see that whatever ZnO concentration or drying, the tendencies are the same. For an increasing gelation time:

- shrinkage is constant,
- mass slightly decreases,
- density slightly decreases,
- and $S_{BET}$ decreases.

Pereira et al. (2018) suggested that the gelation of cellulose solutions is due to precipitation/crystallization of the cellulose hence forming a "cross-linked" network and Sescousse et al. (2011a) and Liu et al. (2011) suggested that gelation is accompanied by micro-phase separation. Cellulose gelation followed by aging can thus be considered as a progressive rearrangement and "packing" of the cellulose chains in a network. This can explain the decrease of specific surface area of aerogels and xerogels with increasing gelation time: when cellulose chains are rearranging and packing, pores become larger and pores' walls thicker. With increasing pores size, we suppose that the metals remaining in the cellulose gels are washed out more easily and more efficiently because of the less steric hindrance of the cellulose chains. This would explain the decrease in mass. It seems that morphology of aerogels and xerogels becomes more heterogeneous with the increase of gelation time (Figure 5.16), however, more precise methods are needed to confirm or not this suggestion.

As suggested above, if pores' size is increased with gelation time, metals are washed out more easily which explains the decrease in mass of the EtOH coagulated xerogels and aerogels. To prove this hypothesis we studied the case when all metals are washed out during coagulation; here the mass of aerogels or xerogels should not vary with gelation time but $S_{BET}$ should decrease because of chains packing. We thus prepared aerogels from 5% cellulose-8% NaOH-0.5% ZnO-$H_2O$ solutions gelled at 50 °C for 4 h and 8 h and coagulated in 2 M HCl. As expected, density and mass were constant and $S_{BET}$ was 388 ± 12 $m^2$ $g^{-1}$ for 4 h ageing and 304 ± 46 $m^2$ $g^{-1}$ for 8 h ageing. It seems that, indeed, longer ageing is changing the cellulose gel, xerogel and aerogel structure at the microscopic scale while this cannot be seen at macroscopic level. It also further emphasise the importance of the influence of the type of coagulation bath and hence metal content in the final material.

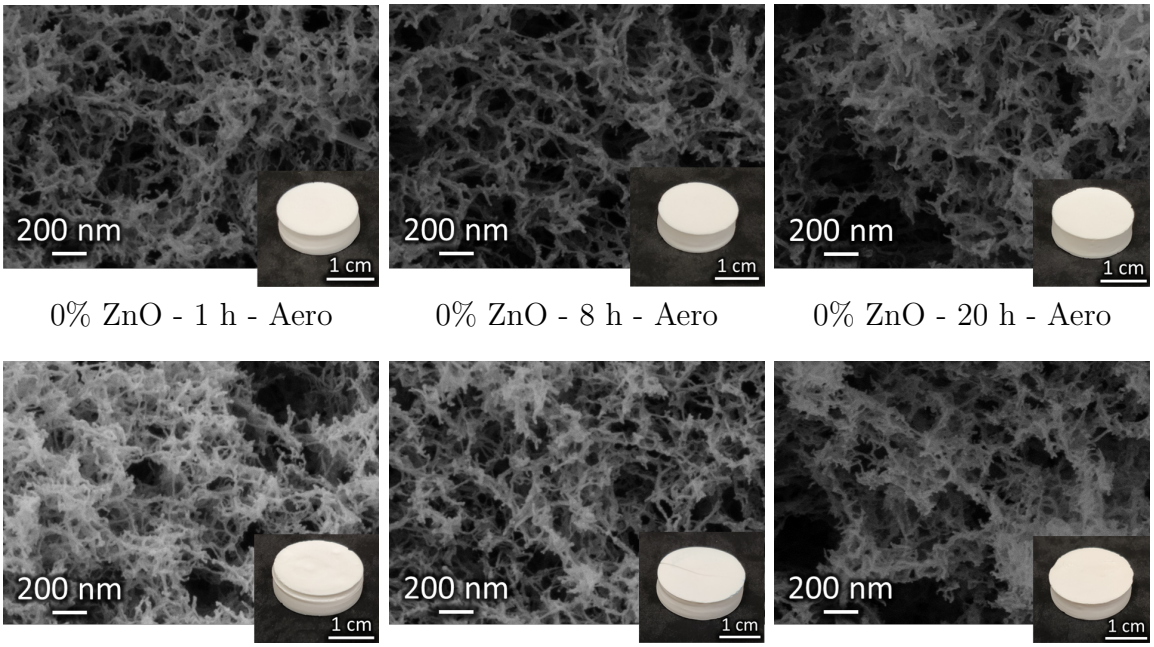


Figure 5.16 – Examples of pictures and morphologies of cellulose aerogels and xerogels from 5% cellulose dissolved in 8% NaOH-$H_2O$ without and with addition of 0.5% ZnO, aged 1 h, 8 h or 20 h at 50 °C, coagulated and washed in EtOH.

### Influence of cellulose solvent

As shown above, porous and high specific surface area cellulose xerogels can be obtained when cellulose is dissolved in 8% NaOH-$H_2O$ (with or without ZnO), coagulated and washed in EtOH. It seems that metals remaining in cellulose structure because of coagulation in EtOH play an important role in keeping certain mesoporosity. The next question is if this holds true when cellulose is dissolved in another solvent?

Thereby, we prepared xerogels from 5% MCC dissolved in [DBNH][Pr], without and with addition of 0.8% ZnO, coagulated and washed in EtOH and dried under vacuum. For comparison, the same solutions were coagulated in water, washed in EtOH and dried under vacuum. Figure 5.17 on the next page presents the obtained xerogels' pictures and morphologies.

A peculiar globular morphology was obtained from water coagulation, similar to what was reported in Section 3.2.3 on page 133 of Chapter 3.

On first sight, we can see that the EtOH coagulated and vacuum dried cellulose-[DBNH][Pr] solutions did not lead to porous xerogels, with and without ZnO. The resulting xerogels were broken and densified (density $\approx$ 1 g cm$^{-3}$) and they showed a very low $S_{BET}$ (below 5 m$^2$ g$^{-1}$). Regarding their $H_2O$ coagulated counterparts, the globular morphology observed for aerogels (Chapter 3, Figure 3.17 on page 135) was preserved even after vacuum drying. The density was lower than that after EtOH coagulation, around 0.3 g cm$^{-3}$ without ZnO and $\approx$ 0.5 g cm$^{-3}$ with ZnO, but their $S_{BET}$ was similar and very low ($\approx$ 5 m$^2$ g$^{-1}$). The lower density of xerogels obtained

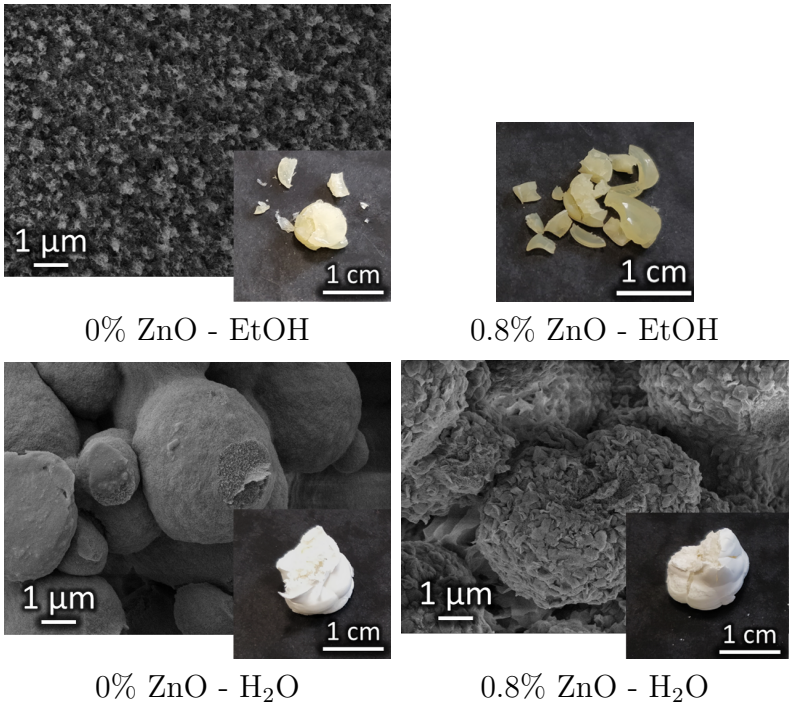


Figure 5.17 – Pictures and morphologies of xerogels of 5% cellulose dissolved in [DBNH][Pr], without and with 0.8% ZnO and coagulated in EtOH or $H_2O$.

from $H_2O$ coagulated cellulose as compared to that from EtOH coagulated one could be a result of the peculiar globular morphology of the first ones. A similar result was observed by Ayadi and Tourrette (2015) in their patent, but they did not report $S_{BET}$.

### Crystallinity of cellulose aerogels and xerogels studied by X-Ray Diffraction

It is well known that there are different cellulose crystals' allomorphs and cellulose can have different degree of crystallinity. Cellulose I is the polymorph of native cellulose with a relatively high crystallinity. When dissolved and "regenerated" or coagulated, cellulose II is obtained. It also has a semi-crystalline structure but usually with a lower degree of crystallinity. X-Ray Diffraction (XRD) measurements were performed on the model cellulose I (MCC), on neat ZnO and on xerogels and aerogels as shown in Table 5.3.

Table 5.3 – Xerogel and aerogel samples chosen for XRD measurements.

| Cellulose concentration | Solvent | ZnO concentration | First Non-solvent | Type of drying |
|---|---|---|---|---|
| 5% | 8% NaOH-$H_2O$ | 0% | EtOH | Vacuum |
| | | 0.8% | EtOH | Sc |
| | | | HCl | |
| | | | $H_2O$ | |
| | [DBNH][Pr] | 0% | EtOH | |

Gelation time of these samples was always 4 h at 50 °C, except when dissolved in [DBNH][Pr] as it does not gel.

Obtained patterns were plotted to highlight the influence of drying (Figure 5.18), non-solvent (Figure 5.19), ZnO concentration (Figure 5.20) and solvent (Figure 5.21) on the resulting cellulose.

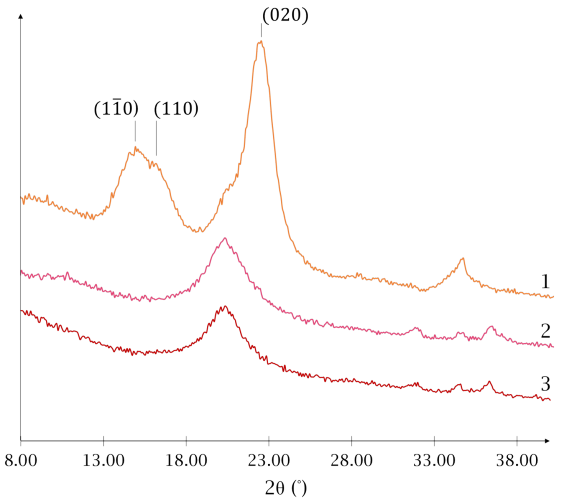


Figure 5.18 – XRD patterns of MCC (1), aerogel (2) and xerogel (3) from 5% cellulose-8% NaOH-0.8% ZnO-$H_2O$ solution, all coagulated with EtOH.

MCC pattern (Figure 5.18) is in agreement with the typical peaks of Cellulose I at $2\theta = 14.8°$, 16.3°, and 22.6°, representing the planes (1$\bar{1}$0), (110) and (020), respectively (Isogai et al. (1989)). Cellulose aerogels and xerogel show cellulose II spectrum.

If we compare the patterns of aerogel and xerogel, not much difference can be seen. It seems that in this case, drying does not have any significant influence on the resulting material. Similar pattern of very low crystallinity cellulose was already reported by Ciolacu et al. (2011) (cellulose dissolved in $SO_2$-diethylamine-dimethylsulfoxide, coagulated in EtOH and air-dried) and by Isobe et al. (2011) (cellulose dissolved in LiOH-urea solvent, coagulated in different non-solvents and freeze-dried) who demonstrated the influence of non-solvent's type on the resulting cellulose structure. For example, the cryogels (freeze-dried gels) obtained from aqueous coagulation show a much stronger (1$\bar{1}$0) peak than the one obtained from non-aqueous coagulation (Isobe et al. (2011)).

As demonstrated in Figure 5.19, the influence of the type of first non-solvent bath on cellulose aerogels' and xerogels' structure is flagrant. $H_2O$ (2) and HCl (3) coagulated aerogels show cellulose II typical pattern with well-defined planes (1$\bar{1}$0), (110) and (020) at $2\theta = 11.9°$ , 20.2° and 21.8°. If we compare these patterns of cellulose coagulated in aqueous solvents with the pattern of cellulose coagulated in EtOH (4), we can clearly see the influence of the non-solvents' type. This confirms what was stated by Isobe et al. (2011) that the intensity of the (1$\bar{1}$0) peak changes as a function of the type of non-solvent bath: with an aqueous non-solvent the intensity of the peak is higher than with an organic non-solvent. The reason for this difference was explained by Yamane

et al. (2006) and Isobe et al. (2011). The crystal plane $(1\bar{1}0)$ of cellulose corresponds to the equatorial position of glucopyranose rings. This plane is the one where the hydrophilic hydroxyl groups are located. It makes sense that when coagulation is done in an aqueous polar solvent, cellulose chains stack through the hydrophobic interaction to expose their hydrophilic groups to non-solvent. Hence the $(1\bar{1}0)$ plane appears with higher intensity in the XDR patterns.

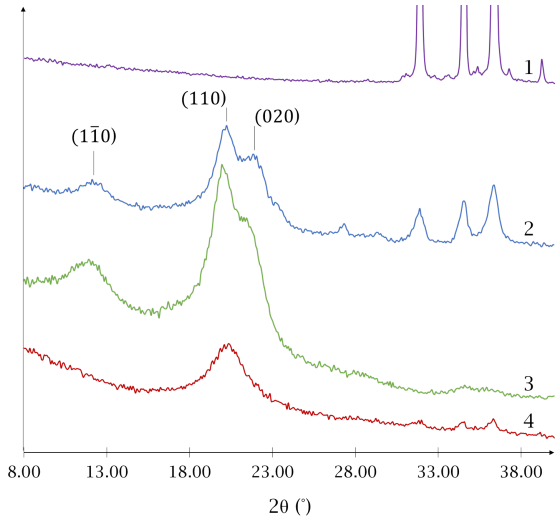


Figure 5.19 – XRD patterns of neat ZnO (1), aerogels from 5% MCC-8% NaOH-0.8% ZnO-$H_2O$ coagulated in $H_2O$ (2), in 2 M HCl (3) and xerogel from the same solvent but coagulated in EtOH (4).

The patterns in Figure 5.19 are also coherent with the metal content measured previously (Table 5.2 on page 189). Indeed, we can clearly see the presence of Zn in $H_2O$ and EtOH coagulated aerogel and xerogel (see similar peaks in neat ZnO pattern, between $2\theta = 30°$ and 40°). No ZnO is recorded for the case when cellulose was coagulated in 2 M HCl as it was washed out (Table 5.2).

The influence of ZnO concentration is shown in Figure 5.20 with the XRD patterns of the neat ZnO (1) and xerogels from 5% MCC-8% NaOH-$H_2O$ coagulated in EtOH with 0.8% ZnO (2) and without ZnO (3).

We can notice the presence of a $(1\bar{1}0)$ peak with no ZnO added to the cellulose solution (3) while almost no peak can be seen when 0.8% ZnO was present (2). It may be possible that the presence of Zn in the xerogel prevents cellulose chains from rearranging and close packing during coagulation, leading to a structure without $(1\bar{1}0)$ peak.

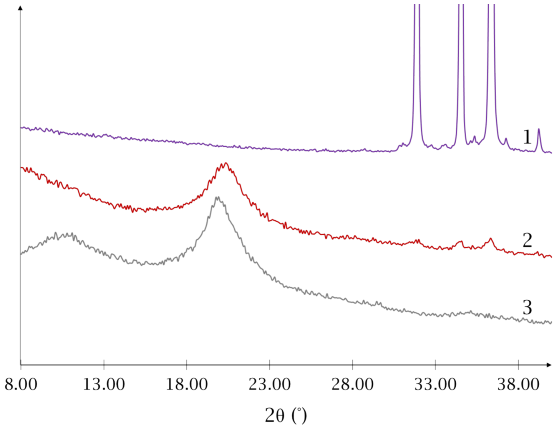


Figure 5.20 – XRD patterns of neat ZnO (1), xerogels from 5% MCC-8% NaOH-$H_2O$ coagulated in EtOH with 0.8% ZnO (2) and without ZnO (3).

We also checked the influence of the solvent, [DBNH][Pr] vs 8% NaOH-$H_2O$, on the structure of cellulose aerogel and xerogel, respectively, both were coagulated and washed in EtOH (Figure 5.21). Both patterns show a very low crystallinity with the presence of small $(1\bar{1}0)$ peak when 8% NaOH-water was used as solvent. It seems that whatever the solvent used for dissolution, it is during cellulose coagulation that chains rearrange. Hence the type of the first non-solvent is the main influencing parameter on final cellulose's structure. Coagulation in EtOH leads to cellulose with very low crystallinity.

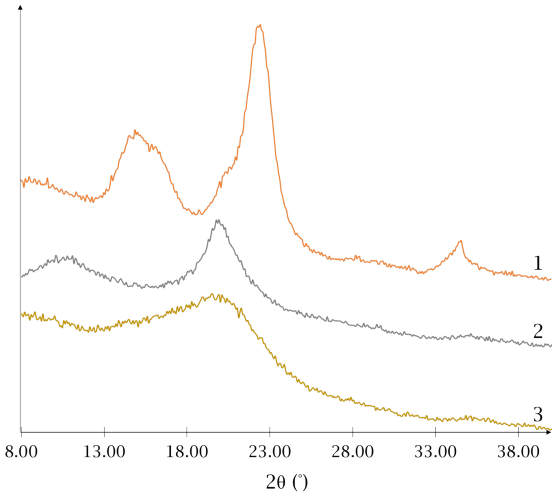


Figure 5.21 – XRD patterns of MCC (1), xerogel from 5% MCC-8% NaOH-$H_2O$ coagulated in EtOH (2), aerogel from 5% MCC dissolved in [DBNH][Pr] and coagulated in EtOH (3).

All patterns were then analysed to determine cellulose crystallinity index (Cr.I.) with the method and equation given in Section 2.2.3 (Equation (2.3) on page 107). The results are shown in Table 5.4. The artificial increase of intensity at very low angles was not taken into account.

Table 5.4 – Xerogels' and aerogels' crystallinity determined by XRD.

| Samples | Cr.I. (%) |
|---|---|
| MCC | 65 |
| 5% MCC - EtOH - Xero | 22 |
| 5% MCC - 0.8% ZnO - EtOH - Xero | 22 |
| 5% MCC - 0.8% ZnO - EtOH - Aero | 27 |
| 5% MCC - 0.8% ZnO - HCl - Aero | 62 |
| 5% MCC - 0.8% ZnO - $H_2O$ - Aero | 53 |
| 5% MCC - [DBNH][Pr] - EtOH - Aero | 9 |

Table 5.4 shows that crystallinity of the aerogels and xerogels mostly depend on the type of the first non-solvent bath used for coagulation. We see a clear difference in cellulose crystallinity between aqueous non-solvent (HCl and $H_2O$) and EtOH. EtOH coagulated aerogels show a very low Cr.I. of 9% when the dissolution was done in [DBNH][Pr] and Cr.I. is around 22 - 27% when it was dissolved in NaOH based solvent. Cr.I of $H_2O$ coagulated aerogel is 53% and Cr.I. of HCl coagulated aerogels is 62%, both showing a significant difference with EtOH. As already mentioned above, the higher crystallinity of aerogels coagulated in aqueous non-solvents can be induced by the way the cellulose rearrange in these polar hydrophilic solvents during coagulation. Regarding the influence of ZnO and of the solvent on cellulose, more studies are needed, for example, characterisation with FTIR spectroscopy. One of the questions is the type of interactions, if any, between cellulose and the remaining Na and Zn.

### 5.2.2 Analysis and discussions

Here we summarise and analyse the results obtained in the previous sections. The influence of the type of the first non-solvent bath, of ZnO concentration, and of the type of solvent on the morphology of cellulose xerogels and aerogels is detailed.

Capillary pressure developed during evaporative drying (see Young-Laplace equation: Equation (1.5) on page 71) usually leads to collapse of pores in "wet" cellulose and great densification, resulting in high density and low specific surface area xerogels. We have demonstrated that *porous* and with high (for cellulose) specific surface area cellulose xerogels can be prepared from low vacuum evaporative drying only when cellulose is dissolved in 8% NaOH-$H_2O$ and when the first and all coagulation baths are EtOH. These xerogels have properties comparable to the ones of their aerogel counterparts and can be even better (higher $S_{BET}$ and lower density) when ZnO is used as additive. The density varies between 0.24 g $cm^{-1}$ and 0.13 g $cm^{-1}$ and $S_{BET}$ from 274 $m^2$ $g^{-1}$ to 136 $m^2$ $g^{-1}$ when no ZnO and when 0.5% ZnO was added to cellulose solution, respectively. The question to answer is "what prevents pore collapse in this specific case?". For example, to make ambient pressure dried silica with properties similar to their supercritically dried counterparts, silylation of silica gels is needed to "re-open"

pores during drying. In the case of cellulose no "on purpose" chemical treatment was performed. Below the experimental results will be summarised and hypotheses trying to answer this question will be made.

There are several facts that should be considered together:

- Presence of non-dissolved Na and Zn in cellulose aerogels and xerogels when first and all coagulation baths are EtOH.
- Very low crystallinity of these aerogels and xerogels.
- High density and low specific surface area of xerogels when cellulose was dissolved in ionic liquid and not in 8% NaOH-$H_2O$, with the same coagulation procedure.
- Peculiar influence of ZnO concentration on xerogels' density and surface area, with still high (for cellulose) $S_{BET}$ and rather low density of xerogels when no ZnO was added to cellulose solutions.
- Presence of two types of ZnO in cellulose solution: dissolved and non-dissolved above the dissolution limit of around 0.4% in 8% NaOH-$H_2O$.

First, we remind that the metals are completely washed away only when coagulation bath is of very low pH (see Table 5.2 on page 189). When $H_2O$ is used, only a part of the Zn is washed away ($\approx$ 47%) while all the Na is. Finally, when coagulated in EtOH, Na takes $\approx$ 5% of the final mass while Zn takes between 2.6% and 8.3% depending on the initial ZnO concentration. The loss of Zn in EtOH is always around 40%, whatever the initial concentration. We suppose that when coagulation happens, cellulose chains rearrange meanwhile Zn precipitates. Part of Zn is thus trapped between cellulose chains and cannot go out from the network during washing. The 40% loss could represent part of precipitated Zn removed from outside layer of the sample or the smallest particles that could be washed out. As all samples had the same size, it makes sense that the loss (in percent) is always the same for all initial ZnO concentrations. If this hypothesis is true, it can be applied to Na as well for the case of coagulation in EtOH.

Considering the presence of non-dissolved metals in cellulose aerogels and xerogels when coagulation is performed in EtOH together with their very low crystallinity allows making the first hypothesis: **non-dissolved metals are acting as spacers preventing cellulose chains to closely pack**. This leads to the formation of pores that remain open after low-vacuum drying and also leads to almost amorphous cellulose. This hypothesis can be illustrated as shown in Figure 5.22.

The suggested hypothesis explains the case of porous cellulose xerogels obtained in the presence of ZnO. However, Figure 5.6 and Figure 5.7 on page 186 show that it is possible to make rather low density (0.24 g $cm^{-3}$) and high specific surface area (263 $m^2$ $g^{-1}$) cellulose xerogels when solvent is 8% NaOH-$H_2O$ without any additives and when coagulation is performed in EtOH. What are the "spacers" here? The answer can be found in literature.

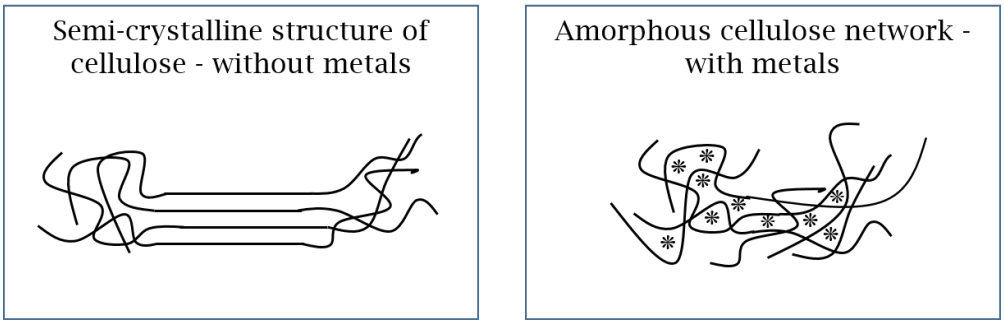


Figure 5.22 – Schematic representation of cellulose structure without and with metals.

Gunnarsson et al. (2017, 2018) suggested that chemisorption of $CO_2$ occurs on the Carbon 6 of the cellulose glucopyranose ring when cellulose is dissolved in NaOH based solvent. Indeed, the $CO_2$ in the surrounding air can diffuse to NaOH(aq) and to deprotonate cellulose creating carbonates. These carbonates can then create bridges between cellulose chains (Elschner et al. (2013)) or hydrogen bonds between carbonates and hydrogens from the hydroxyl groups (Gunnarsson (2017) see Figure 1.8 on page 61). The fact that *"Ethanol, as such, has been shown to preserve chemisorbed $CO_2$ in synthesised organic carbonates, whilst precipitation in water promotes the desorption of $CO_2$."* (Gunnarsson et al. (2018)), allows preserving carbonate bonds created when coagulation is done in EtOH and stabilising (and/or reinforcing) cellulose network. The second hypothesis is thus as follows: **carbonate bridges formed between cellulose chains when dissolved in NaOH-$H_2O$ and coagulated in EtOH prevent cellulose network from collapsing during vacuum drying**. As a consequence, these bridges can be the reason for the amorphous structure of cellulose. This hypothesis also explains why xerogels made from cellulose-ionic liquid solutions were not porous.

The hypothesis of spacers or bridges, whatever is their nature, and the limit of ZnO dissolution in 8% NaOH-$H_2O$ may help the understanding of U-shape curve of specific surface area of aerogels and xerogels as a function of ZnO concentration in solution (Figure 5.7 on page 186). Without ZnO in the solvent, cellulose forms a network stabilised by carbonates. This network is rather resistant to low-vacuum drying, however, certain shrinkage occurs. The pores are kept, the density is moderately low and $S_{BET}$ is high (for cellulose).

When ZnO was added, the density and the $S_{BET}$ of xerogels firstly decreased. Metals, which remain in cellulose network form spacers and thus pores, increase sample weight and prevent shrinkage (Figure 5.8 on page 186). Hence density and $S_{BET}$ of xerogels decrease probably because of the formation of macropores as suggested in Figure 5.22. As for aerogels, their precursors are not shrinking as much as of xerogels: density slightly increases because of the increase of weight due to the presence of metals and $S_{BET}$ decreases because of the formation of macropores as suggested above.

With increasing ZnO concentration the density of aerogels and xerogels continue to slightly increase (Figure 5.7). Above the dissolution limit (around 0.4%), non-dissolved

ZnO appears which form "needle-star" crystals (Figure 5.9 on page 187). We speculate that these crystals may add certain input into the surface area of aerogels and xerogels which would lead to $S_{BET}$ increase (Figure 5.7). The increase in weight due to the presence of more and more metals, and potentially of macropores, both acting towards surface area decrease, is balanced by the presence of "new" crystals.

To conclude, two non-contradicting hypotheses, both explaining the formation of low crystallinity, porous and high (for cellulose) specific surface area cellulose xerogels without drying in supercritical conditions, were suggested:

- The creation of carbonate bridges between cellulose chains during cellulose dissolution in aqueous NaOH solvent and the preservation of these bridges during EtOH coagulation help preserving network during vacuum drying.
- Metals, remaining in cellulose after coagulation in EtOH, play the role of spacers between cellulose chains preventing network collapse during vacuum drying. The dissolution limit of ZnO in 8% NaOH-$H_2O$ may be the reason of $S_{BET}$ variation as a function of ZnO concentration.

### 5.2.3 Cellulose xerogel beads

Thus far, the aim of this thesis was the production of cellulose aerogel beads of different sizes. The discovery of new porous and high (for cellulose) specific surface area xerogels opens a lot of opportunities. Producing them as beads can offer a wider range of applications at a reduced cost, compared to aerogels.

As a first step to prove that the production of porous and high $S_{BET}$ xerogel beads is possible, we used the laboratory scale dropping technique. Two solutions were tested, 5% MCC dissolved in 8% NaOH-$H_2O$, with addition of 0.5% ZnO and without additive. The obtained solutions were then coagulated directly in EtOH by dropping and dried under vacuum and under Sc $CO_2$ conditions, as a comparison. Figure 5.23 shows pictures of xerogel and aerogel beads as well as their specific surface area. Figure 5.24 on page 205 gives their size distribution, mean diameter and standard deviation.

The pictures and $S_{BET}$ given in Figure 5.23 are an excellent proof that the production of high specific surface area cellulose xerogel beads is possible. When comparing with the results obtained in Figure 5.7 on page 186, the properties of beads are very similar to the ones of monolithic xerogels and aerogels. Size distribution, mean diameter and standard deviation of the beads given in Figure 5.24 further emphasise the similarities between aerogels and xerogels. As for the monoliths, the shrinkage is more important for the 0% ZnO xerogels than for all the other xero- and aerogels as the smaller mean diameter of beads can attests (Figure 5.24). Still their $S_{BET}$ stays relatively high with 237 $m^2\ g^{-1}$.

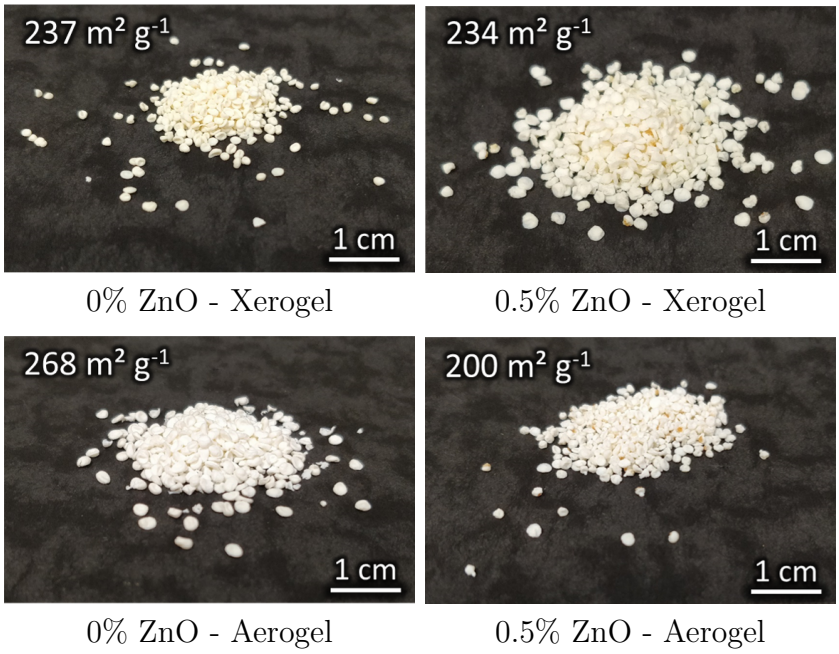


Figure 5.23 – Pictures and $S_{BET}$ of xerogel and aerogel beads from 5% cellulose-8% NaOH-$H_2O$ solutions, without and with 0.5% ZnO, coagulated and washed in EtOH.

Regarding the aerogel beads without and with ZnO, we can see that they show a higher specific surface area than the monoliths:

- without ZnO: 268 $m^2$ $g^{-1}$ for the beads against 212 $m^2$ $g^{-1}$ for the monoliths,
- and with 0.5% ZnO: 200 $m^2$ $g^{-1}$ against 148 $m^2$ $g^{-1}$.

This result is in agreement with what was reported by Voon et al. (2016): the decrease of specific surface, from 498 $m^2$ $g^{-1}$ to 107 $m^2$ $g^{-1}$ with the increase of particle mean diameter from 0.41 $\pm$ 0.03 mm to 2.14 $\pm$ 0.08 mm. A similar tendency can be observed for the xerogel beads and monoliths with addition of 0.5% ZnO as they show a $S_{BET}$ of 234 $m^2$ $g^{-1}$ for the beads against 184 $m^2$ $g^{-1}$ for the monoliths. It may be possible that the Na and the Zn are better washed out from the beads than from the monoliths because of the larger surface to volume ratio.

To conclude on this last part, we can say that we have successfully produced cellulose xerogel beads with the dropping technique. Their properties are comparable to aerogel beads and monoliths and to monolithic xerogels. This laboratory technique is a first step for the mass production of porous cellulose xerogel beads. With this kind of promising results, we can imagine using the JetCutter technique seen in Chapter 3 to produce these beads on a larger scale. Still, more studies are needed to better understand how to tailor the properties of the resulting beads.

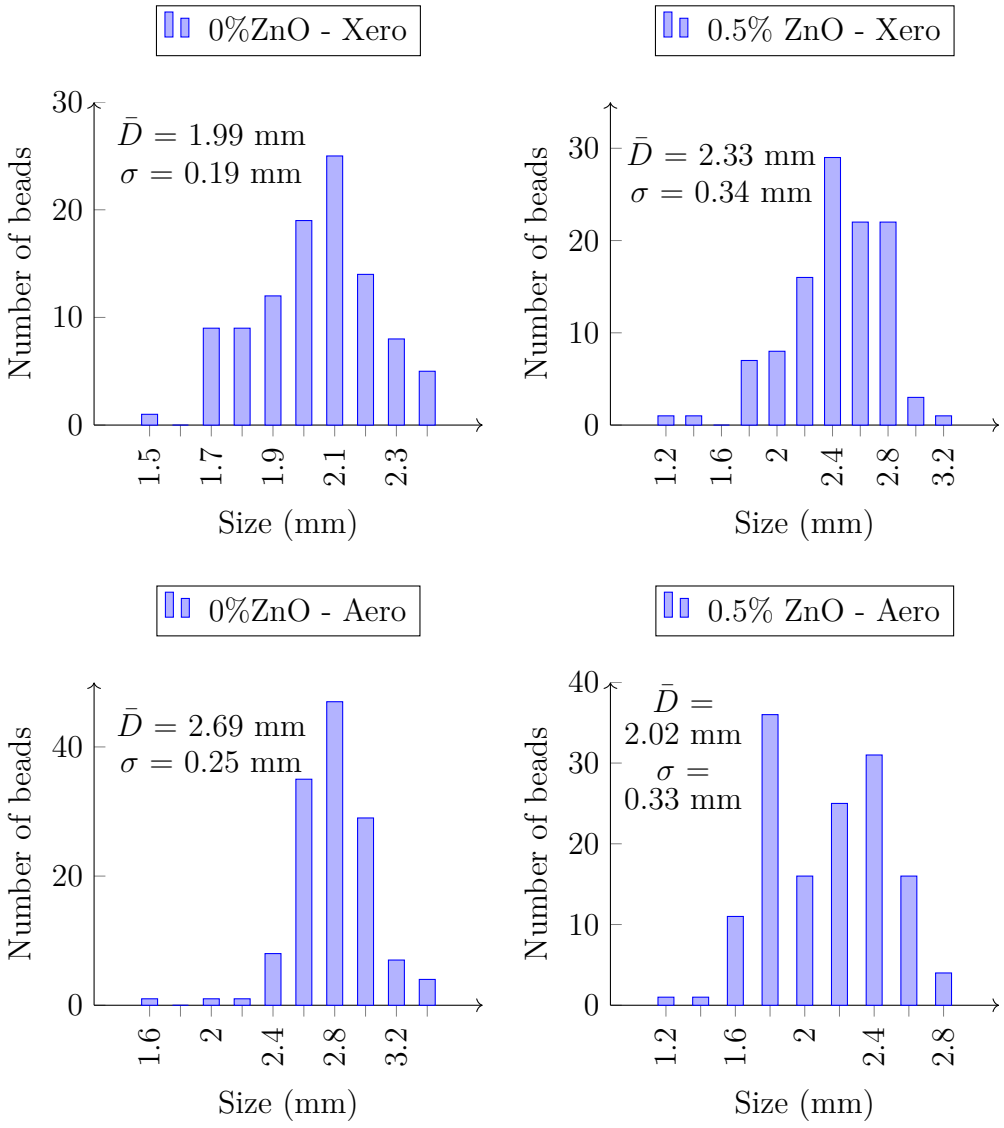


Figure 5.24 – Size distribution of xerogel and aerogel beads from 5% cellulose dissolved in 8% NaOH-$H_2O$ solutions, without and with 0.5% ZnO and coagulated in EtOH. $\bar{D}$ stands for the mean diameter and $\sigma$ for the standard deviation.

# Conclusions

In this study, we have proven that with specific preparation conditions we are able to produce cellulose xerogels, dried under low vacuum, with properties equivalent or even better than the ones of their aerogel counterparts. NaOH-water was used as solvent for cellulose, with different concentrations in additive, here ZnO.

In the first section we have analysed the properties of the cellulose xerogels by evaluating the influence of different preparation parameters. It was demonstrated that ultra-lightweight and high specific area xerogels were only obtained when ethanol was used as first non-solvent for coagulation. The properties of aerogel counterparts confirmed that the influence of the first coagulation bath is specific to xerogels and that the differences in aerogels' properties coagulated with different non-solvents were not that significant.

The influence of ZnO concentration on xerogels' properties was then studied. The property that varied most by changing ZnO concentration was the specific surface area: it has a U-shaped curve with increasing concentration. This trend was also observed for aerogels. Furthermore, when concentration of ZnO was equal or higher than 0.5%, crystals were observed by SEM in the xerogels' and aerogels' structure. We assumed that they were crystals of zinc. Elemental analysis revealed that neither Na nor Zn were completely washed out when coagulation was done in EtOH, while they were washed out when coagulated in HCl.

The influence of gelation time and type of solvent were also checked. Gelation time did not have a significant influence on the resulting xerogels' properties while the type of solvent was critical. When ionic liquid was used as cellulose solvent, the xerogels were dense, with extremely low specific surface area. Finally, crystallinity was evaluated and xerogels and aerogels coagulated with EtOH showed a very low crystallinity as compared to the ones coagulated with HCl or $H_2O$.

The second section of this chapter was devoted to the analysis of all results obtained in the first section. Hypotheses were suggested to explain why these xerogels have outstanding properties. We have observed that when cellulose-NaOH-ZnO-$H_2O$ solutions were coagulated and washed in EtOH, Na and Zn remained in the structure. Our first hypothesis was that the metals are acting as spacer between cellulose chains, hence preventing the network from shrinking and collapsing during vacuum drying. This would also explain why the crystallinity index of aerogels and xerogels coagulated in EtOH is very low: chains cannot reassemble during coagulation because of the remaining metals. Our second hypothesis was based on the work of Gunnarsson et al. (2017) who suggested that carbonate bridges are formed between cellulose chains when dissolved in NaOH-$H_2O$. When coagulated in EtOH, these bridges are not dismantled and they prevent cellulose network from collapsing during vacuum drying. The question on the influence of ZnO on $S_{BET}$ is still open. We suggested that when adding

ZnO to cellulose-NaOH-$H_2O$ solution, ZnO plays the role of spacer and $S_{BET}$ decreases probably because of the formation of macropores. Then, when beyond the limit of solubility of ZnO, the formed "needle-star" crystals are contributing to $S_{BET}$ leading to an increase of the latter.

In the last section we proved that the production of porous and high $S_{BET}$ xerogel beads is possible by using the laboratory scale dropping technique. The properties of beads are very similar to the ones of monolithic xerogels and aerogels. $S_{BET}$ was higher for aerogel beads as compared to the monoliths, with the same preparation conditions.

# Chapter 6

# Pulp based aerogels

## Contents

# Abstract

So far in this manuscript, only model microcrystalline cellulose was used to produce aerogels and xerogels. In this last chapter, we would like to open new possibilities in producing aerogels from pulp. Different types of pulps, with systematic variation of cellulose degree of polymerisation and cellulose, hemicellulose and lignin content were kindly prepared and provided by RISE-Innventia.

In the first section, pulps' characteristics are reminded and solvents and non-solvents used to make aerogels and xerogels are specified. In this study, pulps were dissolved in NaOH-ZnO-$H_2O$ solvent and coagulated in HCl, $H_2O$ or EtOH.

In the second section results are presented and discussed as a function of the different parameters studied. First, the dissolution efficiency of the solvent is evaluated by optical microscope observations and determination of the non-dissolved fraction. Then the influence of different preparation parameters on aerogels' properties are evaluated. Morphology, density, specific surface area, crystallinity and composition changes are analysed as a function of gelation time, type of non-solvent used and pulps' initial composition. In order to have a better understanding of the influence of hemicellulose on pulp aerogels' properties, a short study on the preparation of hemicellulose aerogels is performed. Finally, we confirm that the different studies realised so far in this manuscript are reproducible and applicable to pulps. The most suitable solutions, in terms of pulp type and composition, are selected to be produced as aerogel beads with the JetCutter technology. Ultra-lightweight pulp xerogels are prepared. An application for these aerogels and xerogels is tested for moisture sorption.

# Résumé

Jusqu'à présent dans ce manuscrit, seul la cellulose microcristalline standard a été utilisé pour produire des aérogels et des xérogels. Dans ce dernier chapitre, nous souhaitons ouvrir de nouvelles possibilités en produisant et en analysant des aérogels à partir de pâte à papier. Différents types de pâtes, avec variation systématique du degré de polymérisation de la cellulose et de la teneur en cellulose, en hémicellulose et en lignine ont été aimablement préparés et fournis par RISE-Innventia.

Dans la première section, nous rappelons les caractéristiques des pâtes à papier et nous précisons quels solvants et non-solvants nous sont utilisés pour fabriquer ces aérogels. Dans cette étude, les pâtes à papier sont dissoutes dans le solvent NaOH-ZnO-$H_2O$ et coagulées dans du HCl, de l'$H_2O$ ou de l'EtOH.

Dans la deuxième partie, les résultats sont présentés et discutés en fonction des différents paramètres étudiés. Tout d'abord, l'efficacité de la dissolution du solvant est évaluée par des observations au microscope optique et par la détermination de la fraction de non-dissout. Ensuite, l'influence des différents paramètres de préparation sur les propriétés des aérogels est déterminée. La morphologie, la densité, la surface spécifique, la cristallinité et les changements de composition sont analysés en fonction du temps de gélification, du type de non-solvant utilisé et de la composition initial des pâtes à papier. Afin de mieux comprendre l'influence de l'hémicellulose sur les propriétés des aérogels de pâte à papier, une brève étude sur la préparation d'aérogels d'hémicellulose est réalisée. Enfin, nous confirmons que les différentes études réalisées jusqu'à présent dans ce manuscrit sont reproductibles et applicables aux pâtes à papier. Les solutions de pâte à papier les plus appropriées, en termes de type et de composition, sont sélectionnées pour être produites sous forme de billes d'aérogel avec la technologie JetCutter. Des xérogels de pâte à papier ultra-légers sont préparés. Une application pour ces aérogels et ces xérogels est testée pour la sorption d'humidité.

## 6.1 Materials and methods

### 6.1.1 Materials

In this chapter, MCC, pulps and hemicellulose were used. They were all described in Section 2.1.1 on page 95 of Chapter 2. Table 6.1 summarises the main characteristics of the different pulps, MCC and hemicellulose used to produce aerogels.

Table 6.1 – Pulps', MCC's and hemicellulose's characteristics.

| Pulp type | Pulps | DP | Hemicellulose (%) | Lignin (%) |
|---|---|---|---|---|
| Type 1 | **(1)h-h-h** | 1452 | 12.8 | 5 |
| | **(1)l-h-h** | 755 | | |
| Type 2 | **(2)h-h-l** | 1328 | 16.5 | 0.9 |
| | **(2)l-h-l** | 770 | 7.4 | |
| Type 3 | **(3)h-l-h** | 1384 | 4.8 | 7 |
| | **(3)l-l-h** | 657 | | |
| Type 4 | **(4)h-l-l** | 986 | 2.1 | 0.8 |
| | **(4)l-l-l** | 608 | | |
| | **MCC** | 320 | 0 | 0 |
| | **Hemicellulose** | - | ≈ 60% glucomannan<br>≈ 10% xylan | 3 |

Different solvents were used to make aerogels:

- Pulps were dissolved in NaOH solution with addition of ZnO.
- Hemicellulose and MCC/hemicellulose hybrids were dissolved in freshly prepared [DBNH][Pr].

All these components were already listed and described in Section 2.1.2 on page 99.

### 6.1.2 Methods

#### Pulp aerogels preparation

All pulp aerogels were prepared following the dissolution in NaOH based solvent as described in Section 2.2.1 on page 101. The final solution concentrations were:

- 3% of pulp,
- 0.82% of ZnO,
- and 7.6% NaOH.

After the dissolution, 6 mL of solution was poured in cylindrical containers and they were either directly coagulated or gelled before coagulation at 50 °C for 4 h or 8 h. Three different coagulation baths were used: 1 M HCl, $H_2O$ or EtOH. When the non-solvent was HCl, it was replaced by $H_2O$. Finally, $H_2O$ in the gels was replaced by EtOH for the subsequent Sc Drying (described in Section 2.2.1 on page 102).

### Hemicellulose and hemicellulose-MCC hybrid aerogels' preparation

For hybrid aerogels' preparation, 3% MCC and 10% hemicellulose were dissolved together in [DBNH][Pr] following the procedure described in Section 2.2.1 on page 102. The same procedure was used to obtain the 3% pure cellulose aerogels. However, it was slightly modified for pure hemicellulose dissolution: 30% hemicellulose was dissolved in [DBNH][Pr] at 45 °C and 250 rpm mechanical stirring. As the solution was extremely viscous, the dissolution was done in three steps: a stirring step at 45 °C and 250 rpm for 5 h 30 min, a steady state (no stirring) at room temperature for a night and another stirring step at 45 °C, 250 rpm for 5 h.

For all the prepared solutions, 5 g were poured in cylindrical containers and were kept steady for at least 20 h at 40 °C. This storage allowed the remaining bubbles from the dissolution to make their way out from the solutions.

The solutions were then coagulated in EtOH and washed several times for the Sc drying.

### Determination of non-dissolved fraction in pulp-NaOH-ZnO-$H_2O$ solutions

Pulps were not completely dissolved in NaOH-$H_2O$ even in the presence of ZnO. Pictures were taken with the optical microscope of each pulp solution, to be compared. Non-dissolved fraction of the pulps was determined as follows: immediately after the dissolution, pulp solutions were diluted with cold 8% NaOH solution and centrifuged at 9000 rpm and 10 °C for 15 min. Obtained non-dissolved parts were washed two times with the cold 8% NaOH to better separate the non-dissolved part from the dissolved solution. They were then filtered (filter pores' size $< 2$ µm) and washed several times with water to wash out the remaining NaOH. Finally, the residues from filtration, the non-dissolved part, were dried over night at 70 °C under vacuum and weighted.

The non-dissolved fraction was then calculated as follow:

$$Non - dissolved\ (\%) = \left(1 - \frac{(m_{ini} - m_{non-dissolved})}{m_{ini}}\right) * 100 \tag{6.1}$$

with $m_{ini}$ the initial mass in pulp and $m_{non-dissolved}$ the dried non-dissolved part mass.

### Shaping and different drying modes

Pulp beads were produced with the JetCutter at RISE-Innventia. This technology has already been described in Section 2.2.2 on page 104. The solutions or slightly gelled solutions were cut with the JetCutter and directly coagulated in coagulation bath (1 M HCl, $H_2O$ or EtOH). The obtained wet beads were transferred in EtOH, if not already in it, for the subsequent Sc drying.

Monolithic aerogels of the same were also prepared.

Pulp xerogels were obtained by drying coagulated and washed in EtOH gels (4 h at 50 °C) at 50 °C under vacuum for 24 h.

## 6.2 Results and discussions

### 6.2.1 Dissolution efficiency of NaOH solvent for the pulps

As far as cellulose pulps are only partly soluble in NaOH based solvents (Chapter 1, Section 1.2.1 on page 64), it was important to determine the non-dissolved fraction of our solutions to reveal the potential correlation between the non-dissolved pulp and the resulting aerogel properties. To do so, we have observed pulp solutions at the optical microscope, just after dissolution, and measured the non-dissolved fraction of four different pulps: (1)h-h-h, (3)h-l-h, (1)l-h-h and (4)l-l-l.

Pictures of pulp solutions are shown in Figure 6.1. Note that the pulps (2)h-h-l and (2)l-h-l (pulps of type 2) are not shown in this figure because they were very similar to the pulp of type 4, respectively. Table 6.2 on the next page summarises the pulps characteristics and gives the non-dissolved fraction in percent. Besides, as it was observed in the preceding chapter and will be discussed later in this chapter, the ZnO is not soluble in water. Hence, it is not washed away during the separation of the non-dissolved parts from the solutions. The non-dissolved fraction given here thus includes the remaining Zn, it should consequently be considered as a part of the non-dissolved fraction.

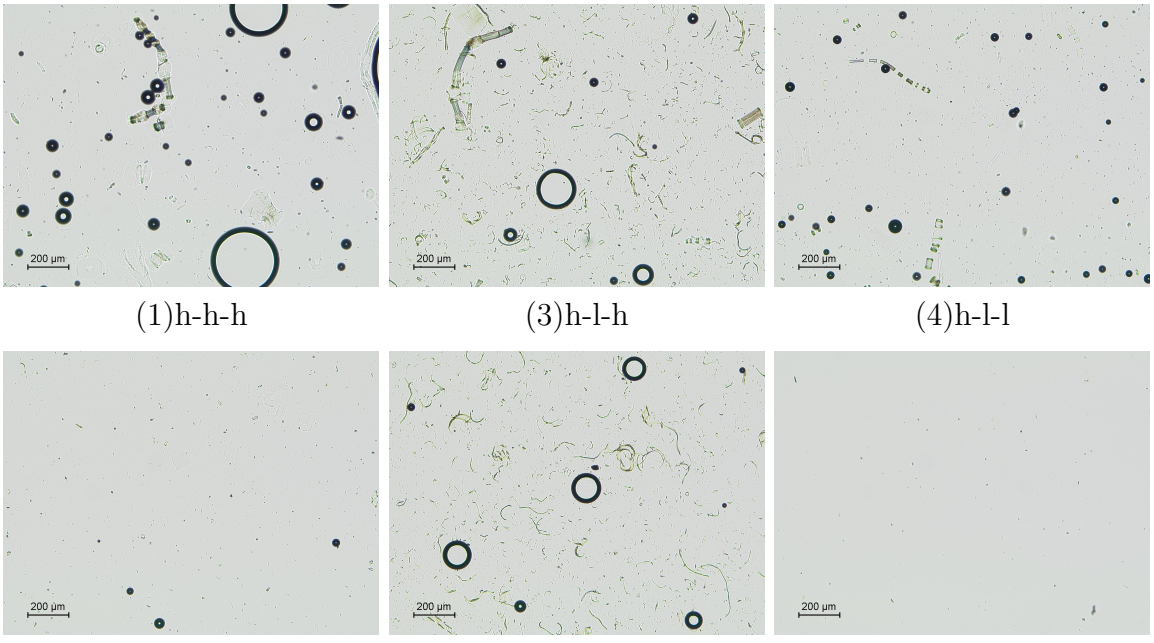


(1)h-h-h (3)h-l-h (4)h-l-l

(1)l-h-h (3)l-l-h (4)l-l-l

Figure 6.1 – Images of pulp solutions. Scale is 200 µm.

Table 6.2 – Pulps' characteristics and non-dissolved fraction calculated from Equation (6.1).

| **Pulps** | **DP** | **Initial hemicellulose content (%)** | **Initial lignin content (%)** | **Non-dissolved (%)** |
|---|---|---|---|---|
| **(1)h-h-h** | 1452 | 12.8 | 5 | 9 |
| **(1)l-h-h** | 755 | | | 1.5 |
| **(2)h-h-l** | 1328 | 16.5 | 0.9 | - |
| **(2)l-h-l** | 770 | 7.4 | | - |
| **(3)h-l-h** | 1384 | 4.8 | 7 | 12.8 |
| **(3)l-l-h** | 657 | | | - |
| **(4)h-l-l** | 986 | 2.1 | 0.8 | - |
| **(4)l-l-l** | 608 | | | 0.7 |

At the first glance it seems that the dissolution fraction mainly depends on cellulose DP. Indeed, the pulp solutions with the highest DP (on the top part of Figure 6.1) show remaining cellulose fibres or part of fibres. We can even clearly distinguish on picture (1)h-h-h the ballooning of cellulose fibres which means that the dissolution is not complete (Le Moigne and Navard (2010)). Measurement of the non-dissolved fraction of the pulps of type 1 confirmed this assumption (Table 6.2). For the same hemicellulose and lignin content, the pulp with a DP of 755 had a non-dissolved fraction of 1.5% whereas the one with a DP of 1452 had a non-dissolved fraction of 9%.

The DP seems not to be the only parameter influencing the dissolution. When looking at the pictures of (3)h-l-h and (3)l-l-h on Figure 6.1, we observe a lot of remaining smaller non-dissolved "parts". These pulps do not have either the highest DP or hemicellulose content, but they do have the highest lignin content (7% of pulp). Hemicellulose and lignin are soluble in NaOH to a certain extent. After the pulping process, the remaining lignin in pulps is relatively unreactive and modified (Gellerstedt and Lindfors (1984); Froass et al. (1998); Melro et al. (2018)) making the dissolution harder. The modification of the lignin could explain its non-dissolution by itself but, when looking at the (1)h-h-h and (1)l-h-h pulps, which have a 5% lignin content on pulp, no non-dissolved lignin can be seen. Two hypothesis can be suggested:

- The lignin solubility limit in 8% NaOH with addition of 0.82% ZnO is included between 0.15% and 0.21% of lignin in the solution (which correspond to 3% pulp dissolved with 5% and 7% of lignin content, respectively).

The pulping process consists of alkaline cooking stages at high temperature, with a maximum 25% effective alkali and 30% sulfidity, and a liquor-to-wood ratios of 5:1. In our study, a small quantity of pulp (3%) was dissolved in more concentrated NaOH than during pulping (8% NaOH solution) with addition of ZnO. It may be possible that even after the pulping, the residual lignin is still soluble, to a certain extent, in our system. The solubility limit of lignin is thus exceeded for (3)h-l-h and (3)l-l-h (7% in the pulp) but not for (1)h-h-h and (1)l-h-h (5% in the pulp).

- The differences during pulping process for the pulps of the type 1 and the type

3 induce a change in lignin dissolution behaviour.
The (3)h-l-h and (3)l-l-h pulps were subjected to a pre-hydrolysis stage while (1)h-h-h and (1)l-h-h did not. The pre-hydrolysis consists on a treatment in water at 170 °C, during which hemicellulose is removed. After the pre-hydrolysis a very similar kraft cooking followed for pulps of both type 1 and type 3. Consequently, the residual lignin in these pulps is not exactly the same. However, deeper studies would be needed to understand why the pre-hydrolysis would lead to a less soluble residual lignin, but it is outside the scope of this work.

Overall, the non-dissolved fraction in solution of high DP pulps is around 10%. The dissolution can be considered as complete for the low DP pulps, except for the (3)l-l-h which have non-dissolved residual lignin. Finally, the hemicellulose seems to be completely dissolved in our system.

### 6.2.2 Parameters influencing pulp aerogels' properties

#### Influence of gelation time

The influence of gelation time on aerogels' properties was studied on:

- two different pulps, chosen for their opposite compositions and DP: (1)h-h-h and (4)l-l-l,
- three gelation times: no gelation (0 h), 4 h or 8 h,
- and one coagulation bath: $H_2O$.

Pictures and morphology of (1)h-h-h and (4)l-l-l aerogels, as a function of gelation time are shown in Figure 6.2. Their properties are given in Table 6.3.

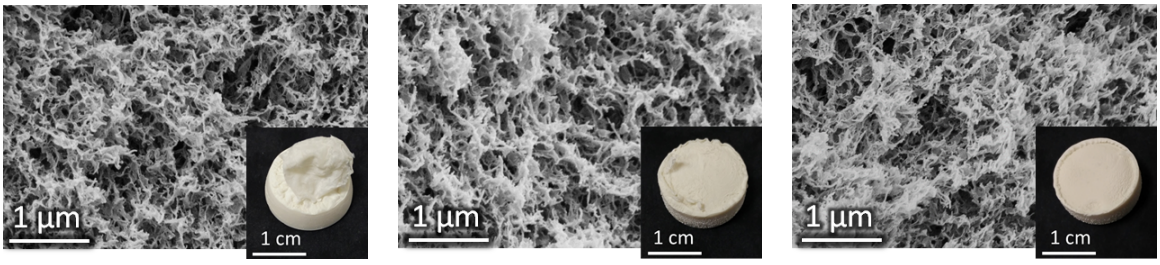


(1)h-h-h - **0 h** - $H_20$ (1)h-h-h - **4 h** - $H_20$ (1)h-h-h - **8 h** - $H_20$

(4)l-l-l - **0 h** - $H_20$ (4)l-l-l - **4 h** - $H_20$ (4)l-l-l - **8 h** - $H_20$

Figure 6.2 – Morphology and pictures of pulp aerogels as a function of gelation time.

Table 6.3 – Pulp aerogels' characteristics as a function of gelation time.

| **Pulps and coagulation bath** | **Gelation time (h)** | **Density (g cm$^{-3}$)** | **$S_{BET}$ (m$^2$ g$^{-1}$)** |
|---|---|---|---|
| **(1)h-h-h** | 0 | 0.13 | 314 |
| | 4 | 0.14 | 318 |
| **$H_2O$** | 8 | 0.14 | 281 |
| **(4)l-l-l** | 0 | 0.10 | 325 |
| | 4 | 0.10 | 326 |
| **$H_2O$** | 8 | 0.10 | 345 |

If we firstly take a look at the visual macroscopic aspect of the aerogels, we can see that when solutions were not gelled, aerogels' shape is not well defined. The sample (1)h-h-h with no gelation shows a sort of aggregated small sheets on its top. The reason is the way the samples are coagulated: the non-solvent is poured on the top of the pulp solutions. If the pouring is not done carefully enough, the coagulated cellulose will not form a 3D object.

Apart from the visual difference, aerogels' density and properties are fairly the same for all gelation times studied. Aerogels have porous structures and specific surface area coherent with what was reported in literature (Sescousse et al. (2011b); Aaltonen and Jauhiainen (2009)).

We can thus conclude that gelation time does not have any significant influence on the intrinsic aerogels' properties. Only the shape and the external aspect of aerogels can appear as less defined and smooth for aerogels made from non-gelled solutions.

### Influence of coagulation bath type

To interpret aerogels' structure and properties, first the composition of aerogels will be investigated as a function of coagulation bath. The reason is that while cellulose is not soluble in all non-solvents used, the solubility of other components, lignin and hemicellulose and also of ZnO and NaOH may vary. For example, it is expected that hemicellulose may be soluble in aqueous media. It is known that the solubility of ZnO is strongly dependent on pH (Dirkse et al. (1954); Reichle et al. (1975); Liu (1998)). As for NaOH, it is obviously soluble in $H_2O$ and 1 M HCl while the solubility in EtOH is lower (Table 6.4). If, for example, Na is not washed out during coagulation because of low solubility in cellulose's non-solvent, its weight will participate to the weight of the cellulose aerogel (as seen in Chapter 5). If looking at the composition of solution: 3%pulp-7.6%NaOH-0.82%ZnO-$H_2O$, the presence of non-washed sodium may be even higher than the weight of the pulp in the final aerogel. Steric hindrance and hydrogen bounds should also be considered as they may "hold" the components in cellulose coagulated network and, as a consequence, in aerogel.

Table 6.4 – Solubility of NaOH and ZnO in the non-solvents in g $L^{-1}$ (Liu (1998)).

| | $H_2O$ | (1 M) HCl | EtOH | 8% NaOH |
|---|---|---|---|---|
| NaOH | $\approx 1.1\ 10^3$ | $> 10^3$ | $< 139$ | - |
| ZnO | $< 10^{-6}$ | $> 10^4$ | $< 0.1$ | $\approx 4$ |

To study the influence of non-solvent on aerogels' properties, two pulps, (1)l-h-h and (3)l-h-h, were dissolved in 7.6%NaOH-0.82%ZnO-$H_2O$, gelled 4 h at 50 °C and coagulated in three different non-solvents: 1 M HCl, $H_2O$ and EtOH. When the non-solvent was HCl, it was then neutralised with $H_2O$ and all samples in $H_2O$ were washed in EtOH. Finally, samples were dried in Sc $CO_2$.

Metal content and cellulose crystallinity as a function of the non-solvent, for the aerogels studied, are presented in Table 6.5.

Table 6.5 – Pulp aerogels' metal content and crystallinity as a function of the type of coagulation bath. Measurement performed by RISE-Innventia.

| **Pulp, DP and initial composition in dry matter (%)** | **non-solvent** | **Final composition (%)** | **Loss (%)** | **Cellulose crystallinity in aerogel (%)** |
|---|---|---|---|---|
| **(1)h-h-h**<br><br>**DP: 1452**<br>**Pulp: 37.36**<br>**Na: 54.42**<br>**Zn: 8.22** | HCl | Na < 0.01<br>Zn < 0.01 | 100<br>100 | 26 |
| | $H_2O$ | Na: 0.02<br>Zn: 8.9 | 100<br>55 | 31 |
| | EtOH | Na: 4.5<br>Zn: 10 | 96<br>46 | 2 |
| **(2)h-h-l**<br><br>**DP: 1328**<br>**Pulp: 37.36**<br>**Na: 54.42**<br>**Zn: 8.22** | HCl | Na < 0.01<br>Zn: 0.18 | 100<br>99 | 31 |
| | $H_2O$ | Na: 0.02<br>Zn: 9.5 | 100<br>52 | 30 |
| | EtOH | Na: 4.6<br>Zn: 11 | 96<br>39 | 7 |

The initial composition in dry matter was calculated from the initial concentrations used for the aerogels' preparation: 3% pulp-7.6% NaOH-0.82% ZnO-$H_2O$. As only Na and Zn were taken into account in the metal content measurements, we need to extract the OH and O from the initial composition. Na represent 57.48% of the NaOH mass and Zn represent 80.36% of the ZnO mass. We thus have the following initial composition:

- 3% pulp,
- 4.37% Na ($7.6 * 0.5748 = 4.37$) and 3.23% OH,
- 0.66% Zn ($0.82 * 0.8036 = 0.66$) and 0.16% O,
- 88.58% $H_2O$.

We can now calculate the initial composition in dry matter:

- Total mass in dry matter: $3 + 4.37 + 0.66 = 8.03$.
- Pulp initial content: $3/8.03 = 37.36\%$,

- Na initial content: $4.37/8.03 = 54.42\%$,
- Zn initial content: $0.66/8.03 = 8.22\%$.

The influence of the type of non-solvent on aerogels' composition, carbohydrate and lignin content, are given in Table 6.6.

Table 6.6 – Composition of pulp aerogels as a function of coagulation bath.

| **Pulp, DP and Initial composition (%)** | **non-solvent (%)** | **Final composition (%)** | **Loss (%)** |
|---|---|---|---|
| **(1)l-h-h**<br>**DP: 755**<br>**Cellulose: 82.2**<br>**Hemicellulose: 12.8**<br>**Lignin: 5** | 1 M HCl | Cellulose: 83.5<br>Hemicellulose: 10.3<br>Lignin: 5.8 | -<br>21<br>0 |
| | $H_2O$ | Cellulose: 89<br>Hemicellulose: 7.7<br>Lignin: 3.3 | -<br>44<br>39 |
| | EtOH | Cellulose: 83.5<br>Hemicellulose: 10.6<br>Lignin: 3.4 | -<br>21<br>35 |
| **(3)l-h-h**<br>**DP: 1384**<br>**Cellulose: 88.2**<br>**Hemicellulose: 4.8**<br>**Lignin: 7** | 1 M HCl | Cellulose: 86.7<br>Hemicellulose: 4.3<br>Lignin: 8.9 | -<br>10<br>0 |
| | $H_2O$ | Cellulose: 89.7<br>Hemicellulose: 3.6<br>Lignin: 6.8 | -<br>26<br>4 |
| | EtOH | Cellulose: 89.7<br>Hemicellulose: 4.9<br>Lignin: 5.6 | -<br>0<br>21 |

The loss in hemicellulose and lignin, given in this table, after coagulation and washing, was calculated as follow:

- All calculation were made knowing the initial pulp composition in percent, with:
  - $\%_{ini}(Cell)$, the initial cellulose content,
  - $\%_{ini}(Hemi)$, the initial hemicellulose content,
  - and $\%_{ini}(Lign)$, the initial cellulose content.
- The final aerogel pulp's composition, also in percent, with:
  - $\%_{final}(Cell)$ the final cellulose content,
  - $\%_{final}(Hemi)$ the final hemicellulose content,
  - and $\%_{final}(Lign)$ the final cellulose content.
- Cellulose content, or mass, was considered constant from the initial to the final composition, it was taken as $\%_{ini}(Cell)$.
- The theoretical initial mass ($m_{ini}$) of the sample was taken as the initial pulp composition: $\%_{ini}(Cell) + \%_{ini}(Hemi) + \%_{ini}(Lign) = 100$.

Considering all the parameters listed above, we have to firstly calculate the final mass of the sample ($m_{final}$):

$$m_{final} = \frac{\%_{ini}(Cell) * m_{ini}}{\%_{final}(Cell)} \tag{6.2}$$

To deduce the final mass of hemicellulose ($m_{final}(Hemi)$) and lignin ($m_{final}(Lig)$):

$$m_{final}(Hemi) = m_{final} * \%_{final}(Hemi) \tag{6.3}$$

$$m_{final}(Lign) = m_{final} * \%_{final}(Lign) \tag{6.4}$$

To finally infer the loss in hemicellulose ($\%_{Loss}(Hemi)$) and in lignin ($\%_{Loss}(Lig)$):

$$\%_{Loss}(Hemi) = \frac{\%_{ini}(Hemi) - m_{final}(Hemi)}{\%_{ini}(Hemi)} * 100 \tag{6.5}$$

$$\%_{Loss}(Lign) = \frac{\%_{ini}(Lign) - m_{final}(Lign)}{\%_{ini}(Lign)} * 100 \tag{6.6}$$

Carbohydrate composition and metal content analyses could not be conducted on exactly the same samples because of the too large amount of matter needed for each measurement. Still, the results shown in Table 6.5 and Table 6.6 provide a lot of interesting information that have never been reported before:

- Whatever the non-solvent, hemicellulose and lignin are partly washed away during solvent exchanges. Lignin is not washed away at all when the gel is coagulated in 1 M HCl.
- Only 1 M HCl allows a complete washing out of both metals.
- In $H_2O$, Na is completely washed while Zn partly remains (up to 50%).
- EtOH seems to be the less effective non-solvent in terms of washing out the metals as the loss in Na and Zn are 96% and only $\approx$ 43%, respectively.
- Finally, both 1 M HCl and $H_2O$ lead to a certain cellulose crystallinity while coagulation in EtOH leads to practically amorphous cellulose.

It should be noted that the exchange from 1 M HCl or $H_2O$ to EtOH (which was needed to perform drying with Sc $CO_2$) seems not to affect the composition of aerogels. As an example, the washing with EtOH of gels coagulated in HCl did not wash away the remaining lignin while the latter is partly washed out when the first coagulation bath is EtOH. It goes the same for the crystallinity: once cellulose is coagulated and cellulose II of certain crystallinity is formed, it does not change to an amorphous state when washed in EtOH, while if coagulated directly in EtOH cellulose becomes amorphous. We can thus conclude that it is the first coagulation bath which determines aerogel properties. This is in agreement with what was reported in previous Chapter 5.

The morphology of pulp based aerogels coagulated in different bathes, together with the photos of the samples, is shown in Figure 6.3. All processing conditions were the same except coagulation bath. From the first glance the morphology does not depend

on the type of non-solvent. The visual aspect of all pulp aerogels is practically the same with samples coagulated in EtOH having less defined shape. A careful check at aerogel morphology shows the presence of non-dissolved Zn crystals when non-solvent is $H_2O$ or EtOH (Figure 6.4). Crystals of Zn could even be found at the surface of aerogels (Figure 6.4). It seems that Zn crystallise differently whether the gel is coagulated in $H_2O$ or in EtOH.

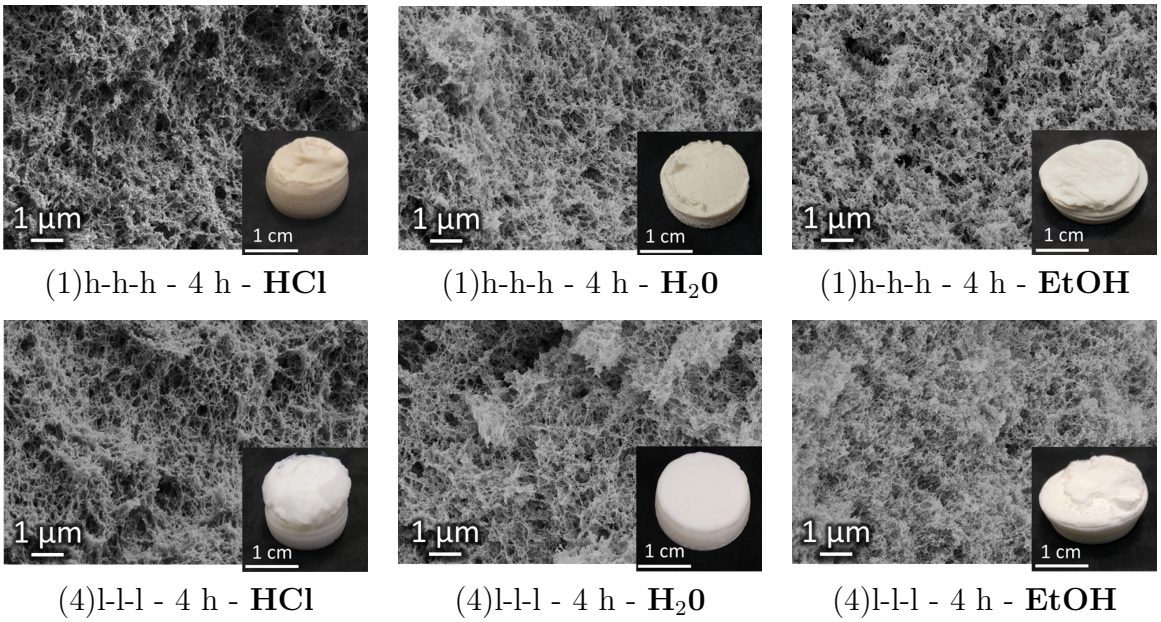


(1)h-h-h - 4 h - **HCl** (1)h-h-h - 4 h - **$H_20$** (1)h-h-h - 4 h - **EtOH**

(4)l-l-l - 4 h - **HCl** (4)l-l-l - 4 h - **$H_20$** (4)l-l-l - 4 h - **EtOH**

Figure 6.3 – Morphology and pictures of pulp aerogels made in different coagulation bathes. Gelation time was 4 h.

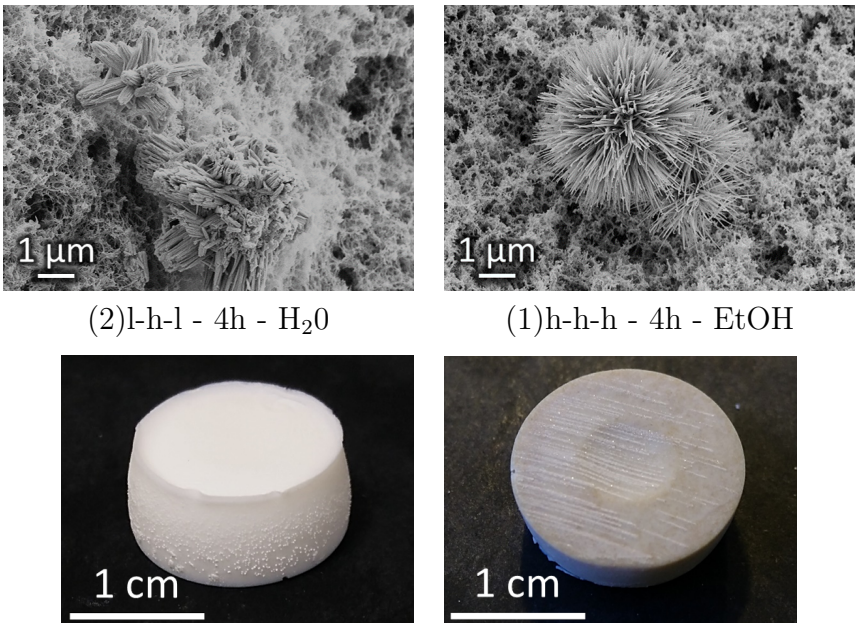


(2)l-h-l - 4h - $H_20$ (1)h-h-h - 4h - EtOH

(2)l-h-l - 4h - $H_20$ (3)l-l-h - 4h - $H_20$

Figure 6.4 – SEM pictures of crystals in the structure (top) and photos of the crystals on the surface (bottom) of aerogels when coagulated in $H_20$ or EtOH.

Knowing the composition of pulp aerogels, we can now better understand their final properties. Density and specific surface area of aerogels from three pulps, coagulated in three different non-solvents are shown in Figure 6.5. Their shrinkage and mass, are given in Figure 6.6.

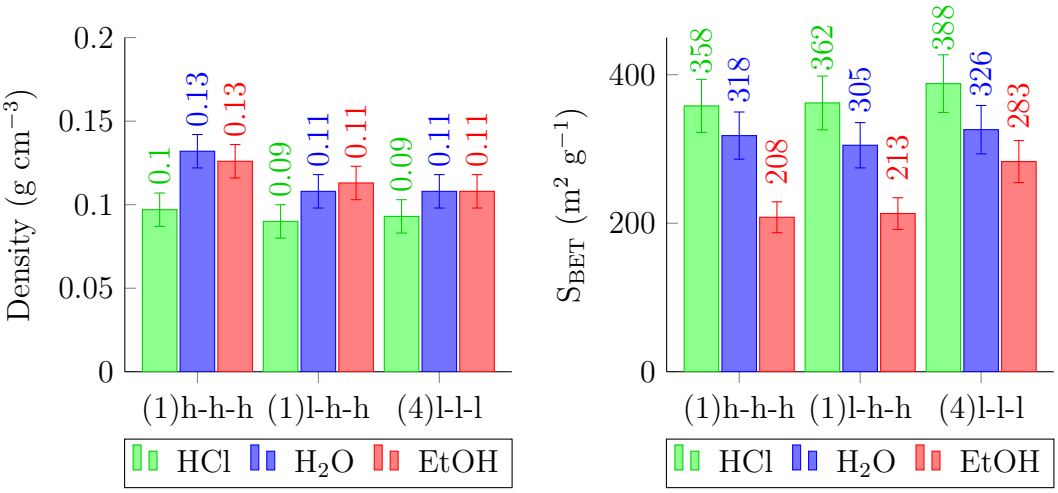


Figure 6.5 – Example of pulp aerogels' density and specific surface area as a function of coagulation bath.

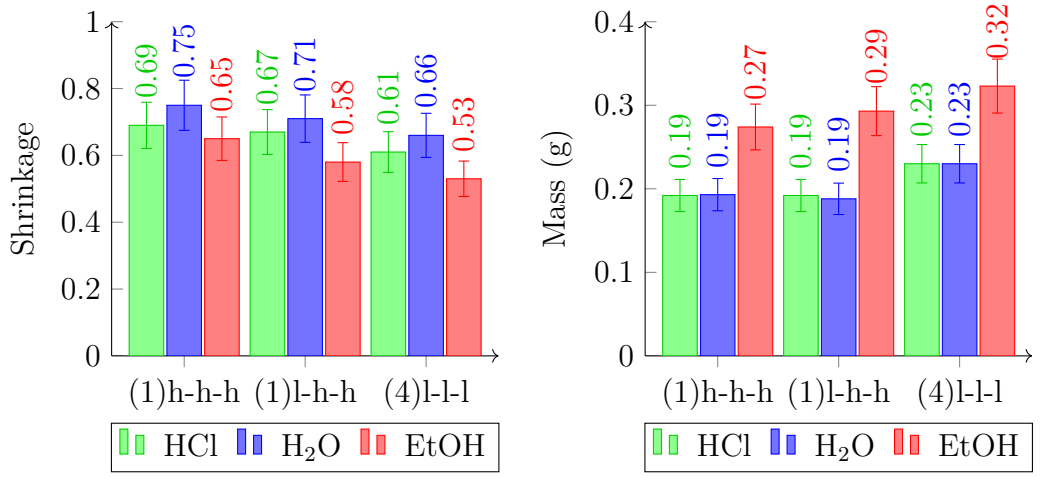


Figure 6.6 – Example of pulp aerogels' shrinkage and mass as a function of coagulation bath.

HCl coagulated aerogels show the lowest density and the highest specific surface area. When coagulated in HCl, all the metals are washed away, as the mass of aerogels in Figure 6.6 can confirm. The shrinkage is slightly lower than when aerogels are coagulated in $H_2O$ but higher than in EtOH. The low mass and shrinkage of HCl coagulated aerogels can explain the noticeably lower density compared to other coagulation bathes. In the same way aerogels coagulated in $H_2O$ show the same density as the ones coagulated in EtOH because of their lower mass but slightly higher shrinkage. To explain the higher surface area of HCl and $H_2O$ coagulated aerogels, various options are possible:

1. Hemicellulose and lignin remaining in the aerogel after coagulation in 1 M HCl (Table 6.6) contribute to specific surface area. As it will be shown in the following, hemicellulose aerogel has very low surface area and thus this option is highly improbable.

2. Metals are not contributing to surface area and thus their presence in $H_2O$- and EtOH-coagulated aerogels would decrease it. This hypothesis is in contradiction with what was suggested in Chapter 5 but if we consider that the additive rule works (case of cellulose aerogel with precipitated-inside silica from Demilecamps et al. (2014)) and taking aerogel from pulp (1)h-h-h as example, a rough estimation can be made to calculate the surface area of $H_2O$- and EtOH-coagulated aerogels:

- Surface area of HCl-coagulated aerogel is around 350 $m^2\ g^{-1}$.
- Metals in EtOH-coagulated aerogels take 15% from aerogel mass and in $H_2O$-coagulated 10%.
- Specific surface area of HCl-coagulated aerogel should thus decrease by 50 $m^2\ g^{-1}$ to be compared with EtOH-coagulated aerogel (i.e. 300 $m^2\ g^{-1}$) and by around 35 $m^2\ g^{-1}$ to be compared with $H_2O$-coagulated aerogel (i.e. 310 $m^2\ g^{-1}$).

This estimation shows that this hypothesis works to explain specific surface area decrease in $H_2O$-coagulated aerogel as compared to HCl-coagulated ones, but does not work for EtOH-coagulated aerogels. We have seen that crystals were different between $H_2O$ and EtOH coagulated aerogels, it may be possible that their influence on properties is not the same either. The influence of ZnO when coagulated in EtOH could also be explained with crystallinity. The very different crystallinities of cellulose in HCl vs EtOH-coagulated aerogels should also be taken into account.

3. Zn and Na crystals act as spacers decreasing close packing of cellulose chains. This means that aerogels made from pulps coagulated in EtOH should have the lowest surface area as far as they are amorphous, while cellulose in aerogels from $H_2O$- and HCl-coagulated routes has similar crystallinity (around 30%). The influence of crystallinity on specific surface area of bio-aerogels had never been studied, and we do not have any proof of the validity of this assumption. More systematic studies would be very useful to confirm or not this idea.

In conclusion, the choice of coagulation bath seems to be primordial for the resulting aerogels composition and properties. With HCl chosen as a non-solvent:

- All the metals are washed away.
- The hemicellulose is partly redissolved and thus washed out.
- The lignin stays in aerogels.
- The density is low and $S_{BET}$ is high.
- $\approx$ 30% crystallinity is expected.

With EtOH as coagulation bath:

- Most of the Zn stays in the aerogel.
- A small part of the hemicellulose and lignin is washed away.
- The aerogels' density is still low and $S_{BET}$ high but it is the "worst" among the pulp aerogels prepared in this study.
- Amorphous structure is expected.

Finally, with $H_2O$:

- Half of the initial quantity of the Zn stays in the aerogel.
- A small part of the hemicellulose and lignin is washed away.
- The aerogels' density is similar to the one of EtOH coagulated aerogels but with a slightly higher $S_{BET}$.
- $\approx$ 30% crystallinity expected.

### Influence of pulp composition

Interestingly, the hemicellulose and lignin contents had much less influence on aerogels' properties compared to the type of coagulation bath, as shown in Figure 6.7.

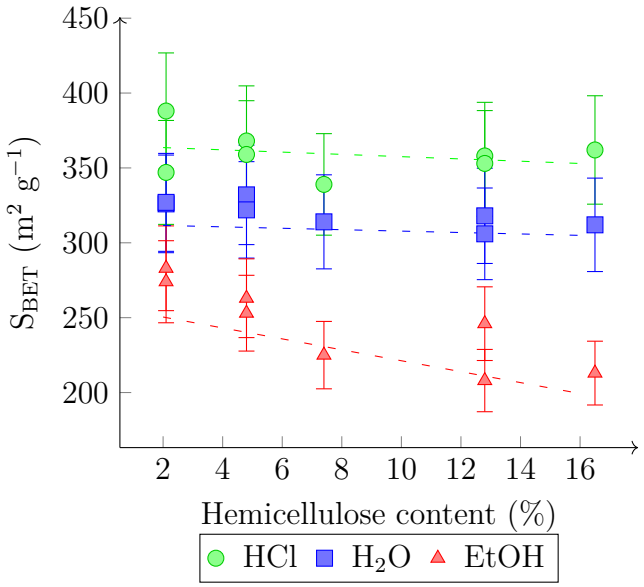


Figure 6.7 – Aerogels' $S_{BET}$ as a function of the initial hemicellulose contents. Dashed lines are linear trend curves.

It seems that the more hemicellulose in the pulp, the lower is specific surface area of the resulting aerogel. This phenomenon is not significant with HCl and $H_2O$ coagulation bathes, but the decrease in $S_{BET}$ is noticeable with EtOH. The reason why specific surface area of aerogels coagulated in EtOH is more sensitive to hemicellulose as compared to its $H_2O$- and HCl- coagulated counterparts is not clear, especially in the view that the loss in hemicellulose was the same when coagulated in HCl and in EtOH and that the metals, and more particularly Na, were not well washed away with EtOH coagulation.

To further understand the behaviour of hemicellulose in the pulps, aerogels were made with hemicellulose and MCC. Our goal was to firstly produce pure hemicellulose aerogels and then hybrid hemicellulose-cellulose aerogels to compare their specific surface area and morphology with each other and with the ones of pulp based aerogels. We have tried to dissolve different concentrations of pure hemicellulose in 8% NaOH, as we wanted to reproduce as much as possible the dissolution conditions of pulps. However, at low hemicellulose concentrations (10%), we could not get any stable network through coagulation: the hemicellulose dispersed in the non-solvent. This is because of the low molecular weight of hemicellulose which is not making "enough" percolated network. And at higher concentration (30%), the hemicellulose dissolution was not complete and the coagulation led to a precipitate rather than a network formation.

We thus decided to dissolve hemicellulose in ionic liquid (IL): [DBNH][Pr]. For low concentrations, the same result as with NaOH was obtained: dispersion of the hemicellulose in the non-solvent instead of formation of a 3D object. At higher concentration, however, the dissolution in IL was complete and a very fragile network was obtained through coagulation in EtOH.

Going further, we dissolved 10% hemicellulose and 3% MCC together in [DBHN][Pr] and made aerogel via coagulation in EtOH. This time, because of the addition of cellulose, a more "resistant" network was obtained from EtOH coagulation. Aerogel based on 3% MCC was also prepared in the same way.

The results are shown in Figure 6.8 and Table 6.7. These first results help us to understand the basic behaviour of hemicellulose in pulp aerogels.

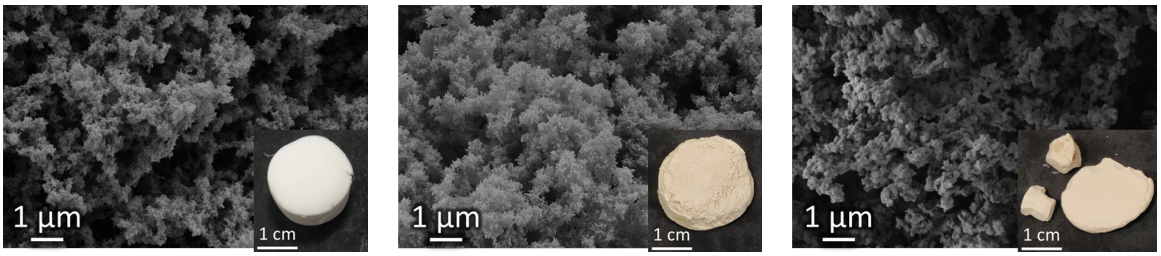


3% MCC in [DBNH][Pr] | 10% hemicellulose 3% MCC in [DBNH][Pr] | 30% hemicellulose in [DBNH][Pr]

Figure 6.8 – Morphology and pictures of 3% cellulose, 10% hemicellulose-3% cellulose and 30% hemicellulose aerogels when dissolved in [DBNH][Pr] and coagulated in EtOH.

Table 6.7 – Specific surface area ($S_{BET}$) of hemicellulose, cellulose and hemicellulose-cellulose hybrid aerogels.

| **Polymer concentration in solution** | 3% cellulose | 3% cellulose 10% hemicellulose | 30% hemicellulose |
|---|---|---|---|
| **$S_{BET}$** | 273 ± 27 | 253 ± 23 | 20 ± 2 |

Pure hemicellulose could only form a network that withstands itself at high concentration (at least 30%). This network was very fragile (the density could not be

measured) and showed a very low specific surface area (20 $m^2$ $g^{-1}$). When mixing hemicellulose with cellulose, a network could be obtained at much lower hemicellulose concentration (10%), thanks to the "supporting" cellulose. Even if the hemicellulose-cellulose hybrid aerogels were really more fragile than the pure cellulose ones, they still had a relatively high specific surface area (253 $m^2$ $g^{-1}$). The difference in specific surface area between cellulose and hybrid aerogels was surprisingly lower that what we could have expected knowing the $S_{BET}$ of pure hemicellulose. We can thus assume that, if hemicellulose concentration is high enough, it can create bonds with cellulose (presumably hydrogen bonds), helping the former to create a viable network and contributing, to a certain extent, to the specific surface area.

The hemicellulose concentrations in the pulp aerogels were much lower than the one we have tested with hybrids. For example, for the pulp with the highest hemicellulose content (16.5%) the concentrations in solution were 2.5% of cellulose and 0.5% of hemicellulose, while it was respectively, 3% and 10% for the hybrids. The decrease in $S_{BET}$, due to the presence of hemicellulose, is then really more important for the pulps than for the hybrids prepared. Several speculations may explain this difference, however, no experimental proof is available. Obviously, "artificial" mixing cellulose and hemicellulose vs their "natural" mix in the pulp is one assumption. Another is the solvent. We have seen earlier that when dissolved in NaOH, the pure hemicellulose did not form any network upon coagulation while it was possible to obtain aerogel when hemicellulose was dissolved in ionic liquid. As suggested previously, in pulp aerogels, the hemicellulose concentration may be too low to form a network thus leading to its simple precipitation. The more hemicellulose in the pulps, the lower the $S_{BET}$.

Despite the non-dissolution of the lignin and its certain concentration in the pulps, it did not have any influence on the resulting aerogels properties, as Figure 6.9 can attest.

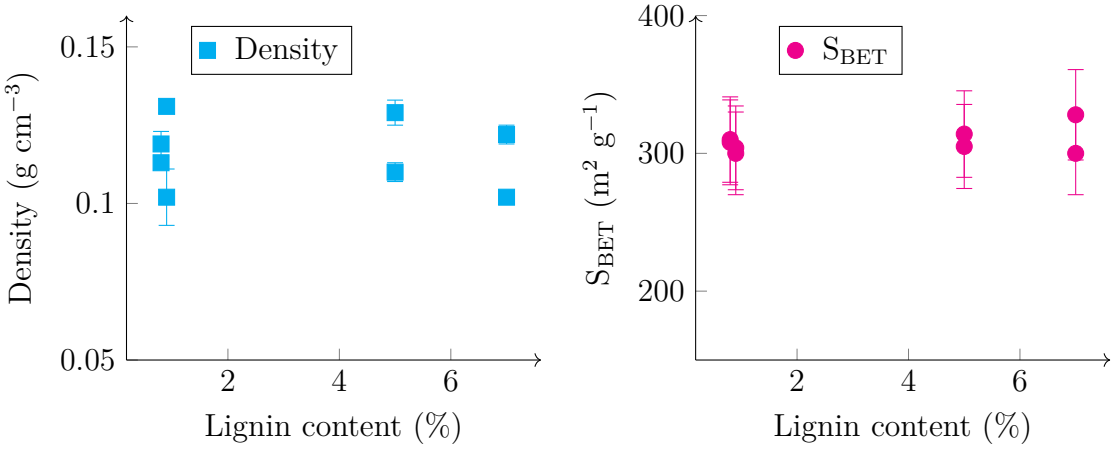


Figure 6.9 – Aerogels' density and $S_{BET}$ when coagulated in $H_2O$ as a function of the initial lignin content.

Yet, what is interesting to see in this same figure is the influence of cellulose DP

on aerogels properties. For each lignin content, one value of density is higher than the other. This corresponds to the difference in DP: pulps with higher DP will lead to denser aerogels as shown in Figure 6.10.

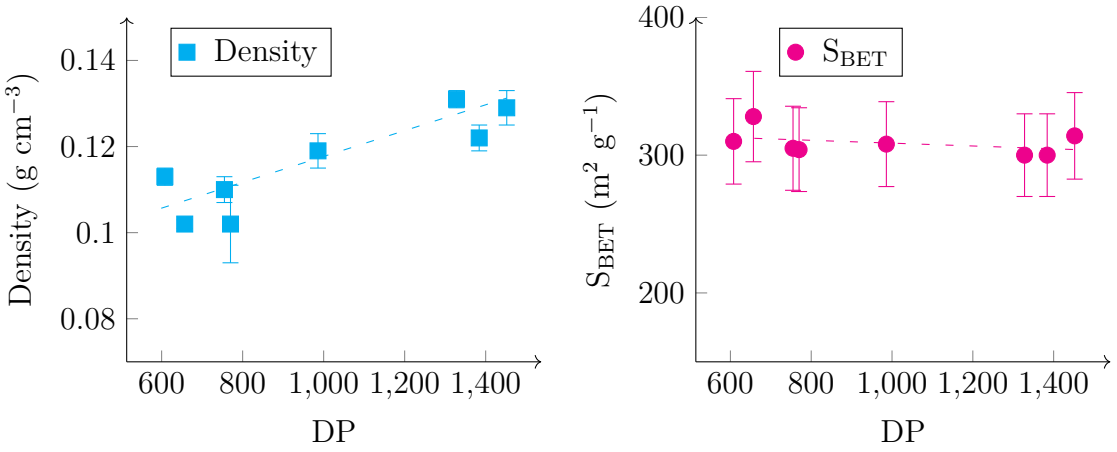


Figure 6.10 – Aerogels' density and $S_{BET}$ when coagulated in $H_2O$ as a function of DP. Dashed lines are trend curves.

Figure 6.10 shows a significant increase of density as a function of DP. The influence on specific surface area is much less significant and can be considered as null. However, pulps of different DP have different compositions which has to be taken into account. To exclude the influence of the composition, pulps have to be compared to each other, type by type. Figure 6.11 makes this comparison for aerogels' density. It really emphasises the fact that with a higher DP, aerogels are more dense.

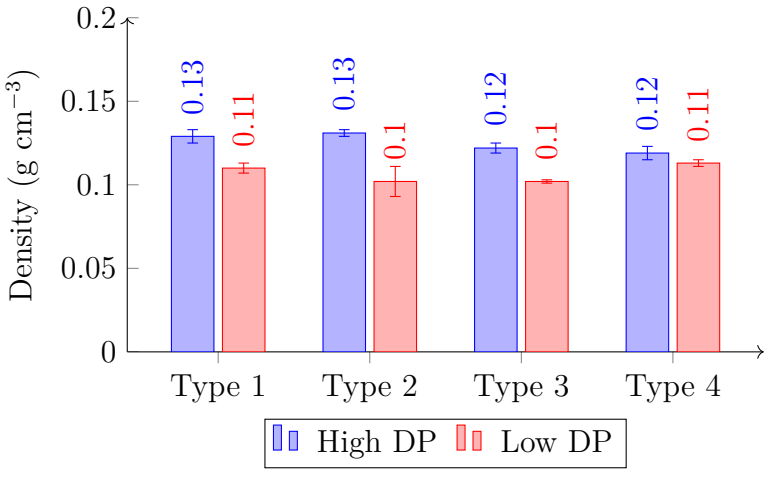


Figure 6.11 – Pulp aerogels' density as a function of type.

This observation makes sense. Indeed, as seen in Section 6.2.1 on page 215 on dissolution efficiency of pulps, a higher DP leads to more non-dissolved cellulose. The cellulose fibres will thus be a part of the aerogel network without contributing to its porous structure. The presence of non-dissolved fibres makes the real concentration of dissolved cellulose lower than 3%. Lower concentration of the dissolved matter leads

to higher shrinkage, as it was demonstrated for aerogels made from MCC and pulps (Innerlohinger et al. (2006); Buchtová and Budtova (2016); Schestakow et al. (2016)), and the same was also obtained here. A higher shrinkage induces a higher density (same mass but in a smaller volume). The shrinkage of pulp aerogels is shown in Figure 6.12 and is coherent with the density reported earlier.

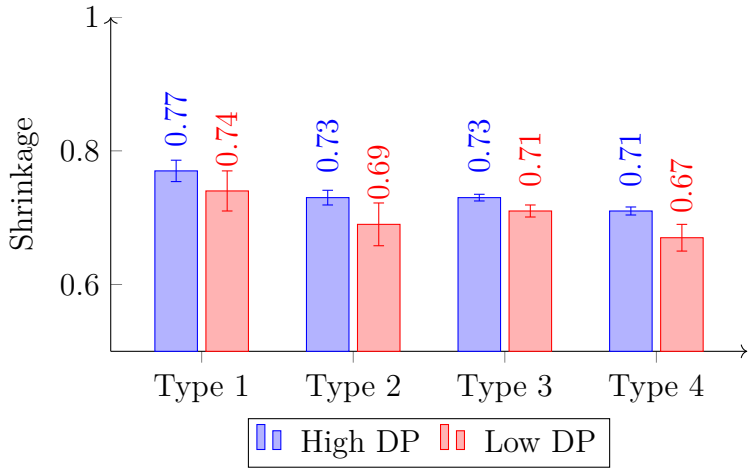


Figure 6.12 – Shrinkage of aerogels as a function of pulp's type.

All these observation were done on $H_2O$ coagulated aerogels, but the same tendency, but less significant, was observed for both HCl and EtOH coagulation bathes (see Figure 6.13).

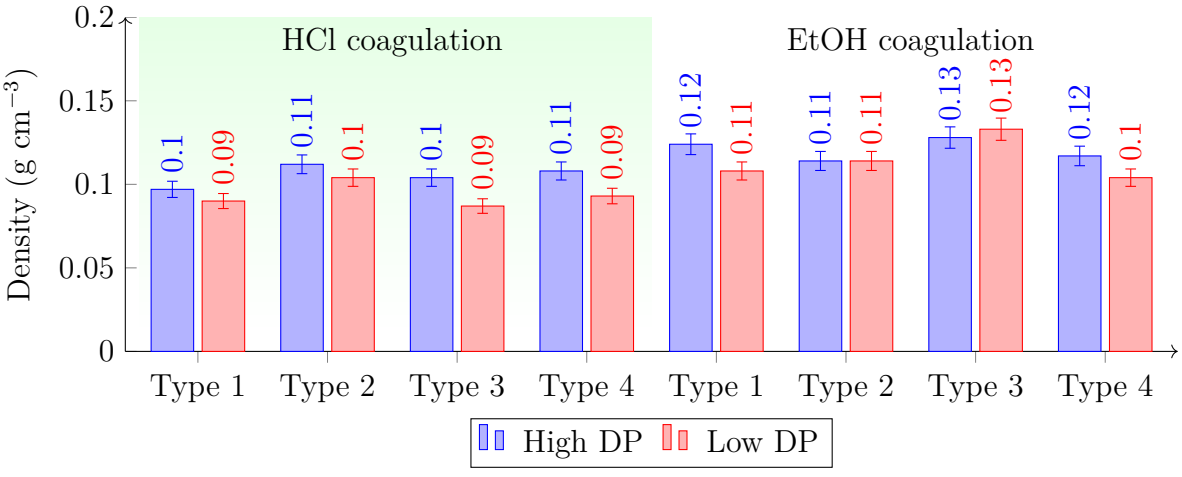


Figure 6.13 – Pulp aerogels' density as a function of DP, by type of pulp for HCl and EtOH non-solvents.

It is interesting to note that the impact of DP on specific surface area seems not as significant as on the density (Figure 6.9). In this case, we should expect lower $S_{BET}$ for higher DP because the non-dissolved cellulose will not contribute to the $S_{BET}$. More trials and replicates would be needed to prove this hypothesis to be true.

### 6.2.3 Prospects: application and variation of shaping and drying

This chapter showed so far the feasibility of making pulp based aerogels with the properties similar to those made from MCC. The next question now is if other findings obtained on MCC based aerogels are applicable to pulp based ones. Three questions were thus investigated:

- Would it be possible to produce pulp aerogels shaped as beads, as it was done with the JetCutter in Chapter 3?
- Does the vacuum drying, used for making low density and high specific surface area MCC based xerogels (Chapter 5), result in pulp based xerogels with similar properties?
- In the view of the applications considered in Nanohybrids project, what are water vapour adsorption properties of pulp based aerogels and xerogels?

#### Pulp based aerogels in shape of beads

As it was already explained in Chapter 3, ionic liquid ([DBNH][Pr]) and MCC were chosen to produce cellulose aerogel beads with the JetCutter technology for two main reasons:

- IL are powerful solvents of cellulose, the solutions are thus homogeneous.
- The selected cellulose-[DBNH][Pr] solutions fitted the required processing parameter range of the JetCutter.

The same restrictions on JetCutter processing window will have to be applied to pulp solutions to successfully produce beads. Hence, the dissolution of pulps will need to be as efficient as possible to ensure homogeneous solutions (the presence of non-dissolved fibres does not allow making beads with the JetCutter). The pulps with the highest DP were thus excluded from bead production. Then, as the behaviour of lignin is not completely understood during pulp dissolution in our NaOH based solvent, only low lignin content pulps were selected. Two pulps were consequently tested: (2)l-h-l and (4)l-l-l.

The visco-elastic behaviour of solutions is also an important factor to match the JetCutter processing window. Rheology of cellulose in NaOH based solvents has been widely studied, hence we decided to base our analysis on the study conducted in Chapter 4 and Chapter 5 and the literature Liu et al. (2011). The gelation of cellulose-NaOH solutions is the most problematic issue. However, this matter can also be turned into an adjustable parameter in terms of viscosity. Indeed, we can use more or less "gelled" solutions depending on viscosity requirements of the JetCutter. The viscosities of MCC dissolved in 8% NaOH with addition of 0.7% ZnO and 1% ZnO were around 170 mPa s and 130 mPa s, respectively, at 20 °C, right after dissolution. It was around 290 mPa

s and 500 mPa s at the gel point. The DP of the pulps chosen is higher than the one of MCC, so we can expect higher viscosity in the same conditions. We have seen in Chapter 3 that the viscosity limit to produce beads was around 5 Pa s for 3% MCC dissolved in [DNNH][Pr]. Even if the DP of the pulps is higher, we should not exceed this value. A complete rheological study is needed to select the suitable parameters of the JetCutter (nozzle size, number of wire of the cutting tool, jet speed...) towards our solutions. However, because of the lack of time, we decided to apply the trials and error method.

Different parameters of the JetCutter (nozzle size, jet speed, size of the wires of the cutting tool...) were tested to produce beads from the "non-gelled" pulp solutions. Yet, we could not produce beads from "fresh" solutions because of their too low viscosity; and surface tension should also be adjusted. No matter the coagulation bath used, the formed droplets crashed on the surface of the coagulation bath leading to dispersed cellulose instead of well shaped beads. We thus decided to let the solutions gel, "just enough", to increase their viscosity and surface tension. A suitable viscosity was reached after solution ageing for around 15 h at ambient temperature and 2 h at 50 °C.

The three coagulation bathes, the same as used for the monoliths, were tested: 1 M HCl, $H_2O$ and EtOH. We could not obtain any intact particles with the $H_2O$ coagulation bath. It is maybe due to "too good" $H_2O$ affinity with the cellulose. Particles were produced using the two other coagulation bathes, 1 M HCl and EtOH, with both pulps, (2)l-h-l and (4)l-l-l.

Pictures of the produced aerogels beads and their microstructure are shown in Figure 6.14. Note that their specific surface area ranged from 300 to 350 $m^2\ g^{-1}$. Their size distribution is given in Figure 6.15 on the next page.

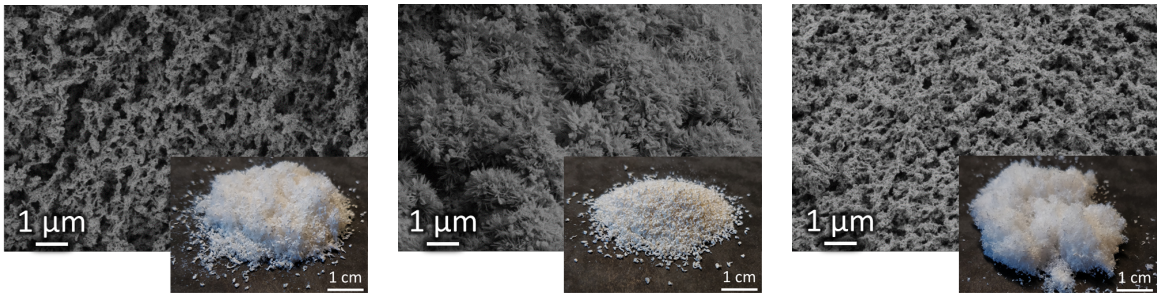


(2)l-h-l - HCl (2)l-h-l - EtOH (4)l-l-l - HCl

Figure 6.14 – Morphology and pictures of pulp aerogel beads.

When looking at the pictures of the beads in Figure 6.14 we can see that whatever the pulp or the non-solvent used, they are neither perfectly round nor mono-dispersed. The mean arithmetic value of the diameter is hence a rough estimation as it was calculated from the area of the beads considering them perfectly round. The large standard deviation is in accordance with this estimation.

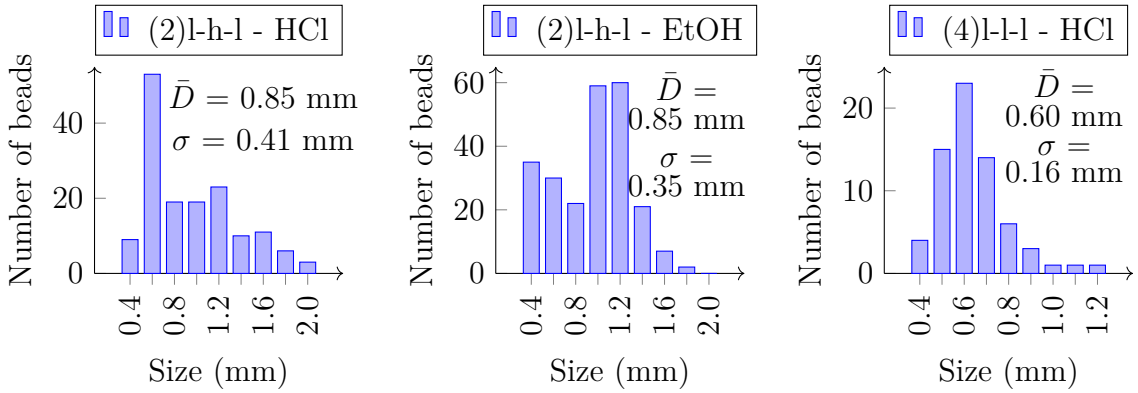


Figure 6.15 – Size distribution of pulp aerogel beads.

Nonetheless, it seems that with EtOH coagulation bath, the shape of the beads is better defined than with HCl. The morphology is preserved for both pulps and both coagulation bathes and, as it was observed for the monoliths, crystals of Zn could be found in the microstructure when coagulated in EtOH. The specific surface area was also kept high as it was up to 350 $m^2$ $g^{-1}$. We can thus conclude that, with the JetCutter processing, the intrinsic properties of pulp based aerogel beads were preserved as compared to their monolithic counterparts.

Before concluding on the influence of the pulps on beads' size, it is important to note that the parameters of the JetCutter were adapted to each pulp to obtain intact and more or less spherical beads. Especially, the nozzle used for (2)l-h-l had a diameter of 800 µm whereas for (4)l-l-l the diameter was only 350 µm. Hence, the size of beads mostly depends on the parameters of the JetCutter rather than on the pulps or the coagulation bath.

Even if these first results are very promising, a deeper study is needed to produce more regular beads with controlled and various sizes, and with a narrower size distribution. We could even consider extending the parameters such as the type of pulp or the coagulation bathes once all the process is well understood. As already said in Chapter 3, this process is very promising for the mass production of aerogel beads. This study opens new prospects in this field.

### Vacuum drying

Since the solvent to dissolve the pulps was the same as the one used to produce the porous cellulose xerogels presented in Chapter 5, we decided to try the same vacuum drying method on pulp samples. The work was performed on monolithic samples and three coagulation bathes were tested: HCl, $H_2O$ and EtOH. Pictures of (1)h-h-h aerogels and xerogels are given in Figure 6.16.

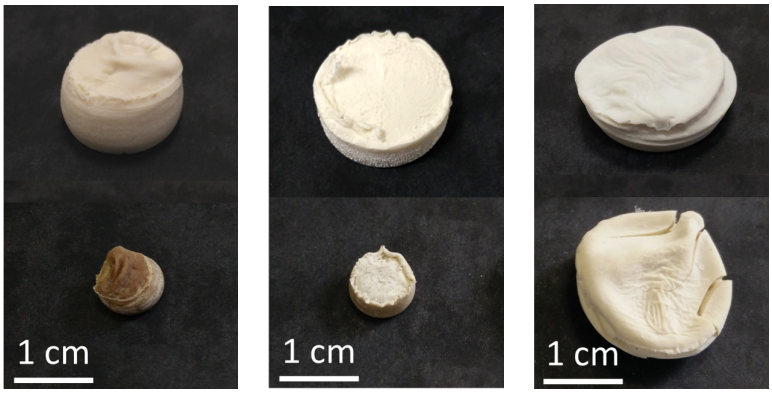


Figure 6.16 – Pictures of pulp (1)h-h-h aerogels (top) and xerogels (bottom) as a function of coagulation bath.

As for the xerogels from MCC, when coagulated in HCl and $H_2O$ the samples based on pulps had a very important shrinkage and their density ranged from 0.7 to 1.1 g cm$^{-3}$. When using EtOH as non-solvent, the results were very promising. EtOH coagulated pulp xerogels showed a low shrinkage and densities ranging from 0.10 to 0.26 g cm$^{-3}$ as shown in Figure 6.17

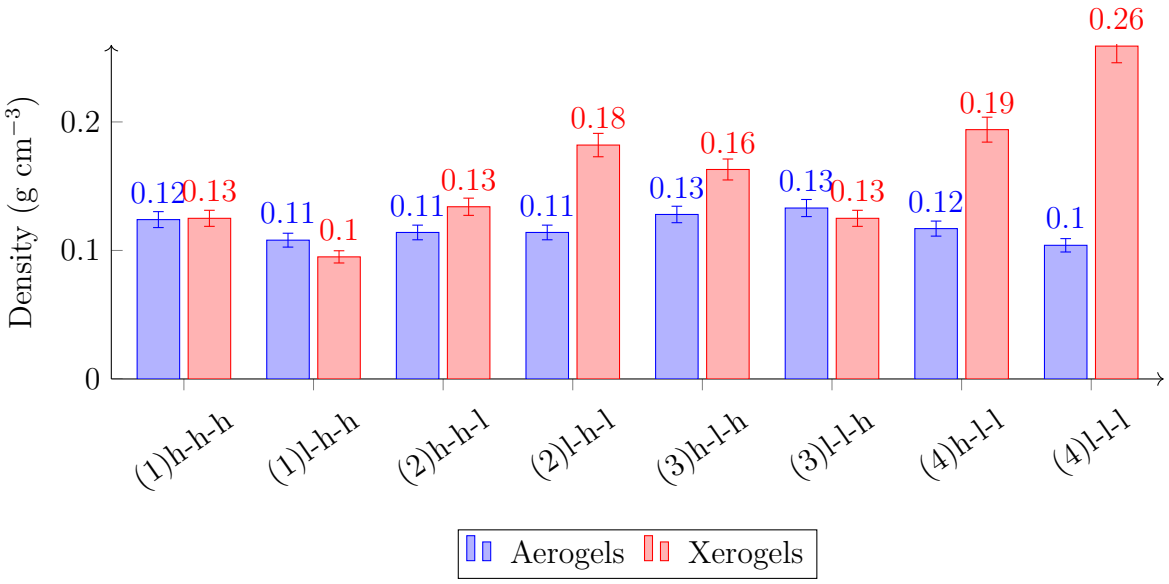


Figure 6.17 – Pulp aerogels' and xerogels' density for EtOH coagulation.

Unfortunately, we did not have enough time to measure the specific surface area nor to analyse the morphology of these xerogels. But their external aspect and their low density are very good indicators to confirm the preparation of porous pulp xerogels. Indeed, when comparing the density of pulp aerogels with the one of their xerogel counterparts, the difference can be so little that we can assume that the process to prepare porous xerogels is reproducible on pulps.

### Moisture sorption

Multiple applications are possible for aerogels. Here we chose to focus on soption capacity of water vapours during several cycles. All moisture sorption experiments were made by RISE-Innventia and we are really grateful for their time and help. Curves for (1)h-h-h and (2)h-h-l pulp aerogels and xerogels coagulated in HCl, $H_2O$ and EtOH are presented in Figure 6.18.

It can firstly be observed from this figure that the type of pulp does not influence moisture sorption behaviour throughout the cycles. Only the coagulation bath and the drying method seem to have an impact, but it is not very significant.

For a relative humidity set at 80%, $H_2O$ coagulated aerogels and EtOH coagulated xerogels show very reversible cycles of sorption and desorption. For HCl coagulated xerogels it evolves through the cycles. In the latter case the first sorption cycle reaches the highest mass uptake of around 12% and then it slowly decreases throughout the cycles to get to 9.5% for the third one. It can also be seen that desorption is far from being perfect, the mass uptake stays at 1% after desorption, for the best one. Very high shrinkage of xerogels coagulated in HCl and hornification phenomenon (pores non-reopening) may be the reason of low moisture adsorption. Xerogels coagulated in EtOH show the highest increase in mass, up to 18.5% and it stays relatively stable along the cycles.

It looks like the behaviour in moisture sorption depends mostly on the structure of the tested network. Overall, a maximum increase in mass of 18.5% is not that outstanding knowing that certain materials such as Zeolites can go up to 38% (Tatlier et al. (2018)). In addition, the small decrease in adsorption throughout the cycles is a sign of deterioration of the aerogels and xerogels structure. For this study, only three cycles were conducted but we can expect that the adsorption capacity will keep decreasing with more cycles.

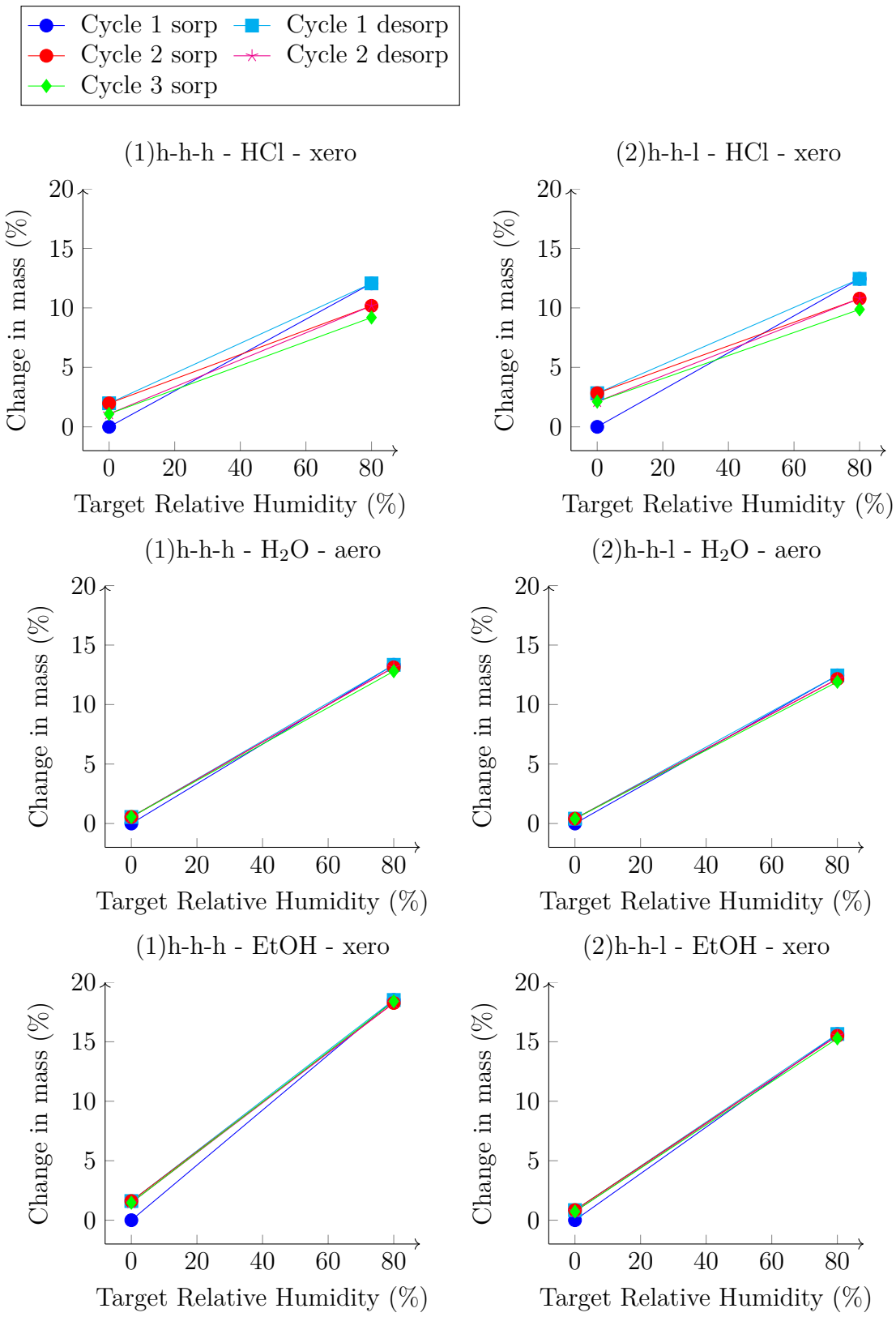


Figure 6.18 – (1)h-h-h (left) and (2)h-h-l (right) aerogels' and xerogels' sorption cycles.

# Conclusions

In this chapter we have proved that the production of aerogels was possible from pulp with different characteristics when they are dissolved in NaOH-ZnO-$H_2O$ solvent. This work would not have been possible without the contribution of RISE-Innventia in preparing the pulps, analysing their composition and the one of aerogels, and testing moisture sorption of aerogels and xerogels.

As expected, pulps were not completely dissolved in NaOH-ZnO-$H_2O$ solvent. The dissolution efficiency was mainly dependent on the degree of polymerisation of cellulose and on the lignin content. Pulps with a low DP and a low lignin content can be efficiently dissolved in the NaOH-$H_2O$ based solvent.

Then, the influence of several processing parameters on the resulting aerogels' properties were analysed. Gelation time were varied but, in the range of temperatures tested, no significant influence on aerogels' properties was observed. The type of non-solvent was varied and it appeared that it has a subsequent influence on aerogels' properties. In the same way as it was observed for xerogels in the preceding chapter, metals are not completely washed away when EtOH or $H_2O$ are used as non-solvent while they are removed from cellulose matrix when coagulating in HCl. Also, crystallinity of EtOH coagulated pulp aerogels is very low as compared to other non-solvents. Coagulation bath also has an influence on the final pulp aerogels' composition as hemicellulose and lignin can be more or less washed away. Finally, the influence of initial pulp's composition was studied on aerogels' properties and it appeared that hemicellulose and cellulose DP were the most influencing parameters. With increasing cellulose DP, density of the aerogels increased and with the increase of hemicellulose content, specific surface area slightly decreased.

A small study to understand the effect of hemicellulose on aerogels' properties was conducted. Hemicellulose, kindly provided by RISE-Innventia, was dissolved in different concentrations in [DBNH][Pr], with or without addition of cellulose and coagulated in EtOH. We successfully obtained both pure hemicellulose aerogels, with very low specific surface area, and hybrid cellulose-hemicellulose aerogels, with $S_{BET}$ slightly lower than the one of pure cellulose aerogels from the same preparation conditions.

Finally, this study on pulp based aerogels was extended to the preparation of pulp aerogel beads and pulp xerogels. Their properties toward moisture sorption was also analysed. After selecting of the lowest cellulose DP and lowest lignin content pulps, aerogel beads were prepared with the JetCutter technology. Beads' diameter was of several hundreds of micrometers and their specific surface area ranged from 300 $m^2\ g^{-1}$ to 350 $m^2\ g^{-1}$. Ultra-lightweight xerogels were successfully prepared, following the same pathway as given in Chapter 5, and density as low as 0.1 g $cm^{-3}$ was reached. Finally, moisture sorption capacity of xerogels and aerogels was tested under cycles and it appeared not that high with a maximum increase in mass of 18.5%.

# General conclusions and perspectives

Our work had both scientific and industrial questions and challenges to tackle. The aims were to prepare and characterise cellulose based aerogels and to shape them as beads of various controlled sizes. To fulfil these tasks, we have used:

- different solvents: NaOH-$H_2O$ based and ionic liquids,
- cellulose from different sources: microcrystalline cellulose and pulps with various characteristics,
- and three shaping techniques: dropping, JetCutter and emulsification.

The selected solvents were used because of their wide range of properties; NaOH based solvents are cheap and bio-compatible, while ionic liquids can dissolve higher concentration of cellulose of higher degree of polymerisation. The pulps were used in order to make raw material cheaper than classically used microcrystalline cellulose. Only few articles describe the preparation and properties of aerogels from pulps, with no systematic study on the influence of pulp composition (cellulose, lignin, hemicellulose) on aerogels' properties. Three shaping techniques were used in order to first adjust processing parameters with dropping, and then to make cellulose beads of different sizes, from few microns to hundreds of micrometers.

The aerogels production route employed is as follows: dissolution - shaping - gelation (if applicable) - coagulation - solvent exchange (if applicable) - drying (mainly with supercritical $CO_2$). Our research also included the preparation of porous materials with a less expensive drying than supercritical drying, low vacuum drying (the material obtained is called xerogel).

This work was performed in the frame of the European project "NanoHybrids" and we would like to thank all partners for the fruitful collaboration.

Four chapters of this manuscript present the results. The chapter 3, *Rheology of cellulose-[DBNH][Pr] solutions and shaping into aerogel beads*, and 4, *Micrometric cellulose aerogel beads production from adapted emulsion technique*, were detailing the production of aerogels shaped as beads and the chapter 5, *Lightweight and mesoporous cellulose xerogels*, and 6, *Pulp based aerogels*, were reporting the preparation of new types of aerogels and aerogel-like cellulose based materials.

In Chapter 3, *Rheology of cellulose-[DBNH][Pr] solutions and shaping into aerogel beads*, we exploited the recently developed ionic liquid, 1,5-Diazabicyclo[4.3.0]non-5-enium propionate ([DBNH][Pr]), to produce aerogel beads with the JetCutter technology. For this purpose, we performed an extended investigation of the rheological properties of cellulose-[DBNH][Pr] solutions. We studied the flow and viscoelastic properties of these solutions as a function of polymer concentration and solution temperature. In the range of conditions studied all solutions showed Newtonian plateau with a beginning of shear thinning regime for higher cellulose concentrations and lower temperatures. Viscoelastic properties of cellulose-[DBNH][Pr] solutions can be described by classical approaches used in polymer physics. Thermodynamic quality of [DBNH][Pr] appeared higher than the one of the well-known 1-ethyl-3-methyl imidazolium acetate ([Emim][OAc]) at the same temperature leading to more swollen polymer coils and lower overlap concentration. These results allowed a selection of solutions viscosity in order to fit into the processing window of the JetCutter.

Aerogel beads were successfully prepared from 2% and 3% of cellulose-[DBNH][Pr] solutions using water, ethanol and isopropanol as coagulation baths and by drying under supercritical $CO_2$ conditions. JetCutter settings were adapted as a function of cellulose viscosity via cellulose concentration and the latter was the major factor controlling the size of the beads. Beads from 2% solution had diameters ranging from 0.5 to 0.7 mm and the ones from 3% solution had mean diameter around 1.8 mm. The properties of beads were similar to their monolithic counterparts, except for monoliths coagulated in $H_2O$ which showed a peculiar globular morphology. More studies are needed to fully understand this phenomenon. The density of the beads was $0.04 - 0.07$ g $cm^{-3}$ and specific surface area ranged from 240 to 340 $m^2$ $g^{-1}$.

The Chapter 4, *Micrometric cellulose aerogel beads production from adapted emulsion technique*, also dealt with the production of cellulose aerogels shaped as beads. However, in this chapter the targeted diameter was of few microns; this size cannot be reached with the JetCutter technique. These small sizes are particularly required for medical, food or cosmetic applications and the use of ionic liquids is not yet recommended in case of the presence of solvent traces. Hence, in our study, we have used NaOH-water based solvents and have implemented a new emulsification technique for the production of cellulose aerogel particles.

Preliminary studies were conducted to highlight different requirements for the cellulose solutions to be emulsifiable. With rheological measurements and rheo-optical observations, it was demonstrated that the use of additives is required to efficiently dissolve cellulose and delay solutions' gelation. Viscosity ratio and surface tension were theoretically promising for a good emulsification of the cellulose solutions in paraffin oil.

The development and implementation of the emulsification method was detailed. Three critical issues appeared during particle production: saponification of the surfac-

tant (due to the high pH of cellulose solutions), impossibility to obtain well shaped "wet" particles when adding the non-solvent directly in the emulsion, and "interface jamming" during phase separation. To overcome these problems, we have developed a new emulsification technique based on mixing of two separate emulsions. One emulsion was containing cellulose solution in oil, without surfactant to avoid saponification, and the other emulsion was made of non-solvent in oil, with surfactant to have better control on droplets' size. These two emulsions were then mixed together to trigger coagulation of the droplets of cellulose solution. This method overcame the problems of saponification and direct coagulation. Regarding interface jamming, two approaches were used: adding a fluid miscible with both aqueous phase and oil (for example, ethanol) just before phase separation, and changing the coagulation mechanism by using a non-solvent partly soluble in oil. The two approaches were successful with particularly good results for the change in coagulation mechanism.

Different parameters of emulsification were varied to determine their influence on the properties of aerogel particles. The mechanism of coagulation, by coalescence or by diffusion of the non-solvent, was evaluated as the most important to obtain well-shaped cellulose aerogel particles. When only coalescence was involved, in the case of HCl as non-solvent, aerogel particles were agglomerated with mean diameter of 5.4 µm and specific surface area around 300 $m^2\ g^{-1}$. When diffusion coagulation was performed, in the case of acetic acid as non-solvent, aerogel particles were individual, with well-defined spherical shape and with a mean diameter of around 20 µm and $S_{BET}$ of around 350 $m^2\ g^{-1}$.

Starting from Chapter 5, other problems were treated. In this chapter, *Lightweight and mesoporous cellulose xerogels*, we have developed ultra-lightweight and high specific surface area cellulose xerogels. It was demonstrated that by using selected preparation parameters, we can obviate the expensive $CO_2$ supercritical drying and obtain materials with properties equivalent to aerogels. Density of the xerogels was between 0.11 g $cm^{-3}$ and 0.24 g $cm^{-3}$ and specific surface area ranged from 180 $m^2\ g^{-1}$ to 275 $m^2\ g^{-1}$. These results are now under patenting.

A complete study was conducted in order to find the best preparation parameters and to understand why such outstanding properties were obtained from simple vacuum dried coagulated cellulose. NaOH-water was used as solvent for microcrystalline cellulose, with different concentrations in additive, here ZnO. Different ageing times and types of the first non-solvent were studied as well as their influence on cellulose crystallinity and on the resulting composition of xerogels. It was highlighted that ultra-lightweight and high specific area xerogels were obtained only when ethanol was used as the first non-solvent for coagulation. To explain this phenomenon two hypothesis were made. It was observed that when cellulose-NaOH-ZnO-$H_2O$ solutions were coagulated and washed in EtOH, Na and Zn remained in the dry cellulose. We suggested that metals are playing the role of "spacer" between cellulose chains. This involved

two main consequences: cellulose chains cannot reassemble during coagulation leading to a low crystallinity and coagulated cellulose does not collapse during vacuum drying. Another non-contradicting hypothesis is based on the work of Gunnarsson et al. (2017) who suggested that carbonate bridges are formed between cellulose chains when dissolved in NaOH-$H_2O$. When coagulated in EtOH, these bridges are not dismantled and they preserve cellulose network from collapsing during vacuum drying. In the view of these results, we found interesting to study the influence of the size and shape on xerogels' properties. We proved that the production of porous and high specific surface xerogel beads is possible by using the dropping technique. The properties of beads were very similar to the ones of monolithic xerogels and aerogels.

The last chapter, Chapter 6, *Pulp based aerogels*, was devoted to the preparation and characterisation of aerogels from pulps with different characteristics. Pulp aerogels were prepared by dissolution of the pulps in NaOH-ZnO-$H_2O$ solvent, partial gelation, coagulation in different non-solvents and drying under supercritical $CO_2$.

Dissolution efficiency of the solvent was evaluated by optical microscope observations and determination of the non-dissolved fraction. The most efficient dissolution was obtained for the pulps with a low DP and a low lignin content. All pulps were used to produce aerogels, whatever their dissolution efficiency. The influence of solution gelation time, type of non-solvent and pulp composition on the resulting aerogel properties was evaluated. The type of non-solvent appeared to be the most influencing parameter. As it was observed for xerogels in the previous chapter, metals are not completely washed away when EtOH or $H_2O$ are used as non-solvent while they are completely removed with HCl which also influenced cellulose aerogels' crystallinity, specific surface area and density. EtOH coagulated pulp aerogels showed higher density, lower $S_{BET}$ and lower crystallinity than the $H_2O$ or HCl coagulated ones.

The influence of pulp composition was not as significant as the type of non-solvents but differences could be noticed as a function of cellulose DP and hemicellulose content. Density of the aerogels increased with increasing cellulose DP and $S_{BET}$ slightly decreased with increasing hemicellulose content. To confirm and understand this last trend, hemicellulose aerogels and cellulose-hemicellulose hybrid aerogels were prepared from [DBNH][Pr] dissolution and coagulation in EtOH. Pure hemicellulose aerogels could only be prepared from its high concentration (30%) and showed very low $S_{BET}$. Hybrids showed a slightly lower $S_{BET}$ than pure cellulose aerogels from the same preparation conditions.

Finally, after selection of the appropriate pulps, aerogel beads were prepared with the JetCutter technology. The diameter of beads was of several hundreds of micrometers and their specific surface area ranged from 300 $m^2\ g^{-1}$ to 350 $m^2\ g^{-1}$, similar to what was obtained for the aerogel monoliths. Ultra-lightweight pulp xerogels were also successfully prepared and moisture sorption capacity of xerogels and aerogels was tested under cycles with the maximum increase in mass up to 18.5%.

Overall, we have demonstrated in this work that by a careful selection of solution properties and processing parameters, cellulose aerogel beads of different sizes can be produced and, in addition, the expensive supercritical $CO_2$ drying can be obviated. Diameters of hundreds of micrometers can be obtained with the JetCutter technology while diameters of only few microns are produced by emulsification. Both of these techniques are potentially up-scalable which brings a lot of value and versatility to these aerogels. The production of porous and high specific surface area xerogels is of great economical interest as high added value materials can be produced with a cheaper cost. This added value is also valid for pulp aerogels, pulp xerogels and pulp aerogel beads.

A lot of perspectives and future work can be drawn from this study. The most evident one is the production, at the industrial scale, of aerogel beads of various sizes for targeted applications. It was demonstrated that [DBNH][Pr] and NaOH based solvents as well as microcrystalline cellulose and pulps can be used with the JetCutter technology. Hence further work is a complete understanding and mastering of this technology in the view of producing all types of cellulose or polysaccharide aerogel beads from a wide range of solvents. Infinite possibilities of applications could thus be reached, from medical to construction industries. The work on emulsification proved that one method could be applied to cellulose-NaOH based solutions for the production of microspheres. Now that this technique is developed, variation of the emulsion parameters to adjust and control the aerogel particle size could lead to even smaller particles. Tests on the bio-compatibility should be performed in the view of their commercialisation and use in medical, food or cosmetic applications.

Literature reports that some bio-aerogel particles, based on "easy-gelling" polysaccharides such as starch or pectin, can be used as carriers for controlled release application with different drugs. The main conclusions were that the release of a drug depends on the type of polysaccharide and on the properties of the aerogel used. The release properties also depend on the type of drug. Only one article of Voon et al. (2017) reports drug controlled release from cellulose aerogel beads. The properties of cellulose aerogel and xerogel beads can be adapted and be different from other bio-aerogels as, for example, cellulose is not water soluble. Hybrid and composite cellulose-organic and cellulose-inorganic aerogels and xerogels as carriers for the release of active compounds can be developed. This opens a huge variety of different applications.

Numerous perspectives involve the production of porous xerogels. In the present state their exploitation might be restricted because of their composition: they still contain Na and Zn. It should be noted that Zn is an antibacterial agent and thus cellulose xerogels may have "naturally" occurring antibacterial properties. The applications involving these metals could be easily found in catalysis or in electrochemical when pyrolysed. Furthermore, low density xerogels were prepared from pulps. The

next step is to fully understand (and confirm our hypotheses or find the reasons) why high specific surface area and lightweight materials are obtained from a simple vacuum drying. Then the results obtained for cellulose could potentially be applied to other cellulose solvents or to other bio-polymers.

Finally, the use of pulp, instead of purified microcrystalline cellulose, reduces the production cost of aerogels. It was proved that different types of materials, with low density and high specific surface area, could be produced from pulp-NaOH-ZnO-$H_2O$ solutions, both aerogels and xerogels of any shape. It could thus be very interesting to use less and less treatments of wood, and understand the corresponding evolution of "cellulose" aerogels' and xerogels' properties.

# References


Aaltonen, O. and O. Jauhiainen

2009. The preparation of lignocellulosic aerogels from ionic liquid solutions. *Carbohydrate Polymers*, 75(1):125–129. (Cited on pages 79, 81, 81, 132, and 218).

Aegerter, M. A., N. Leventis, and M. M. Koebel, eds.

2011. *Aerogels Handbook*, Advances in Sol-Gel Derived Materials and Technologies. New York: Springer-Verlag. (Cited on pages 72, 73, and 73).

Alnaief, M., M. A. Alzaitoun, C. A. García-González, and I. Smirnova

2011. Preparation of biodegradable nanoporous microspherical aerogel based on alginate. *Carbohydrate Polymers*, 84(3):1011–1018. (Cited on pages 85 and 146).

Alnaief, M., R. Obaidat, and H. Mashaqbeh

2018. Effect of processing parameters on preparation of carrageenan aerogel microparticles. *Carbohydrate Polymers*, 180:264–275. (Cited on page 85).

Andanson, J.-M., E. Bordes, J. Devémy, F. Leroux, A. A. H. Pádua, and M. F. C. Gomes

2014. Understanding the role of co-solvents in the dissolution of cellulose in ionic liquids. *Green Chem.*, 16(5):2528–2538. (Cited on page 63).

Atalla, R. H. and D. L. VanderHart

1999. The role of solid state 13c NMR spectroscopy in studies of the nature of native celluloses. *Solid State Nuclear Magnetic Resonance*, (15):1–19. (Cited on page 54).

Ayadi, F. and A. Tourrette

2015. Procédé de préparation d'un matériau poreux a base de cellulose, matériaux obtenus et utilisations. Patent FR 3 042 503 - A1. (Cited on page 196).

Badgujar, K. C. and B. M. Bhanage

2015. Factors governing dissolution process of lignocellulosic biomass in ionic liquid: Current status, overview and challenges. *Bioresource Technology*, 178:2–18. (Cited on page 63).

Baker, A. A., W. Helbert, J. Sugiyama, and M. J. Miles
1997. High-Resolution Atomic Force Microscopy of NativeValoniaCellulose I Microcrystals. *Journal of Structural Biology*, 119(2):129–138. (Cited on pages 35 and 54).

BASF
2019. SLENTITE® – High-performance insulation with organic aerogel. URL : https://www.basf.com/fr/fr/who-we-are/innovation/our-innovations/high-performance-insulation.html. (Cited on pages 11 and 17).

Baudron, V., P. Gurikov, and I. Smirnova
2019. A continuous approach to the emulsion gelation method for the production of aerogel micro-particle. *Colloids and Surfaces A: Physicochemical and Engineering Aspects*, 566:58–69. (Cited on page 85).

Biganska, O. and P. Navard
2008. Morphology of cellulose objects regenerated from cellulose–N-methylmorpholine N-oxide–water solutions. *Cellulose*, 16(2):179. (Cited on page 80).

Blachot, J.-F., N. Brunet, P. Navard, and J.-Y. Cavaille
1998. Rheological behavior of cellulose/monohydrate of n-methylmorpholine n-oxide solutions Part 1: Liquid state. *Rheologica acta*, 37(2):107–114. (Cited on page 127).

Borisova, A., M. D. Bruyn, V. L. Budarin, P. S. Shuttleworth, J. R. Dodson, M. L. Segatto, and J. H. Clark
2015. A Sustainable Freeze-Drying Route to Porous Polysaccharides with Tailored Hierarchical Meso- and Macroporosity. *Macromolecular Rapid Communications*, 36(8):774–779. (Cited on page 72).

Buchtová, N. and T. Budtova
2016. Cellulose aero-, cryo- and xerogels: towards understanding of morphology control. *Cellulose*, 23(4):2585–2595. (Cited on pages 76, 79, 81, 82, 82, 121, 121, 131, 135, 135, 183, 183, and 229).

Budtova, T.
2019. Cellulose II aerogels: a review. *Cellulose*, 26(1):81–121. (Cited on page 82).

Budtova, T. and P. Navard
2016. Cellulose in NaOH–water based solvents: a review. *Cellulose*, 23(1):5–55. (Cited on pages 59, 60, 61, 61, 115, and 116).

CabotCorp
2019. Aerogel. URL: http://www.cabotcorp.com/solutions/products-plus/aerogel. (Cited on page 73).

Cai, J., S. Kimura, M. Wada, S. Kuga, and L. Zhang
2008a. Cellulose Aerogels from Aqueous Alkali Hydroxide–Urea Solution. *ChemSusChem*, 1(1-2):149–154. (Cited on pages 36, 79, 80, 81, 81, 82, 82, 83, and 83).

Cai, J. and L. Zhang
2005. Rapid Dissolution of Cellulose in LiOH/Urea and NaOH/Urea Aqueous Solutions. *Macromolecular Bioscience*, 5(6):539–548. (Cited on page 143).

Cai, J. and L. Zhang
2006. Unique Gelation Behavior of Cellulose in NaOH/Urea Aqueous Solution. *Biomacromolecules*, 7(1):183–189. (Cited on page 147).

Cai, J., L. Zhang, S. Liu, Y. Liu, X. Xu, X. Chen, B. Chu, X. Guo, J. Xu, H. Cheng, C. C. Han, and S. Kuga
2008b. Dynamic Self-Assembly Induced Rapid Dissolution of Cellulose at Low Temperatures. *Macromolecules*, 41(23):9345–9351. (Cited on page 61).

Chan, E.-S., B.-B. Lee, P. Ravindra, and D. Poncelet
2009. Prediction models for shape and size of ca-alginate macrobeads produced through extrusion–dripping method. *Journal of Colloid and Interface Science*, 338(1):63–72. (Cited on page 66).

Chang, X., D. Chen, and X. Jiao
2008. Chitosan-Based Aerogels with High Adsorption Performance. *J. Phys. Chem. B*, 112(26):7721–7725. (Cited on page 78).

Chen, W., H. Yu, Q. Li, Y. Liu, and J. Li
2011. Ultralight and highly flexible aerogels with long cellulose I nanofibers. *Soft Matter*, 7(21):10360–10368. (Cited on page 77).

Ciolacu, D., F. Ciolacu, and V. I. Popa
2011. Amorphous cellulose - Structure and characterization. *Cellulose Chemistry and Technology*, 45:13–21. (Cited on pages 107 and 197).

Ciolacu, D., C. Rudaz, M. Vasilescu, and T. Budtova
2016. Physically and chemically cross-linked cellulose cryogels: Structure, properties and application for controlled release. *Carbohydrate Polymers*, 151:392–400. (Cited on page 74).

Cox, W. P. and E. H. Merz
1958. Correlation of dynamic and steady flow viscosities. *J. Polym. Sci.*, 28(118):619–622. (Cited on page 124).

Cuissinat, C. and P. Navard
2006a. Swelling and Dissolution of Cellulose Part 1: Free Floating Cotton and Wood

Fibres in N-Methylmorpholine-N-oxide–Water Mixtures. *Macromolecular Symposia*, 244(1):1–18. (Cited on page 64).

Cuissinat, C. and P. Navard

2006b. Swelling and Dissolution of Cellulose Part II: Free Floating Cotton and Wood Fibres in NaOH–Water–Additives Systems. *Macromolecular Symposia*, 244(1):19–30. (Cited on page 64).

Cuissinat, C. and P. Navard

2008. Swelling and dissolution of cellulose, Part III: plant fibres in aqueous systems. *Cellulose*, 15(1):67–74. (Cited on page 64).

Cuissinat, C., P. Navard, and T. Heinze

2008. Swelling and dissolution of cellulose, Part V: cellulose derivatives fibres in aqueous systems and ionic liquids. *Cellulose*, 15(1):75–80. (Cited on page 64).

Davidson, G. F.

1934. The Dissolution of Chemically Modified Cotton Cellulose in Alkaline Solutions. Part I: In Solutions of Sodium Hydroxide, Particularly at Temperatures Below the Normal. *Journal of the Textile Institute Transactions*, 25(5):T174–T196. (Cited on pages 59 and 61).

Davidson, G. F.

1937. The Dissolution of Chemically Modified Cotton Cellulose in Alkaline Solutions. Part 3: In Solutions of Sodium and Potassium Hydroxide Containing Dissolved Zinc, Beryllium and Aluminium Oxides. *Journal of the Textile Institute Transactions*, 28(2):T27–T44. (Cited on page 61).

De Bruijn, R.

1993. Tipstreaming of drops in simple shear flows. *Chemical Engineering Science*, 48(2):277–284. (Cited on page 152 and 152).

De Cicco, F., P. Russo, E. Reverchon, C. A. García-González, R. P. Aquino, and P. Del Gaudio

2016. Prilling and supercritical drying: A successful duo to produce core-shell polysaccharide aerogel beads for wound healing. *Carbohydrate Polymers*, 147:482–489. (Cited on page 84).

De Marco, I., L. Baldino, S. Cardea, and E. Reverchon

2015. Supercritical gel drying for the production of starch aerogels for delivery systems. *Chemical Engineering Transactions*, Pp. 307–312. (Cited on page 77).

De Marco, I., S. Riemma, and R. Iannone

2019. Life cycle assessment of supercritical impregnation: Starch aerogel + $\alpha$-

tocopherol tablets. *The Journal of Supercritical Fluids*, 143:305–312. (Cited on page 77).

De Oliveira, W. and W. G. Glasser
1996. Hydrogels from Polysaccharides. I. Cellulose Beads for chromatographic support-Glasser.pdf. *Journal of Applied Polymer Science*, 60:63–73. (Cited on page 66).

Demilecamps, A., G. Reichenauer, A. Rigacci, and T. Budtova
2014. Cellulose–silica composite aerogels from "one-pot" synthesis. *Cellulose*, 21(4):2625–2636. (Cited on page 224).

Desse, M., B. Wolf, J. Mitchell, and T. Budtova
2009. Experimental study of the break-up of starch suspension droplets in step-up shear flow. *Journal of Rheology*, 53(4):943–955. (Cited on page 110).

Ding, B., J. Cai, J. Huang, L. Zhang, Y. Chen, X. Shi, Y. Du, and S. Kuga
2012. Facile preparation of robust and biocompatible chitin aerogels. *J. Mater. Chem.*, 22:5801–5809. (Cited on page 78).

Dirkse, T. P., C. Postmus, and R. Vandenbosch
1954. A Study of Alkaline Solutions of Zinc Oxide. *J. Am. Chem. Soc.*, 76(23):6022–6024. (Cited on page 218).

Druel, L., R. Bardl, W. Vorwerg, and T. Budtova
2017. Starch Aerogels: A Member of the Family of Thermal Superinsulating Materials. *Biomacromolecules*, 18(12):4232–4239. (Cited on pages 73, 77, and 77).

Druel, L., P. Niemeyer, B. Milow, and T. Budtova
2018. Rheology of cellulose-[DBNH][CO2et] solutions and shaping into aerogel beads. *Green Chem.*, 20(17):3993–4002. (Cited on pages 38, 38, 38, 38, 38, 38, 38, 38, 38, 39, 39, 45, 123, 123, 124, 125, 126, 127, 128, 129, 130, 131, 132, and 133).

Dumitriu, S.
2004. *Polysaccharides: Structural Diversity and Functional Versatility, Second Edition*, crc press edition. New York: [publisher unknown]. (Cited on page 51).

Ebringerová, A., Z. Hromádková, and T. Heinze
2005. Hemicellulose. In *Polysaccharides I*, volume 186, Pp. 1–67. Berlin/Heidelberg: Springer-Verlag. (Cited on page 51).

Eckelt, J., A. Knopf, T. Röder, H. K. Weber, H. Sixta, and B. A. Wolf
2011. Viscosity-molecular weight relationship for cellulose solutions in either NMMO monohydrate or cuen. *Journal of Applied Polymer Science*, 119(2):670–676. (Cited on page 127 and 127).

Egal, M.

2006. *Structure and properties of cellulose / NaOH aqueous solutions, gels and regenerated objects*. PhD thesis, École Nationale Supérieure des Mines de Paris, Cemef. (Cited on pages 60, 62, and 147).

Egal, M., T. Budtova, and P. Navard

2007. Structure of Aqueous Solutions of Microcrystalline Cellulose/Sodium Hydroxide below 0 °C and the Limit of Cellulose Dissolution. *Biomacromolecules*, 8(7):2282–2287. (Cited on page 60).

El Seoud, O. A., A. Koschella, L. C. Fidale, S. Dorn, and T. Heinze

2007. Applications of ionic liquids in carbohydrate chemistry: A window of opportunities. *Biomacromolecules*, 8(9):2629–2647. (Cited on pages 62, 115, and 116).

Elschner, T., K. Ganske, and T. Heinze

2013. Synthesis and aminolysis of polysaccharide carbonates. *Cellulose*, 20(1):339–353. (Cited on pages 61 and 202).

Evans, R. and A. F. A. Wallis

1989. Cellulose molecular weights determined by viscometry. *Journal of Applied Polymer Science*, 37(8):2331–2340. (Cited on pages 45, 109, 109, 109, and 110).

Froass, P. M., A. J. Ragauskas, and J. E. Jiang

1998. NMR Studies Part 3: Analysis of Lignin from Modern Kraft Pulping Technologies, Jiang.pdf. *Holzforschung*, 52(4):385–390. (Cited on page 216).

Ganesan, K., T. Budtova, L. Ratke, P. Gurikov, V. Baudron, I. Preibisch, P. Niemeyer, I. Smirnova, and B. Milow

2018. Review on the Production of Polysaccharide Aerogel Particles. *Materials*, 11(11):2144. (Cited on pages 66, 67, and 67).

Ganesan, K., A. Dennstedt, A. Barowski, and L. Ratke

2016. Design of aerogels, cryogels and xerogels of cellulose with hierarchical porous structures. *Materials & Design*, 92:345–355. (Cited on pages 79 and 83).

Ganesan, K. and L. Ratke

2014. Facile preparation of monolithic $\kappa$-carrageenan aerogels. *Soft Matter*, 10(18):3218–3224. (Cited on page 78).

García-González, C., M. Camino-Rey, M. Alnaief, C. Zetzl, and I. Smirnova

2012a. Supercritical drying of aerogels using CO2: Effect of extraction time on the end material textural properties. *The Journal of Supercritical Fluids*, 66:297–306. (Cited on page 77).

García-González, C. and I. Smirnova

2013. Use of supercritical fluid technology for the production of tailor-made aerogel particles for delivery systems. *The Journal of Supercritical Fluids*, 79:152–158. (Cited on page 77 and 77).

García-González, C., J. Uy, M. Alnaief, and I. Smirnova

2012b. Preparation of tailor-made starch-based aerogel microspheres by the emulsion-gelation method. *Carbohydrate Polymers*, 88(4):1378–1386. (Cited on pages 36, 84, and 84).

García-González, C. A., M. Alnaief, and I. Smirnova

2011. Polysaccharide-based aerogels—Promising biodegradable carriers for drug delivery systems. *Carbohydrate Polymers*, 86(4):1425–1438. (Cited on pages 78, 78, and 84).

García-González, C. A., E. Carenza, M. Zeng, I. Smirnova, and A. Roig

2012c. Design of biocompatible magnetic pectin aerogel monoliths and microspheres. *RSC Adv.*, 2(26):9816–9823. (Cited on page 84 and 84).

García-González, C. A., M. Jin, J. Gerth, C. Alvarez-Lorenzo, and I. Smirnova

2015. Polysaccharide-based aerogel microspheres for oral drug delivery. *Carbohydrate Polymers*, 117:797–806. (Cited on pages 84, 84, 84, 85, 85, 141, and 142).

Gardiner, E. S. and A. Sarko

1985. Packing analysis of carbohydrates and polysaccharides. 16. The crystal structures of celluloses IV $_{\mathrm{i}}$ and IV $_{\mathrm{ii}}$. *Canadian Journal of Chemistry*, 63(1):173–180. (Cited on page 56).

Gavillon, R.

2007. *Preparation and characterization of ultra porous cellulosic materials*. PhD thesis, École Nationale Supérieure des Mines de Paris. (Cited on pages 37, 86, 86, and 121).

Gavillon, R. and T. Budtova

2007. Kinetics of Cellulose Regeneration from Cellulose-NaOH-Water Gels and Comparison with Cellulose-N-Methylmorpholine-N-Oxide-Water Solutions. *Biomacromolecules*, 8(2):424–432. (Cited on pages 75 and 132).

Gavillon, R. and T. Budtova

2008. Aerocellulose: New Highly Porous Cellulose Prepared from Cellulose-NaOH Aqueous Solutions. *Biomacromolecules*, 9(1):269–277. (Cited on pages 36, 79, 79, 79, 79, 80, 80, 80, 80, 81, 81, 81, 81, 133, and 135).

Gellerstedt, G. and E. Lindfors

1984. Structural changes in lignin during kraft cooking. Part 4. Phenolic hydroxyl

groups in wood and kraft pulps. *Svensk Papperstidning*, 87(15):R115–R118. (Cited on page 216).

Gericke, M., T. Liebert, O. A. El Seoud, and T. Heinze
2011. Tailored Media for Homogeneous Cellulose Chemistry: Ionic Liquid/Co-Solvent Mixtures. *Macromol. Mater. Eng.*, 296(6):483–493. (Cited on pages 121 and 129).

Gericke, M., K. Schlufter, T. Liebert, T. Heinze, and T. Budtova
2009. Rheological Properties of Cellulose/Ionic Liquid Solutions: From Dilute to Concentrated States. *Biomacromolecules*, 10(5):1188–1194. (Cited on pages 38, 63, 121, 121, 124, 124, 125, 127, 128, and 129).

Gericke, M., J. Trygg, and P. Fardim
2013. Functional Cellulose Beads: Preparation, Characterization, and Applications. *Chemical Reviews*, 113(7):4812–4836. (Cited on pages 66, 66, 67, 115, and 116).

Glenn, G. M. and D. W. Irving
1995. Starch-based microcellular foams. *Cereal chemistry*, 72(2):155–161. (Cited on page 77).

Grace, H. P.
1982. Dispersion Phenomena in High Viscosity Immiscible Fluid Systems and Application of Static Mixers as Dispersion Devices in Such Systems. *Chemical Engineering Communications*, 14(3-6):225–277. (Cited on pages 36, 36, 68, 69, 70, and 152).

Graenacher, C.
1934. Cellulose solution. U.S. Patent 1,943,176. (Cited on page 62).

Green, S. M.
2017. *Understanding Ionic Liquid Properties for Carbohydrate Dissolution*. PhD thesis, University of Leeds, UK. (Cited on page 128).

Groult, S. and T. Budtova
2018a. Thermal conductivity/structure correlations in thermal super-insulating pectin aerogels. *Carbohydrate Polymers*, 196:73–81. (Cited on pages 73, 76, 77, 132, and 135).

Groult, S. and T. Budtova
2018b. Tuning structure and properties of pectin aerogels. *European Polymer Journal*, 108:250–261. (Cited on pages 77, 77, and 194).

Gunnarsson, M.
2017. *Investigation of CO2 interactions with cellulose dissolved in the NaOH(aq)*

*system*. PhD thesis, Chalmers University of Technology, Sweden. (Cited on pages 36, 61, 61, and 202).

Gunnarsson, M., D. Bernin, Å. Östlund, and M. Hasani
2018. The CO2 capturing ability of cellulose dissolved in NaOH(aq) at low temperature. *Green Chem.*, 20(14):3279–3286. (Cited on pages 61, 202, and 202).

Gunnarsson, M., H. Theliander, and M. Hasani
2017. Chemisorption of air CO2 on cellulose: an overlooked feature of the cellulose/NaOH(aq) dissolution system. *Cellulose*, 24(6):2427–2436. (Cited on pages 26, 61, 202, 206, and 240).

Gurikov, P., S. P. Raman, D. Weinrich, M. Fricke, and I. Smirnova
2015. A novel approach to alginate aerogels: carbon dioxide induced gelation. *RSC Adv.*, 5(11):7812–7818. (Cited on page 78).

Haimer, E., M. Wendland, K. Schlufter, K. Frankenfeld, P. Miethe, A. Potthast, T. Rosenau, and F. Liebner
2010. Loading of Bacterial Cellulose Aerogels with Bioactive Compounds by Antisolvent Precipitation with Supercritical Carbon Dioxide. *Macromolecular Symposia*, 294(2):64–74. (Cited on page 77).

Hauru, L. K. J., M. Hummel, A. W. T. King, I. Kilpeläinen, and H. Sixta
2012. Role of Solvent Parameters in the Regeneration of Cellulose from Ionic Liquid Solutions. *Biomacromolecules*, 13(9):2896–2905. (Cited on page 63).

Hauru, L. K. J., M. Hummel, K. Nieminen, A. Michud, and H. Sixta
2016. Cellulose regeneration and spinnability from ionic liquids. *Soft Matter*, 12(5):1487–1495. (Cited on page 63).

Heath, L. and W. Thielemans
2010. Cellulose nanowhisker aerogels. *Green Chemistry*, 12(8):1448. (Cited on page 77).

Hoepfner, S., L. Ratke, and B. Milow
2008. Synthesis and characterisation of nanofibrillar cellulose aerogels. *Cellulose*, 15(1):121–129. (Cited on pages 79, 81, and 82).

Hon, D. N.-S. and N. Shiraishi
2000. *Wood and Cellulosic Chemistry, Second Edition, Revised, and Expanded*. CRC Press. (Cited on pages 51, 51, and 53).

Innerlohinger, J., H. K. Weber, and G. Kraft
2006. Aerocellulose: Aerogels and Aerogel-like Materials made from Cellulose.

*Macromolecular Symposia*, 244(1):126–135. (Cited on pages 79, 80, 81, 81, 81, 81, 86, 87, 132, and 229).

Isobe, N., U.-J. Kim, S. Kimura, M. Wada, and S. Kuga
2011. Internal surface polarity of regenerated cellulose gel depends on the species used as coagulant. *Journal of Colloid and Interface Science*, 359(1):194–201. (Cited on pages 81, 197, 197, 197, and 198).

Isobe, N., S. Kimura, M. Wada, and S. Kuga
2012. Mechanism of cellulose gelation from aqueous alkali-urea solution. *Carbohydrate Polymers*, 89(4):1298–1300. (Cited on page 62).

Isobe, N., K. Noguchi, Y. Nishiyama, S. Kimura, M. Wada, and S. Kuga
2013. Role of urea in alkaline dissolution of cellulose. *Cellulose*, 20(1):97–103. (Cited on page 61).

Isogai, A. and R. H. Atalla
1998. Dissolution of Cellulose in Aqueous NaOH Solutions. *Cellulose*, 5:309–319. (Cited on page 64 and 64).

Isogai, A., M. Usuda, T. Kato, T. Uryu, and R. H. Atalla
1989. Solid-state CP/MAS carbon-13 NMR study of cellulose polymorphs. *Macromolecules*, 22(7):3168–3172. (Cited on page 197).

Jiang, Z., Y. Fang, J. Xiang, Y. Ma, A. Lu, H. Kang, Y. Huang, H. Guo, R. Liu, and L. Zhang
2014. Intermolecular Interactions and 3d Structure in Cellulose–NaOH–Urea Aqueous System. *J. Phys. Chem. B*, 118(34):10250–10257. (Cited on page 61).

Jiménez-Saelices, C., B. Seantier, B. Cathala, and Y. Grohens
2017. Spray freeze-dried nanofibrillated cellulose aerogels with thermal superinsulating properties. *Carbohydrate Polymers*, 157:105–113. (Cited on pages 76, 77, and 132).

Jin, H., M. Kettunen, A. Laiho, H. Pynnönen, J. Paltakari, A. Marmur, O. Ikkala, and R. H. A. Ras
2011. Superhydrophobic and Superoleophobic Nanocellulose Aerogel Membranes as Bioinspired Cargo Carriers on Water and Oil. *Langmuir*, 27(5):1930–1934. (Cited on page 77).

Kamal Mohamed, S. M., K. Ganesan, B. Milow, and L. Ratke
2015. The effect of zinc oxide (ZnO) addition on the physical and morphological properties of cellulose aerogel beads. *RSC Adv.*, 5(109):90193–90201. (Cited on pages 66, 86, 87, 106, 115, 116, 132, and 133).

Kamide, K., K. Okajima, and K. Kowsaka
1992. Dissolution of natural cellulose into aqueous alkali solution: role of supermolecular structure of cellulose. *Polymer Journal*, 24(1):71–86. (Cited on page 60).

Kamide, K., K. Okajima, T. Matsui, and K. Kowsaka
1984. Study on the Solubility of Cellulose in Aqueous Alkali Solution by Deuteration IR and $^{13}$C NMR. *Polymer Journal*, 16(12):857–866. (Cited on page 60).

Karadagli, I., B. Schulz, M. Schestakow, B. Milow, T. Gries, and L. Ratke
2015. Production of porous cellulose aerogel fibers by an extrusion process. *The Journal of Supercritical Fluids*, 106:105–114. (Cited on page 79).

Karatzos, S. K., L. A. Edye, and R. M. Wellard
2012. The undesirable acetylation of cellulose by the acetate ion of 1-ethyl-3-methylimidazolium acetate. *Cellulose*, 19(1):307–312. (Cited on page 63).

Karbstein, H. and H. Schubert
1995. Developments in the continuous mechanical production of oil-in-water macro-emulsions. *Chemical Engineering and Processing: Process Intensification*, 34(3):205–211. (Cited on pages 67 and 68).

Kayser, H., C. R. Müller, C. A. García-González, I. Smirnova, W. Leitner, and P. Domínguez de María
2012. Dried chitosan-gels as organocatalysts for the production of biomass-derived platform chemicals. *Applied Catalysis A: General*, 445-446:180–186. (Cited on page 85 and 85).

Kenar, J. A., F. J. Eller, F. C. Felker, M. A. Jackson, and G. F. Fanta
2014. Starch aerogel beads obtained from inclusion complexes prepared from high amylose starch and sodium palmitate. *Green Chem.*, 16(4):1921–1930. (Cited on page 84).

Kihlman, M., F. Aldaeus, F. Chedid, and U. Germgård
2012. Effect of various pulp properties on the solubility of cellulose in sodium hydroxide solutions. *Holzforschung*, 66(5). (Cited on page 64 and 64).

Kim, K. K. and D. W. Pack
2006. Microspheres for Drug Delivery. In *BioMEMS and Biomedical Nanotechnology: Volume I Biological and Biomedical Nanotechnology*, M. Ferrari, A. P. Lee, and L. J. Lee, eds., Pp. 19–50. Boston, MA: Springer US. (Cited on page 70).

Kistler, S. S.
1931. Coherent Expanded Aerogels and Jellies. *Nature*, 127(3211):741. (Cited on pages 11, 17, 72, 72, 73, 73, and 73).

Kistler, S. S.
1932. Coherent Expanded Aerogels. *J. Phys. Chem.*, 36:52–64. (Cited on page 73 and 73).

Klemm, D., B. Heublein, H.-P. Fink, and A. Bohn
2005. Cellulose: Fascinating Biopolymer and Sustainable Raw Material. *Angewandte Chemie International Edition*, 44(22):3358–3393. (Cited on pages 53 and 58).

Klemm, D., B. Philipp, T. Heinze, U. Heinze, and W. Wagenknecht
1998. *Comprehensive Cellulose Chemistry*, volume 1. Weinheim, FRG: Wiley-VCH Verlag GmbH & Co. KGaA. (Cited on pages 53, 54, 55, and 58).

Kobayashi, Y., T. Saito, and A. Isogai
2014. Aerogels with 3d Ordered Nanofiber Skeletons of Liquid-Crystalline Nanocellulose Derivatives as Tough and Transparent Insulators. *Angewandte Chemie International Edition*, 53(39):10394–10397. (Cited on page 77).

Kroon-Batenburg, L. M. J., J. Kroon, and M. G. Nordholt
1986. Chain modulus and intramolecular hydrogen bonding in native and regenerated cellulose fibers. *Polymer communications*, (27):290–292. (Cited on pages 35 and 55).

Labidi, K., O. Korhonen, M. Zrida, A. H. Hamzaoui, and T. Budtova
2019. All-cellulose composites from alfa and wood fibers. *Industrial Crops and Products*, 127:135–141. (Cited on page 65).

Larsson, P. T., K. Wickholm, and T. Iversen
1997. A CP/MAS13c NMR investigation of molecular ordering in celluloses. *Carbohydrate Research*, 302(1):19–25. (Cited on page 108).

Lavoine, N. and L. Bergström
2017. Nanocellulose-based foams and aerogels: processing, properties, and applications. *J. Mater. Chem. A*, 5(31):16105–16117. (Cited on page 77).

Le, K. A., C. Rudaz, and T. Budtova
2014. Phase diagram, solubility limit and hydrodynamic properties of cellulose in binary solvents with ionic liquid. *Carbohydr. Polym.*, 105:237–243. (Cited on pages 121 and 129).

Le Duc, A., B. Vergnes, and T. Budtova
2011. Polypropylene/natural fibres composites: Analysis of fibre dimensions after compounding and observations of fibre rupture by rheo-optics. *Composites Part A: Applied Science and Manufacturing*, 42(11):1727–1737. (Cited on page 110).

Le Moigne, N. and P. Navard
2010. Dissolution mechanisms of wood cellulose fibres in NaOH–water. *Cellulose*, 17(1):31–45. (Cited on pages 64, 64, 64, and 216).

Liebert, T. and T. Heinze
2008. Interaction of ionic liquids with polysaccharides 5. Solvents and reaction media for the modification of cellulose. *BioResources*, 3(2):576–601. (Cited on page 62).

Liebner, F., E. Haimer, A. Potthast, D. Loidl, S. Tschegg, M.-A. Neouze, M. Wendland, and T. Rosenau
2009. Cellulosic aerogels as ultra-lightweight materials. Part 2: Synthesis and properties 2nd ICC 2007, Tokyo, Japan, October 25–29, 2007. *Holzforschung*, 63(1). (Cited on pages 79 and 81).

Liebner, F., E. Haimer, M. Wendland, M.-A. Neouze, K. Schlufter, P. Miethe, T. Heinze, A. Potthast, and T. Rosenau
2010. Aerogels from Unaltered Bacterial Cellulose: Application of scCO2 Drying for the Preparation of Shaped, Ultra-Lightweight Cellulosic Aerogels. *Macromolecular Bioscience*, 10(4):349–352. (Cited on page 77).

Liebner, F., N. Pircher, C. Schimper, E. Haimer, and T. Rosenau
2016. Aerogels: Cellulose-Based. In *Encyclopedia of Biomedical Polymers and Polymeric Biomaterials*, Taylor and Francis, Pp. 37–75. New York: [publisher unknown]. (Cited on page 54).

Liebner, F., A. Potthast, T. Rosenau, E. Haimer, and M. Wendland
2008. Cellulose aerogels: Highly porous, ultra-lightweight materials. *Holzforschung*, 62(2):129–135. (Cited on pages 79, 81, 81, 82, and 132).

Lin, C.-x., H.-y. Zhan, M.-h. Liu, S.-y. Fu, and L. A. Lucia
2009. Novel Preparation and Characterization of Cellulose Microparticles Functionalized in Ionic Liquids. *Langmuir*, 25(17):10116–10120. (Cited on pages 115 and 116).

Lindman, B., G. Karlström, and L. Stigsson
2010. On the mechanism of dissolution of cellulose. *Journal of Molecular Liquids*, 156(1):76–81. (Cited on pages 57 and 60).

Lindman, B., B. Medronho, L. Alves, C. Costa, H. Edlund, and M. Norgren
2017. The relevance of structural features of cellulose and its interactions to dissolution, regeneration, gelation and plasticization phenomena. *Physical Chemistry Chemical Physics*, 19(35):23704–23718. (Cited on page 60).

Liu, H., K. L. Sale, B. M. Holmes, B. A. Simmons, and S. Singh
2010. Understanding the Interactions of Cellulose with Ionic Liquids: A Molecular Dynamics Study. *J. Phys. Chem. B*, 114(12):4293–4301. (Cited on page 63).

Liu, W. and T. Budtova
2013. Dissolution of unmodified waxy starch in ionic liquid and solution rheological properties. *Carbohydrate Polymers*, 93(1):199–206. (Cited on page 128).

Liu, W., T. Budtova, and P. Navard
2011. Influence of ZnO on the properties of dilute and semi-dilute cellulose-NaOH-water solutions. *Cellulose*, 18(4):911–920. (Cited on pages 61, 147, 180, 187, 191, 191, 192, 192, 192, 192, 192, 194, and 230).

Liu, Y.
1998. Study of Tin Cementation in Alkaline Solution. *J. Electrochem. Soc.*, 145(1):5. (Cited on pages 46, 187, 187, 187, 218, and 219).

López-Iglesias, C., J. Barros, I. Ardao, F. J. Monteiro, C. Alvarez-Lorenzo, J. L. Gómez-Amoza, and C. A. García-González
2019. Vancomycin-loaded chitosan aerogel particles for chronic wound applications. *Carbohydr Polym*, 204:223–231. (Cited on page 78).

Lovskaya, D. D., A. E. Lebedev, and N. V. Menshutina
2015. Aerogels as drug delivery systems: In vitro and in vivo evaluations. *The Journal of Supercritical Fluids*, 106:115–121. (Cited on pages 84 and 85).

Lu, B., A. Xu, and J. Wang
2014. Cation does matter: how cationic structure affects the dissolution of cellulose in ionic liquids. *Green Chem.*, 16(3):1326–1335. (Cited on page 63).

Luo, X., S. Liu, J. Zhou, and L. Zhang
2009. In situ synthesis of Fe3o4/cellulose microspheres with magnetic-induced protein delivery. *Journal of Materials Chemistry*, 19(21):3538. (Cited on page 70).

Luo, X. and L. Zhang
2010a. Creation of regenerated cellulose microspheres with diameter ranging from micron to millimeter for chromatography applications. *Journal of Chromatography A*, 1217(38):5922–5929. (Cited on pages 70, 115, 116, 146, 146, 146, 146, 154, and 155).

Luo, X. and L. Zhang
2010b. Immobilization of Penicillin G Acylase in Epoxy-Activated Magnetic Cellulose Microspheres for Improvement of Biocatalytic Stability and Activities. *Biomacromolecules*, 11(11):2896–2903. (Cited on page 70).

Ma, Y., S. Asaadi, L.-S. Johansson, P. Ahvenainen, M. Reza, M. Alekhina, L. Rautkari, A. Michud, L. Hauru, M. Hummel, and H. Sixta
2015. High-Strength Composite Fibers from Cellulose–Lignin Blends Regenerated

from Ionic Liquid Solution. *ChemSusChem*, 8(23):4030–4039. (Cited on pages 64, 115, and 116).

Manzocco, L., F. Valoppi, S. Calligaris, F. Andreatta, S. Spilimbergo, and M. C. Nicoli
2017. Exploitation of $\kappa$-carrageenan aerogels as template for edible oleogel preparation. *Food Hydrocolloids*, 71:68–75. (Cited on page 78).

Matsumoto, T., D. Tatsumi, N. Tamai, and T. Takaki
2001. Solution properties of celluloses from different biological origins in LiCl · DMAc. *Cellulose*, 8(4):275–282. (Cited on page 127).

Mazza, M., D.-A. Catana, C. Vaca-Garcia, and C. Cecutti
2009. Influence of water on the dissolution of cellulose in selected ionic liquids. *Cellulose*, 16(2):207–215. (Cited on page 63).

Medronho
2015. Probing cellulose amphiphilicity. *Nordic Pulp and Paper Research Journal*, 30(01):058–066. (Cited on page 57).

Medronho, B. and B. Lindman
2014. Competing forces during cellulose dissolution: From solvents to mechanisms. *Current Opinion in Colloid & Interface Science*, 19(1):32–40. (Cited on pages 35 and 58).

Medronho, B., A. Romano, M. G. Miguel, L. Stigsson, and B. Lindman
2012. Rationalizing cellulose (in)solubility: reviewing basic physicochemical aspects and role of hydrophobic interactions. *Cellulose*, 19(3):581–587. (Cited on page 60).

Mehling, T., I. Smirnova, U. Guenther, and R. Neubert
2009. Polysaccharide-based aerogels as drug carriers. *Journal of Non-Crystalline Solids*, 355(50-51):2472–2479. (Cited on page 77).

Melro, E., L. Alves, F. E. Antunes, and B. Medronho
2018. A brief overview on lignin dissolution. *Journal of Molecular Liquids*, 265:578–584. (Cited on pages 51 and 216).

Menshutina, N. V., D. D. Lovskaya, A. E. Lebedev, and E. A. Lebedev
2017. Production of Sodium Alginate-Based Aerogel Particles Using Supercritical Drying in Units with Different Volumes. *Russ. J. Phys. Chem. B*, 11(8):1296–1305. (Cited on page 85).

Mercer, J.
1850. Improvements in the preparation of cotton and others fabrics and other fibrous materials. British Patent 13. (Cited on page 59).

Mi, Q.-y., S.-r. Ma, J. Yu, J.-s. He, and J. Zhang
2016. Flexible and Transparent Cellulose Aerogels with Uniform Nanoporous Structure by a Controlled Regeneration Process. *ACS Sustainable Chem. Eng.*, 4(3):656–660. (Cited on page 79).

Michud, A., M. Tanttu, S. Asaadi, Y. Ma, E. Netti, P. Kääriainen, A. Persson, A. Berntsson, M. Hummel, and H. Sixta
2016. Ioncell-F: ionic liquid-based cellulosic textile fibers as an alternative to viscose and Lyocell. *Textile Research Journal*, 86(5):543–552. (Cited on page 64).

Nanohybrids
2019. Project | nanohybrids.eu. URL: https://nanohybrids.eu/project/. (Cited on pages 12 and 18).

Newman, R. H.
2008. Simulation of X-ray diffractograms relevant to the purported polymorphs cellulose IVI and IVII. *Cellulose*, 15(6):769. (Cited on page 56).

Nishino, T., I. Matsuda, and K. Hirao
2004. All-Cellulose Composite. *Macromolecules*, 37(20):7683–7687. (Cited on page 65).

Obaidat, R. M., M. Alnaief, and H. Mashaqbeh
2018. Investigation of Carrageenan Aerogel Microparticles as a Potential Drug Carrier. *AAPS PharmSciTech*, 19(5):2226–2236. (Cited on page 85).

Okano, T. and A. Sarko
1985. Mercerization of cellulose. II. Alkali–cellulose intermediates and a possible mercerization mechanism. *Journal of Applied Polymer Science*, 30(1):325–332. (Cited on page 59).

Ookuma, S., K. Igarashi, M. Hara, K. Aso, H. Yoshidome, H. Nakayama, K. Suzuki, and K. Nakajima
1993. Porous ion-exchanged fine cellulose particles, method for production thereof, and affinity carrier. US005196527A. (Cited on pages 79 and 85).

Pääkkö, M., J. Vapaavuori, R. Silvennoinen, H. Kosonen, M. Ankerfors, T. Lindström, L. A. Berglund, and O. Ikkala
2008. Long and entangled native cellulose I nanofibers allow flexible aerogels and hierarchically porous templates for functionalities. *Soft Matter*, 4(12):2492–2499. (Cited on page 77).

Parviainen, A., A. W. T. King, I. Mutikainen, M. Hummel, C. Selg, L. K. J. Hauru,

H. Sixta, and I. Kilpeläinen
2013. Predicting Cellulose Solvating Capabilities of Acid-Base Conjugate Ionic Liquids. *ChemSusChem*, 6(11):2161–2169. (Cited on pages 63, 117, and 117).

Parviainen, A., R. Wahlström, U. Liimatainen, T. Liitiä, S. Rovio, J. K. J. Helminen, U. Hyväkkö, A. W. T. King, A. Suurnäkki, and I. Kilpeläinen
2015. Sustainability of cellulose dissolution and regeneration in 1,5-diazabicyclo[4.3.0]non-5-enium acetate: a batch simulation of the IONCELL-F process. *RSC Advances*, 5(85):69728–69737. (Cited on pages 117 and 122).

Pereira, A., H. Duarte, P. Nosrati, M. Gubitosi, L. Gentile, A. Romano, B. Medronho, and U. Olsson
2018. Cellulose gelation in NaOH solutions is due to cellulose crystallization. *Cellulose*, 25(6):3205–3210. (Cited on pages 60, 60, and 194).

Pinnow, M., H.-P. Fink, C. Fanter, and J. Kunze
2008. Characterization of Highly Porous Materials from Cellulose Carbamate. *Macromolecular Symposia*, 262(1):129–139. (Cited on pages 67 and 79).

Pircher, N., L. Carbajal, C. Schimper, M. Bacher, H. Rennhofer, J.-M. Nedelec, H. C. Lichtenegger, T. Rosenau, and F. Liebner
2016. Impact of selected solvent systems on the pore and solid structure of cellulose aerogels. *Cellulose*, 23(3):1949–1966. (Cited on pages 79, 79, 79, 80, 81, and 135).

PlasticsEurope
2019. Market data. URL: https://www.plasticseurope.org/en/resources/market-data. (Cited on page 53).

Poncelet, D., R. Lencki, C. Beaulieu, J. P. Halle, R. J. Neufeld, and A. Fournier
1992. Production of alginate beads by emulsification/internal gelation. I. Methodology. *Appl Microbiol Biotechnol*, 38(1):39–45. (Cited on page 70).

Preibisch, I., P. Niemeyer, Y. Yusufoglu, P. Gurikov, B. Milow, and I. Smirnova
2018. Polysaccharide-Based Aerogel Bead Production via Jet Cutting Method. *Materials*, 11(8):1287. WOS:000444112800024. (Cited on pages 84 and 85).

Prüße, U.
2002. Bead production with JetCutting and rotating disk/nozzle technologies. *Landbauforschung Völkenrode*, P. 11. (Cited on page 67).

Prüsse, U., L. Bilancetti, M. Bučko, B. Bugarski, J. Bukowski, P. Gemeiner, D. Lewińska, V. Manojlovic, B. Massart, C. Nastruzzi, V. Nedovic, D. Poncelet, S. Siebenhaar, L. Tobler, A. Tosi, A. Vikartovská, and K.-D. Vorlop
2008. Comparison of different technologies for alginate beads production. *Chemical Papers*, 62(4). (Cited on page 67).

Prüße, U., F. Bruske, J. Breford, and K.-D. Vorlop
1998a. Improvement of the Jet Cutting Method for the Preparation of Spherical Particles from Viscous Polymer Solutions. *Chemical Engineering & Technology*, 21(2):153–157. (Cited on page 67).

Prüße, U., B. Fox, M. Kirchhoff, F. Bruske, J. Breford, and K.-D. Vorlop
1998b. New Process (Jet Cutting Method) for the Production of Spherical Beads from Highly Viscous Polymer Solutions. *Chemical Engineering & Technology*, 21(1):29–33. (Cited on page 67).

Prüße, U., U. Jahnz, P. Wittlich, and K.-D. Vorlop
2003. Scale-up of the JetCutter technology. *Chem. Ind.*, 57(12):636–640. (Cited on page 67).

Quignard, F., F. Di Renzo, and E. Guibal
2010. From Natural Polysaccharides to Materials for Catalysis, Adsorption, and Remediation. In *Carbohydrates in Sustainable Development I*, A. P. Rauter, P. Vogel, and Y. Queneau, eds., Topics in Current Chemistry, Pp. 165–197. Berlin, Heidelberg: Springer Berlin Heidelberg. (Cited on pages 78 and 85).

Quignard, F., R. Valentin, and F. D. Renzo
2008. Aerogel materials from marine polysaccharides. *New J. Chem.*, 32(8):1300–1310. (Cited on pages 37, 74, 78, 84, and 85).

Rege, A., M. Schestakow, I. Karadagli, L. Ratke, and M. Itskov
2016. Micro-mechanical modelling of cellulose aerogels from molten salt hydrates. *Soft Matter*, 12(34):7079–7088. (Cited on pages 79, 79, 79, 79, and 81).

Reichardt, C.
2006. *Solvents and Solvent Effects in Organic Chemistry*, Wiley-vch, 3rd edition. (Cited on pages 45, 45, 184, and 184).

Reichle, R. A., K. G. McCurdy, and L. G. Hepler
1975. Zinc Hydroxide: Solubility Product and Hydroxy-complex Stability Constants from 12.5–75 °C. *Canadian Journal of Chemistry*, 53(24):3841–3845. (Cited on page 218).

Ricci, A., L. Bernardi, C. Gioia, S. Vierucci, M. Robitzer, and F. Quignard
2010. Chitosan aerogel: a recyclable, heterogeneous organocatalyst for the asymmetric direct aldol reaction in water. *Chem. Commun.*, 46(34):6288–6290. (Cited on page 85).

Robitzer, M., L. David, C. Rochas, F. Di Renzo, and F. Quignard
2008. Nanostructure of Calcium Alginate Aerogels Obtained from Multistep Solvent Exchange Route. *Langmuir*, 24(21):12547–12552. (Cited on page 85).

Robitzer, M., F. D. Renzo, and F. Quignard
2011a. Natural materials with high surface area. Physisorption methods for the characterization of the texture and surface of polysaccharide aerogels. *Microporous and Mesoporous Materials*, 140(1-3):9–16. (Cited on pages 74, 76, 85, and 132).

Robitzer, M., A. Tourrette, R. Horga, R. Valentin, M. Boissière, J. Devoisselle, F. Di Renzo, and F. Quignard
2011b. Nitrogen sorption as a tool for the characterisation of polysaccharide aerogels. *Carbohydrate Polymers*, 85(1):44–53. (Cited on page 85).

Roy, C., T. Budtova, and P. Navard
2003. Rheological Properties and Gelation of Aqueous Cellulose-NaOH Solutions. *Biomacromolecules*, 4(2):259–264. (Cited on pages 60, 146, and 147).

Roy, C., T. Budtova, P. Navard, and O. Bedue
2001. Structure of Cellulose-Soda Solutions at Low Temperatures. *Biomacromolecules*, 2(3):687–693. (Cited on page 60).

Rudaz, C.
2013. *Cellulose and Pectin Aerogels Towards their nano structuration.* PhD thesis, Mines ParisTech, Cemef. (Cited on pages 79, 106, 132, 132, and 132).

Rudaz, C. and T. Budtova
2013. Rheological and hydrodynamic properties of cellulose acetate/ionic liquid solutions. *Carbohydrate Polymers*, 92(2):1966–1971. (Cited on page 128).

Rudaz, C., R. Courson, L. Bonnet, S. Calas-Etienne, H. Sallée, and T. Budtova
2014. Aeropectin: fully biomass-based mechanically strong and thermal superinsulating aerogel. *Biomacromolecules*, 15(6):2188–2195. (Cited on pages 73, 76, 76, 77, 109, 132, 132, and 132).

Rumscheidt, F. D. and S. G. Mason
1961. Particle motions in sheared suspensions XII. Deformation and burst of fluid drops in shear and hyperbolic flow. *Journal of Colloid Science*, 16(3):238–261. (Cited on pages 69, 69, and 152).

Sakai, K., Y. Kobayashi, T. Saito, and A. Isogai
2016. Partitioned airs at microscale and nanoscale: thermal diffusivity in ultrahigh porosity solids of nanocellulose. *Scientific Reports*, 6(1). (Cited on page 77).

Sarko, A., J. Southwick, and J. Hayashi
1976. Packing Analysis of Carbohydrates and Polysaccharides. 7. Crystal Structure of Cellulose IIII and Its Relationship to Other Cellulose Polymorphs. *Macromolecules*, 9(5):857–863. (Cited on page 56).

Scandinavian Pulp, P. a. B. T. C.
1988. SCAN-CM Standard 15:88, Viscosity in cupi-ethylenediamine solution. (Cited on pages 45, 109, 109, and 110).

Schestakow, M., I. Karadagli, and L. Ratke
2016. Cellulose aerogels prepared from an aqueous zinc chloride salt hydrate melt. *Carbohydrate Polymers*, 137:642–649. (Cited on pages 36, 79, 80, 81, 81, 81, 82, and 229).

Seddon, K. R., A. Stark, and M.-J. Torres
2000. Influence of chloride, water, and organic solvents on the physical properties of ionic liquids. *Pure and Applied Chemistry*, 72(12):2275–2287. (Cited on page 63).

Sehaqui, H., Q. Zhou, and L. A. Berglund
2011. High-porosity aerogels of high specific surface area prepared from nanofibrillated cellulose (NFC). *Composites Science and Technology*, 71(13):1593–1599. (Cited on page 77).

Sescousse, R. and T. Budtova
2009. Influence of processing parameters on regeneration kinetics and morphology of porous cellulose from cellulose–NaOH–water solutions. *Cellulose*, 16(3):417–426. (Cited on pages 75, 79, 80, 80, and 80).

Sescousse, R., R. Gavillon, and T. Budtova
2011a. Aerocellulose from cellulose–ionic liquid solutions: Preparation, properties and comparison with cellulose–NaOH and cellulose–NMMO routes. *Carbohydrate Polymers*, 83(4):1766–1774. (Cited on pages 79, 79, 79, 81, 81, 133, and 194).

Sescousse, R., R. Gavillon, and T. Budtova
2011b. Wet and dry highly porous cellulose beads from cellulose–NaOH–water solutions: influence of the preparation conditions on beads shape and encapsulation of inorganic particles. *Journal of Materials Science*, 46(3):759–765. (Cited on pages 66, 86, 115, 116, 121, 132, and 218).

Sescousse, R., K. A. Le, M. E. Ries, and T. Budtova
2010a. Viscosity of Cellulose-Imidazolium-Based Ionic Liquid Solutions. *J. Phys. Chem. B*, 114(21):7222–7228. (Cited on pages 63, 124, and 127).

Sescousse, R., A. Smacchia, and T. Budtova
2010b. Influence of lignin on cellulose-NaOH-water mixtures properties and on Aerocellulose morphology. *Cellulose*, 17(6):1137–1146. (Cited on page 81).

Shen, X., J. L. Shamshina, P. Berton, J. Bandomir, H. Wang, G. Gurau, and R. D. Rogers
2016. Comparison of Hydrogels Prepared with Ionic-Liquid-Isolated vs Commercial

Chitin and Cellulose. *ACS Sustainable Chem. Eng.*, 4(2):471–480. (Cited on page 78).

Shi, Z., Y. Liu, H. Xu, Q. Yang, C. Xiong, S. Kuga, and Y. Matsumoto
2018. Facile dissolution of wood pulp in aqueous NaOH/urea solution by ball milling pretreatment. *Industrial Crops and Products*, 118:48–52. (Cited on page 65).

Shi, Z., Q. Yang, J. Cai, S. Kuga, and Y. Matsumoto
2014. Effects of lignin and hemicellulose contents on dissolution of wood pulp in aqueous NaOH/urea solution. *Cellulose*, 21(3):1205–1215. (Cited on pages 64 and 65).

Silva, S. S., A. R. C. Duarte, A. P. Carvalho, J. F. Mano, and R. L. Reis
2011. Green processing of porous chitin structures for biomedical applications combining ionic liquids and supercritical fluid technology. *Acta Biomaterialia*, 7(3):1166–1172. (Cited on page 78).

Silva, S. S., A. R. C. Duarte, J. F. Mano, and R. L. Reis
2013. Design and functionalization of chitin-based microsphere scaffolds. *Green Chem.*, 15(11):3252–3258. (Cited on page 85).

Sobue, H., H. Kiessig, and E. K. Hess
1939. The cellulose-sodium hydroxide-water system as a function of the temperature. *Z Phys. Chem B*, 43:309–328. (Cited on pages 35, 59, and 59).

Starbird, R., C. A. García-González, I. Smirnova, W. H. Krautschneider, and W. Bauhofer
2014. Synthesis of an organic conductive porous material using starch aerogels as template for chronic invasive electrodes. *Materials Science and Engineering: C*, 37:177–183. (Cited on page 84).

Stone, H. A., B. J. Bentley, and L. G. Leal
1986. An experimental study of transient effects in the breakup of viscous drops. *Journal of Fluid Mechanics*, 173(-1):131. (Cited on pages 36, 69, and 69).

Sun, X., B. Peng, Y. Ji, J. Chen, and D. Li
2009. Chitosan(chitin)/cellulose composite biosorbents prepared using ionic liquid for heavy metal ions adsorption. *AIChE Journal*, 55(8):2062–2069. (Cited on page 66).

Swatloski, R. P., S. K. Spear, J. D. Holbrey, and R. D. Rogers
2002. Dissolution of Cellose with Ionic Liquids. *Journal of the American Chemical Society*, 124(18):4974–4975. (Cited on pages 62 and 63).

Tadros, T. F.
2013. *Emulsion Formation and Stability*, Wiley-VCH. (Cited on pages 67 and 68).

Takahashi, M., M. Ookubo, and H. Takena
1991. Solid state 13c NMR spectra analysis of alkalicellulose. *Polymer Journal*, 23:1009–1014. (Cited on page 60).

Takeshita, S., A. Konishi, Y. Takebayashi, S. Yoda, and K. Otake
2017. Aldehyde Approach to Hydrophobic Modification of Chitosan Aerogels. *Biomacromolecules*, 18(7):2172–2178. (Cited on page 78).

Takeshita, S. and S. Yoda
2018. Upscaled Preparation of Trimethylsilylated Chitosan Aerogel. *Ind. Eng. Chem. Res.*, 57(31):10421–10430. (Cited on page 78).

Tatlier, M., G. Munz, and S. K. Henninger
2018. Relation of water adsorption capacities of zeolites with their structural properties. *Microporous and Mesoporous Materials*, 264:70–75. (Cited on page 234).

Taylor, G. I.
1934. The formation of emulsions in definable fields of flow. *Proc. R. Soc. Lond. A*, 146(858):501–523. (Cited on pages 70, 152, and 152).

Terzić, I., J. Ivanović, I. Žižović, M. L. Škorić, N. Milosavljević, N. Milašinović, and M. K. Krušić
2018. A novel chitosan gels: Supercritical CO2 drying and impregnation with thymol. *Polymer Engineering & Science*, 58(12):2192–2199. (Cited on page 78).

Tjahjadi, M., J. M. Ottino, and H. A. Stone
1994. Estimating interfacial tension via relaxation of drop shapes and filament breakup. *AIChE Journal*, 40(3):385–394. (Cited on page 152).

Tkalec, G., Ž. Knez, and Z. Novak
2015. Formation of polysaccharide aerogels in ethanol. *RSC Advances*, 5(94):77362–77371. (Cited on pages 74 and 77).

Tkalec, G., R. Kranvogl, A. Perva Uzunalić, Ž. Knez, and Z. Novak
2016. Optimisation of critical parameters during alginate aerogels' production. *Journal of Non-Crystalline Solids*, 443:112–117. (Cited on page 78).

Trygg, J., P. Fardim, M. Gericke, E. Mäkilä, and J. Salonen
2013. Physicochemical design of the morphology and ultrastructure of cellulose beads. *Carbohydrate Polymers*, 93(1):291–299. (Cited on pages 66, 86, 86, 115, and 116).

Trygg, J., E. Yildir, R. Kolakovic, N. Sandler, and P. Fardim
2014. Anionic cellulose beads for drug encapsulation and release. *Cellulose*, 21(3):1945–1955. (Cited on pages 86, 115, and 116).

Tsioptsias, C., C. Michailof, G. Stauropoulos, and C. Panayiotou
2009. Chitin and carbon aerogels from chitin alcogels. *Carbohydrate Polymers*, 76(4):535–540. (Cited on page 78).

Tsioptsias, C., A. Stefopoulos, I. Kokkinomalis, L. Papadopoulou, and C. Panayiotou
2008. Development of micro- and nano-porous composite materials by processing cellulose with ionic liquids and supercritical CO2. *Green Chemistry*, 10(9):965. (Cited on page 132).

Tsutsumi, Y., H. Koga, Z.-D. Qi, T. Saito, and A. Isogai
2014. Nanofibrillar Chitin Aerogels as Renewable Base Catalysts. *Biomacromolecules*, 15:4314–4319. (Cited on page 78).

Ubeyitogullari, A. and O. N. Ciftci
2016. Formation of nanoporous aerogels from wheat starch. *Carbohydrate Polymers*, 147:125–132. (Cited on page 77).

Ubeyitogullari, A., R. Moreau, D. J. Rose, J. Zhang, and O. N. Ciftci
2019. Enhancing the Bioaccessibility of Phytosterols Using Nanoporous Corn and Wheat Starch Bioaerogels. *European Journal of Lipid Science and Technology*, 121(1):1700229. (Cited on page 77).

Väisänen, T., O. Das, and L. Tomppo
2017. A review on new bio-based constituents for natural fiber-polymer composites. *Journal of Cleaner Production*, 149:582–596. (Cited on page 65).

Valentin, R., R. Horga, B. Bonelli, E. Garrone, F. D. Renzo, and F. Quignard
2005. Acidity of Alginate Aerogels Studied by FTIR Spectroscopy of Probe Molecules. *Macromolecular Symposia*, 230(1):71–77. (Cited on page 78).

Valentin, R., K. Molvinger, F. Quignard, and D. Brunel
2003. Supercritical CO2 dried chitosan: an efficient intrinsic heterogeneous catalyst in fine chemistry. *New J. Chem.*, 27(12):1690–1692. (Cited on page 85).

Van Heiningen, A., M. Tunc, Y. Gao, and D. Da Silva Perez
2004. Relationship between Alkaline Pulp Yield and the Mass Fraction and Degree of Polymerization of Cellulose in the Pulp. *Journal of pulp and paper science*, 30(8). (Cited on page 109).

Veronovski, A., Ž. Knez, and Z. Novak
2013. Preparation of multi-membrane alginate aerogels used for drug delivery. *The Journal of Supercritical Fluids*, 79:209–215. (Cited on page 85).

Veronovski, A., G. Tkalec, Ž. Knez, and Z. Novak
2014. Characterisation of biodegradable pectin aerogels and their potential use as drug carriers. *Carbohydrate Polymers*, 113:272–278. (Cited on pages 78, 84, and 84).

Voon, L. K., S. C. Pang, and S. F. Chin
2016. Highly porous cellulose beads of controllable sizes derived from regenerated cellulose of printed paper wastes. *Materials Letters*, 164:264–266. (Cited on pages 37, 87, 87, 115, 115, 116, 116, 133, 170, and 204).

Voon, L. K., S. C. Pang, and S. F. Chin
2017. Porous Cellulose Beads Fabricated from Regenerated Cellulose as Potential Drug Delivery Carriers. *Journal of Chemistry*, 2017:11. (Cited on pages 28, 87, 115, 116, and 241).

Vorlop, K.-D. P. D. and J. Breford
1996. Verfahren und Vorrichtung zur Herstellung von Teilchen aus einem flüssigen Medium. DE4424998A1. (Cited on page 67).

Wada, M., L. Heux, and J. Sugiyama
2004. Polymorphism of Cellulose I Family: Reinvestigation of Cellulose IVI. *Biomacromolecules*, 5(4):1385–1391. (Cited on page 56).

Wang, H., G. Gurau, and R. D. Rogers
2012. Ionic liquid processing of cellulose. *Chemical Society Reviews*, 41(4):1519. (Cited on page 63 and 63).

Wang, H., Z. Shao, M. Bacher, F. Liebner, and T. Rosenau
2013. Fluorescent cellulose aerogels containing covalently immobilized (ZnS)x(CuInS2)1-x/ZnS (core/shell) quantum dots. *Cellulose*, 20(6):3007–3024. (Cited on page 79).

Wang, X., Y. Zhang, H. Jiang, Y. Song, Z. Zhou, and H. Zhao
2016. Fabrication and characterization of nano-cellulose aerogels via supercritical CO2 drying technology. *Materials Letters*, 183:179–182. (Cited on page 84).

White, R. J., V. L. Budarin, and J. H. Clark
2010. Pectin-Derived Porous Materials. *Chemistry - A European Journal*, 16(4):1326–1335. (Cited on page 78).

Wickholm, K., P. T. Larsson, and T. Iversen
1998. Assignment of non-crystalline forms in cellulose I by CP/MAS 13c NMR spectroscopy. *Carbohydrate Research*, 312(3):123–129. (Cited on page 108).

Wijmans, J. G., F. W. Altena, and C. A. Smolders
1984. Diffusion during the immersion precipitation process. *Journal of Polymer Science: Polymer Physics Edition*, 22(3):519–524. (Cited on pages 65 and 74).

Wijmans, J. G., J. P. B. Baaij, and C. A. Smolders
1983. The mechanism of formation of microporous or skinned membranes produced by immersion precipitation. *Journal of Membrane Science*, 14(3):263–274. (Cited on pages 65 and 74).

Wolf, B. A.
2007. Polyelectrolytes Revisited: Reliable Determination of Intrinsic Viscosities. *Macromolecular Rapid Communications*, 28(2):164–170. (Cited on page 127 and 127).

Xu, A., J. Wang, and H. Wang
2010. Effects of anionic structure and lithium salts addition on the dissolution of cellulose in 1-butyl-3-methylimidazolium-based ionic liquid solvent systems. *Green Chem.*, 12(2):268–275. (Cited on page 63).

Yamane, C., T. Aoyagi, M. Ago, K. Sato, K. Okajima, and T. Takahashi
2006. Two Different Surface Properties of Regenerated Cellulose due to Structural Anisotropy. *Polymer Journal*, 38(8):819–826. (Cited on page 197).

Yamashiki, T., K. Kamide, K. Okajima, K. Kowsaka, T. Matsui, and H. Fukase
1988. Some Characteristic Features of Dilute Aqueous Alkali Solutions of Specific Alkali Concentration (2.5 mol $l^{-1}$) Which Possess Maximum Solubility Power against Cellulose. *Polymer Journal*, 20(6):447–457. (Cited on page 60).

Zhang, D.-Y., N. Zhang, P. Song, J.-Y. Hao, Y. Wan, X.-H. Yao, T. Chen, and L. Li
2018. Functionalized cellulose beads with three dimensional porous structure for rapid adsorption of active constituents from Pyrola incarnata. *Carbohydr. Polym.*, 181:560–569. (Cited on pages 115 and 116).

Zhang, J., J. Wu, J. Yu, X. Zhang, J. He, and J. Zhang
2017a. Application of ionic liquids for dissolving cellulose and fabricating cellulose-based materials: state of the art and future trends. *Materials Chemistry Frontiers*, 1(7):1273–1290. (Cited on page 63).

Zhang, J., H. Zhang, J. Wu, J. Zhang, J. He, and J. Xiang
2010. NMR spectroscopic studies of cellobiose solvation in EmimAc aimed to understand the dissolution mechanism of cellulose in ionic liquids. *Phys. Chem. Chem. Phys.*, 12(8):1941–1947. (Cited on page 63).

Zhang, S., J. Feng, J. Feng, and Y. Jiang
2017b. Formation of enhanced gelatum using ethanol/water binary medium for fabricating chitosan aerogels with high specific surface area. *Chemical Engineering Journal*, 309:700–707. (Cited on page 78).

Zhao, B., L. Greiner, and W. Leitner
2012a. Cellulose solubilities in carboxylate-based ionic liquids. *RSC Adv.*, 2(6):2476–2479. (Cited on page 63).

Zhao, Y., X. Liu, J. Wang, and S. Zhang
2012b. Effects of Cationic Structure on Cellulose Dissolution in Ionic Liquids: A Molecular Dynamics Study. *ChemPhysChem*, 13(13):3126–3133. (Cited on page 63).

Zhou, J. and L. Zhang
2000. Solubility of Cellulose in NaOH/Urea Aqueous Solution. *Polymer Journal*, 32(10):866–870. (Cited on page 61).

Zhu, S., Y. Wu, Q. Chen, Z. Yu, C. Wang, S. Jin, Y. Ding, and G. Wu
2006. Dissolution of cellulose with ionic liquids and its application: a mini-review. *Green Chemistry*, 8(4):325. (Cited on page 62).

Zugenmaier, P.
2001. Conformation and packing of various crystalline cellulose ®bers. *Prog. Polym. Sci.*, P. 77. (Cited on pages 35 and 55).

## RÉSUMÉ

Les aérogels sont des matériaux ultra-poreux et nanostructurés aux possibilités d'applications variées. Une nouvelle génération d'aérogels à base de polysaccharides est aujourd'hui en plein essor : les bio-aérogels. Ils sont particulièrement prometteurs pour leur respect de l'environnement et leur biocompatibilité. De nos jours, la production de bio-aérogels sous forme de monolithes est maîtrisée. Pour optimiser leur procédé de fabrication et pour répondre à des besoins spécifiques d'applications (pharmaceutiques, alimentaire, absorption ou adsorption, etc), les aérogels doivent avoir la forme de particules.

Ce travail était focalisé sur la préparation et caractérisation de billes d'aérogels à base de cellulose et a été réalisé dans le cadre du projet Européen « Nanohybrids ». Deux objectifs principaux ont été atteints. Le premier était la préparation et la compréhension des propriétés de nouveaux matériaux, tout en diminuant leurs coûts de production. Deux types de matériaux poreux ont été produits et étudiés :

- Des xérogels à base de cellulose (en évitant le séchage sous $CO_2$ supercritique), avec des propriétés comparables à celles de leurs homologues aérogels (densité autour de 0,12 g $cm^{-3}$ et surface spécifique jusqu'à 300 $m^2$ $g^{-1}$).
- Des aérogels à base de pâte à papier. L'influence de chaque composant de la pâte (cellulose, hémicellulose, lignine) et de leur teneur sur la structure et les propriétés des aérogels a été évaluée.

Le deuxième objectif était le développement de méthodes de mise en forme d'aérogels de cellulose sous forme de billes de différentes tailles. Deux techniques ont été appliquées avec succès :

- Le "JetCutting" : des billes d'aérogels à base de cellulose et de pâte à papier, de taille variant de centaines de micromètres à quelques millimètres, dissout dans deux types solvants (NaOH-eau et liquides ioniques) ont été obtenus.
- L'émulsification : des particules d'aérogels de cellulose d'une dizaine de micromètres ont été préparé par le développement d'une nouvelle méthode d'émulsification-coagulation.



## MOTS CLÉS

Bio-aérogels. Cellulose. Porosité. Particules.



## ABSTRACT

Aerogels are ultra-porous and nanostructured materials with a wide range of applications. Bio-aerogels is a new generation of polysaccharide-based aerogels. These fast developing materials are particularly promising for their environmental friendliness and biocompatibility. Nowadays, the production of bio-aerogels in the form of monoliths is mastered. To optimize their manufacturing process and to meet specific application needs (pharmaceutical, food, absorption or adsorption, etc.), aerogels must be in the form of particles.

This work focused on the preparation and characterization of cellulose aerogel beads and was conducted in the framework of the European project "Nanohybrids". Two main objectives were achieved. The first was the preparation and understanding of the properties of new materials while reducing their production costs. Two types of porous materials were produced and studied:

- Cellulose-based xerogels (obviating drying under supercritical $CO_2$), with properties comparable to those of their aerogel counterparts (density around 0.12 g $cm^{-3}$and specific surface area up to 300 $m^2$ $g^{-1}$).
- Pulp-based aerogels. The influence of each pulp component (cellulose, hemicellulose, lignin) and their content on the structure and properties of aerogels was assessed.

The second objective was the development of methods for shaping cellulose aerogels into beads of different sizes. Two techniques were successfully applied:

- JetCutting: aerogel beads based on cellulose and pulps, varying in size from hundreds of micrometres to a few millimetres, dissolved in two types of solvents (NaOH-water and ionic liquids) were obtained.
- Emulsification: cellulose aerogel particles of about few tens of micrometres were prepared by the development of a new method of emulsification-coagulation.



## KEYWORDS

Bio-aerogels. Cellulose. Porosity. Particles.